KATHOLIEKE UNIVERSITEIT
LEUVEN

Arenberg Doctoral School of Science, Engineering & Technology
Faculty of Bioscience Engineering
Department of Biosystems

MONITORING AND MODELING OF A CITRUS PLANT PRODUCTION SYSTEM VIA INTEGRATION OF IN-SITU AND HYPERSPECTRAL REMOTE SENSING DATA

Jan Stuckens

Dissertation presented in partial fulfillment of the requirements for the degree of Doctor in Bioscience Engineering

29 November 2010

Doctoraatsproefschrift nr. 930 aan de faculteit Bio-ingenieurswetenschappen van de K.U.Leuven

MONITORING AND MODELING OF A CITRUS PLANT PRODUCTION SYSTEM VIA INTEGRATION OF IN-SITU AND HYPERSPECTRAL REMOTE SENSING DATA

Jan Stuckens

Promotors:

Prof. P. Coppin, K.U.Leuven, promotor and supervisor
Prof. R. Swennen, K.U.Leuven, promotor
Prof. L. G. Albrigo, University of Florida, co-promotor

Members of the Examination Committee:

Prof. R. Geers, K.U.Leuven, president
Prof. N. Verhoest, Ghent University
Prof. D. Berckmans, K.U.Leuven
Prof. P. Dutré, K.U.Leuven
Dr. W. W. Verstraeten, K.U.Leuven

Dissertation presented in partial fulfillment of the requirements for the degree of Doctor in Bioscience Engineering

29 November 2010

Legal depot number D/2010/11.109/47

ISBN number 978-90-8826-164-0

Dankwoord

Hoe begint een doctoraatsverhaal? Soms rol je er gewoon in na je studies. In mijn geval heeft de roeping wat langer op zich laten wachten. Het begon - een beetje onverwacht - in de stedenbouw, om na een jaartje bij de milieukundige ingenieurstechnieken van Haskoning te landen en dan... ja, waarom terug naar die unief? Doctoreren, was ik daar niet te oud voor geworden? Maar het kriebelde en zo heb ik op een avond, nu vijf jaren geleden en met de nodige nervositeit mijn vroegere thesispromotor gemaild: “konden we nog eens praten over dat meer dan zeven jaar oude voorstel?” Jawel dus, zo niet had dit boekje er niet gelegen. Dit is het dan, resultaat van vier jaren die voorbijgevlogen zijn, gebundeld in zowat tweehonderd bladzijden. Maar onderzoek en ervaringen vat je niet samen in tekst alleen. Was ik nog maar goed en wel gestart, eind 2006, en ik zat op het vliegtuig richting Florida. Daarna volgden nog eens Florida en nadien Stellenbosch, in Zuid-Afrika. Sinaasappelonderzoek heeft zo zijn voordelen.

Uiteraard is niet alles van een leien dakje gelopen. Er waren de nodige moeilijke momenten en frustraties, op wetenschappelijk en op persoonlijk vlak. Niet alles in de natuur werkt mooi volgens je eigen regeltjes. Peperdure wetenschappelijke instrumenten werken niet zo maar naar behoren, zelfs als ze versgebakken uit de doos komen, maar je kan er blijkbaar wel vliegtuigen mee kapen. De ervaring leert: lensdoppen verwijder je voor je begint te meten, in Zuid-Afrika rijden we links, dat is de overkant van de straat. Zonder dit alles was er ook niet zo veel memorabel gebeurd om op terug te blikken. Het is een mooie ervaring geweest, die vier jaren. Ik heb een stuk van een andere wereld mogen proeven, en het smaakt naar meer.

In de eerste plaats wil ik mijn promotor prof. Pol Coppin bedanken voor de kans die hij me gegeven heeft. Hij heeft me de ondersteuning, de vrijheid, het vertrouwen maar ook de nodige kritische commentaar en inzichten bijgebracht, nodig om dit onderzoek tot een goed einde te brengen. Daarbij wil ik ook prof. Rony Swennen bedanken voor de hulp over de hele lijn van het onderzoek en voor de goede samenwerking, die we hopelijk kunnen verderzetten.

Zonder mijn leuke en boeiende collega’s waren het ook maar vier droge jaren geworden. Jullie waren en zijn fijne mensen om mee samen te werken en ook al leidde een en ander tot wat spanningen, we zijn er altijd uitgeraakt. Bedankt Dimi, je hebt me ingewijd in de mysteriën van lasers, online gaming en verdwijnende koffiekoeken. Bedankt Ben, voor je fijne gezelschap in Florida en Zuid-Afrika en alle discussies die we samen gehad

hebben, over de Wetenschap, de toekomst, over mensen en koetjes en kalfjes. Bedankt Willem voor je hulp bij mijn onderzoek, om alles na te lezen, afspraken te regelen en om me niet neer te bliksemen als ik weer eens een verkeerde datum had genoteerd. Bedankt Stephanie, Miguel, Laurent, Mathilde, Ray, Stef, Dimitrios en Sara voor de leuke babbels en de samenwerking. Jullie zorgen ervoor dat ik af en toe van mijn scherm en papieren wegkijk. Bedankt ook, Wouter en Caroline, voor jullie hulp bij de metingen in Zuid-Afrika.

Bedankt aan alle vrienden om me te steunen en gewoon om er te zijn. Ik durf niet beginnen met iedereen op te noemen want ik ga zeker weer iemand vergeten. Maar toch een merci aan Joachim, Leen en Jorg, omdat jullie me hielpen mezelf te overtuigen om hieraan te beginnen. Bedankt ook aan alle collega's bij Haskoning voor jullie vriendschap in de zeven jaren die hieraan vooraf gingen. Dat blijft bij.

Nu wordt het hoog tijd voor het thuisfront. Bedankt mama en papa, Reinhold en Kaatje om me voor de volle 100% te steunen om aan dit avontuur te beginnen. Ook een welgemeende dank aan Brunhilde en Werner, aan al mijn ooms, tantes, neven en nichten in Brabant en het 'verre' West- en Oost-Vlaanderen voor jullie interesse in mijn onderzoek, want met satellieten naar sinaasappels kijken, daar overtuig je niet iedereen mee.

Deze laatste paragraaf is gereserveerd voor de belangrijksten. Bedankt Frederika omdat je me door dik en dun gesteund hebt, dat je naar me luistert als ik er eventjes door zit, dat je zingt in de badkamer, dat je me op tijd komt ambeteren, me terug naar boven stuurt als ik de verkeerde kleren aan heb, dat je er gewoon voor me bent. Adriaan, je kan nog niet zo mooi zingen als mama, maar je bent bij ons. Ik hou van jullie.

Jan

Leuven, november 2010

Acknowledgments

Funding support for this research was provided by the K.U.Leuven, Bijzonder Onderzoeksfonds, OT07048 (Coppin & Swennen, 2007-2011). In the first place, I want to thank prof. Pol Coppin, my supervisor, for giving my this unique opportunity, and my promotors prof. Gene Albrigo from the Citrus Research and Education Center (University of Florida) and prof. Rony Swennen for their contributions to this work over the last four years. Many thanks Gene for your warm welcome during my Florida visits, letting me get a taste of the Florida way of life. A special thanks goes to Reza Ehsani and Ashish Mishra for their help and hospitality. Many parts of this manuscript would not have been made without the help of Dr. Sebinasi Dzikiti (University of Stellenbosch) and Dr. Stephan Verreynne (Citrus Research International). Seb, Stephan, thank you so much for all your help in the data collection, logistics, student coaching and for all the discussions we had over mail and during our exchange visits. Furthermore I want to thank prof. Arnold Schoonwinkel and prof. Herman Steyn for their help in the Sumbandila data request, Dr. Albert Strever for logistic support and scientific input, Mr. Stephan Strauss of the Sandrivier estate and Mr. Kenny Beeton of ALG estates for their willingness to cooperate in our research.

I would also like to express my appreciation to the chairman, prof. Rony Geers and the members of the jury, prof. Niko Verhoest (Ghent University), prof. Phil Dutré, prof. Daniel Berckmans and Dr. Willem W. Verstraeten for their valuable and insightful comments that helped to improve this manuscript.

Abstract

Plant production systems are governed by site management and by biotic and abiotic factors. For annual crops, many of these have been described, modeled and used as a basis for production steering. Existing biophysical production models however lack components for the correct modeling of fruit crops, such as integrated submodels for flowering and fruit growth, adaptation and carbohydrate allocation. Dynamic inputs to these models are being delivered by meteorological records and - increasingly - by remote sensing due to its high spatial and temporal resolution. Specifically hyperspectral satellite data sets offer a high added value as they are capable of detecting a large number of relevant biophysical variables, such as leaf area index, chlorophyll content, soil and crown water content, pigment ratios and biomass production. The major scientific challenge is the robust and unbiased extraction of these variables and their subsequent assimilation in production models.

The first objective of this dissertation, throughout which citrus is used as a model crop, is the development of a bottom-up approach to model, at the different scales, the physiological, structural and optical processes leading to changes in signals as retrieved by hyperspectral satellites. The first step herein encompasses a description of the critical internal processes that lead to detectable changes in biochemical components, with a focus on the carbohydrate flows (chapter 2). In the second step, a dorsiventral leaf model (DLM) is developed (chapter 3) capable of accurately simulating optical properties (reflectance and transmittance) of leaves with known structural properties and biochemical composition. Contrary to existing isolateral leaf models, DLM is adapted to model dorsiventral leaves, typical for dicot species such as citrus. The next step in the up-scaling process establishes the relation between optical properties at the leaf level and those at the canopy (tree crown) level. Using 3D virtualization techniques (ray-tracing), in chapter 4 a model of an existing citrus orchard was constructed and validated using field data. This virtual environment enables simulations of hyperspectral sensor measurements with high accuracy. Innovative aspects are the use of calibrated 3D tree models with an explicit description of the geometry of all leaves, twigs and stems and realistic simulation of both diffuse and direct sunlight. This virtual environment has subsequently been used as a reference for the (in)validation of different assumptions commonly made by simpler but faster algorithmic canopy reflectance models. Tested assumptions concern the shape, distribution and glossy reflections of leaves, the properties of the incident light and the row structure of orchards. This relation between leaf and

tree has not only been studied using simulations, but has also been investigated using a hyperspectral time series of field measurements in a commercial citrus orchard (chapter 5). Changes in leaf, fruit and crown spectra throughout consecutive growth seasons could be explained by interpreting within-canopy mixtures of canopy components (leaf and fruit types) in different phenological stages (flowering, fruit set and growth and leaf drop), stress (sunburn) and management actions (pruning, irrigation and harvest). The last step in the up-scaling process, from crown to satellite level, was made in chapter 7 in which the impact of shadow, viewing geometry and pixel size were investigated.

The second objective in this research was the search for more robust data extraction methods that follow the inverse path: from satellite measurements to biophysical model variables. Chapter 3 introduces an improved model inversion strategy for DLM that allows leaf biochemistry (chlorophyll, carotenoids, dry matter and water) to be determined with higher accuracy. Additional statistical model building (chapter 2) reveals that spectral contact measurements can be used to determine leaf starch and soluble sugar concentrations. For measurements at the crown level, in chapter 6, a new measurement protocol is developed that enables time series collection under variable environmental conditions. This substantially improves measurement opportunities as compared to existing field protocols that demand a cloud free sky. Finally, using the virtualization techniques from chapter 4, chapter 7 finds optimal viewing angles for off-nadir satellite imagery in row plantations that minimize the interfering influence of soil and weeds on the canopy spectrum.

The simulations at the different scale levels of this research (biophysical process, leaf, crown and satellite) are some of the building blocks of a framework. Within this framework, remote sensing measurements capable of monitoring the production process of fruit crops can be simulated in a reliable and physically/physiologically based way. The insights that such an approach has delivered were used to make existing data extraction methods more robust and more accurate. Some parts of this research resulted in technologies that can be employed in an operational context, such as a fast assessment of leaf biochemistry and field protocols for canopy reflectance spectra. The full bottom-up approach as envisaged here, however, requires a substantial amount of sustained fundamental and applied research.

Beknopte samenvatting

Plantproductiesystemen worden aangestuurd door beheer en biotische en abiotische factoren. Voor sommige eenvoudige productiegewassen zijn vele hiervan gekend, gemodelleerd en gebruikt als basis voor productiesturing. In bestaande biofysische productiemodellen ontbreken echter componenten voor het correct modelleren van fruitteeltgewassen, zoals geïntegreerde submodellen voor bloei en vruchtgroei, adaptatie en de allocatie van koolhydraten. Voor de dynamische gegevensinvoer van deze modellen wordt, naast meteorologie, in toenemende mate teledetectie ingezet vanwege de hoge ruimtelijke en temporele resolutie. Met name hyperspectrale satellietwaarnemingen bieden een hoge meerwaarde omwille van het groot aantal relevante biofysische variabelen dat hiermee kan worden opgemeten, zoals bladoppervlakteindex, chlorofylgehalte, pigmentverhoudingen, bodem- en kruinvochtgehalte en biomassaproductie. De belangrijkste uitdaging bestaat erin om deze variabelen op een robuuste en onvertekende manier te extraheren en te assimileren in gewasproductiemodellen.

De eerste doelstelling van dit doctoraatsonderzoek, waarbij citrus wordt gebruikt als modelgewas, is het ontwerp van een eerste bottom-up benadering waarbij op verschillende schaalniveaus de fysiologische, structurele en optische processen worden gemodelleerd die leiden tot veranderingen in signalen zoals gedetecteerd door hyperspectrale satellieten. De eerste stap omvat de beschrijving van de belangrijkste interne processen die leiden tot waarneembare veranderingen in biofysische componenten, hetgeen hier is toegespitst op de koolhydratenhuishouding (hoofdstuk 2). In de volgende stap is een bladmodel, DLM (dorsiventral leaf model), ontwikkeld (hoofdstuk 3) waarmee wijzigingen in optische eigenschappen (reflectantie en transmissie) van een blad accuraat kunnen worden gesimuleerd op basis van gekende biochemische samenstelling en structuurkenmerken. In tegenstelling tot bestaande unilaterale bladmodellen is DLM aangepast voor dorsiventrale bladeren, typisch voor tweezaadlobbigen waaronder citrus. De volgende stap in het opschalingsproces legt de relatie tussen de optische eigenschappen op bladniveau en deze op kruinniveau. Met 3D virtualisatietechnieken (ray-tracing) werd in hoofdstuk 4 een bestaande citrusboomgaard nagebouwd en gevalideerd, waarin met hoge accuraatheid hyperspectrale metingen gesimuleerd kunnen worden. Vernieuwende aspecten zijn het gebruik van gekalibreerde 3D boommodellen met een expliciete geometrische beschrijving van alle bladeren en takken en de waarheidsgetrouwe simulatie van invallend diffuus en direct licht. Deze virtuele omgeving geldt als de referentie waaraan verschillende veronderstellingen worden getoetst die door eenvoudigere maar snellere algoritmische

kruinreflectantiemodellen worden gemaakt. Deze veronderstellingen betreffen de vorm, de verdeling en de spiegelreflectie van bladeren, de eigenschappen van invallend licht en de rijstructuur van boomgaarden. De relatie tussen blad en boom werd niet enkel gesimuleerd, maar werd eveneens in detail onderzocht in een hyperspectrale tijdsreeks van veldmetingen in een commerciële citrusboomgaard (hoofdstuk 5). Wijzigingen in blad-, vrucht- en kruinspectra doorheen opeenvolgende groeiseizoenen konden worden verklaard aan de hand van de expressie van de fenologische stadia (bloei, vruchtzetting en groei, bladval), stress (zonnebrand) en beheer (snoei, irrigatie, pluk). De laatste stap in het opschalingsproces, van kruin- naar satellietniveau, werd gemaakt in in hoofdstuk 7 waarin de effecten van schaduw, waarnemingshoek en pixelgrootte zijn nagegaan.

De tweede doelstelling van dit onderzoek omvat het zoeken naar meer robuuste gegevensextractiemethoden voor algoritmes die de omgekeerde weg bewandelen: van satellietmetingen naar biofysische modelvariabelen. Daarom werd in hoofdstuk 3 een verbeterde modelinversiestrategie voor DLM ontwikkeld waarbij bladparameters (chlorofyl, carotenoïden, droge stof en water) op een meer betrouwbare manier kunnen worden bepaald. Bijkomend statistisch onderzoek (hoofdstuk 2) wijst uit dat gebruik makend van spectrale metingen ook gehaltes van zetmeel en oplosbare suikers met goede nauwkeurigheid kunnen worden bepaald. Voor metingen op kruinniveau werd in hoofdstuk 6 een nieuwe meetstrategie ontwikkeld waarmee tijdreeksen op een onvertekende wijze kunnen worden opgemeten onder variabele weersomstandigheden. Dit vergroot in hoge mate de meetmogelijkheden ten opzichte van de bestaande methoden die een wolkenloze hemel vereisen. Met behulp van de virtualisatietechnieken uit hoofdstuk 4 is ten slotte in hoofdstuk 7 onderzocht welke de optimale kijkhoeken zijn voor oblieke satellietbeelden in rijbeplantingen, waarbij de verstorende invloed van bodem en kruiden op de kruinsignalen wordt geminimaliseerd.

De simulaties op de verschillende schaalniveaus in dit onderzoek (biofysisch proces, blad, kruin en satelliet) vormen de bouwstenen die passen in een omkaderende benadering waarin afstandwaarnemingen, die het productieproces van fruitgewassen opvolgen, op een betrouwbare en fysisch/fysiologisch onderbouwde wijze kunnen worden gesimuleerd. De inzichten die zulke benadering opleverde werden ingezet om bestaande gegevensextractiemethoden robuuster en nauwkeuriger te maken. Sommige deelonderzoeken leverden operationeel inzetbare technologieën op, zoals de snelle bepaling van biochemische bladeigenschappen en meetprotocols voor kruinmetingen. De volledige bottom-up modellering vereist echter een substantiële hoeveelheid bijkomend fundamenteel en toegepast onderzoek.

Abbreviations, symbols and definitions

General abbreviations

ABM-B	Algorithmic Bidirectional surface scattering Model for Bi-facial leaves
ANMB	Area under curve Normalized to Maximal Band depth
ANOVA	ANalysis Of VAriance
AOD	Atmosphere Optical Depth
ARMAX	Autoregressive model with Moving Average and eXogenous input
AVHRR	Advanced Very High Resolution Radiometer
BRDF	Bidirectional Reflectance Distribution Function
BRF	Bidirectional Reflectance Factor
BSFD	Bidirectional Scattering Distribution Function
CI	Contribution Index
COD	Cloud Optical Depth
CS	Clear Sky
DAA	Days After Anthesis
DFOV	Dual Field Of View
DHR	Directional-Hemispherical Reflectance
DHT	Directional-Hemispherical Transmittance
DLM	Dorsiventral Leaf Model
DN	Digital Number
DVOF	Dual Field Of View
ET	EvapoTranspiration
EVI	Enhanced Vegetation Index
EWT	Equivalent Water Thickness
fAPAR	fraction of Absorbed Photosynthetically Active Radiation
FII	Flowering Intensity Index
FOV	Field Of View
GEMI	Global Environment Monitoring Index
GIS	Geographic Information System
HDMR	High Dimensional Model Representation
HLB	Huanglongbing

HPLC	High Performance Liquid Chromatography
HR	High Resolution
IC	Intercalibration term
ICF	InterCalibration Function
IS-HS	In-Situ and HyperSpectral
LAD	Leaf Angle Distribution function
LAI	(one sided) Leaf Area Index
LEO	Low Earth Orbiting
LiDAR	Light Detection And Ranging
LOPEX	Leaf Optical Properties EXperiment
LST	Local Solar Time
MCARI	Modified Chlorophyll Absorption Ratio Index
MCRT	Monte Carlo Ray Tracing
MLR	Multiple Linear Regression
MODIS	MODerate resolution Imaging Spectroradiometer
MSI	Moisture Stress Index
MTVI2	Modified Triangular Vegetation Index
N	Nitrogen
NARMAX	Nonlinear Autoregressive model with Moving Average and eXogenous input
NARX	Nonlinear Autoregressive model with eXogenous input
NDVI	Normalized Difference Vegetation Index
NER	Noise Equivalent Radiance
NIPALS	Non-linear Interactive PArtial Least Squares
NIR	Neaf InfraRed, 700-1400 nm
OS	Obscured Sky
OSAVI	Optimized Soil Adjusted Vegetation Index
PA	Producer's accuracy
PAR	Photosynthetically Active Radiation
PBRT, pbrt	Physically Based Ray Tracer
PCR	Polymerase Chain Reaction
PLS	Partial Least Squares regression
PRI	Photochemical Reflectance Index
PROSPECT	PROpriétés SPECTrales
QCS	Quasi Clear Sky
RAMI	RAdiation transfer Model Intercomparison
RMSE	Root Mean Squared Error
ROMC	RAMI Online Model Checker
RT	Radiative Transfer
RUE	Radiation Use Efficiency
SAA	Solar Azimuth Angle
SAM	Spectral Angle Mapper
SBDart	Santa Barbara DISORT Atmospheric Radiative Transfer
SCI	Soil Contribution Index
SD	Standard Deviation
SDR	Standardized Difference Ratio
SEBAL	Surface Energy BAlance for Land

SID	Spectral Information Divergence
SIWSI	Shortwave Infrared Water Stress Index
sLAIDI	standardized Leaf Area Index Determining Index
SNR	Signal-to-Noise Ratio
SR	Simple Ratio
SRTM	Shuttle Radar Topography Mission
SWIR	Short-Wave InfraRed, 1400 - 3000 nm
SZA	Solar Zenith Angle
TA	Total Acididy
TCARI	Transformed Chlorophyll Absorption Ratio Index
TCI	Temporal Contribution Index
TOC	Top-Of-Canopy
TS	Time Series
TSS	Total Soluble Solids
UA	User's accuracy
UV	Ultra-Violet
VAA	View Azimuth Angle
VGT	SPOT Vegetation
VHR	Very High Resolution
VI	Vegetation Index
VIS	VISible, 400-700 nm
VPD	Vapor Pressure Deficit
VZA	View Zenith Angle
WCI	Weeds Contribution Index

General symbols and definitions

Dimensions are indicated between square brackets, other symbols are abstract or unitless.

α	maximum dispersion angle of light (chapter 3)
	fraction of irradiance under clear sky conditions (chapter 6)
α_f	angle of the facets normals
β_{ep}	fraction of total pigment content in the abaxial epidermis
β_{pigm}	fraction of total pigment content in the palisade layer
β_{wdm}	fraction of fresh mass in the palisade layer
γ	fraction of direct irradiance
δ	diffusion angle of light inside the abaxial epidermis (chapter 3)
θ_a	half-angle between illumination and viewing direction
θ_i,θ_s	incident angle of light
θ_o,θ_v	outgoing (viewing) angle of light
κ	specific absorption spectrum (chapter 3)
	bidirectional BRDF component (chapter 6)
λ	wavelength [nm]

μ	surface roughness modification term for Fresnel reflectance
ν	wavelength independent term
$\bar{\rho}$	Lambertian BRDF component
ρ_{dd}	bidirectional component of BRDF
ρ_{dh}, ρ^{dh}	directional-hemispherical reflectance
ρ^{hd}	hemispherical-directional reflectance
σ	surface roughness coefficient
τ	average transmissivity of a plate layer
φ_v,φ	relative azimuth
χ^2	chi-square statistic
ω_λ	soil single scattering albedo
ω_i	solid incoming angle
ω_o	solid outgoing angle
B	biomass production
b	soil hotspot reflectance peak width (chapter 4)
b'	soil specular reflectance peak width
c	BRDF normalization constant (chapter 3)
	soil hotspot reflectance peak height (chapter 4)
c'	soil specular reflectance peak height
C_x	biochemical content of substance x $[\mu g\, cm^{-2}]$ or $[mg\, cm^{-2}]$
D	normalized microfacets distribution
E	epidermis (chapter 3)
	irradiance $[W\, m^{-2}]$ (chapter 6)
$E(\lambda)$	spectral radiance $[W\, m^{-2}\, nm^{-1}]$
ET_0	reference evapotranspiration
F,Fr	Fresnel reflectance term
f	BRDF function $[sr^{-1}]$ (chapter 3, 7)
	fraction (chapter 5)
f_{air}	fraction of layer separated by air spaces
G	shadowing term
g	target reflectance relative to quasi clear sky target reflectance
H	value of the cost function
h	soil roughness parameter
HI	harvest index
k	absorption coefficient of a layer
Kc	crop coefficient
L, $L(\lambda)$	radiance $[W\, m^{-2}\, sr^{-1}]$ or spectral radiance $[W\, m^{-2}\, sr^{-1}\, nm^{-1}]$
M_x	mesophyll layer
N	PROSPECT structure parameter (number of layers)
nf	BRDF normalization function
OP	vector set of optical properties
P	palisade layer
R	reflectance of a leaf or leaf layer
R^2	coefficient of determination
RT	reflectance and transmittance of a leaf
R_{wh},R_{wp}	absolute reflectance with a whitepanel background

T	transmittance of a leaf or leaf layer (chapter 3)
	scan time (chapter 6)
t	Fresnel transmission coefficient
w	weight function of diffuse irradiance distribution
wp	water productivity factor
Y	yield
z	direction of light (upwards or downwards)

Table of contents

Chapter 1

Introduction

1.1 Modeling, monitoring and steering crop production systems

Fruit producers have, over the last decades, been adopting a wide variety of new technologies to meet increased market demands and environmental standards, to improve production quantity, to avoid losses, and to reduce maintenance costs. Increasing fruit quality and uniformity requirements are met by breeding, post-harvest technology, better management practices and more intensive monitoring (Ladaniya, 2007). Growing environmental concerns on the use of water resources and the contamination of groundwater by pesticides and nutrients have promoted sustainable management in agriculture and orchards (Keeney & Olson, ????; Goulding, 2000). Precision farming techniques such as variable rate technologies (Zaman et al., 2006b) and better irrigation scheduling (Jones, 2004) were introduced to improve management practices and to increase production quantity and quality. The required input parameters could often be measured by novel sensor technologies (De Baerdemaeker, 2001). Moreover, advances in sensor design and technology are proven to provide cost-effective and non-intrusive techniques for pre-symptomatic detection of biotic (pathogens) and abiotic stresses (Delalieux, 2009).

The optimal use of these technologies in commercial production requires a thorough understanding of the production system, which can be provided by crop production models. These range from simple stochastic relations to full-scale biophysical models (Thornley & France, 2007). Crop models can and are being used to control farming systems (currently mainly under greenhouse climates), autonomously or by assisting in the decision making process (Gary et al., 1998). The intricate complexity of horticultural production systems, however, poses new challenges to model all the required interactions, to correctly parametrize each model and to continuously monitor all critical input variables (Goldschmidt & Lakso, 2005).

Current orchard monitoring methods are primarily based on field surveys, meteorology recording and soil or leaf nutrient sampling (Hrubovcak et al., 1999). Most field surveys therefore depend heavily on human interpretation which may cause subjective differences among assessors as well as over time. Meteorological data obtained from local weather stations are important aids in site management (e.g. irrigation steering) as well as inevitable inputs for crop models. A restriction is that meteorological data is a model input and not a direct measure of the internal state (health) or output (yield) of a production system (Thornley & France, 2007). Finally, nutrient analysis provides an objective and direct assessment of the plant state but is generally restricted to a limited number of samples due to the high costs.

The interaction of sunlight with biomass through absorption and scattering reveals many properties of vegetation biochemistry and structure (Liang, 2004) that are expressions of the plant's internal state. This turns remote sensing into a monitoring tool of excellence due to its fast and objective, quantitative nature and the spatial and temporal resolution provided by present day sensors and platforms. Remote sensing technology demonstrated its capability to derive key model parameters and variables (Moulin et al., 1998; Dorigo

et al., 2007). Both active sensors (e.g. microwave or LiDAR[1]) and passive sensors, measuring reflectance or thermal and microwave emission, have been used to monitor agricultural systems (Dorigo et al., 2007), either on satellite or on airborne platforms. Technological advances driven by demands from vegetation sciences and mineralogy exploration have lead to the development of hyperspectral sensors that combine an almost continuous spectrum in the 400-2500 nm domain with a high spatial resolution (Goetz, 2009). Important efforts have been made in porting well-established relations predicting leaf level biochemistry from spectroscopic measurements to their hyperspectral equivalents at canopy and field levels (Goetz, 2009).

Hyperspectral and multi-spectral remote sensing have been widely used in the prediction of chlorophyll content and related stresses (e.g. Haboudane et al., 2002; Zarco-Tejada et al., 2004; Wu et al., 2008), in the estimation of leaf biomass (Baret & Guyot, 1991; Haboudane et al., 2004) and in the detection of water status (e.g. Cheng et al., 2006; Colombo et al., 2008; Suarez et al., 2010). Less common examples are the prediction of phenology (Sakamoto et al., 2005), the prediction of harvest date (El Hajj et al., 2009) and 'direct'[2] yield estimation (Somers et al., 2010b).

Notwithstanding the large potential of hyperspectral sensors, their scope is limited to the retrieval of a set of biochemical or structural variables in plant canopies that can be detected in the optical domain. This set inevitably only reflects a part of a plant system's full physiological functioning. Changes that are not optically detectable, such as alterations in plant hormone balance, or the exact causality of stresses (e.g. is chlorosis caused by nutrient deficiency or by pathogens?) require detailed *in situ* measurements. Hence, integration of *in situ* data with hyperspectral remote sensing is crucial: it combines the high spatial and spectral resolution offered by remote sensing technology with the more accurate analysis of *in situ* sensors.

The realization of this approach in horticultural production systems faces many challenges, that can be related to (i) production modeling, (ii) remote sensing technology and (iii) the establishment of time series of *in situ* and remote sensing data.

i. On the modeling side, the traditional relation between biomass production and system output, often expressed by a harvest factor, that has resulted in successful yield predictions for annual crops (Doorenbos & Kassam, 1986) is often not valid for perennial fruit crops. This is due to the larger number of external (e.g. climatology, drought) and internal factors (e.g. carbohydrate and hormonal balance) that can affect harvest quality and quantity (Davies & Albrigo, 1994; Albrigo et al., 2002; Goldschmidt & Lakso, 2005).

ii. Remotely sensed signals are affected by sensor noise, atmospheric interaction and geometric distortions (Lillesand et al., 2008). With the exception of very high resolution satellites, all space-borne data contain varying mixtures of different cover types, whereby orchards are composed of tree crowns, soils and weeds (Somers,

[1] Light Detection And Ranging

[2] 'Direct' here refers to methods that attempt to detect the presence of (mature) fruit on the trees rather than modeling approaches that derive yield from observations related to tree health such as chlorosis or water stress.

2009). In addition, remote sensing observations are restricted to the expression of a plant's physiological state through only leaf biochemistry and canopy structure. Furthermore, the up-scaling of leaf reflectance to the canopy level is not entirely understood and often not unique (Combal et al., 2003).

iii. Finally, the realization and interpretation of time series of remotely sensed or *in situ* collected data requires robust and sensitive techniques and algorithms in order to capture subtle but important trends.

This dissertation aims at bridging some of these knowledge gaps and at initiating the bottom-up modeling from the expression of physiological state in leaf biochemistry to at-satellite detected trends and changes.

In the following sections, different model types are discussed. Figure 1.1 presents an outline of this chapter. After an introduction on modeling concepts and definitions, biophysical models are treated, starting from the basics of carbon-assimilation (biomass production) and subsequently extending with relations required for horticulture, for which citrus will serve as a proxy. Subsequently the use of remote sensing technology for the retrieval of biophysical variables and parameters is treated with a focus on hyperspectral remote sensing. Thirdly, different *in situ* sensor systems are presented with an emphasis on their complementary role to remote sensing data. The final integration section deals with strategies to assimilate these data into operational or conceptual production models. The introduction chapter concludes with the description of the research framework, objectives and hypothesis and an outline of the following chapters.

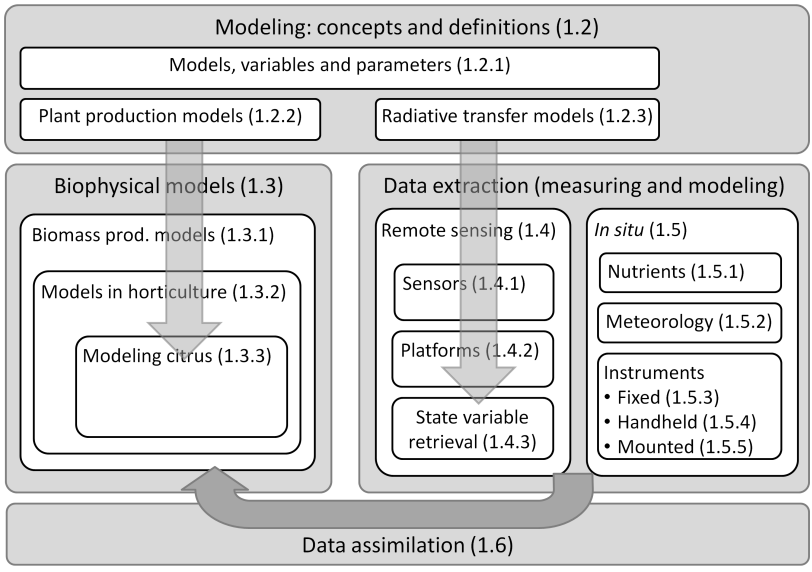

Figure 1.1: *Outline of the introduction chapter. Numbers refer to section numbering.*

1.2 Modeling: definitions and concepts

1.2.1 Models, variables and parameters

In this dissertation, models are discussed and developed that simulate plant production systems as well as models that simulate the propagation of light (radiative transfer) through these vegetative media. This section presents an overview of the main model types, uses, characteristics, assumptions and limitations.

Intrinsically, all models are formal representations of reality, simulating observable processes or systems (Verstraeten, 2006). By reconstructing reality, a model can pave the way to obtain a better understanding of a system. A mathematical model primarily consist of a set of mathematical relationships, which represent a system's state or dynamical behavior.

In model building, the terms 'variable' and 'parameter' are used. In the context of biophysical models, a variable is a system property that changes as part of system dynamics, such as water content or stomatal opening. Within the scope of this dissertation, parameters are considered as fixed system properties for the duration of the model run time. Model variables may be categorized as state, rate or driving variables (Thornley & France, 2007). State variables are those variables that completely describe the state of a system being modeled, at a given moment in time. Rate variables define the rate at which a process occurs, such as the rate of absorption, photosynthesis, growth or transportation processes. Driving variables are external to the system being modeled, but impact the system's dynamics, such as many meteorological variables.

Whether a property is considered as a variable or as a parameter therefore depends on the context in which it is used. For the modeling of water relations on a daily or weekly scale, total leaf area may be a parameter, while for the modeling of seasonal phenology it is a variable that changes due to vegetative flush and leaf drop. In the context of radiative transfer modeling, we adhere to common terminology and use parameter rather than variable for all system properties.

1.2.2 Plant production models

Plant production models attempt to predict economic output of agricultural production systems, in terms of quantity or quality. Depending on their nature, these models can be categorized as *deterministic* or *stochastic*, *dynamic* or *static* and *empirical* or *mechanistic* (Thornley & France, 2007). Deterministic models make definite predictions for quantities, whereas stochastic models include randomness by simulating stochastic distributions of variables. In dynamic models, state variables change over time, even if the final model prediction (e.g. yield) is static. Most plant production models are dynamic since they consider the dynamics of biological processes: growth, senescence, transpiration, etc..

Empirical models - also known as black box models - are data driven and use statistical relations to describe system responses to a set of input variables, without necessarily following the nature of the physical interactions. These models can be static or dynamic.

Examples of dynamic empirical models, fitted on time series of measured inputs and outputs, are state space models such as ARMAX[3] or Box-Jenkins (Box & Jenkins, 1970) that model the dynamic behavior of linear time-invariant systems. Nonlinear dynamic models can be modeled using Neural Networks (e.g. NARX or NARMAX models).

Mechanistic models, conversely, attempt to describe causal relations between variables by means of known physiological processes. This implies an understanding (causality) or explanation of the modeled phenomena. Often mechanistic models rely on two levels of description (e.g. organ - plant or plant - population) in which the higher level is mainly mechanistic while the lower level relies more on a combination of mechanistic and empirical relations since not all (sub)processes are exactly understood (Thornley & France, 2007).

Table 1.1 presents an overview of the characteristics of both model types. Which type of model is the more adequate depends on the intended purpose, on the nature of the system and on the type and quantity of the collected data. Within this dissertation, the focus is on understanding of the functioning of horticultural production systems as a whole rather than on individual processes or on operational use. In addition, horticultural systems are open systems with widely varying dynamics. *'Open'* refers to the many external factors (meteorology, pests, undocumented management interventions) that influence these systems. This increases the demands for both empirical and mechanistic models and increases their complexity and the amount of calibration data. In horticultural systems, processes exist with *fast* (e.g. water relations) *or slow* (alternate bearing) *dynamics*. The system output (yield quality and quantity) is only measured at harvest time, which is at yearly intervals for most non-tropical fruit crops. Establishing large times series as required for empirical time series models would take many years or even decades of dedicated measurements. Such datasets were not available within the scope of this research. Mechanistic models in contrast are less demanding for the length of the dataset, although they often require substantially more variables to be measured.

For the above reasons, the use of biophysical models was preferred within the specific context of this dissertation. No claims are made for which type of model is more adequate to study horticultural systems in general.

[3]Auto-regressive moving average model with exogenous inputs

Table 1.1: Overview of the main properties of empirical and mechanistic dynamic models. Statements are derived from Canham et al. (2003) and Thornley & France (2007) unless mentioned otherwise.

	Empirical	**Mechanistic**
Data requirements	Long time series of a limited number of variables	Shorter time series of a large number of variables
Model structure	Data driven	Physically based or mixed
Prediction power	Optimal for given system if sufficient data	Depends on validity of assumptions and data
Model complexity	Increases with information content of input and output variables (Young, 1993)	Generally large
Portability	Limited: only interpolation within input data rang; extrapolation is uncertain (Ji, 2008)	Model relations are often universal, parameter values are portable under similar conditions; limited extrapolation
Purpose	Applications, study dynamics of unknown processes	Research, understand interactions of mostly known subprocesses
Extensibility/ Modularity	As part of mechanistic model	Yes, if variables are compatible (units, meaning)
Scale	Mainly individual processes with limited external (uncontrollable) influence	From processes to entire systems
Check model validity	Validation data	Validation data + physically realistic parameter bounds

1.2.3 Radiative transfer models

Radiative transfer (RT) models simulate the propagation of light through media. When applied to vegetation, they are named leaf optical models for RT at the leaf level (chapter 3) or canopy models, for RT of canopies (chapter 4). Many canopy models are capable of modeling not only (bidirectional) canopy reflectance, but also light extinction and absorption and albedo (hemispherical reflectance) (Widlowski et al., 2007). RT models are static by nature, although they can be used in a dynamic context if the dynamics of their inputs are known, e.g. the use of trends in leaf area index[4] (LAI) to model changes in canopy reflectance. They can be categorized according to their mathematical nature and to the level of abstraction provided. Analytic models use abstract representations of the distribution of vegetative elements (leaves in a canopy and, at a higher level, trees in a stand or in an orchard). Knowledge of the exact position of each canopy element is not required and stochastic distributions are applied to describe parameters such as the spatial distribution of trees in a stand or the angular distribution of leaves in a

[4]LAI is here defined as the ratio of total one-sided leaf area per unit land cover area.

tree (leaf angle distribution or LAD). Explicit 3D models conversely use an exact 3D representation of all vegetative elements, often including the modeling of the position and shape of each leaf. Such methods have been extended to the cellular level to simulate within-leaf light propagation (Govaerts et al., 1996). An exact solution to the light transfer in these models can only be obtained using ray-tracing techniques. These implement Monte Carlo sampling to follow the path of large numbers of individual light rays (photons) throughout a scene (Pharr & Humphreys, 2004).

RT of the atmosphere is modeled using atmospheric models, that consider the scattering and absorption of incident and reflected light by the different gasses the atmosphere is composed of.

In vegetation remote sensing, atmospheric, canopy and leaf RT models can be integrated to simulate at-sensor measured radiance (Verhoef & Bach, 2007) or - inversely - to obtain vegetation biophysical or structural properties from measured radiance.

Usability of RT models to model system dynamics such as the evolution of canopy reflectance throughout a day or a growing season depends mainly on the nature of the models. For analytical models that have a discrete number of parameters, dynamic modeling depends on the knowledge of the dynamics of the critical parameters such as solar elevation, LAI or leaf angular distribution (LAD). For models with an explicit 3D description of canopy structure, such as Monte Carlo Ray-tracing (MCRT), dynamic modeling may be much more challenging if canopy structure dynamics are considered: for each model time step, a new 3D description may be required.

1.3 Biophysical models

1.3.1 Models driven by biomass production

Historically, the focus in agronomic model development for many annual crops depends on the correct estimation of biomass production, governed by the use of photosynthetically active radiation to assimilate carbohydrates. The progressive accumulation of photosynthesized biomass makes these models inherently dynamic. Most have been targeted at annual crops, starting with zero or a small initial biomass that builds up throughout a single growing season. A fraction of this biomass will constitute the yield. The main assumption is thus that a direct and almost linear relation exists between biomass production (B) and yield (Y) via the definition of a harvest index (HI) (Steduto et al., 2009):

$$Y = B\ HI \tag{1.1}$$

Three growth engine categories have been developed to describe this assimilation, representing different trade-offs between model empiricism and mechanistic behavior: carbon-driven engines, solar-driven engines and water-driven engines (Steduto, 2003).

i. Carbon-driven engines provide the most detailed description of carbon assimilation

as presented in figure 1.2 (dashed line). This includes the dynamic modeling of radiation interception, subdivided into different canopy layers and taking into account leaf density and leaf angular distribution. Biomass production is steered by a crop-specific photosynthetic response curve that establishes a relation between intercepted radiation by a canopy element and its production rate of carbohydrates. This approach has been followed by widespread crop models such as WOFOST (WOrld FOod STudies) and SUCROS (Simple and Universal CROp Simulator) (Bouman et al., 1996).

ii. Difficulties in parametrization and obtaining detailed descriptions of canopy structure lead to simplifications in which the relation between solar radiation and biomass production is given by a single radiation use efficiency (RUE) parameter (gray arrow). Solar driven models use the same path as carbon driven models. Well-known examples are CERES (Crop Environment REsources Synthesis, Ritchie & Otter, 1985) and EPIC (Erosion Productivity Impact Calculator; Williams et al., 1983). Both model categories are based on biophysical relations. Research evidence exists, however, that RUE or photosynthetic response curves may show inconsistent and non-linear behavior over different crop types, locations and years (Sinclair & Muchow, 1999).

iii. The third category of growth engines is based on the relation between transpiration and biomass production (dotted lines). After measuring or modeling crop transpiration, a crop specific water productivity (*wp*) term creates the relation with biomass. This was found to exhibit a robust and conservative behavior even under conditions of mild stress (Steduto et al., 2007). The Aquacrop model (Steduto et al., 2009) provides an implementation of this method.

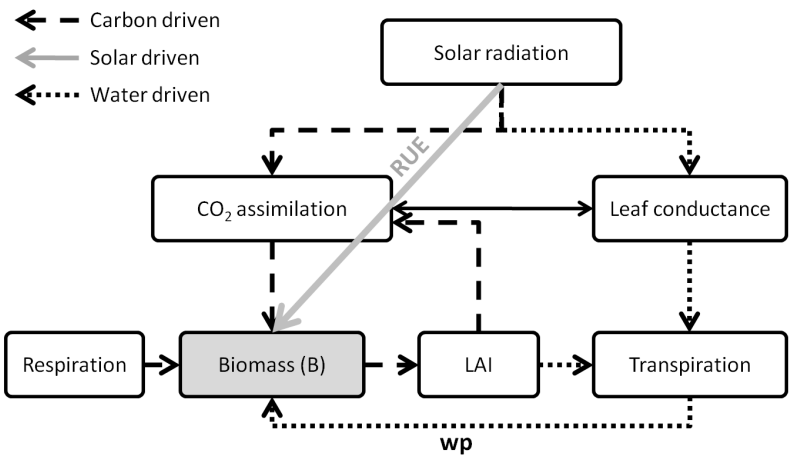

Figure 1.2: *Driving forces for biomass production. RUE: Radiation Use Efficiency, wp: water productivity.*

Most crop growth models will take into account additional sub-models that impact one

or more relations in the scheme of figure 1.2.

A soil-crop water balance sub-model can evaluate the fluxes of water caused by rainfall, irrigation, capillary rise, drainage, soil evaporation, transpiration and run-off (Thornley & France, 2007). This allows simulation of the effects of water shortage on biomass accumulation e.g. through leaf conductance or - for severe stresses - through leaf loss. In addition, it can simulate the impact on different nutrient transport processes.

Partitioning sub-models take care of the allocation of synthesized carbohydrates to respiration, growth or storage in different plant compartments (leaves, stems, roots and fruit) and are therefore critical in the determination of fruit quantity and quality if the production system is source-limited.

Mineral nutrient sub-models are often limited to nitrogen, but can include different sources (soil layers, plant, organic and inorganic fertilizer, fixation) as well as differentiation in nitrates and ammonium (Jones et al., 2003; Stöckle et al., 2003). The impact of deficiencies can be modeled through reductions in photosynthetic activity or through changes in the partitioning.

A senescence sub-model can simulate the effect of aging and leaf drop on photosynthetic efficiency and resource partitioning (Jones et al., 2003).

Crop phenology sub-models simulate the development of reproductive organs (fruit or grains) that generally form the harvestable part (Y in equation 1.1). In its simplest form, phenology is weather driven in the early stages of development (induction, anthesis, fruit set) with an emphasis on negative feedback by both high and low temperatures (Albrigo et al., 2002; Albrigo & Saúco, 2004), but depends on the supply of nutrients (carbohydrates and minerals) and water in the later development stages (Henton et al., 1999). Since fruit in later development stages can be strong sinks (Goldschmidt, 1997), a phenology sub-model may need two-way relations: supply from the plant will affect fruit growth, but growth and presence of fruit can impact partitioning of resources and thus inhibit growth or reserve accumulation in other organs.

Additional refinements are possible by considering within-plant competition (allocation to leaves, fruit, roots and stems), between-plant competition (crop versus weed or inter-cropping) or by integrating population models for pests or diseases (Thornley & France, 2007).

1.3.2 Models for fruit tree horticulture: required extensions

Fruit tree crops share an important number of commonalities with annual crops (Goldschmidt & Lakso, 2005): most processes occurring in annuals will occur in fruit tree crops. Therefore knowledge gathered on the modeling of annual crops provides a first basis to develop more advanced models for perennial fruit crops. Such models may be developed as extensions of existing biophysical models, rather than being created anew.

The main difference between annual and fruit tree modeling is the increased overall complexity of the latter and the higher impact of the fruit quantity and quality in the model development. Yield can no longer be considered as an almost constant fraction of

seasonal biomass production (Steduto et al., 2009).

Stand-alone models have been developed for different aspects of the fruit production process, such as flowering intensity (Albrigo et al., 2002), fruit growth (Bustan et al., 1999) or radiation interception in orchards (Oyarzun et al., 2007). Their integration in existing encompassing models may fill in important requirements for fruit trees. The following paragraphs summarize the required extensions and refinements with an emphasis on the citrus production system.

Light interception

A common approach to describe light interception is to represent a field or block by a horizontal isotropic medium and assume a negative exponential light extinction (Beer-Lambert law). This may be a reasonable approximation for closed canopies (Thornley & France, 2007), but needs refinements for orchards that can form discontinuous canopies with specific row orientations. Detailed interception models have been developed e.g. by Oyarzun et al. (2007) for different orchard configurations from free standing to hedgerow or by Pieri (2010) for vineyards. In both models, orchard trees or rows are represented by simple solid primitives in a fixed geometric configuration and the main fluxes of radiation are quantified. Further refinements and more accurate simulations may need the use of explicit geometric models in a ray tracing environment (Widlowski et al., 2007; Van der Zande et al., 2010).

Photosynthesis

Additional refinements can be made for fruit trees by discriminating different leaf age classes, each of which may have a different radiation use efficiency. The curvilinear response (saturation) of carbon assimilation to photosynthetically active radiation (PAR) is also present and needs to be taken into account, certainly for C3 plants such as citrus, that have lower saturation levels (Taiz & Zeiger, 2006). Shade and sun leaves may require separate treatment, each with their own response curves.

Carbohydrate sink-source relations

In fruit trees, the partitioning of assimilated carbohydrates may follow different rules according to supply/demand ratio and development stage. Under conditions of sufficient supply, each sink can receive its share according to its potential growth, and organ growth is not source-limited (Goldschmidt & Lakso, 2005). Positive feedback may even exist to reduce photosynthesis (Neales & Incoll, 1968). When demand exceeds supply, a partitioning system is required that assigns the assimilates, depending on their sink strength. This is identical to annual crops but with additional emphasis on storage compartments. Sink strength of fruit was found to vary through development, with flowers and young fruitlets having a low priority and expanding leaves and older fruit having a high priority (Bustan & Goldschmidt, 1999). For fruit trees with abundant flowering and where only a small fraction of the flowers develops into fruit, non-productive flowers may need to be considered as a separate sink (Bustan & Goldschmidt, 1998).

Adaptation and acclimation

Adaptation of trees is best known where it concerns their response to either hot or cold temperatures. Cold hardening in citrus was found to be regulated by increased sugar contents in leaves in late autumn to protect against freezes (Yelenosky, 1975).

Ribeiro (2007) discusses evidence of acclimation of the photosynthetic apparatus to increasing growth temperature as well as adaptive photo-protection mechanisms for extreme high temperatures.

Phenology: flowering, fruit set and fruit enlargement

Phenological modeling of fruit trees may require separate sub-models for each of the following stages: initiation/induction, flowering, pollination, fruit set, physiological drop and the different phases of fruit growth: cell division, differentiation, enlargement and maturation (Davies & Albrigo, 1994). For the induction stage that determines flowering intensity, (sub)tropical species may require a cold or drought stress period (Albrigo & Saúco, 2004) that can be modeled by accumulation of chilling units (Albrigo et al., 2002). Additionally, a minimum threshold level of reserve carbohydrates seems to be required (Ruiz et al., 2001). Flower duration and fruit development time is often modeled in thermal time units such as growing degree-days. Physiological drop and the subsequent fruit growth in citrus were found to depend on carbohydrate availability (Ruiz et al., 2001; Goldschmidt & Lakso, 2005).

Fruit quality aspects

Fruit market value is determined by a large number of quality factors. For processed fruit, the major factor is the juice quality. For fresh fruit, also aesthetic aspects such as peel color and appearance, fruit size, shape, toughness and juiciness of the pulp are important (Davies & Albrigo, 1994). Quantitative description of juice quality focuses mainly on relative quantities of soluble solids (TSS) and total acidity (TA) (Davies & Albrigo, 1994). Quality aspects can depend on other plant biophysical processes (certainly for juice content) or can be climatology-driven, such as wind scarring or color break.

In horticulture, market demands concern not only the 'average quality' but also the variability in fruit quality, which may be modeled through stochastic rather than deterministic models (Gary et al., 1998).

Management

Orchard management has an impact on almost all aspects of the production process and established biophysical models often contain dedicated management modules (Jones et al., 2003; Stöckle et al., 2003). Fertilizer applications and irrigation scheduling for orchard trees can be modeled through existing models by changing system nutrient and water inputs. Pruning can be modeled by changes in leaf area and light penetration parameters. Harvest (date of harvest) can be modeled by the removal of the fruit as a

resource sink. In contrast, no quantitative descriptions were found to model the effect of hormonal applications to control fruit drop, flowering intensity, fruit set, thinning, fruit senescence or peel coloration (Spiegel-Roy & Goldschmidt, 1996; Lovatt & Sciences, 2010).

Carry-over effects

The perennial nature of tree crops has as a consequence that the previous year's accumulated history (pests, stresses, climatology) can influence the current year's production. Severe stresses such as those induced by hurricanes may impact tree physiology and fruit for multiple years (Albrigo et al., 2005). In fruit tree crops, certain cyclic carry-over effects have been described as 'alternate' or 'biennial' bearing (Davies & Albrigo, 1994) in which trees alternate heavy crop load ('on') years with low crop load ('off') years. The underlying mechanism, though not fully understood, is believed to be steered by carbohydrate reserves (sugars and starch) (Goldschmidt & Golomb, 1982) and/or by the inhibitory effect of the previous year's fruit present on the trees (Verreynne & Lovatt, 2009). Other carry-over effects include the regrowth after pruning or hedging. Finally, tree death (disease, frost) and replanting may be described as an extreme case of carry-over.

1.3.3 Citrus as a pilot model crop

Throughout this dissertation, orange (*Citrus sinensis* L. [Osbeck]) will be used as the pilot crop for the development and testing of both biophysical and RT models. Reasons as discussed below are (i) the importance of management, (ii) the extensive existing knowledge base, (iii) the economic importance, (iv) the phenology of citrus, and (v) the climatic conditions.

i. The high incidence of continuous management practices in citrus orchards, e.g. with respect to irrigation, fertilization, pruning, pest and weeds management and fruit picking (Davies & Albrigo, 1994; Spiegel-Roy & Goldschmidt, 1996) creates many opportunities for the grower to control in real time the production using information from modeling efforts.

ii. Intensive research on all aspects of the citrus production processes has lead to a large knowledge base. Noteworthy are the existence of extension and research centers such as the University of Florida Citrus Research and Education Center (CREC), grower's organizations such as the Citrus Research International (Southern Africa) and the four-yearly conference of the International Society of Citriculture.

iii. Citrus is one of the important fruit crops worldwide. According to FAO statistics (FAO, 2009), the 2008 total fresh and processed citrus production amounted to 127 million tonnes of which 68 million tonnes were oranges. Technology transfer of relevant modeling results may thus be turned into large economic benefits.

iv. Since citrus is an evergreen crop, the year round monitoring of phenology and physiology is possible. Unlike many crops grown under tropical conditions such as

banana (or non-commercial citrus), most commercial citrus phenology progresses simultaneously through distinct growth stages (flowering, fruit set and color break, etc.), that can therefore be separately monitored.

v. Finally, the majority of commercial citrus is grown in the citrus belt, extending between 20° and 40° latitude on both Northern and Southern hemispheres (Spiegel-Roy & Goldschmidt, 1996). This covers mainly Mediterranean and sub-tropical climates with less cloud cover (Hahn & Warren, 2007) and higher intensity of solar radiation than in temperate climates. This facilitates optical remote sensing data acquisition.

1.4 Remote sensing data

Remote sensing technology is now often used as an instrument to retrieve information on vegetation status for use in biophysical models. While at present the emphasis lays on hyperspectral systems, other approaches have been documented as successful over the years. First an overview is presented of these sensor technologies. Second, the platforms on which these sensors are mounted are described in the view of biophysical modeling needs. Finally, the different variables and parameters that can be retrieved from such technologies are discussed.

1.4.1 Sensor technologies

Depending on their spectral bandwidth and number of bands, sensors are categorized as panchromatic (single broad band), multi-spectral or hyperspectral, where bands are sufficiently narrow to consider the retrieved signal as a continuous spectrum.

Optical reflective

Optical remote sensing detects the reflectance of earth surfaces. It contains the integration of scattering and absorption of electromagnetic radiation between 350 and 2500 nm (Rencz, 1999). This encompasses the higher wavelengths of the ultraviolet (350-400 nm), the visible (400-700 nm), near infrared (NIR or IR-A, 700-1400 nm) and short-wave infrared (SWIR or IR-B, 1400 - 3000 nm)[5]. The differences in chemical bonds and atomic composition of different molecules leads to differences in resonance wavelengths at which light is preferentially absorbed (dissipative absorption) (Hecht, 2002). Combined with the broadening of these resonance wavelenghts due to tight packing of molecules in solids and liquids, it forms the basis of spectral differences in molecular absorption of organic and inorganic materials.

Light that is not absorbed and interacts with molecules is scattered, i.e. redirected without loss of energy, which leads to transmission and reflectance. An important process here is diffraction of light (Snell and Fresnel laws) which is the basis of optical light scattering. Different spatial organizations of materials, at microscopic (e.g. tissue

[5]This manuscript will adhere the International Commission of Illumination (CIE) definitions. In other domains such as astronomy, near-infrared is more commonly defined as the 700-5000 nm region.

organization within a leaf) and macroscopic levels (organization of leaves in a tree or trees in a stand) determine the overall scattering behavior (Liang, 2004). This in turn determines the fraction of incident light that is reflected and retrieved by remote sensors. At-sensor measured radiance (often converted to reflectance factors) therefore contains information on vegetation structure and biochemical composition. Different processes and technological limitations however limit the accuracy by which both can be retrieved (Lillesand et al., 2008). In sequential order these are:

- Atmospheric scattering (Rayleigh and Mie scatter) and absorption of incident light, respectively leading to diffuse skylight and atmospheric absorption windows.
- Overlapping spectral signatures of different biological materials and spectral similarity of different canopy structural changes (e.g. changes in leaf angle or total leaf area).
- Light on the return path to the sensor can also be absorbed or scattered (path radiance)
- Optical sensors rely on the conversion of electromagnetic radiation to electric current, which is influenced by noise (expressed as the signal-to-noise ratio) and sometimes bias (stray light, dark current).
- Finally, positional accuracy, lens distortions, bandpass and spatial point spread ('blurring') of sensors need to be taken into account.

The combination of these processes hampers an accurate retrieval of structural and biochemical information from (vegetative) targets. This is often referred to as an ill-posed inversion problem (Liang, 2007).

Fluorescence

Fluorescence is the re-emission of absorbed electromagnetic radiation at different (higher) wavelengths. Chlorophyll fluorescence is a photo-protective mechanism - next to non-photochemical quenching - dissipating excess energy that is not used for photosynthesis (Taiz & Zeiger, 2006). The amount of fluorescence relative to the incident light intensity (or change in light intensity) is used as a measure of vegetation health. The complexity of the process and the small magnitude of the fluorescence signal (peak at 683-687 nm) superposed on the reflected radiation at the same wavelengths are major challenges for applications in remote sensing (Miller et al., 2005). Fluorescence is successful for monitoring vegetation health using contact measurements (fluorimeters) and short range sensing (Delalieux et al., 2009).

Thermal emission

Thermal emission of earth surfaces including vegetations (temperature around 300 K), occurs in the 8-14 µm range. An important source of vegetation temperature differences is caused by differences in canopy water content. The high thermal capacity of water

combined with the process of evaporative cooling results in overall lower temperatures for well watered vegetations on warm days (Lillesand et al., 2008). Major applications include the detection of vegetation water stress (Pinter et al., 2003) and the calculation of energy budgets for biomass accumulation (section 1.3.1).

Microwave

Active microwave remote sensing relies on sensors emitting radiation in the range of 1 mm - 1 m and collecting the return signal. Passive microwave sensors collect thermally generated microwave radiation emitted from the earth's surface, mainly between 1.5 mm and 0.3 m. The major advantage is the large penetration capacity of microwaves through clouds and haze. Major challenges are the more complicated analysis of radar images due to oblique viewing and low signal-to-noise ratios due to the small magnitude of the emitted or returned signals. Applications in vegetation sciences include canopy structure and vegetation/soil water content retrieval (Wigneron et al., 1997; Lillesand et al., 2008).

LiDAR

Light Detection And Ranging (LiDAR) instruments emit pulses of laser light and detect the time of pulse return to obtain distance information between objects and the sensor (Lillesand et al., 2008). Ground-based and aircraft-mounted LiDAR instruments have been used for topography and vegetation structure mapping.

1.4.2 Platform-sensor combinations

The range of applications for different sensors not only depends on the sensor specifications such as wavelength range and signal-to-noise ratio, but also on platform specifications. Different aspects important for the sensing of vegetations are discussed here, with a special reference to citrus orchards,.

Spatial resolution

Production monitoring in agriculture requires observations at least at the field level so that pixel sizes need to be adjusted to size and shape of the fields. A Geographic Information System (GIS) analysis in two different citrus production regions, Lake Alfred, Florida, USA and Citrusdal, Western Cape province, South Africa (chapter 7), revealed that observations at the field scale require maximum pixels sizes between 20 and 30 m to avoid large admixtures with neighboring fields, even without considering adjacency effects (Richter et al., 2006) and sensor spatial point spread. For larger fields, within-field heterogeneity (e.g. caused by slopes or soil texture gradients) may be taken into account. At this scale level, individual pixels are still composed of mixtures of tree crowns, soil and weeds (Somers et al., 2009c), requiring the use of unmixing algorithms or advanced canopy modeling to extract information from only the tree crowns. Only when pixel sizes are smaller than the tree scale do observations from pure canopy reflectance become feasible. A simulation analysis in chapter 7 estimates these threshold pixel sizes

Table 1.2: *Typical duration of phenological and physiological processes in citrus*

Process	Duration	Region	Reference
Bud development to full bloom	54-88 days	Florida	Valiente & Albrigo, 2002
Full bloom to end of flower drop	14-21 days	Florida	Albrigo & Saúco, 2004
Flower blossoms open (anthesis)	± 17 days	Florida	Bellows et al., 1989
Phloem loading and unloading	< 1 day		Taiz & Zeiger, 2006
Tree wilting after withholding irrigation	3-5 days	Florida	Albrigo, 2000-2002 (unpublished)
	6 days	South Africa, Stellenbosch	Dzikiti et al., 2010
Full bloom to mature fruit	7 months	Palmira, Colombia	Reuther, 1973
	14-17 months	Santa Paula, California	

for typical citrus plantations around 2 m in the Lake Alfred area and around 1 m in Citrusdal.

Temporal resolution and acquisition time

Required temporal resolutions for monitoring applications depend on the nature of the process or stress (e.g. flowering versus fruit growth; water versus nutrient stress) as well as on the goals (monitoring for yield prediction or early warning anticipating the stress). Exact time durations in physiology are hard to define as many physiological processes are highly impacted by temperature, so that the concept of thermal time, expressed in degree-days is more common (Spiegel-Roy & Goldschmidt, 1996). Table 1.2 lists an overview of indicative durations of processes in citrus. Short duration processes such as rapid wilting under severe water stress may be hard to monitor considering (near)nadir revisit times of present and future multi-spectral and hyperspectral satellites (e.g. 16 days for Landsat, 23 days for EnMAP[6], 26 days for SPOT[7]-5). Revisit times can be reduced by constellations of satellites or by off-nadir viewing.

Most low earth orbiting (LEO) satellites have overflight times between 9:30 and 10:30 local solar time (LST) (Campbell, 2002). This may impose restrictions on the monitoring of processes with diurnal dynamics such as evapotranspiration or phloem carbohydrate loading and unloading.

[6]Environmental Mapping and Analyzing Program
[7]Satellite Pour l'Observation de la Terre)

Bidirectional reflectance

For most earth's targets, the reflected radiance at a specific wavelength depends both on the incident angle and on the observation angle. The combined effect is functionally expressed as a bidirectional reflectance distribution function (BRDF) (Schaepman-Strub et al., 2006). The fixed overflight time of LEO satellites implicates that the solar elevation angle at the time of acquisition will vary throughout the year, which will thus impact the measured signal in a time series (see chapter 5).

The row structure of orchards presents an additional complexity, making the BRDF anisotropic (Pharr & Humphreys, 2004) i.e. it also depends on the geographic orientation of the rows and not only on the azimuthal difference between incident and viewing directions (see chapters 4 and 7).

Off-nadir viewing

Limitations in revisit time as well as the use of sensors with a smaller field-of-view have lead to the the development of across and along-track pointing capabilities for satellites enabling off-nadir observations. Although off-nadir viewing complicates mapping applications, researchers also found new ways to exploit the specific nature of off-nadir data. This includes the generation of stereo pairs or the retrieval of vegetation (often forest) structure parameters (Widlowski et al., 2004) using knowledge on bidirectional reflectance. Specifically for orchards, off-nadir viewing has interesting potential to decrease the influence of soil and weeds admixtures and improve the monitoring of canopy physiology and phenology. Chapter 7 describes how this can be achieved by observing from directions with an angle between 45° and 90° relative to the row orientation.

1.4.3 Model variable retrieval

A number of variables reflecting the state of agricultural production systems can be retrieved with remote sensing technology. Retrieval may depend (i) on molecules in leaves with known light absorption or re-emission features (pigments, carbohydrates, proteins and water), (ii) on the computation of energy budgets (light absorption, albedo), or (iii) on direct or indirect changes to the canopy structure. Additionally, information on weed dispersion or soil moisture may be obtained as model inputs. The following section presents an overview.

Retrieval of leaf biochemistry

Chlorophyll

Substantial research has been carried out on canopy and leaf chlorophyll contents detection. Most work is based on the 550 nm and 700-750 nm regions where chlorophyll absorption for healthy vegetations is not saturated (Kumar et al., 2001). Time series of chlorophyll content may have potential to detect time and intensity of vegetative flushes in evergreens (see chapter 5). This can be considered as an alternative to spectral detection of changes in LAI due to new growth since many indices become saturated

at high LAI values (Delalieux et al., 2008) that are common in citrus trees (Davies & Albrigo, 1994; Spiegel-Roy & Goldschmidt, 1996). Detection of chlorophyll content may reveal nutrient deficiencies and occurrence of pests and diseases. In citrus, deficiencies in nitrogen, potassium, sulfur, magnesium, iron, zinc and manganese are known to cause chlorosis and leaf patterns of chlorosis (e.g. full leaf, interveinal, etc.) are associated with specific deficiencies allowing field scouts to identify shortages prior to leaf analysis (Futch & Tucker, 2008). Citrus greening (Huanglongbing, bacterial) and Phytophthora root rot (fungal) are common infections causing leaf chlorosis. Since this type of information is not available from remote sensing at the tree level, ancillary ground data is required for symptom identification.

Differences in action spectra of chlorophyll a and b lead to slight differences in total chlorophyll light absorption that could theoretically be detected by hyperspectral sensors. Both chlorophyll types are often highly correlated (fixed ratios), but differences were found to be relevant for (citrus) stress detection (Bondada & Syvertsen, 2003). No successful processing or measurement technique has yet been developed to enable an accurate differentiation between different chlorophylls (Feret et al., 2008).

Carotenoids

Different carotenoid molecules (carotenes and xanthophylls) absorb in the 400-480 nm wavelength ranges (Kumar et al., 2001). Quantitative assessment of carotenoid contents at the leaf and canopy levels is hampered by the high absorption of chlorophyll in the same wavelengths (masking) leading to only moderate retrieval accuracies (Feret et al., 2008, see also chapter 3) using existing techniques. Carotenoid pigments can act as accessory photosynthetic or as photo-protective pigments (Taiz & Zeiger, 2006). Chlorophyll-to-carotenoid ratios are used to express vegetation health (e.g. chlorophyll breakdown during leaf senescence) and xanthophyll levels have been related to changes in photosynthetic photon flux density (Sims & Gamon, 2002). In citrus, substantially higher carotenoid levels were found in leaves exposed to high (but not damaging) irradiance levels (Felicetti & Schrader, 2009a, see also chapter 5). At the canopy level, the photochemical reflectance index (PRI) has often been related to the xanthophyll cycle and carotenoid-to-chlorophyll ratios (Sims & Gamon, 2002).

Brown pigments (oxidized polyphenols)

Brown pigments are a group of molecules absorbing in the 400-850 region that are synthesized during different stages of leaf senescence by oxidation or polymerization of phenolics (Peñuelas & Filella, 1998). Specifically tannins are expected to play an important role in brown coloration (Boyer et al., 1988). Early senescence stages in sunburn affected citrus leaves were found to affect the reflectance spectrum slope around 800 nm (chapter 5). The diversity of polyphenols, each with difference molecular structure and absorption spectra, hampers a quantitative spectroscopic assessment.

Structural and non-structural carbohydrates and proteins

While LAI can be used as an indicative measure of primary production, the dry mass content is also required to correctly estimate total accumulated dry mass. Good results have been obtained at the leaf level for total dry mass (chapter 3). Discrimination of different dry mass components (lignin, cellulose, hemi-cellulose, sugars, starch and proteins) at the leaf level was not successful with model inversion (Fourty et al., 1996), but statistical approaches were moderately successful for dried leaves (Jacquemoud et al., 1995). Recent experiments revealed that non-structural carbohydrates (starch and soluble sugars) in citrus can be retrieved with good accuracy, not only from dried leaf spectra but also from fresh leaves (Devarrewaere, 2010). Considering their high importance in the citrus production system (see section 1.3.2), the hyperspectral detection of non-structural carbohydrates is treated in more detail in chapter 2. Research at the canopy level shows promising results e.g. for lignin and nitrogen (Serrano et al., 2002).

Water

The broad water absorption bands in the near and short-wave infrared have been the basis of applications for detecting canopy and leaf water contents. Good water content estimates have been obtained at the leaf level (Jacquemoud & Baret, 1990; Feret et al., 2008; chapter 3). Lower accuracies in the retrieval of canopy water content (expressed as equivalent water thickness or EWT) may be attributed to interference of canopy structure in the 800-2500 nm region (Colombo et al., 2008). In physiology research, the relevance of water content as a measure of early stress detection however may be questioned. While severely water-stressed vegetations lead to detectable changes in canopy water content, mild levels of water stress that are most relevant for early warning systems are harder to detect (Carter, 1991; Dzikiti et al., 2010). In addition, water content of the underlying soil can lead to changes in retrieved signals that are hard to separate from those induced by changes in the vegetation. Species-specific secondary order effects of water stress such as changes in leaf angle, leaf curl, leaf facial orientation and ultimately leaf shedding cause changes in vegetation structure that may be easier and earlier to detect (see chapter 5). An important restriction for (space-borne) remote sensing of water stress is the required temporal resolution, as also discussed in section 1.4.2.

Retrieval of energy budgets

Canopy light absorption

Light interception is often expressed as the fraction of absorbed photosynthetically active radiation (fAPAR). Similar to NDVI and EVI, operational time series products from different sensors exist, based on reflectance from visible wavelengths (400-700 nm), supplemented with NIR reflectance (Gobron et al., 2006). fAPAR can be used to estimate gross primary production (carbohydrate assimilation) (Jung et al., 2008; Verstraeten et al., 2010), but requires an estimate of radiation use efficiency. Most applications are on an ecosystem scale.

Surface albedo

Surface albedo estimates the total fraction of light reflected into any direction, taking into account the bidirectional reflectance of targets (Schaepman-Strub et al., 2006). Surface albedo does not directly express vegetation health or phenological status, but is a required parameter to solve the energy budget for evapotranspiration-based production models using thermal emission (Bastiaanssen et al., 1998; Verstraeten et al., 2008). Successful experiments, in addition to those for annual crops, were reported for vineyards and mango orchards (Teixeira et al., 2009).

Retrieval of canopy structure information

Leaf area

Detection on vegetation leaf area, most commonly expressed as the LAI is generally based on near-infrared reflectance, where light scattering (reflectance and transmittance) of healthy leaves is at its maximum due to limited absorption (Kumar et al., 2001). The 3D arrangement (position, orientation and size) of leaves in a canopy leads to multiple scattering whereby the overall reflectance increases with increasing LAI until saturation occurs. Different indices have been developed to improve the saturation point (Delalieux et al., 2008) or to reduce the influence of the soil background or woody elements (Haboudane et al., 2004). Time series of indices sensitive to LAI, such as Normalized Difference Vegetation Index or the MODIS[8] Enhanced Vegetation Index (EVI) are being applied to monitor vegetative phenology of crops and forests.

Crop load

Although yield prediction is a major topic in remote sensing, estimation of crop load for fruit trees, which is often not well correlated with biomass production (see section 1.3.2), is less common. Successful early predictions using canopy visible and near-infrared hyperspectral reflectance are often based on measures of canopy vigor (e.g. Ye et al., 2006 for citrus). A more direct method, based on the presence of fruit and their impact on canopy structure, was developed by Somers et al. (2010b).

Detection of weeds

Specifically in orchards, very high resolution images can be used to map within-field abundance and distribution of weeds (Ye et al., 2007) that may be in competition with trees for resources and water.

Soil moisture

The identical absorption regions of water in both soil matrices and in vegetations is expected to hamper the detection of soil moisture underneath evergreen vegetations using optical remote sensing. For deciduous crops, soil moisture can be derived in the

[8] Moderate Resolution Imaging Spectrometer

absence of vegetation (Muller & Décamps, 2000) i.e. before the start of the growing season or using thermal remote sensing (Verstraeten et al., 2008).

Other parameters

Abundant research exists on the early detection of pests and diseases using remote sensing through their expression in canopy vigor (e.g. leaf loss, chlorosis). Du et al. (2008) present an integrated remote sensing and modeling application for the management of citrus greasy spot (*Mycosphaerella citri* Whiteside).

1.5 *In situ* data

In commercial horticulture, different information sources are consulted to make management decisions such as the time and amount of fertilizer or hormone applications, to determine fruit quality on the tree or to scout for infections. Current practices rely heavily on a combination of field scouting, information of local or regional weather stations, weather forecasts and a limited number of soil and leaf tissue analysis for macro- and micro-nutrients. A substantial number of additional *in situ* measurement systems have been actively researched and developed over the past decades. Some (e.g. sap stream measurements) are more targeted to scientific research, while others (soil moisture probes, optical contact sensing) are targeted for operational use. The following section presents an overview.

1.5.1 Nutrient analysis

Analysis of nutrients, though costly, are currently the main source of information on soil and leaf nutrient levels in agriculture and horticulture. In citrus, seasonal analysis of leaf macro-nutrients of either spring flush (Florida) or fruiting (South Africa) shoots are used to calculate fertilizer requirements (Davies & Albrigo, 1994). Soil nutrient analysis can be used to monitor pH or levels of relatively immobile nutrients such as Mg, Ca, Cu and P (Davies & Albrigo, 1994).

1.5.2 Meteorology

Weather station

Information from weather stations is instrumental in running dynamic biophysical crop growth models. Key variables include rainfall (for water uptake, evapotranspiration), temperature (for respiration, timing of phenological processes and frost prediction), irradiance (for photosynthesis), air moisture and wind speed (for evapotranspiration rate). Some instruments such as temperature sensors can be placed inside tree crowns.

Evapotranspiration (ET)

For water-driven production models (see section 1.3.1), evapotranspiration is an essential parameter.

- The only exact ET measurements, limited to scientific research purposes for individual plants, are provided by lysimeters (Allen et al., 1998), that are limited to experimental conditions (potted trees).
- Energy balance methods require measurements or modeling of net radiation (net radiometers), soil heat flux (heat flux plates) and sensible heat. Sensible heat can be approximated at field scale using remote sensing thermal data (Bastiaanssen, 2000) or by measuring vertical temperature gradients.
- Alternative ET measurements are obtained by eddy covariance methods that require vertical profiles of vapor pressure and temperature or wind speed (Allen et al., 1998).
- A fourth approach exists in the calculation (Penmann-Monteith equation) or measurement (lysimeters) of reference evapotranspiration (ET_0) of an open pan or grass surface. The crop ET is obtained through multiplication by a crop coefficient (Kc) that expresses the crop's cover, phenology and physiology Allen et al. (1998); Steduto et al. (2009).
- An overview of alternative assessment methods and variants can be found in Verstraeten et al. (2008).

1.5.3 Fixed instruments for point sampling

Sap stream

Measurement of sap flow can be achieved by different systems mounted on stems or branches. Each system requires a heat source, warming a section of the stem, and multiple thermocouples measuring the temperature difference or the speed by which heat pulses propagate (Smith & Allen, 1996). Installation and maintenance costs and the relatively large power supply for the heat source impose restrictions for large-scale usage (Verstraeten et al., 2008).

Soil moisture

Volumetric soil moisture measured in the root zone of trees can be used to model irrigation requirements. The high spatial variability of moisture, certainly under irrigated conditions, makes this method questionable, certainly for single-point measurements (Waldo & Schumann, 2009). An overview of assessment methods can be found in Verstraeten et al. (2008).

1.5.4 Handheld instruments and field scouting

Field surveys

Field surveys are required in orchard management for timely detection of stresses (nutrient, water), pests and diseases. Depending on the prevalence of diseases and pests, systematic or occasional surveys are made. Field scout training can be required

to identify specific symptoms or to detect vectors such as the Asian citrus psyllid (*Diaphorina citri* Kuwayama) that transfers Huanglongbing in citrus (Rogers et al., 2009). Use of a PDA and GPS can be an aid for large scale inventories.

Optical contact and close range

Optical contact measurements can be used to obtain non-destructive information on leaf biochemistry. Simple handheld chlorophyll meters and fluorimeters have been commercialized. Chlorophyll meters measure transmission or reflection from an active light source in specific filtered wavelength bands (e.g. SPAD[9] or CCM[10]). Fluorimeters (e.g. OS-30p, Opti-Sciences inc.) detect the fluorescence response to a light pulse of dark adapted leaves in time and magnitude to determine the activity and health of photosystem II.

Leaf reflectance or transmittance spectra obtained from field portable spectrometers can be processed to obtain biochemical information such as leaf chlorophyll, carotenoids, water and dry matter contents (section 1.4.3, chapter 3). The overall better variable retrieval accuracy of optical field measurements can be used to calibrate the same variables extracted from remotely sensed data using similar technology, but extending over a much larger area and time.

Contact spectra on fruit can be used to obtain objective measures on fruit albedo (e.g. coloration of oranges for peel quality). Spectral detection techniques have been developed to determine fruit maturity from contact spectra (e.g. Versita, 2007, for apple fruit).

1.5.5 Mobile mounted instruments

Instruments mounted on tractors, picking platforms or trucks can provide mobile mapping options when coupled with GPS hardware. Monitoring and inventories may be combined with standard orchard maintenance (spraying, fertilizer applications) to reduce the cost of operation.

Fruit counts

Fruit counting can be achieved during harvest, using weighing, LiDAR or camera systems that measure the mass or number of fruits in the tubs in real time (Tumbo et al., 2002). Such systems can be coupled with mechanical harvesting equipment such as shake-and-catch harvesters (Lee et al., 2009) to provide full automation. These systems, although potentially providing exact yield values, are less accurate for mobile mapping at the tree level, since yield coordinates are located in the row middles.

Truck mounted color camera systems, with threshold based fruit detection on digitally processed images have been used to obtain reliable fruit counts weeks before harvest (e.g. Zaman et al., 2009, for blueberry).

[9] Konika-Minolta inc.
[10] Chlorophyll Content Meter, Opti-Sciences inc.

Canopy volume estimates

Canopy size estimates such as tree height and crown volume are important in variable rate technologies to apply optimal amounts of fertilizers and pesticides (De Baerdemaeker, 2001). When data are stored for later processing and mapping, these systems can also provide input for modeling. Ultrasonic detection (Zaman et al., 2006a), cameras systems and 2D terrestrial LiDAR (Rosell et al., 2009) have been successfully applied.

1.6 Integration of remote sensing and *in situ* data in biophysical models

Biophysical models are designed to run on inputs of meteorology, management and site and crop specific parameters, while the values of the (internal) state variables are calculated by the model. A number of these state variables can also be derived from remotely sensed data which provides opportunities to better calibrate models and improve the model's accuracy.

1.6.1 Need for integration

For a biophysical model that simulates all aspects of the production process, only the final output (yield) is available for validation. This approach is however not realistic for modeling of crops:

- The large number of inputs combined with difficulties in parametrization due to a high spatial variability of variables and parameters and difficulties in correct quantification of parameters (e.g. transport capacities) often prevents reliable model calibration, with many parameters set as 'best guesses' based on research of different varieties under different meteorological conditions. This leads to accumulation of errors over the growing season (Thornley & France, 2007).
- For complex production systems such as horticulture, where many processes are not yet fully understood (e.g. hormonal regulation of flowering), large deviations between modeled and measured output can be expected (Goldschmidt & Lakso, 2005).
- Most models are developed for normal production cycles. Anomalies caused by pests, diseases, freeze damage or physical damage (e.g. hurricanes) are often not well predicted (Pinter et al., 2003).

The use of remote sensing offers options for intermediate model calibration: variables such as LAI, chlorophyll content or water content can be derived from optical remote sensing (see section 1.4.3) while they are simultaneously predicted as model state variables (see section 1.2.1). This provides additional calibration opportunities as well as the possibility to model spatial variability between or even within orchard blocks. The exclusive use of remote sensing as a means of intermediate calibration however lacks the detailed information provided by *in situ* instruments:

- Remote sensing often only provides relative measurements of variables, certainly if those are obtained through vegetation indices or statistical techniques, but even inversion of RT models can produce biased estimates (Meroni et al., 2004). Ground measurements on well identified index trees or index sites can be used to convert relative measures to unbiased physical quantities.
- For short duration processes or during periods of continuous unfavorable weather conditions (overcast skies), the temporal resolution of remote sensing can be inadequate. *In situ* instruments measuring the same variable can be used for interpolation in a time series (Moulin et al., 1998).
- *In situ* measurements may allow a more accurate retrieval of remotely sensed parameters, e.g. knowledge of soil moisture and texture can help in more accurate retrieval of canopy spectral reflectance from mixed pixels (i.e. containing factions of tree canopy and soil) (Muller & Décamps, 2000; Somers, 2009).
- For many fruit tree crops, the presence of fruit is largely hidden under the top layer of leaves (see chapter 5). Although the presence of fruit influences the canopy reflectance spectrum either through structural changes or through alteration of the canopy infrared light (Somers et al., 2010b), the majority of the fruit is not directly observed. Information on fruit maturity or health can thus only be provided from *in situ* measurements.

1.6.2 Assimilation strategies

Overview of existing strategies

Different strategies exist in the assimilation of remote sensing data for crop (or ecosystem) production. The following list is based on an extensive review by Moulin et al. (1998):

i. *Empirical models* use statistical model building (e.g. stepwise regression or partial least squares regression) to fit the optimal relation between remotely sensed reflectance or - more commonly - vegetation indices (VI) and yield. Commonly used VI's are NDVI and fAPAR, for which operational time series are available. Most empirical methods rely on the implicit assumption of a strong correlation between dry matter accumulation and yield.

ii. *Semi-empirical models* are popularized by Monteith's efficiency model (Monteith, 1977). This model calculates the total dry matter production as the sum of daily production. Daily production is then estimated as the product of (i) the incident radiation, (ii) the PAR fraction of sunlight, (iii) the radiation interception efficiency and (iv) the conversion efficiency of energy into dry matter. Remote sensing data can be used to estimate the interception efficiency as a measure of total biomass or LAI. Thermal emission (under semi-arid conditions) has been correlated to changes in conversion efficiency of sunlight into biomass (Steinmetz et al., 1990).

iii. *Mechanistic models with driving variables.* The biophysical model component in empirical and semi-empirical models is lacking and strictly speaking these are not

assimilation strategies. Mechanistic models on the other hand rely on a biophysical model to predict production (yield). Driving variables, such as rainfall or PAR, drive the dynamics in the model and require updates at each time step on which the model is run (hours or days). Successful yield predictions have been made with the SEBAL[11] model (Bastiaanssen et al., 1998; Bastiaanssen, 2000; Bastiaanssen et al., 2005; Irmak & Kamble, 2009) using crop latent heat of evapotranspiration as a driving parameter. Other driving parameters such as PAR radiation are highly dynamic (changing over hours and even minutes) and are therefore less commonly retrieved from LEO satellite data considering their revisit time (weeks rather than days). Geostationary meteorological satellites that can continuously capture data at a course spatial scale can be useful to replace missing meteorological data such as PAR (Schiller, 2006).

iv. *Mechanistic models with forcing strategy.* A more common approach is to derive state variables from satellite data. Since state variables are also dynamically calculated by biophysical models, a choice needs to be regarding made how and if to combine both. The most uncomplicated strategy is to replace the model state variable by its equivalent derived from satellite data whenever this is available, i.e. to force the model to agree with the remote sensing data. This approach can correct intermediate errors in state variables but does not allow real-time model calibration: erroneous initial values or model parameters cannot be corrected.

v. *Mechanistic models with re-initialization/re-calibration of state variables.* An integrated approach is to iteratively adjust the model initial values (e.g. initial biomass) or parameters (e.g. specific growth rates) until the best match between the model simulated variables and their remotely equivalent is obtained. Since a main objective of this dissertation is on using RT and biophysical modeling to better understand critical plant production processes, this strategy is worked out below.
Vegetation index time series related to leaf cover or total biomass, such as NDVI, are commonly used in photosynthesis-driven models for annual crops. The model parameters that are re-calibrated or re-initialized depend on modeled crop and site-specific situations: Guérif & Duke (2000) predicted sugar beet yield by re-initialization of the initial LAI (at emergence) and the sowing date while Launay & Guerif (2005) used crop establishment and root settlement as parameters for the same crop. Dente et al. (2008) selected sowing date, soil wilting point and field capacity for the prediction of wheat yield on remotely sensed LAI estimates.

State variables or radiometric data

In the model re-calibration and re-initialization strategy, two alternative approaches exist: (i) retrieving biophysical parameters from remotely sensed data and comparing these to crop model predictions or (ii) coupling the crop model with RT models for leaf, canopy and atmosphere to predict canopy or even at-satellite reflectance (Moulin et al., 1998). Both approaches have strength and weaknesses. Retrieval of state variables such

[11] Surface Energy Balance for Land

as LAI from VI's using standard approaches is sensitive to seasonal BRDF effects without specialized BRDF correction procedures (Qi et al., 2000), while a canopy reflectance model automatically takes this into account. On the other hand, the additional use of canopy models requires additional parameters such as LAD that are not supplied by the crop production model. In addition, predicted state variables such as LAI or chlorophyll content can be verified in the field without the use of specialized equipment.

Reflectance may not necessarily be the best expression of radiometric data: Guérif & Duke (2000) concluded that converting broad-band reflectance (predicted with the SAIL[12] canopy model) into the TSAVI vegetation index improved the data assimilation.

The role of *in situ* data

Meteorological data, preferably from local weather stations, is a requirement to drive almost any crop production model. It can be measured *in situ* for detailed modeling or be interpolated using regional scale data. Different alternative approaches exist in which *in situ* data can be combined with remote sensing in assimilation schemes:

- The most common is using (static) GIS data containing digital elevation, slope and soil type parameters to 'spatialize' a crop model (Mo et al., 2005).
- *In situ* data can also be used to improve the assimilation of remotely sensed data: Guérif & Duke (2000) used field measurements of soil rugosity, texture and moisture to predict soil reflectance. This was transferred to the SAIL canopy reflectance model to improve the accuracy of above-canopy reflectance predictions.
- The energy balance model of Bastiaanssen (1998) requires both *in situ* data (surface rugosity and incident long- and shortwave radiation) and remotely sensed data (LAI and thermal emission) to estimate canopy evapotranspiration.
- Alternatively, Dzikiti et al. (2010) modeled water stress (stem water potential) using sap stream measurements combined with initial estimates of canopy water status derived from hyperspectral reflectance.

Baseline and anomaly detection

The assimilation strategies presented here exclude 'catastrophic' events: production models simulate progressive seasonal dynamics under normal production conditions. This changes in the occurrence of catastrophic or unexpected events such as diseases, pests or frost damage. Unless dedicated sub-models for these events exist (e.g. Thornley & France, 2007, for pest submodels), crop models can no longer make adequate predictions. Deviations between model predicted and remotely sensed state variables beyond certain threshold may indicate anomalies in the production process. In operational systems for well-calibrated models, this can be used as an early warning system.

[12] Scattering by Arbitrarily Inclined Leaves (Verhoef, 1984)

1.7 Research framework, objectives and hypothesis

1.7.1 Research framework

This research fits within the IS-HS framework: *'Integration of In Situ data and HyperSpectral remote sensing for plant production monitoring'*. IS-HS aims at developing automated daily monitoring programs, in which satellites retrieve hyperspectral data and collect up-linked *in situ* data at critical stages in the production process of vegetative systems. Hyperspectral remote sensing can herein provide a cost-efficient technology to retrieve information on biophysical variables at good spatial and temporal resolution. It requires complementary *in situ* measurements and crop management information as inputs to ensure robust and reliable models. On-board software integrates and analyzes this combined information to steer in real-time important aspects of the plantation management such as drip irrigation and nutrition administration. Such a system can additionally provide detailed advice for management aspects such as optimal time for pruning and harvest. Integration of model input with weather forecasting data enables anticipation of stresses. Total system production in terms of yield value (number, size and quality of fruit) can be estimated and automatically adjusted to changes in management interventions. This will allow producers to make important economic decisions at an early stage, to anticipate market trends, and to better organize the management interventions and the harvesting process.

The IS-HS framework is tightly related to the development project of the ZaSat hyperspectral satellite, a joint cooperation between South African (SUNSPACE, University of Stellenbosch, South African government) and Flemish (K.U.Leuven, OIP, Flemish government) partners. ZaSat is part of the African Resource Management (ARM) mini-satellite constellation, that will encompass four satellites and allow daily coverage of any given agricultural area worldwide. ARM will enable true real-time monitoring and active management of vegetation production systems, and will eventually facilitate the extension to field-level applications.

Prior to operational use, modeling issues need to be addressed to further the understanding of plant biophysical responses as well as the translation of these responses to signals received by satellites. This PhD dissertation is a realization of some of these requirements as part of the project OT07048 *'Monitoring and modeling of plant production systems via integration of* in situ *and hyperspectral remote sensing data within the context of the South African/Flemish ZaSat II satellite design project'*. It specifically addresses the OT project goals *(i)* to generate a list of quantitative and qualitative crop production for citrus (chapters 1 and 2), *(ii)* to develop a biophysical citrus model framework (chapter 2), *(iii)* to develop a database of citrus leaf and canopy spectra (chapter 5 and chapter 7) and *(iv)* to develop physically-based hyperspectral indices (chapters 3 and 5).

1.7.2 Research objectives

Even for complex processes, empirical statistical black box methods have proven to establish relations between measured hyperspectral or broad band reflectance signals and state variables such as LAI or chlorophyll content. Those relations have subsequently

been used to predict system production. Due to the inherently limited scope of most empirical research, both in time and space, it is often impossible to make extrapolations and predict how and if these relations are maintained under different conditions (i.e. other regions, different years). As described in the previous sections, substantial amounts of work have been done on the biophysical modeling part, on establishing relations between biophysical state variables and leaf biochemistry or canopy structure, between leaf biochemistry and leaf reflectance and between leaf, canopy and finally at-satellite reflectance. An integrating model that covers each of these steps is, however, lacking for perennial fruit crops. *The **first objective** in this research is therefore to set up a bottom-up modeling approach to understand how changes in plant state are translated into changes as detected by optical remote sensing technology.* It can be used to evaluate under which conditions biophysical or stochastic relations are meaningful.

Figure 1.3 presents an overview of this bottom-up approach. The left part of the figure presents a simplified representation of *plant production modeling*. Changes in system inputs, such as drought stress, nutrient shortages or initiation of flowering controlled by air temperatures will alter the system's state variables (transport capacity, nutrient levels, etc.). Some of these state variables, such as water potential or sap stream, can be readily detected by *in situ* or hyperspectral sensors but others such as hormone levels would require expensive chemical analysis. Dynamics in state variables can initiate a *chain of processes* in which related variables are altered, some of which may affect canopy structure (e.g. changes in leaf angle due to mild drought stress or leaf drop under severe stress) or leaf biochemistry (e.g. decrease in chlorophyll content due to nitrogen or potassium shortages). Most of these processes may eventually also modify system output (yield quantity and quality). Some changes in canopy structure, biochemistry and even changes in yield (fruit load) result in detectable changes of top-of-canopy (TOC) reflectance that can be simulated with *radiative transfer models*. TOC reflectance, mixed with the contributions of weeds, soil and shade and finally the atmosphere, will eventually be recorded in time series of satellite data. In a bottom-up approach, each of these processes needs to be modeled as accurately as possible, since in each step, errors in model structure or parametrization incrementally affect the prediction power of the encompassing model.

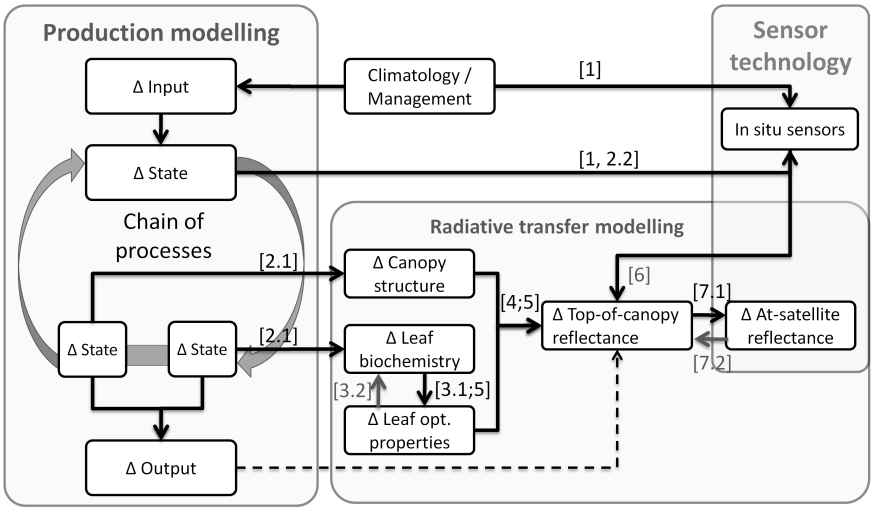

Figure 1.3: *A bottom-up modeling approach that integrates plant production modeling and RT modeling. Relevant chapter numbers as discussed in table 1.3 (section 1.8) are between square brackets. Black numbers: objective one;* gray *numbers: objective two.*

Modeling and monitoring of dynamic systems requires additional considerations.

- During year-round monitoring, crop phenology, such as flowering, fruit set and fruit coloration will impact the remotely sensed vegetation signal but will also contain potentially useful information (e.g. Somers et al., 2010b).
- Many fruit trees such as citrus, banana, olive and mango are evergreens, so that there is no immediate link between the present crop cover or LAI and the biomass production of the current vegetation season.
- Phenological events and stresses (nutrient stress, drought stress, infestations) may only exhibit subtle spectral changes in the retrieved canopy signals (see chapters 4 and 5).
- Orchards are organized in rows or grids leading to open canopies with only partial crown closure. Measured signals thus contain substantial and seasonally variable contributions of (sunlit) soil and weeds between the rows, each having their own seasonal dynamics.

Most changes in remotely sensed signals will thus inevitably reflect a mixture of processes of different nature (biophysical, structural, and also external to the plant system). Some of these processes are of interest for modeling the desired system output (yield) while others are not, causing undesirable variability. The contribution of individual biophysical processes may in addition be limited to subtle changes. *The* ***second objective*** *is therefore to develop sensitive and robust data retrieval technologies to detect relevant but subtle changes or trends in plant state as required in production modeling.*

1.7.3 Hypothesis

The hyperspectral reflectance of perennial fruit tree canopies holds information on the plant's internal state that is expressed in dynamics of leaf biochemistry and in the dynamics of mixtures and the structural organization of canopy components (leaves, fruit, flowers,...). This information can be accurately extracted for integration in biophysical models to improve the prediction of economic output (quantity, quality). Accurate and robust retrieval of this information requires (i) a full understanding - through radiative transfer modeling - of the main interactions from the lowest level of biochemical processes to the highest level of at-sensor measured signals and (ii) robust and sensitive measurement techniques and data extraction methods.

1.8 Dissertation outline

This PhD dissertation is a compilation of six chapters. It includes four published peer reviewed publications in international journals, one manuscript in review and a chapter describing a central part in the biophysical modeling of citrus crop production. Each chapter can be read as an independent research paper, with separate introduction, method, results and conclusions sections.

Table 1.3 lists an overview of the chapters in a logical bottom-up order that does not necessarily correspond to the order in which research was conducted or published. For each chapter, the aspects of time, scale level, research focus and objectives (section 1.7.2) are listed. Corresponding chapter numbers in figure 1.3 and table 1.3 help to explain how these chapters fulfill both research objectives: bottom-up modeling and more sensitive and robust data retrieval.

Table 1.3: *Overview of the aspects of time, model type, scale level, research focus and objectives addressed for each chapter. Original chapter titles are abbreviated. E: empirical; M: mechanistic; RT: radiative transfer; PH: physiology and phenology; I: bottom-up modeling; II: more robust and sensitive data retrieval*

Chapter, Part	**Time scale**	**Type**	**Scale**	**Research focus**	**Objectives**
2. Carbohydrate flows in citrus			leaf	PH	I
2.1. Conceptual model	days to seasons	E+M			I
2.2. *In situ* carbohydrate detection	static	E			I
3. Dorsiventral Leaf Model	static	M	leaf	RT, PH	
3.1. Model development					I
3.2. Inversion strategies					II
4. Assumptions in canopy RT	static	M	tree canopy, field	RT	I
5. Physiology of a hyperspectral time series	seasons	E+M	tree canopy, leaf	PH, RT	I
6. BRDF normalization in field spectroscopy	hours, days	M	tree canopy	RT	II
7. Off-nadir viewing for reducing spectral mixing	hours to seasons	M	field, satellite	RT	
7.1. Spatial resolution, spectral mixtures					I
7.2. Optimal viewing geometry					II

Out of all variables that may be detected using hyperspectral remote sensing, the role of non-structural carbohydrates was found to be one of the most critical. They impact all stages in the production process (section 1.4.3). Internal (e.g. water balance) and external factors (e.g. management, meteorology) that are known to influence their dynamics as well as the effects of these carbohydrates on tree health and fruit quality were treated in a conceptual model (chapter *2*.1) for citrus carbohydrates. Modeling the full citrus production process requires the integration of additional models, such as for nutrient uptake and translocation, flowering, water balance. Each of these models - sub-models in an encompassing model - contain one or more state variables that are expressed in the leaf biochemistry and/or in the canopy structure, both of which influence the hyperspectral canopy reflectance.

The relationship between leaf biochemistry and leaf optical properties is subsequently made through statistical relationships (see chapter 2 for soluble sugars and starch) and through leaf optical models. Existing leaf optical models lack the capacity to discriminate between the leaf top (adaxial) and bottom (side) and can therefore result in substantial errors when used to predict canopy reflectance, as demonstrated in chapter 4. Therefore a Dorsiventral Leaf RT Model (DLM) is presented (chapter *3*.1) to simulate

optical properties in leaves. DLM is based on the well-known plate model PROSPECT (Jacquemoud & Baret, 1990) but provides the transition from symmetric modeling wherein both leaf faces are identical into a dorsiventral representation with different optical properties for adaxial and abaxial sides.

The subsequent step in the up-scaling process is from leaf optical properties to canopy reflectance, which is accomplished by canopy RT models. Many RT models, especially those providing an algorithmically fast implementation, make an important number of assumptions on the nature of the incident light and on the structure of the canopies (mixtures and shape of leaves, spatial organization of the trees). The impact of six of these assumptions was evaluated with a physically based ray tracer (pbrt) that was adapted for spectral rendering (chapter 4). Pbrt was extended with sub-models for realistic illumination (from atmospheric RT code), leaf and soil reflectance and additional camera models. Its accuracy was evaluated in a comparison with other ray-tracing models using the RAMI Online Model Checker tool of the Joint Research Center of the European Commission. Within pbrt, a block of an existing commercial citrus orchard (Wellington, Western Cape province, South Africa) was reconstructed, calibrated using allometric parameters and hemispherical photography and validated against measured spectra.

Subsequently, at the same spatial scale level, the focus is transferred from static modeling to the monitoring of seasonal dynamics. The relationship between leaves and canopies was evaluated using an 18 months time series, measured in a commercial citrus orchard (chapter *5*). This allows creation of a hyperspectral baseline for the citrus production system. Canopy, fruit, leaf, soil and weed spectra were collected and meteorology was recorded on-site. Digitally processed canopy pictures were used to estimate the cover fractions of healthy and sun-burnt leaves, fruit and flowers. Reflectance measurements of different leaf types were inverted using DLM into a time series of biophysical parameters. Using this combined dataset, the dynamics of nine well-established canopy level vegetation indices were interpreted as a combination of changes at the leaf level, changes in canopy structure and changes in cover fractions of the canopy components. Good relations were found to explain the dynamics of chlorophyll content, carotenoid-to-chlorophyll ratios, LAI and leaf water content.

The last step in the bottom-up modeling involved the up-scaling from the field level to satellite level observations (chapter *7.1*). A virtual 3D environment was constructed in which ray-tracing simulations were made for different field orientations and illumination and viewing directions. GIS orchard statistics from citrus growing areas in Florida and South Africa (Western Cape province) were derived from high resolution images. This combined information was used to define the required pixels sizes to obtain good quality tree and field level observations at both locations.

Establishing reliable bottom-up relations that allow the propagate changes in a plant's state to the changes as detected by satellites does not yet imply that these relations can be inverted to retrieve the plant's state from remote sensing observations (ill-posedness). A considerable amount of research has already been dedicated to improve inversion algorithms for more reliable data assimilation. Less attention has been paid to adjusting information retrieval strategies to improve inversions. The focus in this dissertation was

on both.

At the leaf level (chapter *3*.2), different spectrum measurement techniques (white and black background, abaxial and adaxial side) were combined with different inversion strategies for DLM (variable number of inverted parameters, weighting of spectral bands).

At the canopy level, the realization of an uninterrupted time series depends highly on the occurrence of cloudless weather conditions. Dual field of view (DFOV) techniques and instruments exist in field spectroscopy, but data quality of such time series is often limited as differences in illumination conditions (more specifically by the angular distribution of incident light) cause differences in measured reflectance. Therefore, an extension of existing DFOV techniques was developed to normalize illumination conditions so that reflectance measured under overcast skies can be converted into clear sky conditions (chapter 6).

At the satellite level, soil and weeds have a substantial impact on the reflectance of the mixed signal of an orchard (section 1.4.2). Although sophisticated spectral unmixing techniques are being developed to retain only the canopy component of a mixed signal, hitherto, substantial errors remain. The specific row-oriented nature of orchards, combined with off-nadir viewing capabilities of recent platforms offers the potential to reduce these mixture fractions of soils and weeds and thus improve the accuracy of unmixing algorithms. A ray-tracing simulation analysis is made to find optimal off-nadir observation directions for citrus orchards as detected from space-borne platforms (chapter 7.2). A ranking was made based on spectral similarity indices. These indices compared spectral changes in tree crowns that need to be detected with undesirable effects caused by (i) variations in solar elevation, (ii) changes in soil reflectance (e.g. due to soil moisture) and (iii) changes in the reflectance of weeds.

1.9 References

Albrigo, L. & Saúco, V.G. (2004). Flower bud induction, flowering and fruit-set of some tropical and subtropical fruit tree crops with special reference to citrus. *Acta Horticulturae*, 632, 81–90.

Albrigo, L.G., Buker, R.S., Burns, J.K., Castle, W.S., Futch, S., McCoy, C.W., Muraro, R.P., Rogers, M.E., Syvertsen, J.P., & Timmer, L.W. (2005). The impact of four hurricanes in 2004 on the Florida Citrus industry: experiences and lessons learned. *Proceedings of Florida State Horticultural Society*, 118, 66–74.

Albrigo, L.G., Valiente, J.I., & Beck, H.W. (2002). Flowering expert system development for a phenology based citrus decision support system. *Acta horticulturae*, 584, 247–254.

Allen, R.G., Pereira, L.S., Raes, D., & Smith, M. (1998). FAO irrigation and drainage paper no. 56. Crop evapotranspiration. Guidelines for computing crop water requirements. *Technical report*, Food and Agriculture Organisation.

Baret, F. & Guyot, G. (1991). Potentials and limits of vegetation indices for LAI and APAR assessment. *Remote Sensing of Environment*, 35(2-3), 161–173.

Bastiaanssen, W.G.M. (2000). SEBAL-based sensible and latent heat fluxes in the irrigated Gediz Basin, Turkey. *Journal of Hydrology*, 229, 87–100.

Bastiaanssen, W.G.M., Menenti, M., Feddes, R.A., & Holtslag, A.A.M. (1998). A remote sensing surface energy balance algorithm for land (SEBAL) 1. Formulation. *Journal of Hydrology*, 212-213, 198–212.

Bastiaanssen, W.G.M., Noordman, E.J.M., Pelgrum, H., Davids, G., Thoreson, B.P., & Allen, R.G. (2005). SEBAL model with remotely sensed data to improve water-resources management under actual field conditions. *Journal of Irrigation and Drainage Engineering*, 131, 85–93.

Bellows, T.S.J., Morse, J.G., & Lovatt, C.J. (1989). Manipulation of fruiting, chapter Modelling flower development in citrus, pages 115–129. Butterworth & Co, London, UK.

Bondada, B.R. & Syvertsen, J.P. (2003). Leaf chlorophyll, net gas exchange and chloroplast ultrastructure in citrus leaves of different nitrogen status. *Tree Physiology*, 23, 553–559.

Bouman, B.A.M., van Keulen, H., van Laar, H.H., & Rabbinge, R. (1996). The School of de Wit crop growth simulation models: A pedigree and historical overview. *Agricultural Systems*, 52, 171–198.

Box, G.E.P. & Jenkins, G.M. (1970). Time series analysis: forecasting and control. Holden-Day, San Fransisco, CA.

Boyer, M., Miller, J., Belanger, M., & Hare, E. (1988). Senescence and spectral reflectance in leaves of Northern Pin Oak (Quercul palustris Muenchh.). *Remote Sensing of Environment*, 25, 71–87.

Bustan, A. & Goldschmidt, E.E. (1998). Estimating the cost of flowering in a grapefruit tree. *Plant, Cell and Environment*, 21, 217–244.

Bustan, A. & Goldschmidt, E.E. (1999). Examination of 'hierarchical' and 'proportional' dry matter partitioning models with potted citrus trees. *Acta Horticulturae*, 499, 81–90.

Bustan, A., Goldschmidt, E.E., & Emer, Y. (1999). Progress in the development of 'CITROS' - a dynamic model of citrus productivity. *Acta Horticulturae*, 499, 69–80.

Campbell, J.B. (2002). Introduction to remote sensing. Third edition. Taylor and Francis, London, UK.

Canham, C., Cole, J., & Lauenroth, W., editors (2003). Models in ecosystem science. Princeton University Press,.

Carter, G.A. (1991). Primary and secondary effects of water content on the spectral reflectance of leaves. *American Journal of Botany*, 78, 916–924.

Cheng, Y.B., Zarco-Tejada, P.J., Riaño, D., Rueda, C.A., & Ustin, S. (2006). Estimating vegetation water content with hyperspectral data for different canopy scenarios: Relationships between AVIRIS and MODIS indexes. *Remote Sensing of Environment*, 105, 354–366.

Colombo, R., Meroni, M., Marchesi, A., Besetto, L., Rossini, M., Giardino, C., & Panigada, C. (2008). Estimation of leaf and canopy water content in poplar plantations by means of hyperspectral indices and inverse modeling. *Remote Sensing of Environment*, 112, 1820–834.

Combal, B., Baret, F., Weiss, M., Trubuil, A., Macé, D., Pragnère, A., Myneni, R., Knyazikhin, Y., & Wang, L. (2003). Retrieval of canopy biophysical variables from bidirectional reflectance using prior information to solve the ill-posed inverse problem. *Remote Sensing of Environment*, 84, 1–15.

Davies, F.S. & Albrigo, L.G. (1994). Citrus. CABI Publishing, Wallingford, UK.

De Baerdemaeker, J. (2001). Sensors and precision farming in horticulture. *Acta Horticulturae*, 562, 19–27.

Delalieux, S. (2009). Hyperspectral indices for presymptomatic detection of stress in fruit trees. Ph.D. thesis, K.U.Leuven, Groep Science & Technology, Arenberg Doctoral School.

Delalieux, S., Auwerkerken, A., Verstraeten, W.W., Somers, B., Valcke, R., Lhermitte, S., Keulemans, J., & Coppin, P. (2009). Hyperspectral reflectance and fluorescence imaging to detect scab induced stress in apple leaves. *Remote Sensing*, 1, 858–874.

Delalieux, S., Somers, B., Hereijgers, S., Verstraeten, W.W., Keulemans, W., & Coppin, P. (2008). A near-infrared narrow-waveband ratio to determine Leaf Area Index in orchards. *Remote Sensing of Environment*, 112, 3762–3772.

Dente, L., Satalino, G., Mattia, F., & Rinaldi, M. (2008). Assimilation of leaf area index derived from ASAR and MERIS data into CERES-Wheat model to map wheat yield. *Remote Sensing of Environment*, 112, 1395–1407.

Devarrewaere, W. (2010). The use of hyperspectral remote sensing for the detection of carbohydrates in citrus foliage. Master's thesis, K. U. Leuven, Faculty of Bioscience Engineering.

Doorenbos, J. & Kassam, A.H. (1986). Yield Response to Water. FAO Irrigation and Drainage Paper no. 33. *Technical report*, Food and Agriculture Organization of the United Nations, Rome.

Dorigo, W.A., Zurita-Milla, R., de Wit, A.J.W., Brazile, J., Singh, R., & Schaepman, M.E. (2007). A review on reflective remote sensing and data assimilation techniques for enhanced agroecosystem modeling. *International Journal of Applied Earth Observation and Geoinformation*, 9, 165–193.

Du, Q., Chang, N.B., Yang, C., & Srilakshmi, K.R. (2008). Combination of multispectral remote sensing, variable rate technology and environmental modeling for citrus pest management. *Journal of Environmental Management*, 86, 14–26.

Dzikiti, S., Verreynne, J.S., Stuckens, J., Strever, A., Verstraeten, W.W., Swennen, R., & Coppin, P. (2010). Determining the water status of Satsuma mandarin trees [Citrus Unshiu Marcovitch] using spectral indices and by combining hyperspectral and physiological data. *Agricultural and Forest Meteorology*, 150, 369–379.

El Hajj, M., Bégué, A., Guillaume, S., & Martiné, J.F. (2009). Integrating SPOT-5 time series, crop growth modeling and expert knowledge for monitoring agricultural practices - The case of sugarcane harvest on Reunion Island. *Remote Sensing of Environment*, 113, 2052–2061.

FAO (2009). http://faostat.fao.org/.

Felicetti, D.A. & Schrader, L.E. (2009a). Changes in pigment concentrations associated with sunburn browning of five apple cultivars. I. Chlorophylls and carotenoids. *Plant Science*, 176, 78–83.

Feret, J.B., François, C., Asner, G.P., Gitelson, A.A., Martin, R.E., Bidel, L.P.R., Ustin, S.L., le Maire, G., & Jacquemoud, S. (2008). PROSPECT-4 and 5: Advances in the leaf optical properties model separating photosynthetic pigments. *Remote Sensing of Environment*, 112(6), 3030–3043.

Fourty, T., Baret, F., Jacquemoud, S., Schmuck, G., & Verdebout, J. (1996). Leaf optical properties with explicit description of its biochemical composition: Direct and inverse problems. *Remote Sensing of Environment*, 56(2), 104–117.

Futch, S.H. & Tucker, D.P.H. (2008). A guide to citrus nutritional deficiency and toxicity identicifaction. *Technical report*, University of Florida, IFAS.

Gary, C., Jones, J.W., & Tchamitchian, M. (1998). Crop modelling in horticulture: state of the art. *Scienta Horticulturae*, 74, 3–20.

Gobron, N., Pinty, B., Aussedat, O., Chen, J.M., Cohen, W.B., Fensholt, R., Gond, V., Huemmrich, K.F., Lavergne, T., Mélin, F., Privette, J.L., Sandholt, I., Taberner, M., Purner, D.P., M., V.M., & Widlowski, J.L. (2006). Evaluation of fraction of absorbed photosynthetically active radiation products for different canopy radiation transfer regimes: Methodology and results using Joint Research Center products derived from SeaWiFS against ground-based estimations. *Journal of Geophysical Research*, 111, 1–15.

Goetz, A.F.H. (2009). Three decades of hyperspectral remote sensing of the Earth: A personal view. *Remote Sensing of Environment*, 113, S5–S16.

Goldschmidt, E.E. (1997). Citrus Flowering and Fruiting Short Course, chapter Basic and parctical aspects of citrus trees' carbohydrate economy, pages 63–72. University of Florida, Citrus Research and Education Centre, Lake Alfred, FL.

Goldschmidt, E.E. & Golomb, A. (1982). The carbohydrate dynamics of alternate-bearing citrus trees and the significance of reserves of flowering and fruiting. *Journal of the American Horticultural Society*, 107, 206–208.

Goldschmidt, E.E. & Lakso, A.N. (2005). Fruit tree models: scope and limitations. In E. Gelb & A. Offer, editors, Information and Communication Technology (ICT) Development and Adoption: Perspectives of Technological Innovation. European Federation for Information Technologies in Agriculture, Food and the Environment.

Goulding, K. (2000). Nitrate leaching from arable and horticultural land. *Soil Use and Management*, 16, 145–151.

Govaerts, Y.M., Jacquemoud, S., Verstraete, M.M., & Ustin, S.L. (1996). Three-dimensional radiation transfer modeling in a dicotyledon leaf. *Applied Optics*, 35(33), 6585–6598.

Guérif, M. & Duke, C.L. (2000). Adjustment procedures of a crop model to the site speci?c characteristics of soil and crop using remote sensing data assimilation. *Agriculture, Ecosystems and Environment*, 81, 57–69.

Haboudane, D., Miller, J.R., Pattey, E., Zarco-Tejada, P.J., & Strachan, I.B. (2004). Hyperspectral vegetation indices and novel algorithms for predicting green LAI of crop canopies: Modeling and validation in the context of precision agriculture. *Remote Sensing of Environment*, 90, 337–352.

Haboudane, D., MIller, J.R., Tremblay, N., Zarco-Tejada, P.J., & Dextraze, L. (2002). Integrated narrow-band vegetation indices for prediction of crop chlorophyll content for application to precision agriculture. *Remote Sensing of Environment*, 81, 416–426.

Hahn, C.J. & Warren, S.G. (2007). A Gridded Climatology of Clouds over Land (1971-96) and Ocean (1954-97) from Surface Observations Worldwide (NDP-026E). *Technical report*, Climate Change Research Division, Office of Biological and Environmental Research, U. S. Department of Energy.

Hecht, E. (2002). Optics - fourth edition. Addison Wesley, San Fransisco, CA.

Henton, S.M., Piller, G.J., & Gandar, P.W. (1999). A fruit growth model dempendent on both carbon supply and inherent fruit characteristics. *Annals of Botany*, 83, 509–514.

Hrubovcak, J., Vasavada, U., & Aldy, J.E. (1999). Green technologies for a more sustainable agriculture. In Agriculture information bulletin, no. 752. Economic Research Service, US Department of Agriculture, Washington, DC.

Irmak, A. & Kamble, B. (2009). Evapotranspiration data assimilation with genetic algorithms and SWAP model for on-demand irrigation. *Irrigation Science*, 28, 101–112.

Jacquemoud, S. & Baret, F. (1990). PROSPECT: A model of leaf optical properties spectra. *Remote Sensing of Environment*, 34(2), 75–91.

Jacquemoud, S., Verdebout, J., Schmuck, G., Andreoli, G., & Hosgood, B. (1995). Investigation of leaf biochemistry by statistics. *Remote Sensing of Environment*, 54(3), 180–188.

Ji, Z.G. (2008). Hydrodynamics and water quality. Modeling rivers, lakes and estuaries. Wiley-Interscience, Hoboken, New Jersey, USA.

Jones, H.G. (2004). Irrigation scheduling: advantages and pitfalls of plant-based methods. *Journal of Experimental Botany*, 55, 2427–2436.

Jones, J.W., Hoogenboom, G., Porter, C.H., Boote, K.J., Batchelor, W.D., Hunt, L.A., Wilkens, P.W., Singh, U., Gijsman, A.J., & Ritchie, J.T. (2003). The DSSAT cropping system model. *European Journal of Agronomy*, 18, 235–265.

Jung, M., Verstraete, M., Gobron, N., Reichstein, M., Papale, D., Bondeau, A., Robustelli, M., & Pinty, B. (2008). Diagnostic assessment of European gross primary production. *Global Change Biology*, 14, 2349–2364.

Keeney, D. & Olson, R.A. (????).

Kumar, L., Schmidt, K., Dury, S., & Skidmore, A. (2001). Imaging Spectrometry. Basic principles and prospective applications, chapter Imaging spectroscopy and vegetation science, pages 111–156. Kluwer Academic Publishers, Dordrecht, Netherlands.

Ladaniya, M.S. (2007). Citrus fruit: biology, technology and evaluation. Academic Press (Elsevier), San Diego, CA, USA.

Launay, M. & Guerif, M. (2005). Assimilating remote sensing data into a crop model to improve predictive performance for spatial applications. *Agriculture, Ecosystems and Environment*, 111, 321–339.

Lee, W.S., Chinchuluun, R., & Ehsani, R. (2009). Citrus fruit identification using machine vision for a canopy shake and catch harvester. *Acta Horticulturae*, 824, 217–222.

Liang, S. (2004). Quantitative remote sensing of land surfaces. John Wiley & Sons.

Liang, S., editor (2007). Advances in land remote sensing: system, modelling, inversion and application. Springer Science+Business Media B. V.

Lillesand, T.M., Kiefer, R.W., & Chipman, J.W. (2008). Remote sensing and image interpretation. 6th edition. John Wiley & Sons, inc.

Lovatt, C.J. & Sciences, B..P. (2010). Plant Growth Regulators. In UC IPM Pest Management Guidelines: Citrus. university of California, Davis.

Meroni, M., Colombo, R., & Panigada, C. (2004). Inversion of a radiative transfer model with hyperspectral observations for LAI mapping in poplar plantations. *Remote Sensing of Environment*, 92, 195–206.

Miller, J., Berger, M., Goulas, Y., Jacquemoud, S., Louis, J., Mohammed, G., Moise, N., Moreno, J., Moya, I., Pedrós, R., Verhoef, W., & Zarco-Tejada, P. (2005). Development of a vegetation fluorescence canopy model. Final report. *Technical report*, European Space Agency.

Mo, X., Liu, S., Lin, Z., XU, Y., Xiang, Y., & McVicar, T.R. (2005). Prediction of crop yield, water consumption and water use efficiency with a SVAT-crop growth model using remotely sensed data on the North China Plain. *Ecological Modelling*, 183, 301–322.

Monteith, J.L. (1977). Climate and the efficiency of crop production in Britain. *Philosophical Transactions of the Royal Society of London*, B281, 277–294.

Moulin, S., Bondeau, A., & Delécolle, R. (1998). Combining agricultural crop models and satellite observations: from field to regional scales. *International Journal of Remote Sensing*, 19, 1021–1036.

Muller, E. & Décamps, H. (2000). Modeling soil moisture-reflectance. *Remote Sensing of Environment*, 76, 173–180.

Neales, T.F. & Incoll, L.D. (1968). the control of leaf photosynthesis rate by the level of assimilate concentration in the leaf - a review of the hypothesis. *Botanical Reviews*, 34, 107–125.

Oyarzun, R.A., Stöckle, C.O., & Whiting, M.D. (2007). A simple approach to modeling radiation interception by fruit-tree orchards. *Agricultural and Forest Meteorology*, 142(1), 12–24.

Peñuelas, J. & Filella, I. (1998). Visible and near-infrared reflectance techniques for diagnosing plant physiological status. *Trends in Plant Science*, 3, 151–156.

Pharr, M. & Humphreys, G. (2004). Physically based rendering. From theory to implementation. Morgan Kaufmann, San Fransisco, USA.

Pieri, P. (2010). Modelling radiative balance in a row-crop canopy. Cross-row distribution of net radiation at the soil surface and energy available to clusters in a vineyard. *Ecological Modelling*, 221, 802–811.

Pinter, P.J.J., Hatfield, J.L., Schepers, J.S., Barnes, E.M., Moran, M.S., Daughtry, C.S.T., & Upchurch, D.R. (2003). Remote sensing for crop management. *Photogrammetric Engineering and Remote Sensing*, 69, 647–664.

Qi, J., Kerr, Y.H., Moran, M.S., Weltz, M., Huete, A.R., Sorooshian, S., & Bryant, R. (2000). Leaf area index estimates using remotely sensed data and BRDF models in a semi-arid region. *Remote Sensing of Environment*, 73, 18–30.

Rencz, A.N., editor (1999). Remote sensing for the earth sciences. John Wiley & Sons, New York, NY.

Reuther, W. (1973). The citrus industry, 2nd ed. Vol. 3, chapter Climate and citrus behavior, pages 280–337. Berkeley, University of California Press.

Ribeiro, R.V. (2007). Some aspects of citrus ecophysiology in subtropical climates: re-visiting photosynthesis under natural conditions. *Brazilian Journal of Plant Physiology*, 19, 393–411.

Richter, R., Bachmann, M., Dorige, W., & Muller, A. (2006). Influence of the adjacency effect on reflectance measurements. *Transactions on Geoscience and Remote Sensing Letters*, 3(4), 565–569.

Ritchie, J.T. & Otter, S. (1985). Description and performance of CERES-Wheat: A user-oriented wheat yield model. ARS wheat yield project. ARS-38. *Technical report*, National Technical Information Service, Springfield, VA.

Rogers, M.E., Timmer, L.W., & Spann, T.M. (2009). Florida Citrus pest management guide, SP 043. University of Florida, IFAS, Lake Alfred, Florida, USA.

Rosell, J.R., Llorens, J., Sanz, R., Arnó, J., Ribes-Dasi, M., Masip, J., Escolà, A., Camp, F., Solanelles, F., Gràcia, F., Gil, E., Val, L., Planas, S., & Palacín, J. (2009). Obtaining the three-dimensional structure of tree orchards from remote 2D terrestrial LIDAR scanning. *Agricultural and Forest Meteorology*, 149, 1505–1515.

Ruiz, R., García-Luis, A., Monerri, C., & Guardiola, J.L. (2001). Carbohydrate availability in relation to fruitlet abscission in citrus. *Annals of Botany*, 87, 805–812.

Sakamoto, T., Yokozawa, M., Toritani, H., Shibayama, M., Ishitsuka, N., & Ohno, H. (2005). A crop phenology detection method using time-series MODIS data. *Remote Sensing of Environment*, 96, 366–374.

Schaepman-Strub, G., Schaempan, M.E., Painter, T.H., Dangel, S., & Martonchik, J. (2006). Reflectance quantities in optical remote sensing - definitions and case studies. *Remote Sensing of Environment*, 103, 27–42.

Schiller, K. (2006). Derivation of Photosynthetically Available Radiation from METEOSAT data in the German Bight with Neural Nets. *Ocean Dynamics*, 56, 79–85.

Serrano, L., Peñuelas, J., & Ustin, S.L. (2002). Remote sensing of nitrogen and lignin in Mediterranean vegetation from AVIRIS data: decomposing biochemical from structural signals. *Remote Sensing of Environment*, 81, 355–364.

Sims, D.A. & Gamon, J.A. (2002). Relationships between leaf pigment content and spectral reflectance across a wide range of species, leaf structures and developmental stages. *Remote Sensing of Environment*, 81(2-3), 337–354.

Sinclair, T.R. & Muchow, R.C. (1999). Radiation use efficiency. *Advances in Agronomy*, 65, 215–265.

Smith, D.M. & Allen, S.J. (1996). Measurement of sap plow in plant stems. *Journal of Experimental Botany*, 47, 1833–1844.

Somers, B. (2009). Hyperspectral unmixing for plant production system monitoring. Ph.D. thesis, K. U.Leuven, Groep Science & Technology, Arenberg Doctoral School.

Somers, B., Delalieux, S., Verstraeten, W.W., Vanden Eynde, A., Barry, G., & Coppin, P. (2010b). The contribution of the fruit component to the hyperspectral citrus canopy signal. *Photogrammetric Engineering and Remote Sensing*, 76, 37–47.

Somers, B., Delalieux, S., Verstraeten, W.W., & Coppin, P. (2009c). A conceptual framework for the simultaneous extraction of sub-pixel spatial extent and spectral characteristics of crops. *Photogrammetric Engineering and Remote Sensing*, 75(1), 57–68.

Spiegel-Roy, P. & Goldschmidt, E.E. (1996). Biology of citrus. 229. Cambridge University Press.

Stöckle, C.O., Donatelli, M., & Nelson, R. (2003). CropSyst, a cropping systems simulation model. *European Journal of Agronomy*, 18, 289–307.

Steduto, P. (2003). Biomass water-productivity. Comparing the growth-engines of crop models. In FAO Expert Consultation on Crop Water Productivity Under Deficient Water Supply. Romy, Italy.

Steduto, P., Hsiao, T.C., & Fereres, E. (2007). On the concervative behavior of biomass water productivity. *Irrigation Science*, 25, 189–207.

Steduto, P., Hsiao, T.C., Raes, D., & Fereres, E. (2009). AquaCrop - the FAO crop model to simulate yield response to water: I. concepts and underlying principles. *Agronomy Journal*, 101, 426–437.

Steinmetz, S., Guérif, M., Delécolle, R., & Baret, F. (1990). Spectral estimates of the absorbed photosynthetically active radiation and light-use effciency of a winter wheat crop subjected to nitrogen and water deficiencies. *International Journal of Remote Sensing*, 11, 1797–1808.

Suarez, L., Zarco-Tejada, P.J., González, V., Berni, J.A.J., Sagardoy, R., Morales, F., & Fereres, E. (2010). Detecting water stress effects on fruit quality in orchards with time-series PRI airborne imagery. *Remote Sensing of Environment*, 114, 286–298.

Taiz, L. & Zeiger, E. (2006). Plant physiology, fourth edition. Sinauer Associates, Sunderland, Massachusetts.

Teixeira, A.H.d.C., Bastiaanssen, W.G.M., Ahmad, M.D., & Bos, M.G. (2009). Reviewing SEBAL input parameters for assessing evapotranspiration and water productivity for the Low-Middle São Francisco River basin, Brazil. Part B: Application to the regional scale. *Agricultural and Forest Meteorology*, 149, 477–490.

Thornley, J.H.M. & France, J. (2007). Mathematical models in agriculture. Quantitative methods for the plant, animal and ecological sciences. CABI.

Tumbo, S.D., Whitney, J.D., Miller, W.M., & Wheaton, T.A. (2002). Development and testing of a citrus yield monitor. *Applied Engineering in Agriculture*, 18, 399–403.

Valiente, J.I. & Albrigo, L.G. (2002). Modeling flowering date of sweet orange [Citrus sinensis (L.) Osbeck] trees in Central Florida based on historical weather records. *Proceedings of the International Society of Citriculture*, 1, 186–190.

Van der Zande, D., Stuckens, J., Verstraeten, W.W., Muys, B., & Coppin, P. (2010). Assessment of light environment variability in broadleaved forest canopies using terrestrial laser scanning. *Remote Sensing*, 2, 1564–1574.

Verhoef, W. (1984). Light scattering by leaf layers with application to canopy reflectance modeling : The SAIL model. *Remote Sensing of Environment*, 16, 125–141.

Verhoef, W. & Bach, H. (2007). Coupled soil-leaf-canopy and atmosphere radiative transfer modeling to simulate hyperspectral multi-angular surface reflectance and TOA radiance data. *Remote Sensing of Environment*, 109, 166–182.

Verreynne, J.S. & Lovatt, C.J. (2009). The ffect of crop load on budbreak influences return bloom in alternate bearing 'Pixie' mandarin. *Journal of the American Horticultural Society*, 134, 299–307.

Versita, W. (2007). Non-destructive evaluation of apple fruit maturity on the tree. *Vegetable Crops Research Bulletin*, 66, 161–169.

Verstraeten, W.W. (2006). Integration of Remotely Sensed Hydrological Data into an Ecosystem Carbon Flux Model. Ph.D. thesis, K.U.Leuven.

Verstraeten, W.W., Veroustraete, F., & Feyen, J. (2008). Assessment of evapotranspiration and soil moisture content across different scales of observation. *Sensors*, 8, 70–117.

Verstraeten, W.W., Veroustraete, F., Wagner, W., Van Roey, T., Heyns, W., Verbeiren, S., & Feyen, J. (2010). Remotely sensed soil moisture integration in an ecosystem carbon flux model. The spatial implication. *Climatic Change*, (online).

Waldo, L.J. & Schumann, A.W. (2009). Spatial variability of soil water under citrus tree canopies in central Florida. *Acta Horticulturae*, 824, 147–154.

Widlowski, J.L., Pinty, B., Gobron, N., Verstraete, M.M., Diner, D.J., & Davis, A.B. (2004). Canopy structure parameters derived from multi-angular remote sensing data for terrestrial carbon studies. *Climatic Change*, 67(2), 403–415.

Widlowski, J.L., Taberner, M., Pinty, B., Bruniquel-Pinel, V., Disney, M., Fernandes, R., Gastellu-Etchegorry, J.P., Gobron, N., Kuusk, A., Lavergne, T., Leblanc, S., Lewis, P.E., Martin, E., Mottus, M., North, P.R.J., Qin, W., Robustelli, M., Rochdi, N., Ruiloba, R., Soler, C., Thompson, R., Verhoef, W., Verstraete, M.M., & Xie, D. (2007). Third Radiation Transfer Model Intercomparison (RAMI) exercise: Documenting progress in canopy reflectance models. *Journal of Geophysical Research*, 112, 1–28.

Wigneron, J.P., Kerr, Y., & Prévot, L. (1997). Retrieval of soil and vegetation features from passive microwave measurements. *Remote Sensing Reviews*, 15, 157–177.

Williams, J.R., Dyke, P.T., & Jones, C.A. (1983). Analysis of Ecological Systems: State-of-the-Art in Ecological Modeling, chapter EPIC: a model for assessing the effects of erosion on soil productivity, pages 553–572. Elsevier, Amsterdam, Netherlands.

Wu, C., Niu, Z., Tang, Q., & Huang, W. (2008). Estimating chlorophyll content from hyperspectral vegetation indices: Modeling and validation. *Agricultural and Forest Meteorology*, 148, 1230–1241.

Ye, X., Sakai, K., Asada, S.I., & Sasao, A. (2007). Use of airborne multispectral imagery to discriminate and map weed infestations in a citrus orchard. *Weed Biology and Management*, 7(1), 23–30.

Ye, X., Sakai, K., Garciano, L.O., Asada, S.I., & Sasao, F. (2006). Estimation of citrus yield from airborne hyperspectral images using a neural network model. *Ecological Modelling*, 198, 426–432.

Yelenosky, G. (1975). Cold hardening in citrus stems. *Plant Physiology*, 56, 540–543.

Young, P. (1993). Concise encyclopedia of environmental systems. Pergamon press, U.K.

Zaman, Q., Schumann, A.W., & Hostler, K.H. (2006a). Estimation of citrus fruit yield using ultrasonically-sensed tree size. *Applied Engineering in Agriculture*, 22, 39–44.

Zaman, Q., Schumann, A.W., & Shibusawa, S. (2006b). Impact of variable rate fertilization on nitrate leaching in a citrus orchard. In 8th International Conference on Precision Agriculture. Minneapolis, Mn.

Zaman, Q.U., Percival, D.C., Gordon, R.J., & Schumann, A.W. (2009). Estimation of wild blueberry fruit yield using digital color photography. *Acta Horticulturae*, 824, 57–65.

Zarco-Tejada, P.J., Miller, R., Morales, A., Berjón, A., & Agüera, J. (2004). Hyperspectral indices and model simulation for chlorophyll estimation in open-canopy tree crops. *Remote Sensing of Environment*, 90, 463–476.

Chapter 2

A conceptual model of carbohydrate flows in citrus

Abstract

This chapter presents a conceptual model for the carbohydrate flows in citrus. Internal and external factors impact tree health, yield (fruit number, size and juice quality), alternate bearing and freeze tolerance through their effect on carbohydrates. External relations involve climatology, with an emphasis on irradiance, air moisture, temperature, and management, including pruning, thinning and hormone sprays. Internal factors involve the soil-tree water balance, mineral nutrition, storage and partitioning.

Subsequently the seasonal dynamics in non-structural carbohydrate levels (soluble sugar and starch) in unstressed conditions are described, with a focus on leaf storage, to establish a link between remote sensing and *in situ* measurements. The vegetative flush, followed by flowering and fruit set were found to be the periods exhibiting the largest dynamics in starch levels, with smaller changes in soluble sugar contents, although the pattern in seasonal dynamics is different under different climatological regions. Monitoring of leaf non-structural carbohydrate contents has the potential infer information about yield losses caused by physiological fruit drop, about the tendency of trees towards alternate bearing, about cold hardiness in cooler climates and as an indicator for infections that block phloem transport such as citrus greening (Huanglongbing).

Estimation of soluble sugar and starch concentrations was evaluated using near infrared spectroscopy as a potential low-cost *in situ* technique. Different methods of leaf preparation, spectrum collection, preprocessing and statistical regression were compared side-by-side. Prior drying of leaves did not substantially improve the results over the direct use of fresh leaf material. The use of white backgrounds as an alternative to the standard black background improved predictions. Multiple stepwise regression consistently provided better results than partial least squares regression and standardized difference band ratios. First derivative spectra generally outperformed the use of normal spectra.

2.1 Introduction

As explained in section 1.3.2 in the introduction chapter, the modeling of fruit tree crops using existing biophysical models requires different sub-models. These include (i) carbohydrate sink-source relations, (ii) light interception, mainly due to the row oriented structure, (iii) photosynthesis (C3 metabolism, leaf age classes), (iv) intra-annual carry-over effects such as alternate bearing, (v) adaptation, (vi) phenology, (vii) fruit internal and external quality and (viii) management. This chapter introduces a conceptual model for non-structural carbohydrate sink-source relations, with a special reference to citrus. Evidence is given on the critical role of carbohydrates in fruit quality and seasonal and intra-annual dynamics such as alternate bearing and adaptation (e.g. cryo-protection). An encompassing treatment of the carbohydrate economy, embedded in a biophysical modeling approach, can thus initiate a solution for many of the aforementioned modeling aspects.

Carbohydrate relations in fruit trees cannot be contained into a single sub-model, but are linked to the photosynthetic apparatus, the partitioning system, the storage pool and the reproductive phenology (fruit quantity and quality). Since no subsystem can be conceived as a self-contained 'black box', links to related subsystems (water balance, mineral nutrients and management) are described.

Carbohydrates as referred to in this chapter are non-structural saccharides whose physiological role is the storage and transportation of energy and carbon, as opposed to structural carbohydrates such as (hemi)cellulose. Two groups are identified: *oligosaccharides* such as glucose, fructose and sucrose and *starch*, a group of polysaccharides consisting of linear (amylose) or branched (amylopectin) glycosidic chains. The soluble oligosaccharides are important for transportation and direct energetic use. The main physiological function of starch, which is largely insoluble in water, is storage. This can occur in leaves (amyloplasts), stems and roots.

In the next section, a schematic model is presented in which carbohydrate relations, including positive and negative feedback mechanisms are described. Subsequently, seasonal dynamics are discussed and ideas are presented about how these can be integrated in a carbohydrate monitoring system. The last section focuses on non-destructive *in situ* assessment with near-infrared spectroscopy (NIRS).

2.2 Modeling non-structural carbohydrates

2.2.1 Conceptual models

This section presents a conceptual model of carbohydrate relations in fruit trees. Conceptual models, as defined by Greca & Moreira (2000) are external representations that facilitate the comprehension or the teaching of systems or states of affairs in the world. They are simplified representations of real objects, phenomena or situations. A conceptual approach was preferred over quantifying all possible relationships, many which have only been demonstrated in specific cases and cannot be extrapolated to fruit tree horticulture (and not even to citrus production). The aim is to further the understanding of the manifold factors that influence carbohydrate assimilation, allocation, storage and consumption in fruit trees. Such an understanding may improve experiment designs by knowing beforehand the external factors that are expected to influence experiments and need to be controlled or accounted for. In addition, it can be used to predict cascades of interactions[1]. When such considerations are not made, experiments can lead to different conclusions depending on the time-specific (e.g. did a cold spell occur during measurements, or drought stress, or photodamage) or site specific (irrigated versus non-irrigated, sand versus clay) conditions. From such conclusions, made without an encompassing framework, it would be difficult to derive general relationships on species physiology.

While this model attempts to cover most of the known interactions of the carbon subsystem at the level of plants and organs, this does not imply that any model, either mechanistic or empirical, should inherit this full complexity. Rather, simplified models can be derived as long as the context and environment in which they are applied are understood.

[1] As an example: mineral nutrient deficiencies can lead to chlorosis which will in turn decrease photosynthesis; this will impact the partitioning system and - depending on the plant's phenology - might lead to decreased root storage, lower fruit count, smaller fruits or lower fruit juice quality.

2.2.2 General relations

Figure 2.1 presents a simplified scheme of the carbohydrate relationships in fruit trees. Main relations are indicated with roman numerals. The driving force for carbohydrate production is the use of intercepted solar irradiance to convert carbon dioxide and water into triose phosphate for the production of sucrose or starch (rel. I). The dominant factor in light interception is the total area of leaves receiving photosynthetically active radiation to support carbon assimilation (rel. III). Light interception however is not linearly related to total production and in semi-arid climates, a mild shade that prevents photo-inhibition and stomatal closure can even stimulate carbon assimilation in citrus (Raveh et al., 2003). Light interception is determined by canopy structure parameters such as tree height, Leaf Area Index (LAI) and pruning system and by orchard layout parameters (row and tree spacing, row orientation) (rel. II; Oyarzun et al., 2007; Thornley & France, 2007). Of specific interest for woody perennial crops is the impact of the previous year's foliage in the provision of photosynthates during the emergence of the spring flush (rel. II, IV; Shimizu et al., 1978).

Assimilated carbohydrates are partitioned either for direct allocation to the leaves (rel. VI) or transportation to the roots, stems, sink leaves or fruit compartments (rel. VII, VIII). Within each compartment, these may be allocated for maintenance respiration, growth and storage (Léchaudel et al., 2005). For most crops, respiration has the highest priority, followed by growth and finally storage (Thornley & France, 2007). Priority between different compartments in simple models is either hierarchical or proportional (Le Roux et al., 2001). More advanced approaches include allometric partitioning (ratios depend on the organ development stage), functional equilibrium models based on root-shoot ratios, canonical models, models based on sink strength or models based on transport resistance between organs (Marcelis & Heuvelink, 2007).

For modeling purposes, leaf, root and stem storage are pooled together (rel. X), although more fine scale of modeling requires separate pools. Supply and demand for photosynthates determine the conversion of sucrose into either oligosaccharides or starch. Reallocation of starch (rel. XI) can occur on a short time scale (e.g. diurnal conversion of leaf starch into sugars for respiration at night, (Taiz & Zeiger, 2006) or on a seasonal time scale. Storage of carbohydrates in fruit as sugar and acid content of the sap (rel. XII) is considered as final, with no reallocation to other compartments. This may be a simplification: water stress experiments by Goldschmidt & Koch (1996) revealed that water/juice can be withdrawn from juice sacs and some mandarin cultivars can lose juice content during the maturation phase (Agustí et al., 2002).

2.2.3 Citrus-specific relations

Figure 2.2 shows a more detailed version of figure 2.1 with additional and species-specific interactions, indicated with Arabic numerals.

A first set of relations (rel. 1-11) involves the impact of climatology, mineral nutrition, water status and management on photosynthesis and thus determines the rate of carbohydrate assimilation (rel. V). The assimilation rate in all species not only depends

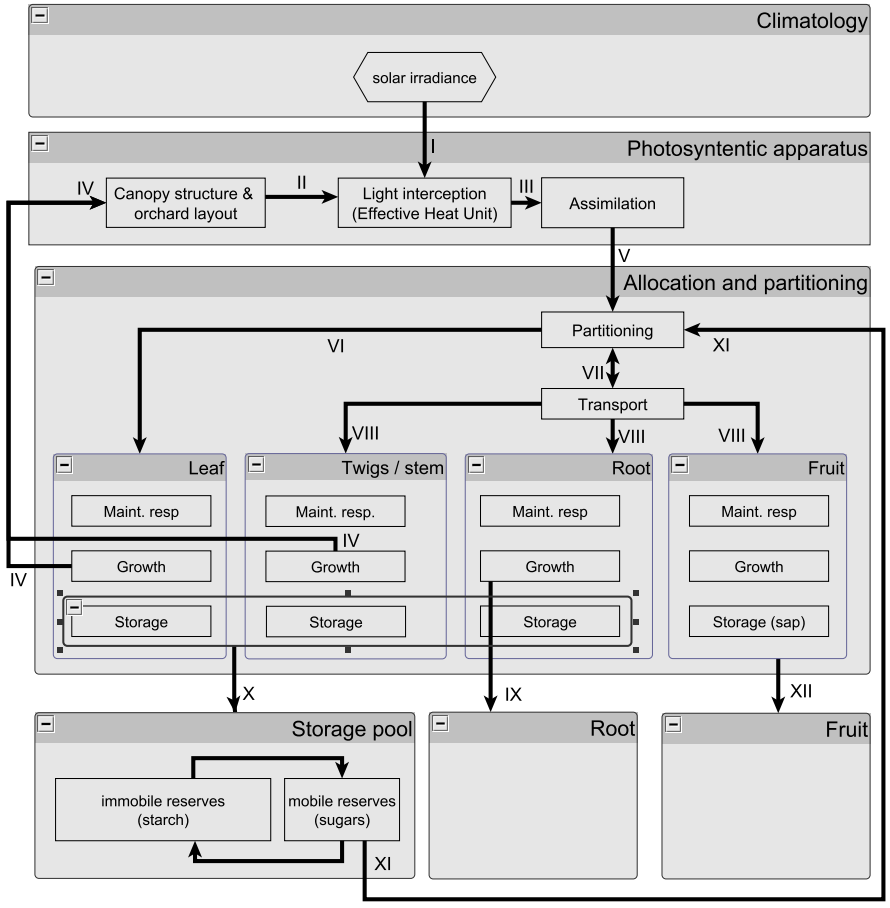

Figure 2.1: The influence of carbohydrate flows on fruit tree growth and development as affected by internal and external factors: simplified representation. Numbers correspond to relations discussed in the text. Boxes are used for internal elements, hexagons for external inputs.

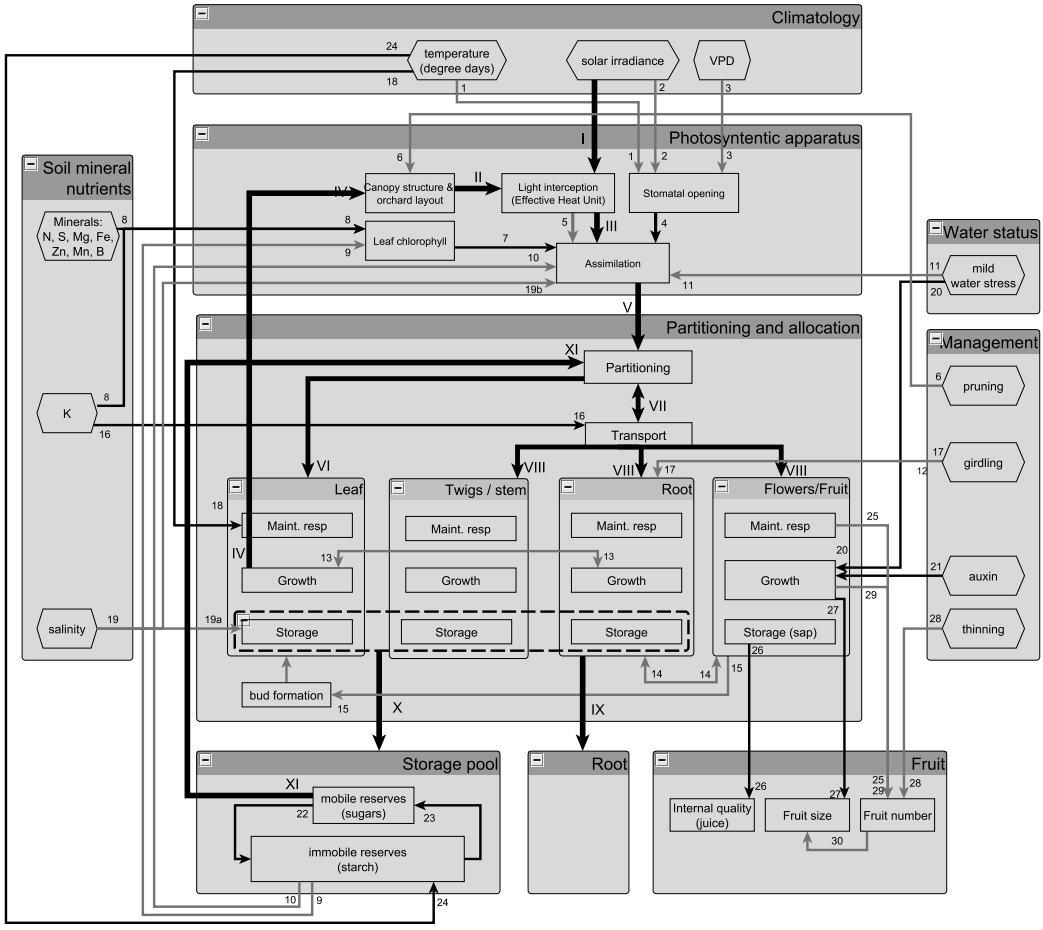

Figure 2.2: The influence of carbohydrate flows on fruit tree growth and development as affected by internal and external factors: detailed representation. Medium black arrows: positive interactions, gray arrows: negative interactions, thin arrows: internal conversions, thick black arrows: main interactions as on figure 2.1. Numbers correspond to relations discussed in the text. Boxes are used for internal elements, hexagons for external inputs.

on light interception, but also on stomatal opening (rel. 4; Taiz & Zeiger, 2006). This in turn is regulated by the vapor pressure deficit (VPD, rel. 3), temperature (rel. 1) and solar irradiance (rel. 2) (Syvertsen & Lloyd, 1994). Commonly the Penmann-Monteith equation (Allen et al., 1998) is used for quantitative modeling. In citrus, Ribeiro (2007) found stomatal closure to occur from VPD above 1.5 kPa, while for temperature an optimal range between 25 and 40°C was suggested rather than a single optimum. Carbon assimilation can be downregulated under conditions of high irradiance as a photo-protective mechanism (rel. 5; Gussakovsky & Salomon, 1993). Light intensity levels during leaf development, leading to differentiation into shade and sunlit leaves, were found to have a high impact on photosynthetic efficiency in citrus due to differences in leaf structure and chlorophyll content (rel. 5,7; Nii, 1987). Whether the total tree leaf area has a net positive contribution to the tree photosynthesis may be questioned considering the high LAI common for citrus (Davies & Albrigo, 1994). Yuan et al. (2005) found little effect on tree growth, yield quantity and fruit quality after defoliation of up to 50% of the leaf area, whereas Eissenstat & Duncan (1992) report a large impact on yield of pruning about one third of the canopy cover (rel. 6). In citriculture, the high demand of nitrogen (N) fertilization as well as the impact of shortages leading to chlorosis has been well described (rel. 8; Davies & Albrigo, 1994; Spiegel-Roy & Goldschmidt, 1996). A quantitative and linear relation between leaf N and chlorophyll contents was established by Bondada & Syvertsen (2003). In addition to N, other minerals such as potassium, sulfur, magnesium, iron, zinc, boron and manganese cause chlorosis (Futch & Tucker, 2008), all of which are expected to decrease photosynthetic efficiency (rel. 7). Large accumulations of starch in amyloplasts can cause damage to the thylakoid structure in case of extreme chlorophyll accumulation (rel. 9; Schaffer et al., 1986). Similarly but more generally, Iglesias et al. (2002) report feedback inhibition of photosynthesis by starch accumulation (rel. 10). The commonly encountered down-regulation of photosynthesis under water stress is also encountered in citrus, mainly around solar noon where the leaf water potential is at its minimum (Vu & Yelenosky, 1988).

The second set of relations (rel. 13-21) more directly impact the partitioning and allocation sub-systems. In citrus it is expected that generally, (i) leaf growth has the highest priority, followed by (ii) growth and storage of fruit after the physiological drop, next (iii) roots and stems, followed by (iv) growth of young fruitlets (rel. 12; Goldschmidt & Koch, 1996; Iglesias et al., 2002). Different refinements can be made:

- Partitioning priority between roots and leaf shoots has a dynamic aspect, with alterations between root and shoot growth occurring in annual cycles (rel. 13; Bevington & Castle, 1985).
- Goldschmidt & Monselise (1977) found that under carbohydrate shortage, root growth may be prioritized to fruit growth on a short term, but fruit have priority on the longer term (rel. 14). Heavy fruit load was also found to reduce the following vegetative summer flush (rel. 15; Goldschmidt, 1997)
- Shimizu et al. (1978) found starch accumulation in the fruit to depend on demands by the fruit itself (sink strength).

- Little indications were found on the priority of stem growth, but it can be hypothesized that stem growth and leaf growth both have equal priority, since stems and twigs are required to support the canopy structural development.

Although storage is generally accepted to have the lowest priority, the sink strength of reserves has been demonstrated by Goldschmidt & Koch (1996). Carbohydrate storage occurs in all organs. Goldschmidt & Golomb (1982) emphasize the role of the roots as the most important reserve organ, whereas Raveh et al. (2003) found the highest carbohydrate accumulation in the stems. The storage function of leaves was described by Kriedermann (1969). Defoliation and stem girdling experiments have indicated that leaf storage mostly serves nearby flowers and fruit (Mehouachi et al., 1995; Iglesias et al., 2007), although Goldschmidt & Golomb (1982) found root storage (rel. IX) to be the most critical factor in the development of the following season's spring flush. Considering the relations described here, a combination of allometric and sink strength based partitioning is suggested (see section 2.2.2), although Eissenstat & Duncan (1992) and Syvertsen & Hanlon (2008) also express the importance of plant root/shoot ratios in tree growth and fruit quality.

The partitioning subsystem is also affected by concentrations of other minerals, management and environmental factors. Low potassium levels were found to impair the transportation of carbohydrates (rel. 16; Marschner, 1995). Stem girdling, although less common in citriculture except for research purposes, leads to carbohydrate accumulation in leaves by inhibiting the sap stream towards the roots (rel. 17). Temperature largely controls organ respiration and for many crops, the relation between respiration and temperature is approximately linear between 15 and 35°C (rel. 18; Amthor, 1989). Salinity in citrus causes leaf abscission, reduced flowering and fruit drop, which correlated with decreased leaf carbohydrate storage (rel. 19a) and may indicate reduced photosynthesis (rel. 19b; Lloyd & Howie, 1989). Water stress was found to decrease the accumulation of sugars in fruit (decreased sink strength). This was explained by Barry et al. (2004)as a consequence of osmotic adjustment, although this theory is contradicted in Syvertsen & Albrigo (1980), who found experimental evidence that leaf and fruit water potentials are largely independent and by Albrigo (1977) who found that high water availability in the root zone contrarily decreases the total soluble solids due to a dilution effect (increase in fruit size). The same effect could also be explained by a decrease in carbohydrate production following a down-regulation of photosynthesis by stomatal closure. Finally also hormonal control impacts the partitioning system. The role of auxins has been of demonstrated to improve fruit growth (rel. 21; Guardiola & Lázaro, 1987) and auxin applications are now part of commercial production practices in Spain.

The third set of relations (rel. 22-24) concern the storage pool. Internal conversions (rel. 22) are simplified: both starch (larger pool, reserve) and sucrose (smaller pool, energy supply, transport) are synthesized directly from assimilated triose phosphate (end product of the Calvin cycle). Starch can be either directly converted back into triose phosphate for nightly respiration or into sucrose to be transported via the phloem (phloem loading and unloading) (rel. 23; Taiz & Zeiger, 2006). In citrus, this relation was found to help in sustaining early leaf respiration and development (Shimizu et al., 1978), although mobilization of starch (rel. 23 and VIII) was slow, thereby limiting

supply to young fruitlets (Ruiz et al., 2001). Cold hardening in citrus in late autumn impacts the starch/sugar ratio, leading to increased concentrations of soluble sugars in leaves (Yelenosky, 1975, 1985).

Finally, a number of relations (rel. 25-30) directly impact fruit set, drop, size and the quality of the fruit. Increased carbohydrate consumption for fruit growth and maintenance and growth respiration leads to self-thinning in the physiological fruit drop (rel. 25 and 29; Bustan et al., 1999). Experiments with shade nets (Jifon & Syvertsen, 2001) as well as early research by Sites & Reitz (1949) support evidence that photosynthesis, through carbohydrate allocation to fruit, has an impact on juice quality (e.g. total soluble solids) (rel. 26), although research by Bustan et al. (1996) found direct climatological control by temperature (degree days) to be the dominant factor. Thinning experiments reveal the role of carbohydrates in the determination of fruit size (rel. 28; Guardiola & Gacriá-Luis, 2000). Inverse relations (source limitation) were found between total fruit number and average fruit size (rel. 26 and 30; Goldschmidt & Monselise, 1977).

Note that this review is restricted to the role of carbohydrates on fruit quality and does not consider other factors such as the direct impact of water stress, mineral nutrients or physical damage.

2.3 Dynamics in carbohydrates

From the schemes presented in section 2.2, it can be interpreted that both seasonal climatological changes in irradiance and temperature as well as internal changes (flowering, fruit set, drop and development) lead to seasonal and even biennial changes in non-structural carbohydrate contents. The following paragraphs present an overview of available literature describing such seasonal trends in leaf and fruit peel non-structural carbohydrates and how such trends can be used in a monitoring strategy.

2.3.1 Seasonal and diurnal dynamics

Most research on carbohydrates in citrus is focused on flowering, fruit set and fruit drop. This was found to be the most critical period where carbohydrate limitations (and excesses) are expressed and impact future fruit production. Experiments include ringing, partial defoliation, sucrose supplements, irradiance reduction (shade nets) and CO_2 elevation, each of which was found to impact the carbohydrate economy. Figure 2.3, adapted from Sanz et al. (1987) shows a typical seasonal trend under Mediterranean conditions, in which old and new leaves are treated separately. A fast accumulation of carbohydrates in old leaves occurs from leafy bud break (S) until flowering (B), followed by a decrease at an approximately constant rate until mid-August, when fruit drop has ended. The overall trend is determined by changes in starch contents, with only limited dynamics in soluble sugars. In young leaves, both starch and soluble sugars accumulate until the beginning of the fruit drop period, during which there is a rapid and transient decrease, followed by a recovery. The subsequent more gradual decrease is analogous to the pattern in old leaves. Similar trends are reported by Garcia-Luis et al. (1988) and

Iglesias et al. (2002) for the post-bloom period. Research confirms a clear link between carbohydrate levels and abscission (Sanz et al., 1987; Garcia-Luis et al., 1988; Iglesias et al., 2007) with peaks of abscission coinciding with low leaf carbohydrate levels. This can be explained by the plant's response to internal competition (figure 2.2, relations 25 and 29): low carbohydrate levels in citrus fruit were found to stimulate ethylene production, which is the main abscission hormone in citrus (Ruiz et al., 2001). Not all reported trends however are similar: in Ruiz et al. (2001) the peak in carbohydrates for old leaves occurs around 45 days after anthesis (DAA), at the start of fruitlet abscission and slightly earlier for the inflorescence leaves. The impact of climate on seasonal carbohydrate dynamics was reviewed by Ribeiro (2007): under Mediterranean conditions (California, US), levels are minimal during the summer season, while under subtropical conditions (Brazil), summer and winter carbohydrate contents are similar. The highest contents however were invariably found in early spring, just before the flowering and vegetative flushes. The overall seasonal trend in carbohydrates is the resultant of a budget equation: in winter a lower solar intensity (Figure 2.2, rel. I) can decrease photosynthesis and thus decrease supply (rel. III, V). This can be compensated for by a lower amount of photo-inhibition (rel. 5), higher air moisture (rel. 3) and higher root water availability (rel. 11) leading to less frequent stomatal closure. Lower winter temperatures will also lead to lower respiratory demands by leaves, roots and fruit (rel. 12).

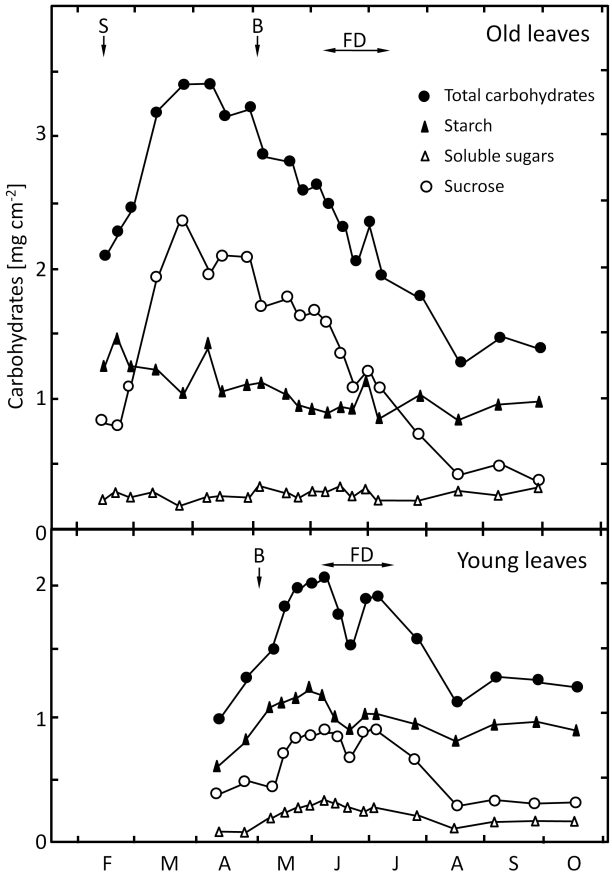

Figure 2.3: Changes in starch, ethanol-soluble sugars, sucrose and metabolizable carbohydrates (starch + soluble sugars) in old and young leaves from sprouting until the end of drop. S: bud sprouting; B: bloom; FD: fruit drop (adapted from Sanz et al., 1987).

Dry matter accumulation of the fruit is the net result of the summation of sink source processes in the leaves. Accumulation occurs in waves (García-Luis et al., 2002), with minima concurring with abscission peaks. The overall yearly photosynthate consumption for commercial grapefruit trees was estimated by Bustan & Goldschmidt (1998), with 11.3% allocated to flowers, 16.0% to fruit that eventually dropped, 51.6% to harvestable fruit and only 21.1% to maintenance (respiration, leaf and stem growth and non-reproductive reserve accumulation).

Soluble sugar contents in leaves were found to increase strongly when air temperatures drop from 15 to 10°C while starch contents did not increase significantly (Yelenosky, 1975, 1982). Combined with a decrease in leaf water content, this leads to elevated sap concentrations and freezing point depression. This confirms research by Dugger &

Palmer (1969) who emphasize the inverse relation between the soluble sugar fraction, peaking in mid winter, and starch, reaching a minimum at that time.

Knowledge on seasonal dynamics may enable carbohydrate monitoring applications based on fixed thresholds as reference values or on trends in time series. Carbohydrate balances under normal production conditions depend on local climate, site characteristics and species/variety/rootstock. Therefore, general and absolute thresholds may be hard to define. For well described seasonal trends (i.e. gradual or cyclic behavior), three basic properties can be considered: the magnitude of a change (max - min), the rate of change (maximum slope) and the time of a change (e.g. time of initiation or maximum rate of change). These can be compared to previous years for the same trees or fields or between structurally similar fields for the same year. If the relations presented in section 2.2 can be quantitatively described and integrated into an adequately parametrized biophysical model, predictions can be made for the current or even future levels (meteorological forecasting) of carbohydrates. These may be a better alternative to detect deviations from an optimal production cycle as they can integrate the current year's weather and management.

An important requirement is the separation of seasonal dynamics from diurnal dynamics. On days with optimal photosynthesis (high irradiance, no water shortage not photoinhibition), photosynthate production may exceed transportation from the late morning until the evening and as a consequence, starch accumulates in the leaves until it is transported again during late evening or night to the other organs. Heavier crop load can diminish this buildup due to large sinks near the leaf source while unusual starch buildup early in the day indicates anomalies, such as HLB if in Florida or Brazil. Hence, diurnal dynamics need to be taken into account e.g. by monitoring at a constant time of day (e.g. predawn or solar noon), by explicitly modeling the expected dynamics or by measuring at higher frequencies during a day (*in situ* hyperspectral).

2.3.2 Carbohydrates for predicting alternate bearing and diseases

Alternate bearing is the tendency of trees to produce a heavy crop load in one year ('on' year) followed by a very light or no crop in the next year ('off' year) (Goldschmidt & Golomb, 1982). Recently, Verreynne & Lovatt (2009) confirmed that for the 'Pixie' mandarin in California, the alternating cycles of on and off crops appear to be perpetuated by a crop load-dependent inhibitory effect of fruit on bud-break. Early in their development, fruit suppresses the growth of the vegetative shoots that would comprise the summer flush and, subsequently, the fall flush. Later in their development, fruit inhibit spring bud-break on the parent shoots and the summer/fall vegetative shoots borne on the parent shoot. The role of carbohydrates as a possible signaling agent has been duly researched, although results are not conclusive and the underlying mechanism is not yet fully understood. The year-to-year fluctuation in carbohydrate availability has been related to the alternate bearing in some citrus varieties (Syvertsen & Lloyd, 1994), although roots rather than stems or leaves may have a central role (Goldschmidt & Golomb, 1982; Goldschmidt & Koch, 1996; Li et al., 2003). This hypothesized relation between carbohydrates and alternate bearing is not exclusive for citrus, but has been detected in other tree crops such as olive (Seyyednejad et al., 2001) and avocado

(Scholefield et al., 1985).

Elevated starch concentrations can indicate the presence of diseases such as citrus Huanglongbing (HLB), also known as citrus greening disease[2]. HLB is associated with the bacterium *Candidatus liberibacter asiaticus* and the Asian Citrus psyllid (*Diaphorina citri* Kuwayama) is the vector. The disease, which slowly weakens and kills all types of citrus trees, causes fruit to become lopsided and taste bitter, making it unmarketable. Fruit does not develop the desired color, hence the greening name. Infection leads to the plugging of sieve pores, primarily by callose deposition. The phloem blockage or damage then leads to massive accumulation of starch in leaves and nutrient deficiencies in sink organs (Kim et al., 2009). Recently, an iodine reaction kit was developed (Onuki et al., 2002) to identify leaves with high starch contents as a pre-screening test for HLB[3].

2.4 Hyperspectral *in situ* detection of carbohydrates

As explained in sections 2.2 and 2.3, the carbohydrate economy in citrus has a large impact on both physiology and phenology and therefore on the overall production process. Robust and frequent monitoring of trends and sudden changes in (leaf) soluble sugars and starch can be an indicator for variations in flowering intensity, fruit set and drop, juice quality, alternate bearing, freeze tolerance and infections such as HLB. This section describes the development of a hyperspectral technique for the detection for soluble sugars and starch from *in situ* non-destructive leaf contact measurements. It contains a summary of the master thesis work by Devarrewaere (2010), which can be consulted for more detailed information.

A calibration dataset of leaf samples was collected in orange groves near Wellington (33°35'00"S; 18°55'30"E) and Stellenbosch (33°55'12"S 18°51'36"E), South Africa on Valencia and Navel orange trees (*Citrus sinensis* L. (Osbeck)) and on Clementine mandarin trees (*Citrus reticulata* Blanco). Both sites have a Mediterranean climate. Data was collected on three dates between July and September 2009. A total of 72 samples were selected to maximize the variations in expected sugar and starch contents. Each sample consisted of ten leaves from the same tree. The selection includes shaded, sunlit, chlorotic and senescent leaves from different species on both harvested and fruit bearing trees.

Hyperspectral reflectance data from 350 to 2500 nm was obtained with a plant probe attached to a FieldSpec Pro JR spectroradiometer[4]. A Spectralon whitepanel (Labsphere inc.) was used as a white reference. Leaf reflectance spectra were collected using both a standard black background (4% uniform reflectance) and a white Spectralon background that normalizes for leaf internal scattering (see chapter 3). Spectra were taken on fresh leaves and on the same leaves after over-drying at 60° for 48 to 72 h. For each sample, spectra of all ten leaves were averaged.

[2]HLB was first detected in China in the early 20th century and is now common in most of Asia and has been imported to Brazil and the USA

[3]The most popular diagnostic method for HLB is PCR (polymerase chain reaction) analysis. PCR analysis, however, is time-consuming and expensive, and is not suitable for large numbers of samples.

[4]Analytical Spectral Devices Inc., Boulder, USA. The spectral resolutions were 3 nm from 350 to 1050 nm and 30 nm from 1050 to 2500 nm.

Starch and soluble sugar contents of each sample were determined using the Dreywood anthrone method (Dreywood, 1946; Yemm & Willis, 1954), combined with amyloglucosidase reaction to break down starch into glucose after prior extraction of soluble mono- and oligosaccharides. Measurements were made with triplicate readings and replicate outliers (relative standard deviation $> 15\%$) were removed prior to statistical model fitting.

Statistical calibration models for soluble sugar and starch and total non-structural carbohydrates (soluble sugar + starch) were developed by correlating the reflectance spectra as well as their first derivatives to the chemical analysis of each sample. Original spectra were smoothed using a Savitzky-Golay (Savitsky & Golay, 1964) filter prior to computation of the derivatives. Since both soluble sugars and starch have no absorption features in the 350 - 950 nm range (Curran, 1989), reflectance and derivative reflectance spectra were constrained to the 950 - 2500 nm range to avoid non-causal correlations between pigment contents and carbohydrates. The statistical methods evaluated in this study are multiple stepwise linear regression (MLR), partial least squares (PLS) regression and ratio indices. For MLR, stepwise model building was applied (Draper & Smith, 1981) and constrained to a maximum of five independent variables to avoid model over-fitting. PLS was implemented using the Non-linear Interactive (NIPALS) implementation (Wold, 1973) in which the optimum number of latent variables was determined using leave-one-out cross-validation. Ratio indices were calculated as standardized difference ratio indices (SDR)[5] for each possible pair of wavelengths. A total of 72 statistical models were fitted for all possible combinations of predicted variable (sugars, starch and total carbohydrates), model type (MRL, PLS and SDR), type of input spectrum (reflectance and reflectance derivative; black and white background) and leaf type (fresh and dry). Calibration models were tested with leave-one-out cross-validation.

The statistics of the three analysis methods are summarized in Table 2.1 in which the quality of the models was expressed by their coefficient of determination R^2 of cross-validation. Additional statistical measures (root mean squared error or RMSE) can be found in Devarrewaere (2010).

[5] A standard difference ratio for reflectance (ρ) at wavelengths $\lambda 1$ and $\lambda 2$ is calculated as $(\rho_{\lambda 1} - \rho_{\lambda 2}) / (\rho_{\lambda 1} + \rho_{\lambda 2})$

Table 2.1: Coefficients of determination (R^2) using cross-validation for the prediction of concentrations of starch, soluble sugars and total non-structural carbohydrates using multiple linear regression (MLR), partial least squares regression (PLS) and standardize difference band ratios (SDR) on spectra of leaf reflectance (ρ) or the first derivative of leaf reflectance ($d\rho$).

Leaf type	Background	MLR		PLS		SDR	
		ρ	$d\rho$	ρ	$d\rho$	ρ	$d\rho$
Starch							
fresh	black	0.87	0.91	0.81	0.83	0.80	0.89
fresh	white	0.88	0.90	0.81	0.84	0.85	0.89
dry	black	0.78	0.81	0.74	0.72	0.76	0.79
dry	white	0.87	0.89	0.85	0.85	0.86	0.86
Soluble sugars							
fresh	black	0.10	0.28	0.13	0.25	0.21	0.33
fresh	white	0.28	0.46	0.18	0.26	0.24	0.40
dry	black	0.57	0.70	0.45	0.51	0.27	0.39
dry	white	0.44	0.42	0.37	0.47	0.39	0.46
Total carbohydrates							
fresh	black	0.86	0.89	0.78	0.78	0.71	0.86
fresh	white	0.88	0.87	0.81	0.80	0.79	0.88
dry	black	0.78	0.81	0.72	0.74	0.73	0.74
dry	white	0.88	0.88	0.83	0.84	0.76	0.82

Results for total carbohydrates and starch produced the best R^2, with lower R^2 values for soluble sugar concentrations. This is consistent for all spectra and leaf types and for the three statistical methods. Analysis of prediction errors (RMSE) reveals that soluble sugar concentrations are predicted with equal or better accuracy than starch. The lower R^2 for soluble sugars is therefore mainly attributed to the smaller range of variation in soluble sugar concentrations as compared to starch. In citrus physiology, variations in leaf soluble sugar concentrations are indeed less pronounced than those in starch, which can reach high levels around anthesis while dropping to low levels during the fruit maturation period (figure 2.3, Sanz et al., 1987; Garcia-Luis et al., 1988). The more subtle dynamics in soluble sugar contents may thus be harder to monitor using *in situ* spectral measurements.

White backgrounds that partly normalize for multiple scattering inside leaves (chapter 3) produced slightly better results than black backgrounds, except for the prediction of soluble sugars using dry leaves. Drying leaves prior to spectrum collection did not consistently improve prediction accuracy, which contrasts with the common assumption that water masks most of the critical absorption features of the leaf dry matter components (Curran, 1989; Jacquemoud et al., 1995, 1996).

Of the three tested methods, MLR produced the best results, followed by PLS and finally SDR. The lower performance of SDR can be expected since standardized difference ratios only use two independent variables for the prediction, while MLR was constrained here to five and PLS uses latent variables that are linear combinations of all independent

variables. Therefore the relatively low performance of PLS was unexpected: in NIR spectrometry, where the number of independent variables (wavelengths) is usually larger than the number of observations, the use of latent variables generally makes PLS more robust to over-fitting than MLR (Tobias, 1995). Many wavelengths selected by both MLR and SDR could be related to known absorption features of soluble sugars or starch (Curran, 1989). The use of first derivative spectra instead of reflectance spectra consistently improved the prediction accuracy, for almost any combination of method, spectrum type and leaf type.

2.5 Conclusions

A conceptual model for the carbohydrate flows in citrus was constructed in which carbohydrates were described as critical factors in that have an impact on fruit number, size and internal quality, alternate bearing and freeze tolerance. The main internal factors of the model involve the sink-source relations, including assimilation, partitioning and mobilization/immobilization of reserves. External inputs (climate and management) and related subsystems (mineral nutrition and tree-soil water balance) have an impact on tree health and production through their impact on the carbohydrate economy. Climatological variables include solar irradiance, air moisture and temperature. The most important factors in mineral nutrition were nitrogen, potassium and salinity. Management interferes through pruning, thinning, girdling and hormone sprays.

The second section of this chapter focuses on the seasonal dynamics in soluble sugars and starch, specifically at the leaf level as this is the easiest to monitor using remote sensing and *in situ* detectors. Most research agrees on the impact of the vegetative flush, followed by flowering and fruit set as the period exhibiting the largest dynamics in starch, with smaller changes in soluble sugar contents. Monitoring of leaf carbohydrate contents has potential to infer information about possible yield losses due to physiological fruit drop, about the tendency of trees towards alternate bearing, about temperature conditioning or cold hardiness in cooler climates and to scout for possible infections that block phloem transport such as HLB.

Near infrared spectroscopy (1000 - 2500 nm) as an *in situ* technique for the estimation of soluble sugars and starch has a reasonable to good prediction power (R^2 of 0.91 for starch and 0.70 for soluble sugars). The use of white backgrounds improved predictions, while prior drying of leaves did not substantially improve the results. Multiple linear stepwise regression consistently provided better results than partial least squares regression and standardized difference band ratios. The small difference in performance between stepwise regression (linear, using up to five wavelengths) and band ratios (non-linear, only two wavelengths) underlines the potential of non-linear regressions. Pre-processing of spectra by taking the first derivative improved the prediction accuracy.

2.6 References

Agustí, M., Martínez-Fuentes, A., & Mesejo, C. (2002). Citrus fruit quality. Physiological basis and techniques of improvement. *Agrciencia*, 6, 1–16.

Albrigo, L.G. (1977). Rootstocks affect 'Velencia' orange fruit quality and water balance. *Proceedings of the International Society of Citriculture*, 1, 62–65.

Allen, R.G., Pereira, L.S., Raes, D., & Smith, M. (1998). FAO irrigation and drainage paper no. 56. Crop evapotranspiration. Guidelines for computing crop water requirements. *Technical report*, Food and Agriculture Organisation.

Amthor, J.S. (1989). Respiration and crop productivity. Springer-Verlag, Berlin.

Barry, G., Castle, W.S., & Davies, F.S. (2004). Rootstocks and plant water relations affect sugar accumulation of Valencia sweet orange via osmitic adjustment. *Acta Horticulturae*, 632, 159–165.

Bevington, K.B. & Castle, W.S. (1985). Annual root growth pattern of young citrus trees in relation to shoot growth, soil temperature and soil water content. *Journal of the American Horticultural Society*, 110, 840–845.

Bondada, B.R. & Syvertsen, J.P. (2003). Leaf chlorophyll, net gas exchange and chloroplast ultrastructure in citrus leaves of different nitrogen status. *Tree Physiology*, 23, 553–559.

Bustan, A. & Goldschmidt, E.E. (1998). Estimating the cost of flowering in a grapefruit tree. *Plant, Cell and Environment*, 21, 217–244.

Bustan, A., Goldschmidt, E.E., & Emer, Y. (1999). Progress in the development of 'CITROS' - a dynamic model of citrus productivity. *Acta Horticulturae*, 499, 69–80.

Bustan, A., Goldschmidt, E.E., & Erner, Y. (1996). Integrating temperature effects on fruit growth into a citrus productivity model. In Proc. Int. Soc. Citriculture, pages 938–944.

Curran, P.J. (1989). Remote sensing of foliar chemistry. *Remote Sensing of Environment*, 30, 271–278.

Davies, F.S. & Albrigo, L.G. (1994). Citrus. CABI Publishing, Wallingford, UK.

Devarrewaere, W. (2010). The use of hyperspectral remote sensing for the detection of carbohydrates in citrus foliage. Master's thesis, K. U. Leuven, Faculty of Bioscience Engineering.

Draper, N. & Smith, H. (1981). Applied regression analysis, 2nd edition. John Wiley & Sons, Inc., New York, NY.

Dreywood, R. (1946). Qualitative test for carbohydrate material. *Ind. Eng. Chem. Anal.*, 18, 499.

Dugger, W.M. & Palmer, R.L. (1969). Seasonal changes in lemon leaf carbohydrates. In Proc. First Int. Citrus Symp. I, pages 339–343.

Eissenstat, D.M. & Duncan, L.W. (1992). Root growth and carbohydrate responses in bearing citrus trees following partial canopy removal. *Tree Physiology*, 10, 245–257.

Futch, S.H. & Tucker, D.P.H. (2008). A guide to citrus nutritional deficiency and toxicity identicifaction. *Technical report*, University of Florida, IFAS.

García-Luis, A., Oliveira, M.E.M., Bordón, Y., Siqueira, D.L., Tominaga, S., & Guardiola, J.L. (2002). Dry matter accumulation in citrus fruit is not limited by transport capacity of the pedicel. *Annals of Botany*, 90, 755–764.

Garcia-Luis, A., Fornes, F., Sans, A., & Guardiola, J.L. (1988). The regulation of flowering and fruit set in citrus: relationschip with carbohydrate levels. *Israel Journal of Botany*, 37, 189–201.

Goldschmidt, E.E. (1997). Citrus Flowering and Fruiting Short Course, chapter Basic and parctical aspects of citrus trees' carbohydrate economy, pages 63–72. University of Florida, Citrus Research and Education Centre, Lake Alfred, FL.

Goldschmidt, E.E. & Golomb, A. (1982). The carbohydrate dynamics of alternate-bearing citrus trees and the significance of reserves of flowering and fruiting. *Journal of the American Horticultural Society*, 107, 206–208.

Goldschmidt, E.E. & Koch, K.E. (1996). Photoassimilate distribution of plants and crops, chapter Citrus, pages 797–823. Marcel Dekker Inc., New York.

Goldschmidt, E.E. & Monselise, S.P. (1977). Physiological assumptions toward the development of a citrus fruiting model. In Proc. Int. Soc. Citriculture 2, pages 668–672.

Greca, I. & Moreira, M. (2000). Mental models, conceptual models, and modelling. *International Journal of Science Education*, 22, 1–11.

Guardiola, J.L. & Gacriá-Luis, A. (2000). Increasing fruit size in Citrus. Thinning and stimulation of fruit growth. *Planth Growth Regulation*, 31, 121–132.

Guardiola, J.L. & Lázaro, E. (1987). The effect of synthetic auxins on fruit growth and anatomical development in Satsuma mandarin. *Scienta Horticulturae*, 31, 119–130.

Gussakovsky, E.E. & Salomon, E. (1993). Photoinhibition (light stress) in citrus leaves. *Acta Horticulturae*, 349, 139–143.

Iglesias, D.J., Cercós, M., Colmenero-Flores, J.M., Naranjo, M.A., Ríos, G., Carrera, E., Ruiz-Rivero, O., Lliso, I., Morillon, R., Tadeo, F.R., & Talon, M. (2007). Physiology of citrus fruiting. *Brazilian Journal of Plant Physiology*, 19, 333–362.

Iglesias, D.J., Lliso, I., Tadeo, F.R., & Talon, M. (2002). Regulation of photosynthesis through source: sink imbalance in citrus is mediated by carbohydrate content in leaves. *Physiologia Plantarium*, 116, 563–572.

Jacquemoud, S., Ustin, S.L., Verdebout, J., Schmuck, G., Andreoli, G., & Hosgood, B. (1996). Estimating leaf biochemistry using the PROSPECT leaf optical properties model. *Remote Sensing of Environment*, 56(3), 194–202.

Jacquemoud, S., Verdebout, J., Schmuck, G., Andreoli, G., & Hosgood, B. (1995). Investigation of leaf biochemistry by statistics. *Remote Sensing of Environment*, 54(3), 180–188.

Jifon, J.L. & Syvertsen, J.P. (2001). Effects of moderate shade on citrus leaf gas exchange, fruit yield, and quality. *Proceedings of Florida State Horticulture Society*, 114, 177–181.

Kim, J.S., Sagaram, U.S., Burns, J.K., Li, J.L., & Wang, N. (2009). Response of sweet orange (Citrus sinensis) to 'Candidatus Liberibacter asiaticus' infection: Microscopy and microarray analyses. *Phytopathology*, 99, 50–57.

Kriedermann, P.E. (1969). 14C distributions in lemon plants. *Journal of Horticultural Science*, 44, 273–279.

Léchaudel, M., Génard, M., Lescourret, F., Urban, L., & Jannoyer, M. (2005). Modeling effects of weather and source-sink relationships on mango fruit growth. *Tree Physiology*, 25, 583–597.

Le Roux, X., Lacointe, A., Escobar-Gutierrez, A., & Dizes, S. (2001). Carbon-based models of individual tree growth: a critical appraisal. *Annals of Forest Science*, 58, 583–597.

Li, C.Y., Weiss, D., & Goldschmidt, E.E. (2003). Girdling affects carbohydrate-related gene expression in leaves, bark and roots of alternate-bearing citrus trees. *Annals of Botany*, 92, 137–143.

Lloyd, J. & Howie, H. (1989). Response of orchard 'Washington navel orange', Citrus sinensis (L.) Osbeck to saline irrigation water I. Canopy characteristics and seasonal patterns in leaf osmotic potential, carbohydrates and ion concentrations. *Australian Journal of Agricultural Research*, 40, 359–369.

Marcelis, L.F.M. & Heuvelink, E. (2007). Wageningen UR Frontis Series. Volume 22. Functional-structural plant modelling in crop production, chapter Concepts of modelling carbon allocation among plant organs, pages 103–111. Wageningen University.

Marschner, H. (1995). Mineral nutrition of plants. Academic press, London.

Mehouachi, J., Serna, D., Zaragoza, S., Agusti, M., Talon, M., & Primo-Millo, E. (1995). Defoliation increases fruit abscission and reduces carbohydrate levels in developing fruits and woody tissues of Citrus unshiu. *Plant science*, 107, 189–197.

Nii, N. (1987). Anatomical changes including chloroplast structure in citrus leaves under different light conditions in relation to photosynthesis. *Scientific Reports 23*, Fac. Agr., Meijo University.

Onuki, M., Truc, N.T.N., & Hong, L.T.T. (2002). Useful histological method for distinguishing citrus yellowing leaves infected with huanglongbing from those caused by other factors. In Proc the 2002 Annual workshop of JIRCAS Mekong Delta Project.

Oyarzun, R.A., Stöckle, C.O., & Whiting, M.D. (2007). A simple approach to modeling radiation interception by fruit-tree orchards. *Agricultural and Forest Meteorology*, 142(1), 12–24.

Raveh, E., Cohen, S., Raz, T., Yakir, D., Grava, A., & Goldschmidt, E.E. (2003). Increased growth of young citrus trees under reduced radiation load in a semi-arid climate. *Journal of Experimental Botany*, 54, 365–373.

Ribeiro, R.V. (2007). Some aspects of citrus ecophysiology in subtropical climates: revisiting photosynthesis under natural conditions. *Brazilian Journal of Plant Physiology*, 19, 393–411.

Ruiz, R., García-Luis, A., Monerri, C., & Guardiola, J.L. (2001). Carbohydrate availability in relation to fruitlet abscission in citrus. *Annals of Botany*, 87, 805–812.

Sanz, A., Monerri, C., González-Ferrer, J., & Guardiola, J.L. (1987). Changes in carbohydrates and mineral elements in Citrus leaves during flowering and fruit set. *Physiologia Plantarium*, 69, 93–98.

Savitsky, A. & Golay, M.J.E. (1964). Smoothing and differentiation of data by simplified least squares procedures. *Analytical Chemistry*, 36, 1627–1639.

Schaffer, A.A., Lin, K.C., Goldschmidt, E.E., Boyer, C.D., & Goren, R. (1986). Citrus leaf chlorosis induced by sink removal: starch, nitrogen and chloroplast ultrastructure. *Journal of Plant Physiology*, 124, 111–121.

Scholefield, P.B., Sedgley, M., & Alexander, D. (1985). Carbohydrate cycling in relation to shoot growth, floral initiation and development and yield in the avocado. *Scienta Horticulturae*, 25, 99–110.

Seyyednejad, M., Ebrahimzadeh, H., & Talaie, A. (2001). Carbohydrate content in Olive Zard c. v. and alternate bearing pattern. *International sugar journal*, 103, 84–87.

Shimizu, T., Torikata, H., & Torii, S. (1978). Studies on the effect of crop load on the composition of Satsuma mandarin trees. V. Analysis of production processes of bearing and non-bearing trees based on the carbohydrate economy. *Journal of the Japanese Horticultural Society*, 46, 465–478.

Sites, J.W. & Reitz, H.J. (1949). The variation in individual Valencia oranges from different locations of the tree as a guide to sampling and spot-picking quality. Part 1. Soluble solids in the juice. *Proc. Am. Soc. Hort. Sci.*, 55, 73–80.

Spiegel-Roy, P. & Goldschmidt, E.E. (1996). Biology of citrus. 229. Cambridge University Press.

Syvertsen, J. & Hanlon, E.A. (2008). Citrus tree stresses: effects on growth and yield. *Technical report*, University of Florida, IFAS.

Syvertsen, J.P. & Lloyd, J. (1994). Handbook of environmental physiology of fruit crops: sub-tropical and tropical crops, chapter Citrus, pages 65–99. CRC Press, Boca Raton.

Syvertsen, J. & Albrigo, L. (1980). Seasonal and diurnal citrus leaf and fruit water relations. *Botanical Gazette*, 141, 440–446.

Taiz, L. & Zeiger, E. (2006). Plant physiology, fourth edition. Sinauer Associates, Sunderland, Massachusetts.

Thornley, J.H.M. & France, J. (2007). Mathematical models in agriculture. Quantitative methods for the plant, animal and ecological sciences. CABI.

Tobias, R.D. (1995). An introduction to partial least squares regression. In Proceedings of the Twentieth Annual SAS Users Group International Conference, pages 1250–1257. Cary, NC.

Verreynne, J.S. & Lovatt, C.J. (2009). The ffect of crop load on budbreak influences return bloom in alternate bearing 'Pixie' mandarin. *Journal of the American Horticultural Society*, 134, 299–307.

Vu, J.C.V. & Yelenosky, G. (1988). Water deficit and assiciated changes in siome photosynthetic parameters in leaves of 'Valencia' organge (Citrus sinensis [L.] Osbeck). *Plant Physiology*, 88, 375–378.

Wold, H. (1973). Multivariate Analysis, III, chapter Nonlinear iterative partial least squares (NIPALS) modelling. Some current developments, pages 391–420. Academic Press, New-York, NY.

Yelenosky, G. (1975). Cold hardening in citrus stems. *Plant Physiology*, 56, 540–543.

Yelenosky, G. (1982). Indicators of citrus cold-hardening in the field. *Proc. Fla. State Hort. Soc.*, 95, 7–10.

Yelenosky, G. (1985). Cold hardiness in citrus. *Horticultural Reviews*, 7, 201–238.

Yemm, E.W. & Willis, A.J. (1954). The estimation of carbohydrates in plant extracts by anthrone. *Biochemistry Journal*, 57, 508–514.

Yuan, R., Alferez, F., Kostenyuk, I., Singh, S., Syvertsen, J.P., & Burns, J.K. (2005). Partial defoliation can decrease average leaf size but has little effect on orange tree growth, fruit yield and juice quality. *Horticultural Science*, 40, 2011–2015.

Chapter 3

A dorsiventral leaf radiative transfer model: development, validation and improved model inversion techniques

Published as: Stuckens, J., Verstraeten, W.W., Delalieux, S., Swennen, R., Coppin, P., 2009. A dorsiventral leaf radiative transfer model: development, validation and improved model inversion techniques. Remote Sensing of Environment 113, 2560-2573.

Contents lists available at ScienceDirect

Remote Sensing of Environment

journal homepage: www.elsevier.com/locate/rse

A dorsiventral leaf radiative transfer model: Development, validation and improved model inversion techniques

Jan Stuckens [a,*], Willem W. Verstraeten [a], Stephanie Delalieux [b], Rony Swennen [c], Pol Coppin [a]

[a] Katholieke Universiteit Leuven, Biosystems department, M3-Biores, Willem de Croylaan 34, BE-3001 Heverlee, Belgium
[b] Flemish Institute for Technological Research (VITO), Center for Remote Sensing and Earth Observation Processes (TAP) Boeretang 200, BE-2400 Mol, Belgium
[c] Katholieke Universiteit Leuven, Biosystems Department, Division of Crop Biotechnics, K.U. Leuven, Kasteelpark Arenberg 13, BE-3001 Heverlee, Belgium

ARTICLE INFO

Article history:
Received 1 December 2008
Received in revised form 18 July 2009
Accepted 18 July 2009

Keywords:
Leaf optical properties
Asymmetry
Radiative transfer
Absorption
Scattering
Pigments

ABSTRACT

A Dorsiventral Leaf Model (DLM) is presented to simulate leaf radiative transfer. DLM was conceived as a plate model with a stochastic distribution of different groups of layers. Leaf asymmetry was modeled by assigning non-uniform distributions of pigments, water and dry matter to palisade and mesophyll layers and by simulating different amounts of light diffusion for adaxially and abaxially incident light. Surface reflections are based on micro-facets theory enabling the simulation of directional–hemispherical reflectance and a range of bidirectional reflectance factors. Adaxial and abaxial optical properties could be accurately simulated for a variety of leaf types with an overall error in reflectance and transmittance below 1.3%.
Sensitivity analysis focused on optimizing model inversion schemes improves parameter estimation accuracy. Different inversion schemes were compared for two independent datasets. Results underpin most of the propositions of the sensitivity analysis: (i) masking the near-infrared wavelengths (band weighting) to account for variability in the dry matter composition consistently increased predicted accuracies for dry matter content, (ii) white reflectance measurements (reflectance with a 100% diffusely reflecting background) provided results superior to other optical measurements, making it a valuable and fast alternative and (iii) combining reflectance and transmittance into absorptance however did not result in improvements. Comparisons of DLM with the PROSPECT 5 model indicate an almost equal performance in content estimations. Improvements were thus not related to differences in model structure but to techniques that reduce the impact of leaf structure and compensate for sampling errors and variations in specific absorption spectra. DLM has important potential in the study of leaf radiative transfer and in the integration with canopy radiative transfer models.

1. Introduction

Leaf optical properties have been recognized as key variables in the description and modeling of radiative transfer in canopies. The interaction of electromagnetic radiation with leaves, resulting in reflection, transmission, absorption and fluorescence, depends on their chemical and physical characteristics (Allen et al., 1969, 1970; Jacquemoud & Baret, 1990). In modeling leaf optical properties in the 400–2500 nm range, a wide variety of radiative transfer models exist. They are classified by Jacquemoud and Ustin (2001) in increasing order of complexity into plate models (of which the PROSPECT model of Jacquemoud and Baret (1990) is the best known example), N-flux models, stochastic models, models based on the radiative transfer equation and ray tracing models. Models of each class have been used to obtain accurate and coherent simulation of reflectance and transmittance of broad-leaved and needle-shaped leaves.

Major factors impacting the scientific success of existing models, in no specific order, are the model's validation, the ability to invert the model, its integration with canopy radiative transfer models, the availability of the model to the scientific community and the model's complexity.

Recent research has focused on modeling of the leaf bidirectional reflectance distribution function (BRDF) (Bousquet et al., 2005), modeling of fluorescence (Zarco-Tejada et al., 2006) and the possibility of separating pigments such as carotenoids and chlorophyll a versus b (Feret et al., 2008). Attempts to apply inversion techniques of leaf radiative transfer models to separate different components of leaf dry mass such as lignin, cellulose and sugars on fresh leaf spectra were largely unsuccessful (Fourty et al., 1996), although statistical approaches proved successful for dry and – to some extent – for fresh material (Jacquemoud et al., 1995).

The impact of leaf internal structure on its optical properties has been subject to extensive research. The differences in optical properties of dorsiventral (also called bi-facial or asymmetric) leaves have been well described. Woolley (1971) reports higher directional hemispherical reflectance of abaxial soybean faces than of adaxial

* Corresponding author. Tel.: +32 16 32 97 49.
E-mail address: Jan.Stuckens@biw.kuleuven.be (J. Stuckens).

0034-4257/$ – see front matter © 2009 Elsevier Inc. All rights reserved.
doi:10.1016/j.rse.2009.07.014

faces for most of the 400–2700 nm spectrum, but an inversion of this effect in the near infrared (NIR, 800–1300 nm). Directional hemispherical transmittance of the abaxial face in the NIR was found to be higher than of the adaxial side. Analogous results were described in Baldini et al. (1997). Different models have been developed that account for the dorsiventral structure of leaves. Yamada and Fujimura (1991) developed a four layer reflectance and transmittance model based on Kubelka–Munk theory and subsequently applied this model to predict chlorophyll content. Richter and Fukshansky (1996) developed and extended a four-flux radiative transfer model for predicting radiation fluxes inside a leaf using optical microprobe measurements for calibration. Ma et al. (2007) extended PROSPECT into the dorsiventral model QSPECT that counts four layers: adaxial epidermis, palisade mesophyll, spongy mesophyll and abaxial epidermis. Each layer's optical properties were calculated with the PROSPECT model with different values for biochemical content and structure. In addition, leaf optical properties have also been simulated using Monte Carlo sampling: Govaerts et al. (1996) developed the ray-tracing model RAYTRAN to simulate photon transport in a 3D dorsiventral leaf and Baranoski (2006) developed an Algorithmic Bidirectional surface scattering Model for Bi-facial leaves (ABM-B) that uses random walk Monte Carlo sampling to compute optical properties. The influence of leaf asymmetry into the model's structure on the retrieval of biochemical properties (model accuracy and bias) has hitherto not been assessed. A precise modeling of both adaxial and abaxial optical properties for broadleaved species is of importance in remote sensing research since research provided evidence that ignoring differences between both faces may introduce significant errors in the simulation of canopy reflectance (Stuckens et al., 2009). While aforementioned research focused on broad-leaved species, (Dawson et al., 1998) were able to construct a model that simulated optical properties of fresh and dried needle-shaped leaves.

Model inversion problems of either leaf or canopy radiative transfer models are most often tackled by least squares minimization or table look-up approaches. Both unconstrained and constrained (e.g. (Kuusk, 1991) who uses a penalty term for unrealistic parameter values) minimizations are applied. Least squares minimization relies on important assumptions: the errors between wavebands have to be uncorrelated with each other and with the independent variables and have equal variance (Björck, 1996). As these assumptions are rarely met in hyperspectral remote sensing it can be expected that more successful inversion schemes can be designed by using band weighting, alternative definitions of independent variables (spectra) or neural networks (e.g. Atzberger, 2004; Bacour et al., 2006).

For leaf optical models further improvements in parameter prediction are expected by coherent improvements in the model's architecture (e.g. including asymmetry) and in inversion techniques. Additional improvements may be obtained by more accurate estimations of spectral constants such as specific absorption spectra. The first objective of this research is to develop and validate an algorithmically fast, invertible model for dorsiventral broad-leaved leaves that can be implemented in different types of canopy reflectance models. The second objective is to design an optimized measurement and inversion procedure that allows a more accurate prediction of biochemical contents.

The Materials and methods section describes the collection and properties of reference datasets that include spectral measurements and contents determination. The model description section presents an analysis of leaf anatomical structure that will be used as a template for a mathematical formulation of a dorsiventral leaf model (DLM). The interaction between model parameters and the consequences of model and measurement errors will be interpreted in the sensitivity analysis. The validation section investigates spectral approximation of measured spectra for both adaxial and abaxial reflectances and the accuracy of parameter estimations for different model inversion schemes.

2. Materials and methods

Three datasets were collected. The first dataset, LeuvenC, is a model calibration dataset consisting of 20 leaves from 12 different species for which adaxial and abaxial directional-hemispherical reflectance and transmittance were recorded in March 2009 with a RTS-3ZC integrating sphere (updated version) coupled to an ASD Fieldspec spectroradiometer (Analytical Spectral Devices, Boulder, Co) measuring from 350 to 2500 nm with a spectral resolution of 3 nm in the 350–1050 nm range and 10 nm in the 1050–2500 nm range. Sample holders were removed from the sphere to avoid reduced port reflectance errors. Scans of 5–10 s per leaf were taken from different positions and averaged. Leaves were kept on their stems during measurements to minimize water loss. Data were noise filtered with a zero phase forward and reverse fourth order Butterworth filter (Oppenheim & Schafer, 1989). From the same leaves, five 1 s scans were made with an ASD leaf probe for instrument intercomparison. The leaf probe measurement chamber has an incandescent light source with illumination perpendicular to the leaf and a viewing angle centered at 40°, measuring biconical reflectance (Schaepman-Strub et al., 2006). Given the limited solid viewing and illumination angles it will further be approximated by bidirectional reflectance. All spectra were corrected to absolute reflectance using the manufacturer provided reflectances of the Spectralon (Labsphere, USA) white-panels. Additionally an intercalibration between the whitepanels of the integrating sphere and leaf probe was established. Intercompatibility of both measurement types for modeling purposes is theoretically treated in Section 4.3 and tested in Section 6.1.

A validation dataset (LeuvenV) was collected in June 2008 consisting of coupled measurements of optical properties and leaf biochemistry for 107 leaves of 10 species with varying leaf structure: *Citrus sinensis* L. (orange), *Malus domestica* Borkh. (apple), *Prunus avium* L. (sweet cherry), *Zea mais* (corn), *Solanum tuberosum* L. (potato), *Musa* sp. (banana), *Populus*×*canadensis* (poplar), *Fagus sylvatica* L. (beech), *Acer pseudoplatanus* (Norway maple) and *Euonymus fortunei* (albino leaves of a variegated cultivar). Leaf samples were taken in and spectral and biochemical analysis were made on the day of sample collection. No indications of senescence were present in the samples. Sealed plastic bags and refrigerator storage were used to prevent intermediate dehydration. Spectral measurements were made with an ASD spectroradiometer and a leaf probe. For each leaf, two measurements were made of adaxial and abaxial reflectance using a matte plastic background with a flat reflectance spectrum of 4%. The effect of the background on reflectance measurements was included into the model structure as described in Section 4.8. An additional pair of measurements was made of the adaxial reflectance with the same Spectralon whitepanel as a background, hereafter called 'white (adaxial) reflectance'. This spectral measurement set comprises a fast method (1 s scan time per measurement) that can easily be adapted to field work. Per leaf, dry mass and water contents were determined by weighting three up to five fixed area (2.4 cm^2) tissue disks in fresh state and after drying at 85 °C in an oven for at least 16 h. In additional drying experiments, the difference in measured water content between 16 h and a four days extended drying period was below 0.04 mg/cm^2, which is one order of magnitude smaller than the accuracies obtained in this research. Chlorophyll a and b and carotenoids were determined on five tissue samples of 0.79 cm^2 by absorption spectroscopy using an UV–VIS Perkin Elmer Lambda 12 spectrophotometer and an acetone–Tris extraction solvent. Contents were calculated using the equations described by Sims and Gamon (2002) which includes a correction for the absorption by anthocyanins. These authors report the accuracy of their method when compared to High Performance Liquid Chromatography (HPLC) pigment determinations with a coefficient of determination (R^2) of 0.96 for chlorophylls.

As a third dataset, the LOPEX dataset (Hosgood et al., 1994) was used which contains a larger number of biochemical properties and

leaf reflectance and transmittance spectra of 60 broad-leaved species. As reported by Feret et al. (2008), the pigment contents in LOPEX are questionable possibly due to inefficient pigment extraction procedures. Accuracies on LOPEX chlorophyll content estimation are included in the analysis to facilitate comparison with other published results but should be treated with care. Table 1 summarizes relevant properties of the LeuvenV and LOPEX datasets.

3. Analysis of abaxial and adaxial optical properties

Fig. 1 shows the structure of a dorsiventral leaf, typical for most broad-leaved dicot species. The palisade mesophyll layer consists of densely packed cells with few intercellular spaces. The underlying spongy mesophyll is loosely packed with large intercellular spaces. The adaxial (top) and abaxial (bottom) sides of the leaf are bound by an epidermal layer with a cuticle of varying thickness. Quantification studies in sun-lit and shade leaves of *Spinacia oleracea* (Cui et al., 1991) and *Acer platanoides* (McCain et al., 1993) reveal that the highest chloroplast concentrations are found in the palisade tissue, with lower concentrations in the spongy tissue and almost no chloroplast concentrations in the epidermal layers.

Fig. 2 shows typical directional–hemispherical reflectance and transmittance spectra of the adaxial and abaxial sides of two leaves, *Urtica dioica* L. (nettle) and *Hedera helix* L. (ivy) with different dorsiventral structures. Marked differences between adaxial and abaxial optical properties exist (i) in the VIS region (400–700 nm) where abaxial reflectance exceeds adaxial reflectance with approximately equal transmittances, (ii) in the NIR region (700–1400 nm), where the adaxial reflectance is higher and the adaxial transmittance is lower and (iii) in the SWIR region (1400–2500 nm) where abaxial reflectance is higher in the water absorption bands and both positive and negative differences are found in the 1600–1800 and 2000–2400 nm regions. In addition, Baldini et al. (1997) report additional reflectance and transmittance plots between 400 and 1100 nm from which similar conclusions can be drawn. An important observation from Fig. 2, which confirms observations by Woolley (1971) and Baldini et al. (1997) is that the (NIR) transmittance of the abaxial side is systematically higher than on the adaxial side. This observation is in seeming conflict with the reciprocity relation (or polarity property) for transmitted light (Kubelka, 1954) which states that scattering and absorption are unaffected when the path of light is exactly reversed. For a directional–hemispherical configuration this implicates that at the opposite face of the leaf the hemispherical–directional transmittance is measured, under the same zenith angle. This is not applicable

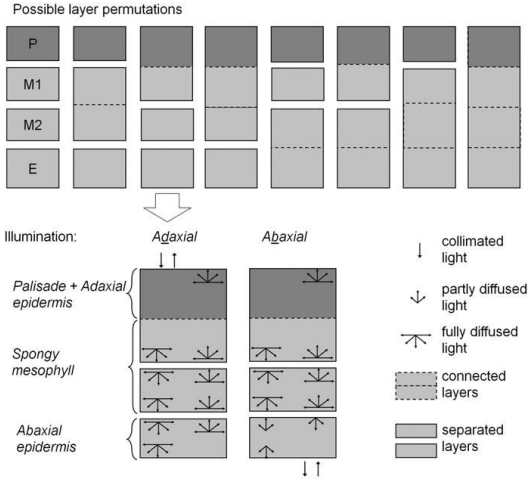

Fig. 1. Structure of a typical dorsiventral leaf.

to our model and measurements that consider a directional–hemispherical configuration at both faces. As a consequence differences in transmittance from both faces of a surface are physically plausible and should not be attributed to measurement errors.

Aforementioned observations can be explained by considering the cross-section of a dorsiventral leaf:

1. The compact structure of the palisade layer was found to facilitate penetration of adaxial light into the spongy tissue (Vogelmann & Martin, 1993), where the light is scattered due to the large amount of cell–air interfaces of the more loosely packed cells. Elevated concentrations of chlorophyll in the palisade layer will further reinforce this effect. For abaxial illumination, the scattering by the spongy mesophyll cells occurs before light can be guided into the leaf interior, which increases the reflectance.
2. The difference between adaxial and abaxial directional–hemispherical transmittance can be explained by representing a leaf as a stack of 'optical' layers separated by air spaces (Fig. 1). The adaxial epidermis and palisade tissue are connected over most of their surface with almost no intercellular spaces and are therefore be represented by a

Table 1
Characteristics of the datasets.

	Dataset	Leuven	LOPEX
	Year	2008	1993
	Number of samples	107	64 (pigments)/330 (water and dry matter)
	Number of species	10	50
	Instrument	ASD FieldSpec FR	Perkin Elmer Lambda 19
	Spectral range	400–2500 nm	400–2500 nm
	Solvent	Acetone 80% w. Tris buffer (pH 7.8)	Acetone 100%
	Pigment extraction method	Sims and Gamon (2002)	Lichtenthaler (1987)
Total chlorophyll (g/cm^2)	Min	0.4	0.5
	Max	113.8	72.6
	Mean	39.2	20
Carotenoids (g/cm^2)	Min	0.3	0.6
	Max	8.5	15.8
	Mean	22.2	4.4
Water (mg/cm^2)	Min	3.9	4.3
	Max	41.2	43.9
	Mean	13.7	11.3
Dry matter (mg/cm^2)	Min	1.8	1.7
	Max	12	15.2
	Mean	6.2	5.3

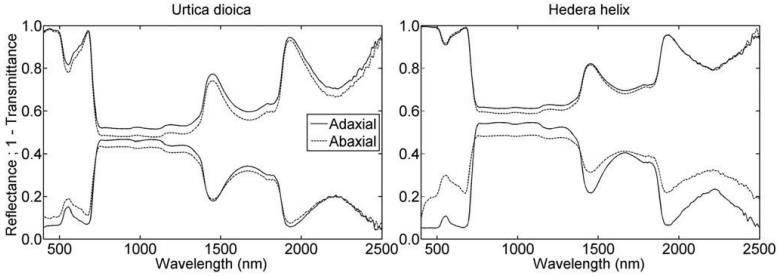

Fig. 2. Reflectance and transmittance of abaxial an adaxial faces of *Urtica dioica* and *Hedera helix*.

single optical layer of which the mesophyll tissue causes light scattering (Vogelmann & Martin, 1993). The abaxial epidermis is disconnected from the spongy tissue over a large fraction of its surface and is therefore expected to optically function as a separate layer. The generally smooth oblate shape of epidermal tissue (Baranoski, 2006; Taiz & Zeiger, 2006) is expected to cause low amounts of scattering and even focusing of light (Vogelmann et al., 1996). Abaxial collimated light is thus not fully diffused upon entering the abaxial epidermis (bottom layer) but only upon entering the spongy tissue (middle layers) while adaxial collimated light is immediately diffused by the top optical layer. As a consequence, abaxial transmittance can be higher than adaxial transmittance due to the lower total amount of light scattering.

3. The effects in the SWIR region can be considered as a mixture of the previous items, with the concentration effect dominating in high absorption regions and the dispersion effect dominating in low absorption regions.

In the following sections, an analytical Dorsiventral Leaf Model (DLM) is developed that takes into account the described asymmetric behavior of light scattering and absorption.

4. Model description

DLM is based on the well known plate generalized model (Allen et al., 1970) that simulates reflectance and transmittance of leaves represented by a set of horizontal layers separated by air spaces. First, the adaxial and abaxial optical properties of a single layer are determined for a generalized case of partly diffused light. Next, the optical properties of a stack of non-identical layers is derived. For the top layer on which light is incident, the model formulation is extended to either directional–hemispherical reflectance (DHR) and transmittance (DHT) or bidirectional reflectance factor (BRF) (Schaepman-Strub et al., 2006). In the subsequent sections, default model parameters are established, the refractive index of cell walls is re-calibrated and the plate model is extended to calculate leaf reflectance with a background of known reflectance.

4.1. Reflectance and transmittance of a single layer

Reflectance and transmittance of a single layer in DLM are a generalization of the formulation derived in Jacquemoud and Baret (1990), for conditions where light inside a layer is not necessarily fully diffused. Consider a layer illuminated by either a collimated or diffuse light source. The layer's hemispherical reflectance and transmittance are derived from the average of the Fresnel transmission coefficients (t) at the air-to-cell and cell-to-air interfaces and the average transmissivity (τ) of light passing through it. The value of t depends on the maximum dispersion angle of the light (α for light outside of the layer and $\tilde{\alpha}$ for light inside the layer), the relative refractive index of the layer (η) and the direction in which light crosses the interface.

An analytical formulation is given in Allen et al. (1969). We will use t_o for light entering a layer (air-to-cell interface) and t_i for light leaving the layer (cell-to-air interface). The angular distribution of incident light may be different for both faces of a layer, so α and $\tilde{\alpha}$ depend on the direction of illumination (z), which is abaxial ($z='b'$) or adaxial ($z='d'$). The average transmissivity $\tau(\tilde{\alpha},k)$ is found by averaging the Beer–Lambert law over $\tilde{\alpha}$:

$$\tau(\tilde{\alpha},k)=\frac{\int_0^{\tilde{\alpha}} e^{-k/\cos(\theta)}\cos\theta\sin\theta\,d\theta}{\int_0^{\tilde{\alpha}}\cos\theta\sin\theta\,d\theta}=\frac{1}{1-\cos^2\tilde{\alpha}}\left[e^{-k}(1-k)+e^{-k/\cos\tilde{\alpha}}\cos\tilde{\alpha}(k-\cos\tilde{\alpha})+E_1(k)-E_1\left(\frac{k}{\cos\tilde{\alpha}}\right)\right] \quad (1)$$

where k is the absorption coefficient of a layer and E_1 stands for the exponential integral (for a mathematical proof, see online documentation). For $\tilde{\alpha}=90$ the formula simplifies to the version used in Jacquemoud and Baret (1990). The reflectance (R_z) and transmittance (T_z) of a layer with light incident from direction z can now be expressed as:

$$R_z=R_s+\frac{T_s\tau(\widetilde{\alpha_z},k)^2 t_i(\widetilde{\alpha_z},\eta)(1-t_i(\widetilde{\alpha_z},\eta))}{1-\tau(\widetilde{\alpha_z},k)(1-t_i(\widetilde{\alpha_z},\eta))^2}$$
$$T_z=\frac{T_s\tau(\widetilde{\alpha_z},k)t_i(\widetilde{\alpha_z},\eta)}{1-\tau(\widetilde{\alpha_z},k)(1-t_i(\widetilde{\alpha_z},\eta))^2} \quad (2)$$

with R_s the surface reflectance and T_s the surface (hemispherical) transmittance of the layer (see Section 4.3). For leaf internal scattering (all layers except the top layer), we will use Allen's approximation where $T_s=t_o(\alpha,\eta)$ and $R_s=1-T_s$. For the top layer a more detailed treatment is presented in Section 4.3. The reflectance and transmittance of a layer illuminated by either adaxial or abaxial sides will be represented by a four element vector: $[R_{z=d}, T_{z=d}, R_{z=b}, T_{z=b}]$.

4.2. Reflectance and transmittance of a group of layers

In calculating the reflectance and transmittance of a group of homogeneous layers, Jacquemoud and Baret (1990) extended the 'generalized plate model'. In this symmetric model, abaxial and adaxial optical properties are equal. This plate model theory is further improved here to model the asymmetry of dorsiventral leaves. A four-layer representation of a leaf (Fig. 3) was developed for DLM. The top layer (P) represents the aggregate of adaxial epidermis and palisade mesophyll. Both are assumed to optically represent a single layer, as motivated in Section 3) and will henceforth be simply named 'palisade layer'. This assumption agrees with the results of Ma et al. (2007) who treated the adaxial epidermis as a separate layer, but assigned to it a very low structure parameter. The second and third layers represent the spongy mesophyll (M_1 and M_2). The lower epidermis (E) is treated as a fourth layer since it is not always tightly connected to the spongy mesophyll (see Fig. 1 and Section 3). The

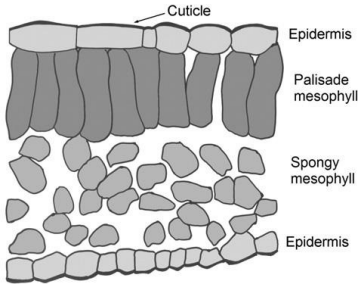

Fig. 3. Schematic structure of the Dorsiventral Leaf Model for three out of eight layer groups with adaxial and abaxial illumination. The bottom line shows the group probabilities.

choice of two spongy mesophyll layers and thus a four layer leaf representation has no direct physical basis, but was chosen as an upper bound in representing the (near-infrared) scattering behavior that is expected to be dominant in the spongy layers. Simulations with different model structures revealed that a four-layer leaf structure was sufficient to model the scattering of all leaves in the Leuven and LOPEX datasets while a three layer representation was insufficient for thicker leaves.

Contrary to the traditional interpretation of layers in plate models, in DLM two adjacent layers are separated by air spaces for only a fraction (f_{air}) of their surface area and are connected for the remainder fraction ($1-f_{air}$). The parameter f_{air} determines the scattering behavior and is analogous to the structure parameter N in the PROSPECT model. It is equal for each pair of adjacent layers. The adaxial and abaxial reflectance and transmittance of two adjacent layers (A and B) for the area over which they are separated by air spaces, can be given in the four-element notation:

$$\left[R_{AB,d}, T_{AB,d}, R_{AB,b}, T_{AB,b}\right] = \left[R_{A,d} + \frac{T_{A,d}R_{B,d}T_{A,b}}{1-R_{A,b}R_{B,d}};\ \frac{T_{A,d}T_{A,d}}{1-R_{A,b}R_{B,d}};\ R_{B,b} + \frac{T_{B,b}R_{A,b}T_{B,d}}{1-R_{A,b}R_{B,d}};\ \frac{T_{B,b}T_{B,b}}{1-R_{A,b}R_{B,d}}\right] \quad (3)$$

The fractional area over which A and B are connected (no air spaces) on the other hand, can be represented by a single layer with a layer absorption coefficient $k_{AB}=k_A+k_B$. The above formulas for two layers can be iteratively applied to find reflectance and transmittance of three and finally four layers. The reflectance and transmittance of an entire leaf consists of a combination of reflectances and transmittances of the eight possible permutations in which four layers can either be separated or connected: [$P.M_1.M_2.E$]; [$PM_1.M_2.E$]; [$P.M_1M_2.E$]; [$P.M_1.M_2E$]; [$PM_1M_2.E$]; [$P.M_1M_2E$]; [$PM_1.M_2E$]; [PM_1M_2E]. In this notation a dot indicates separation by air spacing and connected letters indicate connected layers. The upper part of Fig. 3 visualizes these combinations, while the lower part illustrates a detail of a single permutation ([$PM_1.M_2.E$]). The total leaf reflectance and transmittance (RT_{leaf}) is then a weighted average of the reflectances and transmittances of the individual permutations (RT_i):

$$RT_{\text{leaf}} = \sum_{i=1}^{8} (w_i RT_i) \quad (4)$$

with the weights given as $w_i = f_{\text{air}}^{n} f_{\text{air}}^{3-n}$ where n equals the number of air layers (number of dots) in the permutation. The eight weights form a binomial distribution and sum up to one so no normalization is required.

4.3. Reflectance of the top layer

In this section we will derive expressions for BRF and DHR of leaf surfaces for implementation in DLM. BRDF modeling of leaf surfaces has been subject to research in domains of computer graphics (e.g. Habel et al., 2007) and remote sensing (Bousquet et al., 2005; Govaerts et al., 1996). Surface reflectance is derived from the Bousquet micro-facets model (calibrated on beech, laurel and hazel leaves) and allows an intercompatibility relationship to be established between DHR and BRF of leaf surfaces. The leaf BRDF in Bousquet's model is represented as the sum of a diffuse component ($BRDF_d$) representing the leaf interior absorption and scattering and a glossy/specular component ($BRDF_s$) related to the cuticle surface reflectance: $BRDF = BRDF_s + BRDF_d$. This formulation is not directly compatible with plate models (Eq. (2)) and does not assure energy conservation (Ashikhmin & Shirley, 2000) as it does not account for Fresnel-based reduced reflectance i.e. light reflected off a surface does not enter the leaf interior and does not contribute to diffuse reflectance. The previous equation is therefore extended to: $BRDF = BRDF_s + (1-DHR_s)BRDF_d$ where DHR_s is the directional–hemispherical surface reflectance obtained by hemispherical integration of $BRDF_s$. $BRDF_s$ is calculated using the Cook and Torrance (1981) model:

$$BRDF_s(\eta(\lambda), \theta_s, \theta_v, \varphi_v, \sigma) = \frac{Fr(\eta(\lambda), \theta_a) D(\alpha, \sigma) G(\theta_s, \theta_v, \varphi_v)}{4 \cos\theta_s \cos\theta_v} c \quad (5)$$

with λ the wavelength, θ_s the light incident angle, θ_v the viewing angle, φ_v the relative azimuth, $\eta(\lambda)$ the refractive index of the cuticle that is assumed to be equal to cell walls, θ_a the half-angle between illumination and viewing directions, α the angle of the facets normals, σ a surface roughness parameter, Fr the Fresnel reflectance, D a (normalized) micro-facets distribution function, G a shadowing term and c a normalization constant. Of these terms only the Fresnel term depends on wavelength (λ).

For implementation in DLM we restrict calculations to collimated light incident perpendicular to the leaf surface ($\theta_s=0$) and viewing angles between 0 and 45° ($\theta_a<22.5°$) which conforms with optical designs of commonly used measurement instruments such as leaf probes and integrating spheres. Under such conditions it can be derived (see online documentation) that $\theta_a=\alpha=\theta_v/2$, $BRDFs$ no longer depends on φ_v and the Fresnel reflectance almost equals the Fresnel reflectance at normal incidence: $Fr(\eta,\theta_a) \approx Fr(\eta,0)$ (relative error<1%). The BRF_s (equal to $\pi BRDF_s$) can be closely approximated by the product of two separate terms: the Fresnel factor and a wavelength-independent term (ν) that depends on viewing geometry and surface roughness:

$$BRF_s(\eta(\lambda), \theta_v, \sigma) \approx m(\theta_v, \sigma) Fr(\eta(\lambda), 0);\ \theta_v < 45^{\circ} \quad (6)$$

Monte Carlo simulations on the Bousquet micro-facets model with a wide range of refractive indices (between 1.1 and 1.6) and surface roughnesses (between 0.2 and 1) show that errors of this approximation were below 10^{-4} for $\theta_v<45°$ (see online documentation). In a second Monte Carlo experiment equal accuracy standards were obtained for the DHR_s so that:

$$DHR_s(\eta(\lambda), \sigma) \approx \mu(\sigma) Fr(\eta(\lambda), 0) \quad (7)$$

with μ a different constant that only depends on surface roughness. Now the values of R_s and T_s of Eq. (2) can be determined. For DHR simulations, $R_s=DHR_s$ and $T_s=1-DHR_s$ and for BRF simulations, $R_s=BRF$ and $T_s=1-DHR_s$ since T_s stands for hemispherical transmittance in both cases. BRF and DHR for these conditions only differ in their specular components and the difference between both is independent of biochemical content or leaf internal scattering. While DHR can be measured with an integrating sphere, derivations made for BRF can be

ported, without loss of accuracy, to biconical reflectance (e.g. measured with a leaf probe) since this integrates bidirectional reflectance over viewing and illumination directions (Schaepman-Strub et al., 2006).

4.4. Model parameters

The absorption coefficients (k) of the palisade and spongy mesophyll layers and the abaxial epidermis are expressed as linear combinations of the different layer biochemical contents (in mass per unit area) with their respective specific absorption spectra ($\kappa(\lambda)$ in unit area per mass). Further analysis will be restricted to the four main components of a leaf's biochemical composition (Fourty et al., 1996; Feret et al., 2008): total chlorophyll a+b (C_{chl}), total carotenoids (C_{car}), water (C_{wat}) and total dry matter (C_{dm}). For easier parametrization the following generalizations are made: (i) water and dry matter contents in each layer are present in equal proportions with respect to the total leaf contents, (ii) the chlorophyll and carotenoids contents in each layer are also present in equal proportions, (iii) the biochemical contents in the spongy mesophyll layers are equal and (iv) the adaxial epidermis contains a reduced chlorophyll content (only in stomatal cells; (Taiz & Zeiger, 2006)). The absorption coefficient of each layer can now be found for known values of these four components and the fractions of the total pigment content (β_{pigm}) and water and dry matter content (β_{wdm}) in the palisade layer and the fraction of pigments in the abaxial epidermis (β_{ep}).

The arrows on the bottom drawing of Fig. 3 show the scattering of light between the different layers. Light incident upon a leaf is collimated with normal incidence. Leaf surface roughness is modeled as described in Section 4.3 and parametrized by μ for DHR and by μ and ν for BRF. Adaxially incident light is assumed to be diffused inside the palisade layer so that $\overline{\alpha_d} = 90°$ for all layers. The abaxial epidermis on the other hand is expected to cause only partial light diffusion ($\overline{\alpha_b} = \delta$; $\delta < 90°$) considering its relative smoothness, light focusing and optical thinness of the epidermal tissue (Section 3). After crossing the first cell–air boundary light will become fully diffuse ($\overline{\alpha_b} = 90°$), as is the light in intercellular air spaces ($\alpha_d = \alpha_b = 90°$). Fully and partly diffused light beams are indicated in Fig. 3. An important consequence of different values for $\overline{\alpha_b}$ and $\overline{\alpha_d}$ inside a single layer is that the layer and overall leaf directional–hemispherical transmittance can be different for abaxial and adaxial illumination.

Since the refractive index spectrum ($\eta(\lambda)$) and the specific absorption spectra of the leaf components ($\kappa(\lambda)$) are treated as optical constants, the leaf optical properties can be represented by the following parameters: C_{chl}, C_{car}, C_{wat}, C_{dm}, β_{pigm}, β_{wdm}, β_{ep}, f_{air}, μ, ν and δ.

4.5. Default leaf asymmetry and roughness parameters

Since a total number of 11 parameters is expected to decrease the performance of inversion algorithms, causing them to become ill-posed, default average values are determined for the asymmetry parameters β_{pigm}, β_{wdm} and β_{ep} and for the leaf roughness parameter μ. This allows choosing between inversion schemes in which these parameters are either fixed or free (estimated by the inversion algorithm). Knapp et al. (1988) report more than 50% of the chlorophyll content in the upper 270–300 μm of a leaf cross-section with a 400 μm palisade layer thickness. Measurements of paradermal sections made by McCain et al. (1993) reveal approximately 67% of the leaf chlorophyll in the palisade layer, 31% in the spongy tissue and 4% in both epidermal layers together. Estimates of fractional mass in different layers can be obtained from measurements of intercellular space volume and layer thickness in epidermal, spongy and palisade tissues. Values derived from Evans et al. (1996) on six different species range between 49 and 62% of leaf mass present in the upper epidermis and palisade tissue, while values derived from Pääkkönen et al. (1995) on fresh and aging Birch leaves range between 44% and 51%. Model inversion on directional–hemispherical abaxial and adaxial reflectance and transmittance leaves of the LeuvenC dataset return average values of 0.52 for β_{pigm} and 0.44 for β_{wdm} which is within the range of values reported in literature. Since DLM is an abstraction of leaf structure, its parameters should be treated as effective parameters (i.e. different from the true values they are supposed to represent but resulting in equal optical interactions). Therefore inverted values are preferred. Inverted values for β_{ep} (chlorophyll in lower epidermis) range between 7% and 25% with an average of 11%, which is relatively high. It may be assumed that the bottom layer effectively represents the abaxial epidermis and a fraction of the spongy tissue.

An average value for leaf roughness (μ) was estimated on the LOPEX dataset that consists of a larger number of directional–hemispherical adaxial reflectance measurements. A first estimate is based on model inversion (see Section 6) with μ as an additional free parameter, resulting in an average value of 1.19. A second estimate is based on the reflectance in the 400–450 nm range. Model calculations reveal that in leaves with moderate to high chlorophyll (>40 μg/cm^2) and carotenoid (>10 μg/cm^2) contents the diffuse part of the reflectance is less than 0.1% so that almost the entire reflectance is due to glossy reflections of the leaf cuticle. Using moderate or high chlorophyll and carotenoid contents as a selection criterion an average value of 1.14 was obtained, which is close to the previous estimate.

4.6. Specific absorption spectra

While the specific absorption coefficient of water has been directly measured (κ), the spectra of the other components have been determined by Jacquemoud and Baret (1990), Jacquemoud et al. (1996) and later by Feret et al. (2008) using model inversion. These spectra are being used in DLM, assuming that their shape is determined by the underlying physics, while their level (scaling) may be model-dependent.

4.7. Refractive index of cell walls

The refractive index spectrum of cell walls has been re-calibrated since its values were found to be significantly influenced by the difference in model structure between DLM and PROSPECT and more specifically by the assumptions of asymmetry. The calibration is made on 67 measurements of reflectance and transmittance of fresh leaves in the LOPEX dataset (five spectra averaged per species) for which ν (directional hemispherical) and δ (only adaxial) are not required. For each leaf C_{chl}, C_{car}, C_{wat}, C_{dm}, f_{air} and μ are determined from model inversions or measurements while fixed values (Section 4.5) are used for β_{pigm}, β_{wdm} and β_{ep} so that for each model layer, κ (Eq. (2)) can be found. The resulting values of $\eta(\lambda)$ were averaged resulting in the spectrum of Fig. 4. This spectrum significantly differs from values obtained by Feret et al. (2008) in their recalibration of the cell walls refractive index and its shape is closer to a monotonically decreasing line from approximately 1.5 at 400 nm down to 1.3 at 2500 nm. To evaluate whether these differences may be caused by differences in estimation procedures rather than by differences in model asymmetry, the procedure was repeated with parameter settings representing a perfectly symmetric leaf, analogous to the PROSPECT model (β_{pigm}, β_{wdm} and β_{ep} equal to 0.25). This result shows a shape similar to the spectrum of Feret et al. (2008). The effect of a symmetric model structure on the estimation of $\eta(\lambda)$ applied on dorsiventral leaves thus seems to cause a bias that is most pronounced in the 450–700, 1400–1550 and 1850–2000 nm wavelength ranges. A plausible cause is that at wavelengths of high absorption, most of the light entering a leaf is absorbed regardless of leaf asymmetry so that cuticular reflectance determines the estimated refractive index; at low absorption wavelengths, scattering dominates absorption so that biochemical content distributions (and thus asymmetry) have little

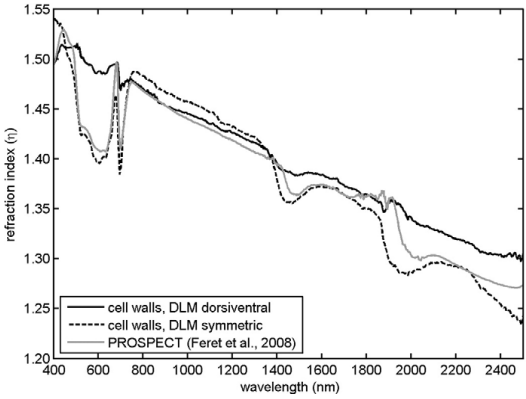

Fig. 4. Inverted spectra of the cell refraction index obtained from (i) DLM with a dorsiventral leaf assumption (ii) DLM with a symmetric leaf assumption and (iii) Feret et al. (2008).

effect; at zones of moderate absorption however, leaf reflectance and transmittance are more sensitive to biochemical content distributions and leaf asymmetry. The refractive index used in symmetric radiative transfer models such as PROSPECT is thus likely to be considered as an effective variable.

4.8. White reflectance and reflectance with a background

Inversion procedures for the estimation of biophysical content from optical measurements often require both reflectance and transmittance spectra. Different attempts have been made to replace both properties with one comprehensive measurement of which the concept of *infinite reflectance* (Allen et al., 1969; Lillesaeter, 1982) is the most widely known. It is defined as the reflectance of an optically thick stack of leaves, where the reflectance no longer increases with an increasing number of leaves. Even though infinite reflectance has important properties for the estimation of scattering and absorption coefficients and for the simulation of canopy reflectance, its practical use in the simulation of leaf optical properties is constrained by the requirement of a pile of almost identical leaves. An alternative and more convenient measure is the adaxial reflectance of leaves with a matte high reflective background (Lillesaeter, 1982), hereafter named *white (adaxial) reflectance* or R_{wh}. Using plate theory, white reflectance can be calculated for an asymmetric layer as:

$$R_{wh} = R_{d,c} + \frac{T_{d,c}T_{b,s}R_{wp}}{1 - R_{wp}R_{b,s}} \quad (8)$$

with $R_{d,c}$ and $T_{d,c}$ the adaxial reflectance and transmittance for collimated light, $R_{b,s}$ and $T_{b,s}$ the abaxial reflectance and transmittance of diffusely scattered light and R_{wp} the (absolute) reflectance of the whitepanel. White reflectance was combined with adaxial reflectance by Merzlyak et al. (2004) to estimate leaf transmittance. This procedure however required the additional assumptions that abaxial and adaxial reflectances and transmittances are equal and that differences between collimated and diffuse light can be ignored. Since this violates both our observations (Section 3) and our model structure and considering the significant errors produced by this estimation procedure, it was preferred here to directly measure and model white reflectance (see Section 2) rather than converting to transmittance. Important optical properties of white reflectance as an alternative to reflectance and transmittance are treated in the sensitivity analysis. Analogously to white adaxial reflectance, also white abaxial reflectance can be defined, but to reduce the total number of optical measures and inversion schemes being discussed in this text, this is not further discussed.

By replacing R_{wp} in Eq. (8) by the reflectance of any other (Lambertian) background, the reflectance of a leaf with different backgrounds can easily be calculated.

5. Sensitivity analysis

The sensitivity analysis is set up to provide more insights into the mechanisms that can cause random or systematic differences between predicted and measured biochemical variables. It breaks down into three modules. The first module assesses the sensitivity of simulated spectra to the model parameters. The second module focuses on the sensitivity to natural variability in a specific absorption spectra. The last module deals with the effects of sampling errors on model inversions.

5.1. Sensitivity of DLM to varying parameter values

The sensitivity of DLM was tested by evaluating differences in model output by the 11 parameters that drive the model. Model outputs considered here are adaxial and abaxial reflectance and transmittance, white reflectance and absorptance. The applied method is a variance based sensitivity analysis using the high dimensional model representation (HDMR) implementation developed by Ziehn et al. (2009). HDMR methods use a large number of randomly generated inputs (within operational parameter ranges) and their corresponding outputs to construct a high-dimensional Analysis of Variance (ANOVA) decomposition of the output dataset. The sensitivity of a parameter is often expressed by the Sobol' index (SI) (Sobol', 2001) that expresses the fraction of the total variance in a dataset explained by an individual parameter x_i (first order terms) or by the cooperative effect (interaction) of two parameters i and j: x_{ij} (second order terms). For a perfect high-dimensional representation, all first and second order terms sum up to one. Lower values indicate unexplained variance. A dataset of 2000 random parameters was generated with stochastic distributions of biochemical contents (C_{chl}, C_{car}, C_w and C_{dm}) derived from the LeuvenV and LOPEX datasets. The stochastic distributions of the seven structure parameters were estimated from initial model inversions of the LOPEX and LeuvenC datasets. For easier visualization the asymmetry effects (β_{pigm}, β_{wdm}, β_{ep} and δ) and BRDF effects (μ and ν) were grouped together. The second order terms of all interaction effects were relatively small and are represented as a single group. Fig. 5 shows the Sobol' indices per wavelength for adaxial and abaxial reflectance, absorptance and white reflectance. For all outputs the chlorophyll and water contents have a large impact on model sensitivity within their respective absorption regions. Dry matter content has a much smaller impact on adaxial and abaxial reflectance indicating that it may be significantly harder to retrieve with good accuracy. This agrees well with reported results of model inversions (Feret et al., 2008; Jacquemoud et al., 1996). Sensitivity to carotenoid content is low for all outputs, but abaxial reflectance and absorptance provide the highest sensitivity. Sensitivity to dry matter content of white reflectance and absorptance in contrast is far higher and dominates the NIR region. This indicates that use of either of both properties may result in more accurate content estimations. f_{air} has a large impact on adaxial and abaxial reflectance in the NIR and noticeable effects in the SWIR but almost no effect on white adaxial reflectance and absorptance. BRDF effects dominate the 400–500 nm region for most outputs and have small but noticeable effects in the higher wavelengths. Adaxial reflectance has a limited sensitivity to leaf asymmetry, mainly for wavelengths in the 1400–2500 nm range while abaxial reflectance is much more sensitive to leaf asymmetry over the entire spectrum. This may complicate the use of abaxial reflectance in content estimations. All outputs are to some extent sensitive to second order terms, which were found to be

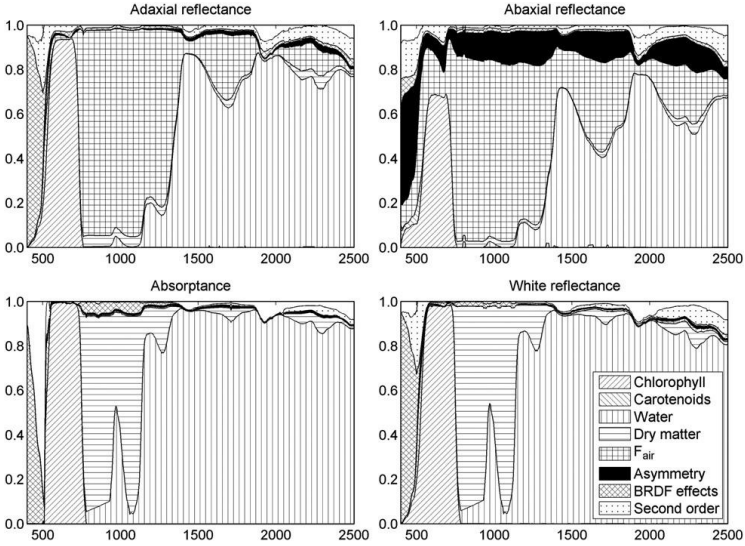

Fig. 5. Sobol' sensitivity index for individual and grouped model parameters and four different optical measures.

mainly composed of interactions between leaf structure and biochemical contents and interactions among biochemical contents (results not shown). For all outputs, a small fraction of the total variance (white part of the graphs) could not be explained by HDMR.

Both absorptance and white reflectance as alternatives to adaxial reflectance and transmittance may improve model inversions in applications where only content estimations (and not leaf structure) are targeted. Sensitivity is highly dependent on the input parameter ranges, which are derived here for fresh and relatively healthy (non-chlorotic) leaves of vegetations grown in temperate climatic conditions. Therefore generalization of these conclusions to other datasets including tropical, chlorotic or senescent leaves should be avoided.

5.2. Sensitivity to variations in specific absorption spectra

This section will focus on (inherent) variability in specific absorption spectra of dry matter and chlorophylls. For water, multiple measured and congruent specific absorption spectra have been published (e.g. Buiteveld et al., 1994; Kou et al., 1993; Segelstein, 1981). We assume that this spectrum is a physical constant – ignoring any variations that may be due to within-leaf chemical bonds with other molecules – and that its published values are sufficiently accurate to ignore any impact on model sensitivity. For chlorophylls and carotenoids, measured spectra in acetone or ethanol are available but with different shifts in peak absorption regions according to the polarity of the solvents. In vivo spectra have been determined by model inversion (Feret et al., 2008). These model based spectra are implicitly based on average proportions of chlorophyll a and b and the different carotenoids, while variations in these proportions can impact model sensitivity. The specific absorption spectrum for dry matter is subject to high uncertainty. The spectrum applied in multiple versions of the PROSPECT model for example, uses a constant value for wavelengths between 450 and 1200 nm which illustrates the difficulties in its estimation. In addition and analogously to chlorophylls and carotenoids, the dry matter specific absorption spectrum is a weighted average of the molecular absorption spectra of all the dry matter components of which (hemi)cellulose, lignin, starch, proteins and sugars are the major groups that are present in different relative proportions in each leaf. The impact of variations in chlorophyll and dry matter specific absorption spectra is assessed with the HDMR global sensitivity analysis as described in Section 5.1. For this purpose, DLM was extended so that the chlorophyll a and b fractions (of the total chlorophyll content) and the (hemi)cellulose, lignin, starch, sugar and protein factions (of the total dry matter content) can be used as inputs. For chlorophyll a and b, specific absorption spectra were used from Maier (2000). Although these spectra were not obtained in vivo and therefore cannot be directly used for model inversions, we assume here that their relative shapes are adequate for assessing the sensitivity to variations in chlorophyll a and b fractions. The stochastic distribution of the chlorophyll fractions is obtained from measured values in the LOPEX dataset (Hosgood et al., 1994). Spectra of different dry matter components as well as their relative distributions were obtained from Fourty et al. (1996). Considering the uncertainty of these estimated spectra, results should only be interpreted qualitatively. Fig. 6 shows an area plot of the Sobol' first order sensitivity indices for leaf absorptivity. For better visualization, all structure parameters and second order terms are grouped together. The influence of different proportions of chlorophyll a and b is almost not noticeable and is limited to a small (<1%) peak between 700 and 750 nm. In contrast, the combined sensitivity to different proportions of (hemi)cellulose, lignin, starch, sugars and proteins suggests a large effect between 700 and 1000 nm that decreases at higher wavelengths. For models where such variations cannot be taken into account, variations in the total leaf dry matter composition will increase the fraction of unexplained variance in optical properties. The NIR region in leaf absorptance spectra, although highly sensitive to total dry matter content, may thus be subject to a significant variability that cannot be explained by only considering the total leaf dry matter content. In addition to the effects of mixture compositions treated here, other factors such as shifts in specific absorption spectra may further increase the fraction of leaf optical properties that cannot be explained.

5.3. Sensitivity of model inversion to sample variability

Thus far we have assumed the measured spectra to be perfect representations of the average biochemical and structural composition. This contrasts to real measurements of leaf spectra where only a

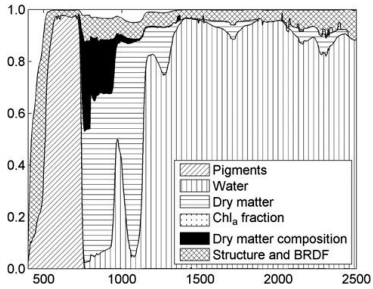

Fig. 6. Sobol' sensitivity index for absorptivity spectrum and variations in dry matter specific absorption spectrum due to differences in fractional contents of lignin, (hemi) cellulose, proteins, sugar and starch.

fraction of the leaf is sampled. In the LeuvenV dataset for example, two measurements per leaf were taken with a spot size of 10 mm. As pointed out by Castro-Esau et al. (2006), the within leaf variability in optical properties can be large compared to the between-leaf variability. This relates well to research by Rascher (2003) who demonstrated that leaves exhibit distinct spatial heterogeneity in photosynthetic efficiency. Using a single or a small number of measurements over a limited area of a leaf may lead to noticeable errors in representing average leaf optical properties. In addition, also reference measurements (spectroscopy and dry and fresh weight) are made on samples (disks) rather than on the whole leaf. The deviation between reference measurements and parameters derived from inversion may thus be significant.

Fig. 7 shows the average within-leaf standard deviation in reflectance of the measurements of the leaves in the LeuvenV dataset. Although these values are relatively small for adaxial and abaxial reflectance (<1%), their impact on the agreement between measured and predicted values of biochemical contents may be significant. The comparably large standard deviation of white reflectance in the NIR can be explained by high amounts of lateral (sideways) scattering due to the interaction of the irregular (nerves) abaxial side with an almost 100% reflecting background: a variable fraction of laterally scattered light is not captured within the sensor field of view. This was confirmed (for both measurements with integrating sphere and leaf probe) by applying different amounts of pressure between the leaf and the whitepanel. Although this effect is ignored in the following analysis, it will be instrumental in explaining observed differences in inversion accuracy in Section 6.2.

To simulate the effects of within-leaf variability, 500 reference model parameter sets were generated, each being a random draw from the distributions of chlorophyll, water, carotenoids and dry matter content in the LeuvenV dataset. Distributions of the structure

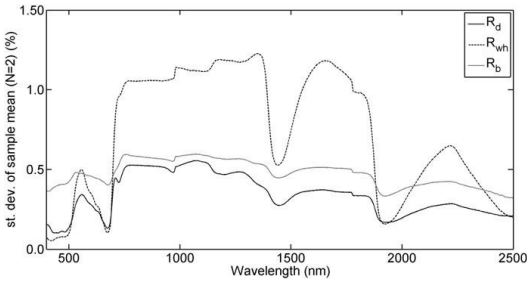

Fig. 7. Average standard deviation in measured adaxial (R_d), abaxial (R_b) and white (R_{wh}) reflectance between two samples per leaf in the Leuven dataset.

and asymmetry parameters were estimated. From each reference set, two subsets (a and b) were derived, each with small random fluctuations in their parameters to simulate the sampling effect. Within-leaf parameter distributions were adjusted to produce standard deviations in reflectance spectra approximately equal to measured values in the Leuven dataset (Fig. 7). From both subsets optical properties were simulated and combined in different inversion schemes to estimate the original parameters in the reference set. All inversion schemes are based on least squares minimization of a cost function H:

$$H = \sum_{\lambda}\left(\widehat{OP}_{a,\lambda} - OP_{a,\lambda}\right)^2 + \sum_{\lambda}\left(\widehat{OP}_{b,\lambda} - OP_{b,\lambda}\right)^2 \quad (9)$$

in which $\widehat{OP}$ denotes the modeled and OP the measured optical properties and depending on the scheme, OP_a and OP_b may stand for reflectance, transmittance or white reflectance. A constrained Nelder–Mead minimization algorithm (Nelder & Mead, 1964) was used. The four biochemical parameters and the structure parameter were estimated while other parameters were fixed at their average values (see also Section 4.5). A larger number of free parameters (e.g. including the asymmetry parameters) resulted in lower accuracies due to ill-posedness (multiple set of parameters exists that results in almost the same optical properties). Six inversion schemes were included:

- a standard inversion using the reflectance (R) from a and the transmittance (T) from b;
- an inversion in which reflectance of a and transmittance of b were combined into absorptance;
- an inversion using the mean of the white reflectance (R_{wh}) of a and b;
- three additional inversions using the previous schemes with the NIR (720–1350 nm) masked out as a rudimentary weighted least squares technique. Masking was motivated by the conclusions of Section 5.1 in which the NIR reflectance and transmittance showed almost no sensitivity to biochemical contents but high sensitivity to leaf structure.

For each biochemical content and for each scheme the root mean square error (RMSE) between reference and inverted values was calculated (Table 2). The rightmost column of the table lists the RMSE between the reference parameters and the averages of subsets a and b. This is the best possible estimate given only subsets a and b as inputs and acts therefore as a lower bound. The standard inversion scheme (column 1) using reflectance and transmittance and the full range of wavelengths has a good accuracy (compared to the optimum) for chlorophyll and water, but produces large errors for carotenoids and dry matter. This agrees with the conclusions from Feret et al. (2008) and expresses the common assumption that only chlorophyll and water contents can be accurately predicted with model inversions. Combining both spectra into absorptance does not change this conclusion although carotenoid estimations improve. Using only white reflectance leads to significant improvements that are not much larger than the lower bound. Masking of the NIR region (columns 4–6) results in a remarkable improvement in dry matter prediction and moderate improvements in carotenoid prediction for all three schemes. This sensitivity analysis marks the importance of an optimal choice of inversion schemes when combining different measurements (e.g. reflectance and transmittance) or when model inversion cannot estimate the full set of model parameters. Optimal results are not assured by the standard inversion scheme that minimizes both errors in reflectance and transmittance over the entire 400–2500 nm range. Since this analysis is entirely model-based, the conclusions do not express a lack of validity in model structure, but rather express errors inherent to sample variability and ill-posedness.

Table 2
RMSE for retrieval of biochemical parameters with different inversion schemes using simulated adaxial reflectance (R) and transmittance (T).

Scheme	R_a; T_b	R_a+T_b	$R_{w,ab}$	R_a; T_b	R_a+T_b	$R_{w,ab}$	Lower bound
Spectral range (nm)	400–2500			400–720; 1350–2500			–
Chlorophyll (g/cm^2)	5.87	5.70	5.18	6.28	6.00	6.44	4.15
Carotenoids (g/cm^2)	5.86	3.06	4.80	3.84	2.74	4.24	0.93
Water (mg/cm^2)	1.17	1.13	0.98	1.29	1.27	1.01	0.97
Dry matter (mg/cm^2)	1.79	1.72	0.56	0.73	0.71	0.43	0.39

Subscripts refer to datasets a and b. $R_{w,ab}$ is the inversion of the average white reflectance of a and b. The last column (lower bound) lists the RMSE for the average parameters of a and b compared to the reference.

6. Validation

In a first validation section the model's capabilities for approximating abaxial and adaxial reflectance and transmittance spectra of different broad-leaved species are tested and an intercalibration between DHR and BRF is made. The second subsection addresses the use of DLM in estimating biochemical content from model inversion.

6.1. Simulation of reflectance and transmittance

A model inversion procedure was set up to jointly fit measured adaxial and abaxial reflectance and transmittance of the LeuvenC dataset (20 leaves) that was collected with an integrating sphere. In a first inversion experiment, the contents of chlorophylls, carotenoids, water and dry matter, the structure parameter (f_{air}), leaf asymmetry parameters (β_{pigm}, β_{wdm} and β_{ep}), the abaxial diffusion parameter (δ) and the BRDF parameter μ were determined by the inversion procedure resulting in a ten parameter inversion. A second experiment compared these results to an inversion using default parameter values for β_{pigm}, β_{wdm}, β_{ep}, δ and μ as determined in Section 4.4 resulting in a five parameter inversion. To assess the relative improvements of a dorsiventral model over a symmetric model, the same dataset was inverted using the PROSPECT model for which simulated abaxial and adaxial optical properties are equal. The quality of the fit is expressed as the root mean squared error (RMSE) between the measured and simulated spectra.

Fig. 8 shows the agreement between measured and simulated (ten parameter inversion) adaxial and abaxial reflectance and transmittance spectra for *Citrus sinensis* L., a species with considerable differences between both faces. The fits of all four spectra show a good approximation between measured and modeled data. The largest differences are present in the NIR and around the 1850 nm water absorption region.

The statistics for all leaves are summarized in Table 3 and show that DLM is capable of representing the optical properties of the reference spectra with an average RMSE of 1.3%. The five parameter version produced overall larger fitting errors (average RMSE is 1.6%) with the largest differences in the abaxial reflectance. The inversions using PROSPECT produced for all spectra larger errors as could be expected for a symmetric model. The spectral fits using DLM in either a five or ten parameter version on combined abaxial and adaxial spectra are equal to or better than those reported in Feret et al. (2008) using the PROSPECT model on only adaxial spectra (RMSE between 1.6% and 3.9%).

An additional experiment was set up to test the theory of Section 4.3 stating that for a specified range of viewing and illumination conditions differences between DHR and BRF only depend on leaf surface structure and not on biochemical content or internal structure. This experiment used adaxial and abaxial reflectance of 12 leaves of the LeuvenC dataset taken with either integrating sphere or leaf probe. The integrating sphere measurements were inverted with a five parameter inversion scheme, identical to the scheme of Section 6.1. The leaf probe measurements were inverted with the same five parameters and the additional parameter ν required for BRF (Section 4.3). Predicted water ($R^2=0.99$), dry matter contents ($R^2=0.97$) and chlorophyll contents ($R^2=0.97$) from both datasets show a good agreement, while predicted carotenoid content had a moderate agreement ($R^2=0.76$). These observations suggest that model inversions with leaf probe and integrating sphere provide consistent results, if model structure accounts for differences between both instruments.

6.2. Parameter estimation

The performance of DLM in the estimation of biochemical contents was evaluated on both the LeuvenV and LOPEX datasets. Multiple inversion schemes are compared implementing the knowledge gathered in the sensitivity analysis (Sections 5.2 and 5.3). In addition,

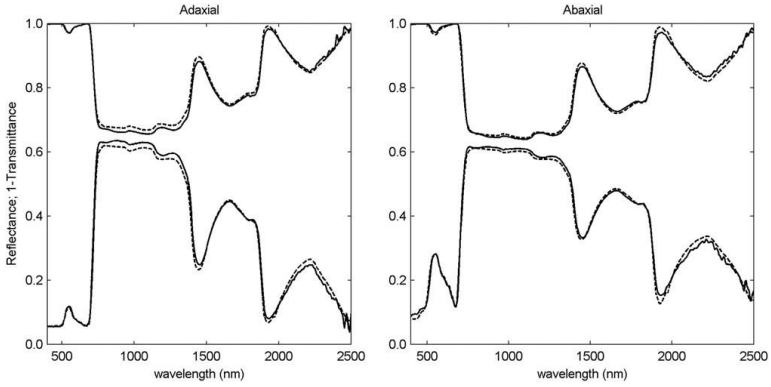

Fig. 8. Measured and simulated spectra of reflectance and transmittance for *Citrus sinensis*.

Table 3
Average and maximum RMSE (% reflectance) of the fit between measured and simulated directional–hemispherical reflectance and transmittance spectra of the LeuvenC dataset using ten and five parameter versions of DLM and PROSPECT.

	Mean RMSE (%)			Maximum RMSE (%)		
	DLM10 param.	DLM5 param.	PROSPECT	DLM10 param.	DLM5 param.	PROSPECT
Adaxial reflectance	1.25	1.59	4.22	2.04	2.88	9.48
Abaxial reflectance	1.39	1.85	6.26	2.95	4.25	10.93
Adaxial transmittance	1.02	1.14	4.82	2.29	2.4	13.06
Abaxial transmittance	1.26	1.37	4.09	2.07	2.43	9.78
Average LeuvenV	1.27	1.56	4.95	1.96	2.51	9.90

DLM is compared to PROSPECT version 5 to investigate whether the prediction of biochemical contents benefits from the use of a dorsiventral model. The four biochemical parameters and the structure parameter are included (free parameters) while for β_{pigm}, β_{wdm}, β_{ep}, δ and μ the average estimated parameters from Section 4.4 are used. For the LeuvenV dataset also ν was included. Attempts to improve the inversion by including one or more additional parameters produced lower prediction accuracies which is ascribed to over-fitting.

The LeuvenV dataset inversion schemes used combinations of adaxial reflectance, white reflectance and abaxial reflectance. For the LOPEX dataset, inversion schemes included combinations of reflectance and transmittance. For both datasets, inversions were made on either the full 400–2500 nm spectral range or with the NIR region (720–1350 nm) masked out. The headers of Tables 4 and 5 give an overview of all schemes.

The schemes and results for the LeuvenV inversion schemes are listed in Table 4. The schemes using only adaxial reflectance (schemes 1 and 2) produce good results for chlorophyll, water and dry matter, but low accuracies of carotenoids. Excluding the NIR (scheme 2) leads to a decrease in accuracy, which indicates that for content estimations from reflectance an accurate estimation of the leaf structure is required. The inversion using unweighted white reflectance (scheme 3) has a large penalty on the accuracy of the dry matter prediction while white reflectance with exclusion of the NIR (scheme 4) provided superior results, with very accurate predictions for chlorophyll, water and dry matter. The accuracy of the dry matter prediction (RMSEr = 0.4 mg/cm^2; R^2 = 0.97) is remarkable since this is traditionally assumed to be hard to estimate on fresh leaf material due to masking by water absorption (Fourty et al., 1996). The cause of the impact of the NIR on estimated dry matter accuracy may be found in different fractional constitutions of the total dry mass, that is expected to be spectrally most pronounced in the NIR (Section 5.2). In addition the large within-leaf variability of white reflectance in the NIR (Fig. 7), attributed to variable amounts of lateral scattering between the leaf and the background (see Section 5.3), may negatively impact the accuracy. Combinations of adaxial and abaxial reflectance (scheme 5) only provided results of moderate accuracy, which indicates that incorporation of abaxial reflectance, which is significantly more sensitive to leaf asymmetry, provides no additional benefits. This conclusion is in agreement with the findings of Section 5.3 since combining two spectra of different types into one inversion may degrade rather than improve results due to sampling errors. Schemes using DLM show a bias (overestimation) of the dry matter contents (RMSE > RMSEr), indicating that the dry matter specific absorption spectrum needs to be scaled when porting from PROSPECT to DLM. The accuracies using PROSPECT 5 (scheme 6) are not noticeably different from those using DLM (scheme 4), although the chlorophyll estimates are more biased while the dry matter estimates are less biased.

Table 5 lists the results of the inversions of the LOPEX dataset. Inversions using only reflectance (scheme 1) or only transmittance (scheme 2) produce good accuracies for water and moderate accuracies for dry matter. The combined use of reflectance and transmittance without band weighting (scheme 3) improves the accuracy for chlorophylls and water, but decreases the accuracy for dry matter. Excluding the NIR (scheme 4) further improves accuracy, with an important decrease in dry matter RMSEr from 1.8 to 1.1 mg/cm2. The combination of reflectance and transmittance into absorptance

Table 4
Statistics of inversion schemes for the Leuven dataset using adaxial reflectance (R_d), abaxial reflectance (T_b) and white reflectance (R_{wh}).

Scheme nr.	1	2	3	4	5	7
Model	DLM					PROSPECT 5
Spectra	R_d	R_d	R_{wh}	R_{wh}	R_d; R_b	R_{wh}
Weighting	Equal	Excl. NIR	Equal	Excl. NIR	Excl. NIR	Excl. NIRs
R^2						
Chlorophyll	0.91	0.87	0.95	0.95	0.81	0.94
Carotenoids	0.53	0.50	0.52	0.58	0.27	0.53
Water	0.90	0.86	0.90	0.94	0.87	0.92
Dry matter	0.90	0.91	0.28	0.97	0.56	0.97
RMSE regression						
Chlorophyll (g/cm^2)	5.6	6.6	4.1	4.1	9.7	4.8
Carotenoids (g/cm^2)	2.7	2.6	2.9	2.5	4.3	2.6
Water (mg/cm^2)	2.0	2.3	2.1	1.6	2.2	1.8
Dry matter (mg/cm^2)	1.0	0.9	2.5	0.4	1.9	0.5
RMSE no regression						
Chlorophyll (g/cm^2)	5.9	6.9	5.6	5.6	11.7	9.7
Carotenoids (g/cm^2)	6.0	4.7	8.4	5.9	5.8	5.5
Water (mg/cm^2)	2.0	2.3	2.5	1.7	2.3	2.0
Dry matter (mg/cm^2)	2.0	1.7	3.0	1.7	3.2	0.8
RMSE spectrum fit	0.5%	0.5%	1%	0.8%	1.2%	0.8%

Table 5
Statistics of inversion schemes for the LOPEX dataset using spectra (adaxial) reflectance (R) and transmittance (T).

Scheme nr.	1	2	3	4	5	6
Model	DLM					PROSPECT 5
Spectra	R	T	R; T	R; T	$R+T$	$R+T$
Weighting	Equal	Equal	Equal	Excl. NIR	Excl. NIR	Excl. NIR
R^2						
Chlorophyll	0.41	0.46	0.57	0.58	0.63	0.64
Water	0.91	0.90	0.94	0.95	0.93	0.95
Dry matter	0.64	0.69	0.49	0.81	0.80	0.80
RMSE regression						
Chlorophyll (g/cm^2)	14.1	15.6	12.4	11.9	11.1	11
Water (mg/cm^2)	2.1	2.7	1.7	1.7	1.8	1.8
Dry matter (mg/cm^2)	1.5	1.4	1.8	1.1	1.1	1.2
RMSE no regression						
Chlorophyll (g/cm^2)	15.0	15.6	12.4	12.7	11.3	11.0
Water (mg/cm^2)	2.4	2.9	1.8	1.8	1.8	1.8
Dry matter (mg/cm^2)	2.2	2.6	4.7	3.1	3.6	3.8
RMSE spectrum fit	0.9%	0.9%	1.4%	1.2%	1.9%	1.8%

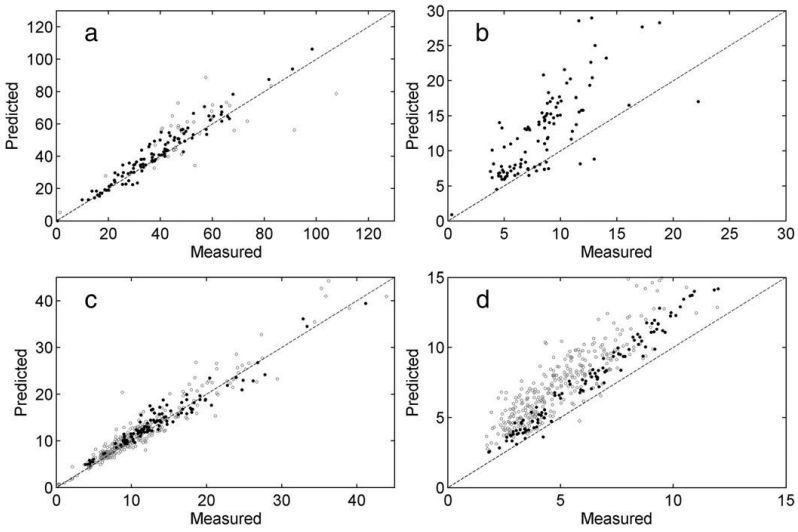

Fig. 9. Comparison between measured and predicted contents of (a) chlorophylls (μg/cm), (b) carotenoids (μg/cm), (c) water (mg/cm) and (d) dry matter (mg/cm) using DLM with parameters from Table 6. (● Leuven, ○ LOPEX).

(scheme 5) provides no clear benefit. The PROSPECT 5 scheme produced almost equal accuracies.

For Tables 4 and 5, the bottom line lists the RMSE of reflectance or transmittance of the fit of the measured on the predicted spectrum. For none of the inversion schemes could this value be related to the accuracy of biochemical content estimates, indicating that improvements in approximating the exact shape of reflectance or transmittance curves may not necessarily lead to a better prediction of leaf biochemistry.

Care should be taken when directly comparing the LOPEX results to the Leuven results. The coefficients of determination should not be compared since they also reflect the variability of the dataset (parameter range), but RMSE values can be compared. The overall accuracies for the predicted water contents are almost equal to the Leuven dataset. The LOPEX accuracies for chlorophyll are significantly lower which may be caused by errors in pigment extraction procedures as reported by Feret et al. (2008). This result agrees with the lower accuracies reported by Jacquemoud et al. (1996) and Feret et al. (2008). The accuracy of dry matter contents is comparable to schemes 1 and 2 of the Leuven dataset that use only adaxial reflectance.

Fig. 9 shows scatter-plots of the measured and predicted values of the four inverted components for the best inversion schemes on both datasets and Table 6 lists extended statistics for these schemes. Two additional parameters were included: the water content as fraction of the total leaf fresh weight and the ratio of chlorophylls to carotenoids. The fraction of water can be estimated with a very high accuracy for both datasets. This also indicates that prediction errors for water and dry matter may be correlated. The low accuracy of the car/chl ratio on the other hand may limit the usability of the carotenoids estimates in biochemical applications. The slope of the regression indicates the bias in the prediction which is acceptable for chlorophyll and water contents. The dry matter content is overestimated (slope < 1) for both the LeuvenV and LOPEX datasets, which indicates that its specific absorption spectrum should be scaled. The same applies to the carotenoid estimates of the LeuvenV dataset. Note that only measured values of the water specific absorption spectrum are available, while other spectra (dry matter, carotenoid and chlorophyll) are determined by inversion procedures and can therefore be model dependent (specific absorption spectra were used from the PROSPECT 5 model). Differences in biases between both datasets may be explained in procedural differences in content estimations (e.g. pigment extraction, weighting).

Table 6
Extended statistics for the best inversion schemes for the Leuven and LOPEX datasets.

Dataset	Leuven	LOPEX
Spectra	R_{wh}	$R+T$
Weighting	Excl. NIR	Excl. NIR
# parameters	6	5
R^2		
Chlorophyll	0.95	0.63
Carotenoids	0.58	
Water	0.94	0.93
Dry matter	0.97	0.80
Car/Chl ratio	0.24	
Fraction of water	0.98	0.93
Slope regression		
Chlorophyll	0.92	1.04
Carotenoids	0.62	
Water	0.97	1.00
Dry matter	0.81	0.63
Car/Chl ratio	0.93	
Fraction of water	1.04	1.16
RMSE regression		
Chlorophyll (g/cm^2	4.1	11.1
Carotenoids (g/cm^2)	2.5	
Water (mg/cm^2)	1.6	1.8
Dry matter (mg/cm^2)	0.4	1.1
Car/Chl ratio (–)	6.4%	
Fraction of water (%)	2.4%	4.1%
RMSE no regression		
Chlorophyll (g/cm^2)	5.6	11.3
Carotenoids (g/cm^2)	5.9	
Water (mg/cm^2)	1.7	1.8
Dry matter (mg/cm^2)	1.7	3.5
Car/Chl ratio (–)	6.7%	
Fraction of water (%)	3.7%	10%
RMSE spectrum fit	0.8%	1.9%

Knowledge gathered from the inversion of leaf optical models can also be applied to the inversion of canopy radiative transfer models. Although governed by different processes, the principles of band weighting and alternative methods to combine different (multi-angular) reflectance spectra may significantly improve the retrieval of canopy biochemistry and structure parameters.

The comparable performance of DLM and PROSPECT 5 on both datasets may imply that no large gains in accuracy are to be expected by introducing more sophisticated models that provide a better representation of leaf internal structure. In explanation of these results, the implicit inclusion of leaf asymmetry into the PROSPECT 5 model (Section 4.7) via the refractive index as an effective parameter can be pointed out. An explicit treatment of leaf asymmetry as is provided by DLM may however become an important factor when a further breakdown of pigments (e.g. chlorophyll a and b) or dry matter (e.g. lignin, cellulose, sugars…) is targeted.

7. Conclusions

In this research, the impact of leaf asymmetry on radiative transfer was modeled and investigated. A dorsiventral leaf model was introduced that considers the asymmetric distribution of pigments, water and dry matter. The differences in light diffusion between adaxially and abaxially incident collimated light are modeled by introducing an abaxial diffusion parameter. Both adaxial and abaxial reflectance and transmittance of a wide variety of leaves can be accurately simulated with good precision. The precise simulations of optical properties of both faces may facilitate improvements in canopy radiative transfer modeling, since dorsiventral properties of leaves can have a significant impact on canopy reflectance. Continued research efforts are required to evaluate this potential.

The sensitivity analysis focused on optimizing the model inversion process. Results indicate that parameter estimation from model inversion may be improved by (i) combining reflectance and transmittance measurements to minimize the impact of leaf structure (ii) adjusting procedures to account for variability in the dry matter specific absorption spectrum and (iii) inversion schemes that minimize the impact of sampling errors. The white reflectance was found to exhibit favorable qualities making it a suitable candidate to replace reflectance and transmittance measurements for parameter estimations.

Knowledge gathered in the sensitivity analysis was applied in different model inversion schemes to retrieve pigment, water and dry matter content for two independently collected datasets, LeuvenV (2008, abaxial, adaxial and white reflectance) and LOPEX (1994, reflectance and transmittance). For the LeuvenV dataset, the white reflectance measure returned the most accurate estimates for all four parameters, provided the NIR (720–1350 nm) was excluded from the inversion process. Additional knowledge on the leaf abaxial reflectance could not improve these estimates. Inversions of the LOPEX dataset demonstrated that by excluding the NIR significant improvements in the estimation of leaf dry matter can be achieved. Overall accuracies for water and dry matter contents in LOPEX were equal to the accuracies in the Leuven dataset for equal inversion schemes. Combinations of two spectra of a different type into a single inversion did not improve accuracies, as was predicted in the sensitivity analysis. The good accuracies for dry matter content estimation may encourage attempts breaking down the total dry matter estimates into cellulose, lignin, protein, sugar and starch components. No impact on content prediction accuracy was found by the use of biconical reflectance measurements instead of DHR. The major improvements in content predictions were found by procedures that account for sampling errors, uncertainly in the specific absorption spectra and variability in specular reflectance rather than by the use of a more sophisticated (dorsiventral) model structure.

Since DLM is designed for broad-leaved species, no tests were performed on coniferous needle-shaped leaves, although the dorsiventral structure of some species with differentiated mesophyll such as *Abies* sp. (Johnson et al., 2005) may prove to be compatible.

DLM has important potential in the study of leaf radiative transfer while it can also be used to relate anatomic differences causing asymmetric scattering and absorption to evolutionary and ontological strategies of plants to optimize the interaction with their light environment.

Acknowledgments

Funding support for this project has been provided by the K.U. Leuven as part of the Special Research Fund program OT04047. The Authors are grateful to the Joint Research Center, Institute for Remote Sensing Applications of the European Commission for freely providing the LOPEX dataset and to professors Stéphane Jacquemoud (Institut de Physique de Globe de Paris & Université Paris Diderot) and Christophe François (Laboratoire Ecologie, Université Paris-Sud) for valuable comments on the model construction.

Appendix A. Supplementary data

Supplementary data associated with this article can be found, in the online version, at doi:10.1016/j.rse.2009.07.014.

References

Allen, W., Gausman, H., Richardson, A., & Thomas, J. (1969). Interaction of isotropic light with a compact plant leaf. *Journal of the Optical Society of America*, *59*(10), 1376—1379.

Allen, W., Gausmann, H., & Richardson, A. (1970). Mean effective optical constants of cotton leaves. *Journal of the Optical Society of America*, *60*, 542—547.

Ashikhmin, M., & Shirley, P. (2000). An anisotropic phong BRDF model. *Journal of Graphics Tools*, *5*, 25—32.

Atzberger, C. (2004). Object-based retrieval of biophysical canopy variables using artificial neural nets and radiative transfer models. *Remote Sensing of Environment*, *93*, 53—67.

Bacour, C., Baret, F., Béal, D., Weiss, M., & Pavageau, K. (2006). Neural network estimation of LAI, fAPAR, fCover and LAIxCab, from top of canopy MERIS reflectance data: Principles and validation. *Remote Sensing of Environment*, *105*, 313—325.

Baldini, E., Facini, O., Nerozzi, F., Rossi, F., & Rotondi, A. (1997). Leaf characteristics and optical properties of different woody species. *Trees*, *12*(2), 73—81.

Baranoski, G. V. (2006). Modeling the interaction of infrared radiation (750 to 2500 nm) with bifacial and unifacial plant leaves. *Remote Sensing of Environment*, *100*(3), 335—347.

Björck, A. (1996). *Numerical methods for Least Squares problems*. Philadelphia, Penn: SIAM books.

Bousquet, L., Lachérade, S., Jacquemoud, S., & Moya, I. (2005). Leaf BRDF measurements and model for specular and diffuse components differentiation. *Remote Sensing of Environment*, *98*(2–3), 201—211.

Buiteveld, H., Hakvoort, J. M. H., & Donze, M. (1994). The optical properties of pure water, in Ocean Optics XII. In J. S. Jaffe (Ed.), *Proc. SPIE, vol. 2258*. (pp. 174—183).

Castro-Esau, K., Sanchez-Azofeifa, G., Rivard, B., Wright, S., & Quesada, M. (2006). Variability in leaf optical properties of Mesoamerican trees and the potential for species classification. *American Journal of Botany*, *93*(4), 517—530.

Cook, R., & Torrance, K. (1981). A reflectance model for computer graphics. *Computer Graphics*, *15*, 307—316.

Cui, M., Vogelmann, T., & Smith, W. (1991). Chlorophyll and light gradients in sun and shade leaves of *Spinacia oleracea*. *Plant, Cell and Environment*, *14*, 493—500.

Dawson, T., Curran, P., & Plummer, S. (1998). LIBERTY — modeling the effects of leaf biochemical concentration on reflectance spectra — Pigments of photosynthetic biomembranes. *Remote Sensing of Environment*, *65*(1), 50—60.

Evans, L., Albury, K., & Jennings, N. (1996). Relationships between anatomical characteristics and ozone sensitivity of leaves of several herbaceous dicotyledonous plant species at Great Smoky Mountains national park. *Environmental and Experimental Botany*, *36*, 413—420.

Feret, J. B., François, C., Asner, G. P., Gitelson, A. A., Martin, R. E., Bidel, L. P., et al. (2008). PROSPECT-4 and 5: Advances in the leaf optical properties model separating photosynthetic pigments. *Remote Sensing of Environment*, *112*(6), 3030—3043.

Fourty, T., Baret, F., Jacquemoud, S., Schmuck, G., & Verdebout, J. (1996). Leaf optical properties with explicit description of its biochemical composition: Direct and inverse problems. *Remote Sensing of Environment*, *56*(2), 104—117.

Govaerts, Y., Jacquemoud, S., Verstraete, M., & Ustin, S. (1996). Three-dimensional radiation transfer modeling in a dicotyledon leaf. *Applied Optics*, *35*(33), 6585—6598.

Habel, R., Kusternig, A., & Wimmer, M. (2007). Physically based real-time translucency for leaves. Rendering Techniques 2007. *Proceedings Eurographics Symposium on Rendering* (pp. 253—263).

Hosgood, B., Jacquemoud, S., Andreoli, G., Verdebout, J., Pedrini, A., & Schmuck, G. (1994). Leaf Optical Properties EXperiment 93 (LOPEX93). *Technical report, Joint*

Research Centre, Institute for Remote Sensing Applications, Unit for Advanced Techniques, TP 272, Ispra (VA), Italy.

Jacquemoud, S., & Baret, F. (1990). PROSPECT: A model of leaf optical properties spectra. *Remote Sensing of Environment*, *34*(2), 75—91.

Jacquemoud, S., & Ustin, S. (2001). Leaf Optical Properties: A state of the art. *8th International Symposium of Physical Measurements & Signatures in Remote Sensing*.

Jacquemoud, S., Verdebout, J., Schmuck, G., Andreoli, G., & Hosgood, B. (1995). Investigation of leaf biochemistry by statistics. *Remote Sensing of Environment*, *54*(3), 180—188.

Jacquemoud, S., Ustin, S. L., Verdebout, J., Schmuck, G., Andreoli, G., & Hosgood, B. (1996). Estimating leaf biochemistry using the PROSPECT leaf optical properties model. *Remote Sensing of Environment*, *56*(3), 194—202.

Johnson, D., Smith, W., Vogelmann, T., & Brodersen, C. (2005). Leaf architecture and direction of incident light influence mesophyll fluorescence profiles. *American Journal of Botany*, *92*, 1425—1431.

Knapp, A., Vogelmann, T., McClean, T., & Smith, W. (1988). Light and chlorophyll gradients within Cucurbita cotyledons. *Plant, Cell and Environment*, *11*, 257—263.

Kou, L., Labrie, D., & Chylek, P. (1993). Refractive indices of water and ice in the 0.65–2.5 µm spectral range. *Applied Optics*, *32*, 3531—3540.

Kubelka, P. (1954). New contributions to the optics of intensely light-scattering materials. Part II: Nonhomogeneous layers. *Journal of the Optical Society of America*, *44*, 330—335.

Kuusk, A. (1991). Determination of vegetation canopy parameters from optical measurements. *Remote Sensing of Environment*, *37*, 207—218.

Lichtenthaler, H. K. (1987). Chlorophylls and Carotenoids: Pigments of Photosynthetic Biomembranes. *Methods in Enzymology*, *148*, 350—382.

Lillesaeter, O. (1982). Spectral reflectance of partly transmitting leaves: Laboratory measurements and mathematical modeling. *Remote Sensing of Environment*, *12*, 247—254.

Ma, K., Baret, F., Barroy, P., & Bousquet, L. (2007). A leaf optical properties model accounting for differences between the two faces. *10th International Symposium on Physical Measurements and Signatures in Remote Sensing, 2007. ISPMSRS07*. International Society for Photogrammetry and Remote Sensing.

Maier, S. (2000). Modeling the radiative transfer in leaves in the 300 nm to 2.5 um wavelength region taking into consideration chlorophyll fluorescence. The leaf model SLOPE. Ph.D. thesis, Technische Universität München, Oberpfaffenhofen (Germany).

McCain, D., Croxdale, J., & Markley, J. (1993). The spatial distribution of chloroplast water in *Acer platanoides* sun and shade leaves. *Plant, Cell and Environment*, *16*, 727—733.

Merzlyak, M. N., Melo, T., & Naqvi, K. R. (2004). Estimation of leaf transmittance in the near infrared region through reflectance measurements. *Journal of Photochemistry and Photobiology. B, Biology*, *74*, 145—150.

Nelder, J., & Mead, R. (1964). A simplex method for function minimization. *Computer Journal*, *7*, 308—313.

Oppenheim, A., & Schafer, R. (1989). *Discrete-time signal processing.* Prentice-Hall.

Pääkkönen, E., Holopainen, T., & Kärenlampi, L. (1995). Ageing-related anatomical and ultrastructural changes in leaves of birch (*Betula pendula* Roth.) clones as affected by low ozone exposure. *Annals of Botany*, *75*, 285—294.

Rascher, U. (2003). Imaging and imagining spatiotemporal variations of photosynthesis of simple leaves. *Nova Acta Leopoldina*, *88*(332), 367—380.

Richter, T., & Fukshansky, L. (1996). Optics of a bifacial leaf: 1. A novel combined procedure for deriving the optical parameters. *Photochemistry and Photobiology*, *63*(4), 507—556.

Schaepman-Strub, G., Schaepman, M., Painter, T., Dangel, S., & Martonchik, J. (2006). Reflectance quantities in optical remote sensing — Definitions and case studies. *Remote Sensing of Environment*, *103*, 27—42.

Segelstein, D.J. (1981). The complex refractive index of water. Master's thesis, Department of Physics. University of Missouri-Kansas City.

Sims, D. A., & Gamon, J. A. (2002). Relationships between leaf pigment content and spectral reflectance across a wide range of species, leaf structures and developmental stages. *Remote Sensing of Environment*, *81*(2–3), 337—354.

Sobol', I. (2001). Global sensitivity indices for nonlinear mathematical models and their Monte Carlo estimates. *Mathematics and Computers in Simulation*, *55*, 271—280.

Stuckens, J., Somers, B., Delalieux, S., Verstraeten, W. W., & Coppin, P. (2009). The impact of common assumptions on canopy radiative transfer simulations: A case study in Citrus orchards. *Journal of Quantitative Spectroscopy and Radiative Transfer*, *110*, 1—21.

Taiz, L., & Zeiger, E. (2006). *Plant physiology*, fourth edition Sunderland, Massachusetts: Sinauer Associates.

Vogelmann, T., & Martin, G. (1993). The functional significance of palisade tissue: Penetration of directional versus diffuse light. *Plant, Cell and Environment*, *16*, 65—72.

Vogelmann, T. C., Bornman, J. F., & Yates, D. J. (1996). Focusing of light by leaf epidermal cells. *Physiologia Plantarum*, *98*(1), 43—56.

Woolley, J. (1971). Reflectance and transmittance of light by leaves. *Plant Physiology*, *47*, 656—662.

Yamada, N., & Fujimura, S. (1991). Nondestructive measurement of chlorophyll pigment content in plant leaves from three-color reflectance and transmittance. *Applied Optics*, *30*, 3964—3973.

Zarco-Tejada, P., Miller, J., Pedrùos, R., Verhoef, W., & Berger, M. (2006). FluorMODgui V3.0: A graphic user interface for the spectral simulation of leaf and canopy chlorophyll fluorescence. *Computers & Geosciences*, *32*, 577—591.

Ziehn, T., Hughes, K., Griffiths, J., Porter, R., & Tomlin, A. (2009). A software tool for global sensitivity analysis of complex models. *Environmental Modelling & Software*, *24*, 775—785.

Background documentation

This document provides background information on various topics in the article.

Section 3, figure 1

Additional abaxial and adaxial directional-hemispherical reflectance and transmittance spectra

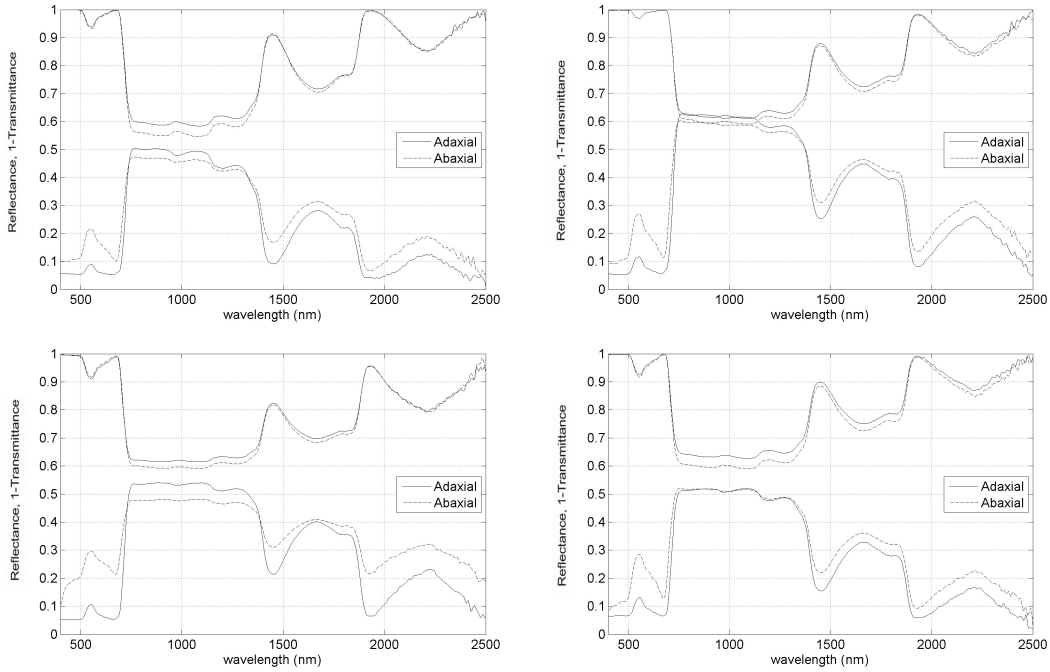

Figure 1: *Schefarella* sp.(top left), *Citrus sinensis* L. (Osbeck) (top right), *Rubus fruticosus* agg. (bottom left), *Prunus laurocerasus* (bottom right)

Section 4.1, equation 1

The analytical solution can be found as follows:

$$
\begin{aligned}
&\frac{\int_0^{\widetilde{\alpha}} e^{-k/cos(\theta)}\ \cos\theta\ \sin\theta\,\mathrm{d}\theta}{\int_0^{\widetilde{\alpha}} \cos\theta\ \sin\theta\,\mathrm{d}\theta} \\
= &\ \frac{-2}{1-\cos^2\widetilde{\alpha}} \int_1^{\cos\widetilde{\alpha}} e^{-k/t} t\,\mathrm{d}t \\
= &\ \frac{-2}{1-\cos^2\widetilde{\alpha}} \left[\left(\frac{e^{-k/t}t^2}{2} \right) |_{t=\cos\widetilde{\alpha}}^{t=1} - \int_{\cos\widetilde{\alpha}}^{1} \frac{t^2}{2}\,\frac{e^{-k/t}}{t^2}\,k\,\mathrm{d}t \right] \\
= &\ \frac{1}{1-\cos^2\widetilde{\alpha}} \left[e^{-k} - e^{-k/\cos\widetilde{\alpha}}\cos^2\widetilde{\alpha} - k\left(e^{-k/t}t\right)|_{t=\cos\widetilde{\alpha}}^{t=1} + k\int_{\cos\widetilde{\alpha}}^{1} \frac{t\,e^{-k/t}}{t^2}\,k\,\mathrm{d}t \right] \\
= &\ \frac{1}{1-\cos^2\widetilde{\alpha}} \left[e^{-k} - e^{-k/\cos\widetilde{\alpha}}\cos^2\widetilde{\alpha} - k\,e^{-k} + k\,e^{-k/\cos\widetilde{\alpha}}\cos\widetilde{\alpha} - k^2 \int_{\frac{k}{\cos\widetilde{\alpha}}}^{k} \frac{e^{-u}}{u}\,\mathrm{d}u \right] \\
= &\ \frac{1}{1-\cos^2\widetilde{\alpha}} \left[e^{-k}(1-k) + e^{-k/\cos\widetilde{\alpha}}\cos\widetilde{\alpha}\,(k-\cos\widetilde{\alpha}) + \int_k^{\infty} \frac{e^{-u}}{u}\,\mathrm{d}u - \int_{\frac{k}{\cos\widetilde{\alpha}}}^{\infty} \frac{e^{-u}}{u}\,\mathrm{d}u \right] \\
= &\ \tfrac{1}{1-\cos^2\widetilde{\alpha}} \left[e^{-k}(1-k) + e^{-k/\cos\widetilde{\alpha}}\cos\widetilde{\alpha}\,(k-\cos\widetilde{\alpha}) + E_1(k) - E_1\left(\tfrac{k}{\cos\widetilde{\alpha}}\right) \right]
\end{aligned}
$$

Section 4.3, equation 5

We will provide the proof that when light is perpendicular to the surface, $\theta_a = \alpha = \theta_v/2$ and $BRDFs$ no longer depends on φ_v.

If $\theta_s = 0$ then

$\cos 2\theta_a = \cos\theta_s\cos\theta_v + \sin\theta_s\sin\theta_v\cos\phi = \cos\theta_v$ so that $\theta_a = \frac{\theta_v}{2}$

$\cos\alpha = \frac{\cos\theta_s + \cos\theta_v}{2\cos\theta_a} = \frac{1+\cos\theta_v}{2\cos\frac{\theta_v}{2}} = \frac{2\cos^2\frac{\theta_v}{2}}{2\cos\frac{\theta_v}{2}} = \cos\frac{\theta_v}{2}$ so that $\alpha = \frac{\theta_v}{2}$

Since θ_a and α no longer depend on φ_v, of the terms in equation 5, only G (shadowing term) is defined as a function of φ_v. However:

$G(\theta_s, \theta_v, \varphi_v) = \min(1, E_1, E_2)$

with $E_1 = \frac{2\cos\alpha\ \cos\theta_v}{\cos\theta_a} = 2\ \cos\theta_v$ and $E_2 = \frac{2\cos\alpha\ \cos\theta_s}{\cos\theta_a} = 2$

so $G = \min(1,\ 2\ \cos\theta_v)$

Therefore, for normal incidence, $BRDF_s$ does not depend on the relative azimuth.

Section 4.3, equations 6 and 7

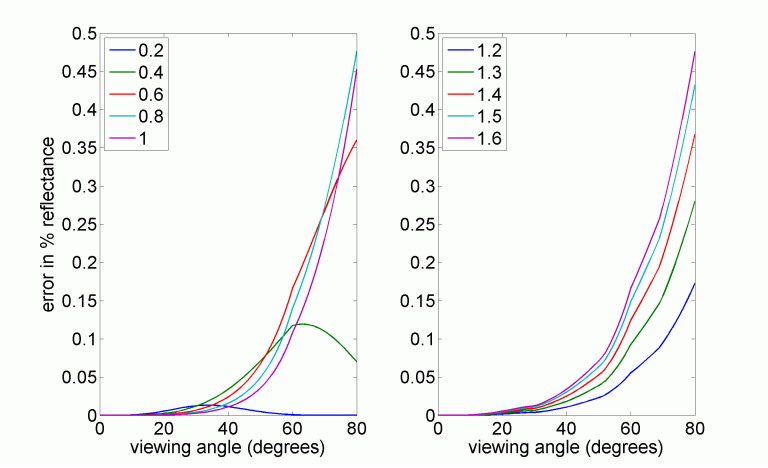

Figure 2: Maximum error of the approximation of equation 6 (BRF). Left: maxima (over all values of refractive index) for different values of surface roughness (σ). Right: maxima (over all values of surface roughness) for different values of refractive index (η)

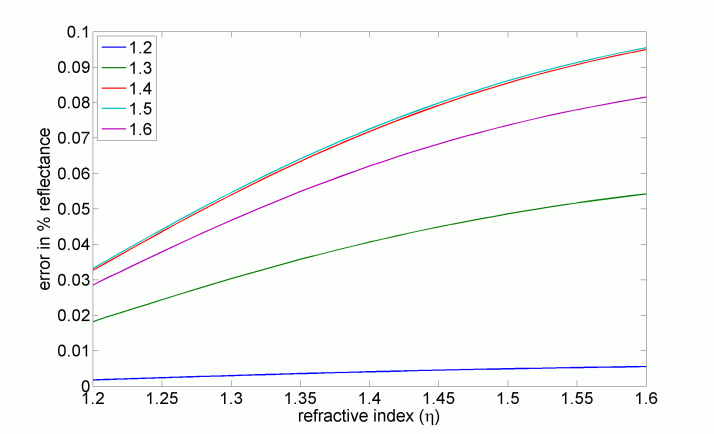

Figure 3: Error of the approximation of equation 7 (DHR) for different values of surface roughness (σ) as a function of the refractive index (η)

Section 6.1, comparison between leaf probe and integrating sphere

The following six figures show adaxial (top) and abaxial (bottom) reflectance of six leaves of the LeuvenC dataset, measured with an integrating sphere (blue line) and with a leaf probe (red line). According to the theory developed in section 4.3, the difference between the red and blue lines should only be determined by the glossy/specular reflectance of the leaves and should not reflect the leaf interior structure or biochemical contents. For a spectrally constant refraction index, this difference would be spectrally constant. For wavelength dependent refractive index (decreasing with increasing wavelength, according to figure 4) , the difference would be expected to monotonically decrease. The difference graph at the bottom shows that differences for the six leaves are within a 2% range.

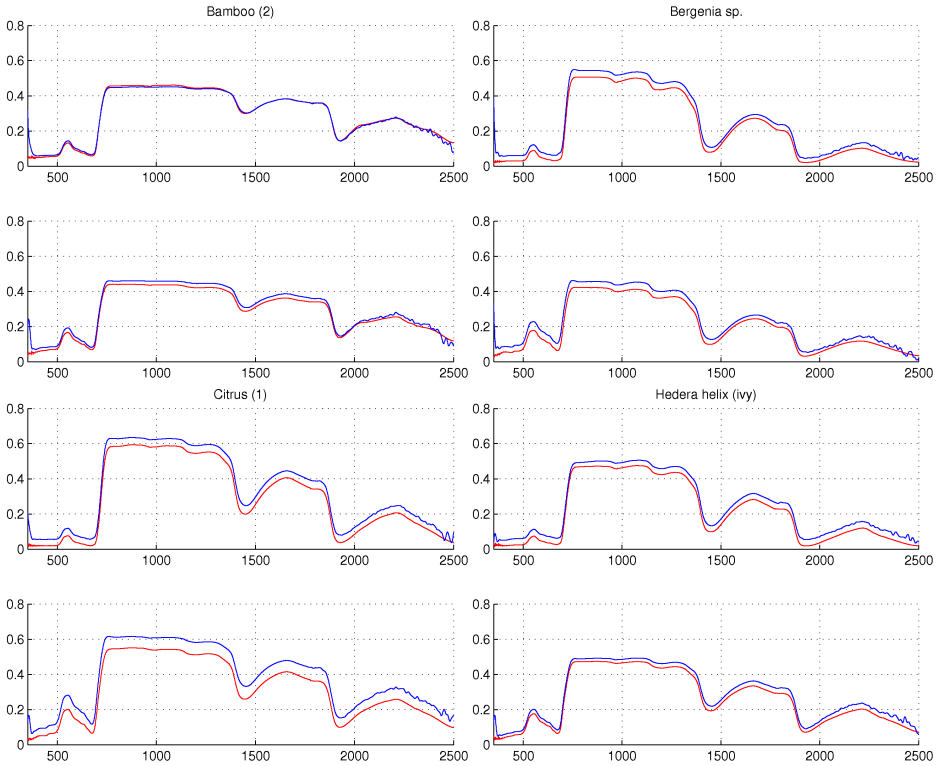

Figure 4: Adaxial (top) and abaxial (bottom) reflectance spectra measured with leaf probe (red) and integrating sphere (blue) for six different leaves.

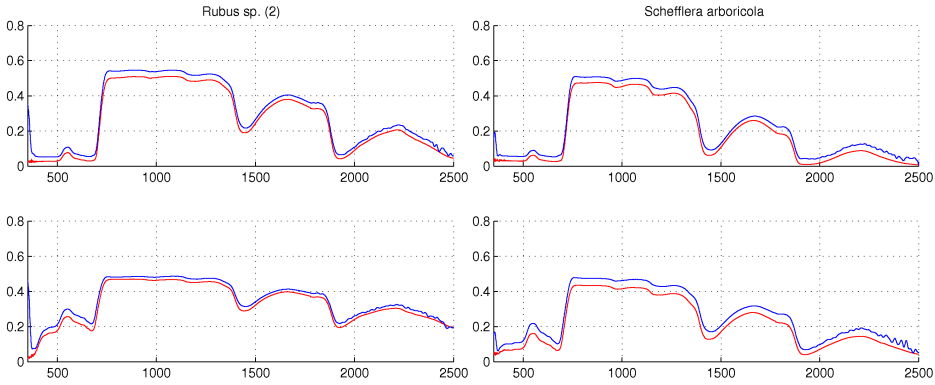

Figure 5: Adaxial (top) and abaxial (bottom) reflectance spectra measured with leaf probe (red) and integrating sphere (blue) for six different leaves (continued).

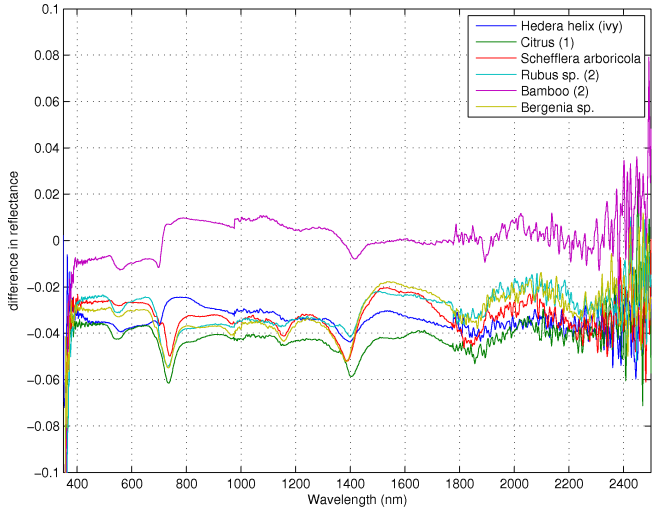

Figure 6: Differences in reflectance between leaf probe and integrating sphere for six leaves.

Errata

Section 5.1:

"The sensitivity of a parameter is often expressed by the Sobol' index (SI) (Sobol', 2001) that expresses the fraction of the total variance in a dataset explained by an individual parameter x_i..."

should be:

"The sensitivity of a parameter is often expressed by the Sobol' index (SI) (Sobol', 2001). SI expresses the fraction of the total variance of an output variable by the variation of the constant value of an individual parameter x_i..."

Section 6.2, table 6:

Ideally, R^2 values for both the LeuvenV and LOPEX datasets should be compared with inversions using equal numbers of inverted model parameters (now 6 and 5 respectively). Due to the inherent difference between both datasets with respect to spectrum collection, the LeuvenV required an additional parameter (ν) to account for less stable glossy reflections by the contact probe. The LOPEX dataset was collected using an integrating sphere and did not require this additional parameter.

Chapter 4

The impact of common assumptions on canopy radiative transfer simulations: a case study in Citrus orchards

Published as: Stuckens, J., Somers, B., Delalieux, S., Verstraeten, W.W., Coppin, P., 2009. The impact of common assumptions on canopy radiative transfer simulations: A case study in Citrus orchards. Journal of quantitative spectroscopy & radiative transfer 110, 1-21.

Contents lists available at ScienceDirect

Journal of Quantitative Spectroscopy & Radiative Transfer

journal homepage: www.elsevier.com/locate/jqsrt

The impact of common assumptions on canopy radiative transfer simulations: A case study in *Citrus* orchards

J. Stuckens *, B. Somers, S. Delalieux, W.W. Verstraeten, P. Coppin

M3-BIORES, Biosystems Department, Katholieke Universiteit Leuven, W. De Croylaan 34, 3001 Leuven, Belgium

ARTICLE INFO

Article history:
Received 2 June 2008
Received in revised form
2 September 2008
Accepted 2 September 2008

Keywords:
Canopy model
Ray tracing
Bidirectional reflectance
Row orientation
Diffuse illumination

ABSTRACT

Radiative transfer (RT) models for canopies entail multiple implicit and explicit assumptions. In this case study six different commonly used assumptions were evaluated on a detailed virtual orchard model. This model was constructed in a physically based ray-tracing environment using detailed sub-models for the description of tree geometry, leaf and soil bidirectional reflectance and diffuse illumination. After calibration and validation with both the RAMI Online Model Checker (ROMC) and field data obtained in a Citrus orchard in Wellington, South Africa, the model was used as a reference to analyze the different assumptions. A first set of three assumptions focused on leaf optical properties, evaluating the effect of the spectral mixing of randomly distributed leaves and trees, leaf asymmetry and leaf bidirectional reflectance and transmittance. The fourth assumption investigated the structure effects of variations in leaf shape and leaf curl. Finally, the last two assumptions were tested at the orchard level and dealt with the row orientation of trees and the angular distribution of diffuse irradiance. Errors induced by each assumption were evaluated in side-by-side comparisons with the reference. Only for the first assumption no measurable error could be detected. All other assumptions caused variable relative errors of up to 70%. The size of the errors was found to be spectrally variable and depends on canopy structure, leaf optical properties and illumination conditions. Corrections with minimal additional complexity in implementation in 3D RT models were suggested.

1. Introduction

1.1. Advances in canopy radiative transfer modeling

Description and simulation of radiative transfer (RT) processes in canopies are an active research topic in the remote sensing community. RT in canopies has been described and investigated by plane–parallel models, geometric optical models and computer simulation models [1]. Plane–parallel models represent a canopy as a horizontally infinite turbid or discrete scatterers medium. Geometric optical models represent a (forested) canopy macrostructure by simple geometric primitives such as ellipsoids or cones shaped as a hull around the foliage. Computer simulation models represent a canopy by an exact positioning of leaves and branches as ensembles of simple geometric primitives such as triangles and disks. Implementations of these models may be achieved by using analytic or stochastic methods or a combination thereof [2]. Analytic techniques attempt to obtain an exact or approximate solution to the RT equation. To make such a solution

* Corresponding author. Tel.:+32 16 32 97 49; fax: +32 16 32 97 60.
E-mail addresses: Jan.Stuckens@biw.kuleuven.be, Jan.Stuckens@hotmail.com (J. Stuckens).

0022-4073/$ - see front matter © 2008 Elsevier Ltd. All rights reserved.
doi:10.1016/j.jqsrt.2008.09.001

feasible, multiple generalizations and assumptions are made on the nature of the medium (canopies), on the distribution of light or on the nature of light-matter interactions. Stochastic techniques, which are usually applied for solving computer simulation models, most often rely on a Monte-Carlo approach in which a large number of rays are traced through the canopy. The reflection and transmission of light are governed by separate sub-models that may simulate specular, glossy or matte surface properties. The accuracy of this approach is mainly limited to the level of detail of the geometric primitives and the appropriateness of the used sub-models. While expected to be potentially more accurate than plane–parallel or geometric optical models [3], the challenge for most Monte-Carlo methods is the required relatively large amount of processing power due to their stochastic nature. Continuous advances in algorithmic efficiency [4], the use of lookup tables and neural networks for model inversion [5] and the continuous increase in computer processing power may be able to overcome these limitations in the near future.

As knowledge on the nature of light interactions in vegetation canopies advanced, models of all types have gone through an evolution of increased consistency and a more precise representation of the 'ground truth'. While becoming more holistic, the number of parameters required for running these models increases, demanding a larger knowledge of the characteristics of the investigated plots. As such, limitations in accuracy may shift from the algorithmic nature to the users' knowledge on the modeled system.

1.2. Overview of assumptions

In both model construction and use, assumptions are made concerning the nature of the system, which includes canopy architecture, incident light distribution and surface reflection. While the implications of some assumptions have already been scope of active research (e.g. the effect of leaf elevation angle [6]), many other assumptions are often being overlooked by model users or have not yet been implemented in frequently used RT models. The goal of this research is the evaluation of a selection of assumptions for which a detailed and validated reference model exists or can be constructed to evaluate the validity of and the errors introduced by these assumptions. Six assumptions have been tested. The first set of four concerns individual tree canopies and is relevant for all spatial scales of remote sensing. The last set of two concerns entire orchards or orchard blocks and is relevant for medium- and low-resolution remote sensing, for which the individual pixel size exceeds the size of an individual tree crown:

1. *The averaging of the optical properties of randomly distributed leaves (scatterers) in a canopy.* Spectral/spatial variability of scatterers has been implemented in RT models in different ways: plane–parallel models may subdivide the canopy into multiple homogeneous parallel layers, each with a different set of optical properties [7,8]. Geometric optical models may discern different categories of crowns in a scene, each with its own size, shape, distribution and optical properties. Computer simulation models are theoretically capable of simulating any distribution of optical properties, including the effects of woody elements [9], but most implementations assume constant optical properties of all scatterers within a crown. Moreover, field studies tend to rely on measured averaged spectra of a sufficiently large sample of randomly picked leaves and neglect the stochastic (e.g. variance, skewedness) and/or spatial distribution of the data. Testing of this assumption, however, is limited to the stochastic variability and does not include non-random spatial distribution patterns of optical properties such as the occurrence of shadow leaves in the interior and lower parts of the canopy.
2. *Ignoring of the abaxial optical properties of leaves.* Most models and field studies ignore leaf asymmetry that causes different reflectance and transmittance of adaxial and abaxial sides due to the asymmetric distribution of chlorophyll in the parenchyma and mesophyll layers or due to different cuticular wax layers. Generally, only adaxial reflectance and transmittance data are collected.
3. *Representation of leaves as Lambertian scatterers.* The bidirectional scattering distribution function (BSDF) of leaves is often represented by a simple Lambertian (matte) reflectance and transmittance. Models have been developed to accurately represent the specific BSDF of leaves, which is generally assumed to be caused by glossy reflection of leaf wax [10]. Some of these have been implemented in canopy reflectance models either by applying a correction for specular reflectance of the wax layer [5–7] or as a full BSDF sub-model integrated in a ray tracer [11]. Obtaining validated and realistic parameter settings for surface roughness, however, is often a practical issue. Moreover, the Lambertian model has been validated by Chelle [12], who did not find any notable difference in canopy light absorption (not reflectance) between a Lambertian and a non-Lambertian model for dense crop canopies. Hence, the simplicity of the Lambertian model, from a practical point of view, is appealing.
4. *Representation of leaves as simple geometric surfaces.* The specific shape of leaves is generally not considered in practical applications and only the average leaf area is being used as an input parameter. Although computer simulation models are capable of simulating leaves of complex geometries, typical representations for broadleaved species still rely on simple and flat surfaces of triangles, disks or ellipses, ignoring any reduction in exposed leaf area due to curling or folding of leaves. The importance of leaf shape in coniferous trees has already been pointed out by Disney et al. [13], who simulated significant differences in off-nadir canopy reflectance when using different models for needle cross-section. Future applications may replace the factual geometric representation of leaves by integrating the spectral invariants theory in analytic RT models [14] combined with the use of effective leaf area values.

5. *Ignoring of row orientation when simulating radiative transfer for orchards, row crops and plantations.* When row orientation is not considered, radiative transfer reverts to the case of sparse canopies with randomly positioned trees. Row orientation was found to have a significant impact on canopy reflectance and absorption [15]. While the implementation of row orientation is not really limiting for Monte-Carlo computer simulation models (may allow exact positioning of tree crowns), most fast and invertible analytic solutions have not been adapted so far. Some simplified analytical implementations exist that focus on the effect of row orientation on the first-order scattering [16], while for higher orders of scattering, solutions for homogeneous media are applied on the vegetated fractions within the rows. As a consequence, in such analytical models lateral fluxes, which can be significant [17], are often not correctly modeled.
6. *Ignoring of diffuse sky irradiance or approximation by a homogeneous distribution of diffuse irradiance.* Many recent RT models consider diffuse light, but assume an isotropic sky model and ignore the angular distribution that is typically higher in the circumsolar region (corona). Research in atmospheric sciences has resulted in multiple models to describe the angular distribution of diffuse irradiance, ranging from simple formula-type models such as the CIE sky models [18] to atmospheric radiative transfer models [19]. The importance of this item has already been pointed out by Govaerts [20], who implemented a CIE formula for diffuse illumination.

1.3. Testing environment

In order to test the aforementioned assumptions, a physically based Monte-Carlo ray tracer, an accurate representation of tree geometries and state-of-the art sub-models for leaf and soil reflectance and diffuse illumination are applied. Due to the high variability inherent to natural environments and the associated difficulties of obtaining accurate and representative ground data, all assumptions have been tested using simulated data. In this case study, an orchard block of Sweet orange (*Citrus sinensis* (L.) Osbeck var. Valencia Midknight) was used as a proxy for assumption testing. The main motivation is that *Citrus* combines multiple aspects that allow testing of important RT model assumptions in a realistic simulation including row orientation of trees, glossy reflection, asymmetric leaf structure and leaf curl. The use of a real crop rather than one or more 'synthetic' trees or crops allows calibration of spectral and structure properties and a validation of the reference situation prior to simulations. While RT models are being constructed for multiple ranges of the electromagnetic spectrum, including radar and thermal domains, this research focuses on the visible (VIS, 400–700 nm), near-infrared (NIR, 700–1400 nm) and short-wave infrared (SWIR, 1400–2500 nm) wavelengths.

The basic assumption of this study is that more simplified models can be validated—to a certain degree—using more detailed and holistic models as a reference. Such detailed analysis is expected to provide new insights by exposing weaknesses in current assumptions. Meanwhile, it provides users with insight on the magnitude of errors inherent to each model and may lead to new advances in canopy RT modeling.

1.4. Limitations of the research

As this research focuses on the within-canopy RT, atmospheric effects are not explicitly taken into account with the notable exception of diffuse incident radiance. This is treated with higher detail as variation in illumination geometry is expected to cause differences in within-canopy RT. Atmospheric effects not being considered here include path radiance and adjacency effects, both of which are expected to play no vital role in the within-canopy RT. The simulated output is thus top-of-canopy (TOC) rather than top-of-atmosphere. The default ray-tracer output in radiance units was converted into directional reflectance factors by dividing the radiance by the radiance of an infinite 100% reflective Lambertian horizontal surface at the TOC.

Assumptions on the characteristic of the ray-tracing environment include linearity (the combined effect of two inputs equals the sum of both), energy conservation (light scattering can never produce additional energy [21]) and the absence of fluorescence and polarization effects. Note that a fluorescence-enabled canopy RT model was introduced in [22]. Additional assumptions made in this study are mostly related to the canopy architecture and include:

- The random distribution of optical properties of leaves within a tree canopy (see assumption 1).
- Representation of leaves by two-dimensional surfaces, ignoring the within-leaf RT that is a result of the specific 3D organization of cells and organelles [23] or photo-orientation of chloroplasts.
- Random leaf azimuthal angles. This ignores growth or diurnal rotations of leaves towards (heliotropism) or away from the sunlight. See also Cohen and Fuchs [24], who found a south-east azimuthal preference in north-east-oriented citrus orchards.
- The simulations concern non-flowering and non-fruiting trees.
- Excluding the effects of participating media. This involves all processes of absorption and scattering by the air layer within and between the canopies.
- Assumptions related to the architecture of the different sub-models, such as the representation of leaf cuticles by microfacets, the simulation of backscatter in soil bidirectional reflectance distribution functions (BRDF) [25] or the scattering theories in atmospheric RT models [19].

2. Materials and methods

2.1. Field data collection

All reference data for calibration and validation were collected in a 9-year-old Valencia 'Midknight' orange grove near Wellington, South Africa (33°36′S; 18°56′E, altitude 100 m), during two field campaigns from August until October in 2006 and 2007. The orchard block had a row spacing of 4.5 m, a tree spacing of 2 m and a row azimuth of 7.3°. Average tree height was 3 m.

Canopy and leaf reflectance spectra were collected using an ASD FR spectroradiometer (Analytical Spectral Devices, Boulder, CO) ranging from 350 to 2500 nm with a spectral resolution of 3 nm in the VIS and NIR and 10 nm in the SWIR. A 25° field of view (FOV) bare fiber optic was used. Within the orchard, 60 trees were selected that span the range of structural and spectral variability encountered in the orchard. For each tree, structure parameters were collected including tree height, crown width and crown diameter. Additionally, per tree eight hemispherical photos were taken near the trunk of the tree with a Kodak DCS 660 6.2 megapixel digital camera using a Sigma 8 mm fisheye lens with a 137° FOV. For a more detailed description of the field campaign, see [26]. For 45 reference trees, leaf reflectance spectra were taken per tree from 60 randomly picked leaves in the TOC. For the reference trees, five canopy spectra per tree were taken from 1.5 to 2 m above the TOC.

2.2. Reference model development within a ray-tracing system

All results have been simulated using an extended version of the PBRT ray tracer [21]. This is a 'physically based' rendering system to model the interaction of light and matter. The PBRT system is designed as an extensible software package by the use of a plug-in architecture. This enables the implementation of different models for surface reflection, illumination and camera types. Within the ray-tracing environment, a scene is made up of different components each corresponding to a sub-model: (i) illumination sources, (ii) a sensor platform, (iii) geometry descriptions, (iv) material optical properties and (v) an integrator. The sub-model implementations are described in the sections below.

2.2.1. Illumination

The scene illumination was simulated using the combination of two light sources: a directional light source for the direct (unscattered) light and a skymap that contains the angular distribution of diffuse light. Both direct and diffuse light were calculated using the SBDart RT code [19]. This code was configured to compute the at-ground (ir)radiance after atmospheric interaction, including gaseous absorption, Rayleigh and Mie scattering. Aerosols, water vapor and ozone concentrations were determined by presets for rural areas at mid-latitudes (2.9 g cm^{-2} H_2O and 0.32 atm-cm O_3). The sky was assumed to be cloud-free with a good horizontal visibility (30 km at 550 nm).

Both direct and diffuse illuminations were calculated from 350 to 2500 nm with a 10 nm interval. Because of the relatively small bandwidth, a filter function was not applied. Direct illumination was calculated as the total direct downward flux (W m^{-2} μm^{-1}) at ground altitude. Diffuse illumination (radiance units or W m^{-2} μm^{-1} sr^{-1}) was calculated for the entire hemisphere in steps of 2° in azimuth angle and 1° in zenith angle.

Skymaps were generated for different solar elevations and azimuths that correspond to different points in time. For tree-level calculations, the reference solar elevation and azimuth were 56.4° and 356.4° (March 21, 13 h local time, maximum solar elevation) unless stated otherwise. For orchard-level simulations, solar positions were calculated for six points in time on March 21, June 21 and December 22 (spring equinox, summer and winter solstice) and for each day at 10 and 13 h local time. The corresponding azimuths and elevations can be found in Table 1. The three simulations at 13 h cover the minimal, average and maximal annual solar elevations with the sun near 0° azimuth (no row shadowing for a north–south-oriented orchard), while the 10 h simulations with different solar azimuths cause variable amounts of row shadowing.

Table 1
Solar positions and percentage of direct irradiance at 400 and 2400 nm for six different illumination conditions

Time	Solar elevation (°)	Solar azimuth (°)	% Direct irradiance	
			400 nm	2500 nm
December 22, 10 h	52.9	85.0	53	97
December 22, 13 h	79.2	339.6	60	97
March 21, 10 h	37.5	59.4	44	96
March 21, 13 h	56.4	356.4	54	97
June 21, 10 h	20.6	40.5	23	93
June 21, 13 h	32.8	356.1	39	95

Table 2
Structure parameters of measured and simulated trees

	Field data		Simulation	
	Average	St. dev.	Average	St. dev.
Tree height (m)	2.92	0.31	2.98	0.32
Crown width within row (m)	2.00	0.22	2.10	0.19
Crown width perp. to row (m)	2.56	0.37	2.45	0.32
Leafless part of the trunk (m)	0.51	0.08	0.54	0.12
Leaf area (m^2)	–	–	25.7	9.6
Leaf area index	7.0	2.6	6.3	2.1
Leaf angle (°)	–	–	57	22
Leaf number	–	–	8269	3123
Trunk base width (m)	0.40	0.05	0.39	0.05
Average leaf area (m^2)	0.0029	0.0012	0.003	0
Leaf length/width	–	–	1.6	
Leaf curl (%)	–	–	20	

The percentage of total direct irradiance depends on wavelength and solar position and ranged from 23% for a low solar elevation at 400 nm to 97% for a high solar elevation at 2400 nm. Minimum (400 nm) and maximum (2400 nm) values are reported in Table 1.

2.2.2. Camera and detector

A 216 band hyperspectral sensor was simulated with spectral range from 350 to 2500 nm and a 10 nm spectral resolution. Sensor noise, drift, stray light and spatial and spectral point spread functions are ignored, assuming a perfect sensor.

The scenario simulations used an orthographic projection camera without any geometric distortions for which outputs are expressed as hemispherical–directional reflectance. In simulations at the tree level, the same virtual camera type with a rectangular spot size of $1.5 \times 1.5\ m^2$ was placed over the canopy center. This ensured that the sensor's retrieved signal contained no significant fraction of soil with the exception of soil visible through canopy gaps. The simulations in the validation experiment used a 25° FOV projective camera that produces hemispherical–conical reflectance to better approximate the spectroradiometer FOV. Additional simulations used a goniometer camera model for obtaining the canopy bidirectional reflectance distribution of the hemisphere. The goniometer was modeled as a rotating sensor positioned in all hemispherical positions above the target, for each position looking at a central representative area of the tree or orchard.

2.2.3. Geometry description

The scene geometry involved the construction of 3D tree geometry. Leaves, branches and trunk were built as triangular meshes using an implementation tree geometry algorithm developed by Weber and Penn [27]. The original program code, called Arbaro [28], was modified to allow more realistic simulation of *Citrus* trees. Modifications include different options for trunk splitting (grafting), pruning, topping, leaf angle changes and leaf curling. Note that leaf curl is modeled as a triangle mesh by folding the lateral ends of a leaf around an imaginary cylinder with the adaxial side inwards (Fig. 2, bottom right). A curl of 100% means that both lateral ends touch. For curled leaves, the triangles that form a leaf mesh each have a different normal. As a consequence, leaf angle distributions are computed by weighting each triangle of each leaf with respect to its area.

From the test plot, ten representative trees were selected and their structure was reconstructed as accurate as possible. Calibration parameters include branch width and height, crown width, crown height, average leaf width and length. The number and distribution of leaves for each tree were calibrated by comparative analysis of gap fraction distributions and fractal dimension of both real and ray-tracing-simulated hemispherical photos. The procedure for gap fraction and fractal dimension analysis steps is described in [29]. Important structure parameters of the simulated trees are listed in Table 2. Fig. 1 shows an example of a hemispherical photograph of a reference and a simulated tree.

For the orchard-level simulations, random instances (clones) of the reconstructed prototype trees were placed in the correct orchard geometry as illustrated in Fig. 2. Within the rows, 11% of the tree positions were left void to account for an equal fraction of missing trees in the field plot. Between the rows, weeds were simulated. As weeds did not have a homogeneous but rather a clustered distribution, weed patches were simulated and randomly distributed between the rows to allow a more realistic simulation of 'clumped' weed occurrence. Within each patch, leaves were simulated as randomly placed disks with a fixed leaf area of $5\ cm^2$, a random height between 0.0 and 0.5 m above the ground and a total LAI per patch of one. For the leaf orientation, the elliptical distribution of Kuusk [7] was used with an eccentricity ε of 0.9 and an average leaf angle of 45°, to simulate partly erectophile grasses. Weed height and LAI were obtained from field estimates. Leaf area was determined by the minimal area that was computationally possible since the true average leaf area of the dominant species (*Lolium* sp.) was smaller. The total size of the simulated block was $130 \times 130\ m^2$ and simulations were limited to the $100 \times 100\ m^2$ central area to avoid errors due to lateral radiation fluxes.

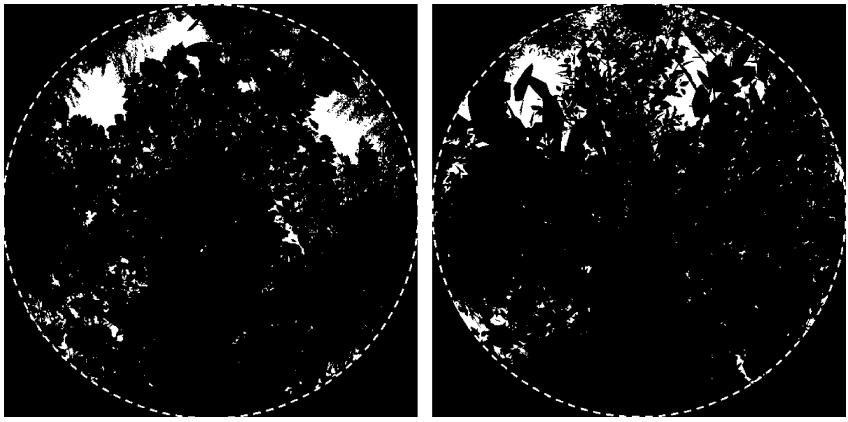

Fig. 1. Real (left) and simulated (right) pictures of B/W threshold images of a hemispherical view positioned at the trunk base (bottom).

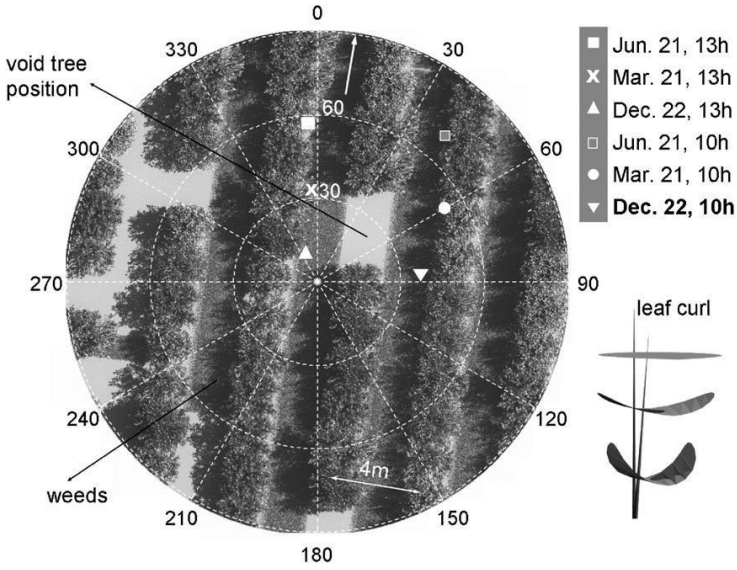

Fig. 2. Overview of orchard layout and solar illumination positions. The top arrow indicates the row orientation. Simulation for a clear sky illumination of December 22, 10 h (elevation 52.9°; azimuth 85°). The bottom-right image shows three leaves with from top to bottom 0%, 20% and 40% curl.

2.2.4. Material optical properties

2.2.4.1. Tree leaves. For tree leaves a BSDF model was developed consisting of (i) an implementation of the microfacets model of Bousquet et al. [10] to simulate the specular/glossy reflectance of leaves, (ii) a Lambertian component for the diffuse reflectance, (iii) Lambertian transmittance and (iv) different optical properties for abaxial and adaxial sides.

(i) The Bousquet microfacets model calculates BRDF (f) as the product of a Fresnel reflectance term (F), a microfacets distribution term (D) and a shading term (G):

$$f_{\mathrm{dd,microfacets}}(\theta_\mathrm{i},\theta_\mathrm{o},\varphi,\eta,\sigma)=\frac{F(\eta,\theta_\mathrm{a})G(\theta_\mathrm{i},\theta_\mathrm{o},\phi)}{4\pi\,\cos(\theta_\mathrm{i})\cos(\theta_\mathrm{o})}\frac{\exp(-\tan^2\alpha/\sigma)}{\sigma\cos^4\alpha} \tag{1}$$

$$G(\theta_\mathrm{i},\theta_\mathrm{o},\phi)=\min\left(1,\frac{2\cos\alpha\cos\theta_\mathrm{o}}{\cos\theta_\mathrm{a}},\frac{2\cos\alpha\cos\theta_\mathrm{i}}{\cos\theta_\mathrm{a}}\right) \tag{2}$$

with θ_i the incident angle, θ_o the outgoing angle, φ the azimuthal difference between incident and viewing directions, η the refraction coefficient of the surface, σ the surface roughness coefficient, α the angle between the surface normal and the facet normal and θ_a the angle between the facet normal and the incident angle. Both α and θ_a can be computed from θ_i and θ_o using simple geometric relationships.

(ii) To ensure a correct energy-preserving simulation, the principles of Fresnel-based reduced reflectance, as explained in [30], were implemented. The Ashikhmin model assumes a two-layer material with a top layer of microfacets (cuticle) and a diffusely reflecting bottom layer (mesophyll). The light incident on the bottom layer is reduced by the fraction of light reflected by the first layer. The total BRDF (f_{tot}) is

$$f_{tot} = f_{dd,microfacets}(\theta_i, \theta_o, \varphi) + \frac{1}{\pi}\rho_{diffuse}(1 - \rho_{dh,microfacets}(\omega_i)) \quad (3)$$

where $\rho_{diffuse}$ is the diffuse component of the BRDF reflectance and $\rho_{dh,microfacets}$ is the directional–hemispherical reflectance of the microfacets or the hemispherical integral of $f_{dd,microfacets}$ over all outgoing directions. To avoid the numerically costly evaluation of a full hemispherical integral for each ray scattering event, $\rho_{dh,microfacets}$ was approximated with a quadratic regression model f:

$$\rho_{dh,microfacets} = f(\log(\sigma), \eta, \cos(\theta_i)) \quad (4)$$

In this model θ_i is the angle between the incident light and the leaf normal, σ is the roughness coefficient and η is the refraction index. A total of nine regression terms were used including interaction and second-order terms to obtain an adjusted R^2 of 0.997.

(iii) Transmittance was assumed to be Lambertian. This approximation was validated by Bousquet [31] for low-absorption wavelengths. For high-absorption wavelengths (e.g. the 350–670 nm), transmittance at high incident angles is reduced due to the higher path length of rays within a leaf and due to the non-Lambertian character of the bidirectional transmittance.

(iv) Leaf bifacial properties were introduced by differentiating according to the angle between an incident ray and the leaf normal. For angles $<90^\circ$ the ray is incident on the adaxial side and for angles $>90^\circ$ it is incident on the abaxial side. This implementation imposes an additional requirement on the leaf geometry to ensure that all triangles of a leaf mesh (Section 2.2.3) have their normals pointing to the adaxial side.

Simulation of a full-leaf BSDF requires thus inputs of (i) surface roughness coefficients, (ii) an index of refraction of the leaf surface (iii) abaxial and adaxial diffuse reflectances and transmittances.

The adaxial leaf roughness parameter (σ) was calibrated by inverting the Bousquet BRDF model over a set of measurements of a *Citrus* leaf using a compact laboratory spectro-goniometer [33]. The best fit (RMSE of 2% in reflectance) was obtained for $\sigma = 0.248$. For the abaxial side a roughness parameter of 0.5 was assumed. Simulations with different settings for abaxial roughness (results not reported here) have shown that the influence of this parameter on the canopy reflectance can be considered negligible. The refraction index was 1.5.

Reflectance and transmittance of the *Citrus* leaves were obtained with the following procedure: for each of the ten selected reference trees, 60 leaf reflectance spectra were averaged and each averaged spectrum was inverted using the PROSPECT model [32] to estimate leaf structure and biochemical composition. The transmittance was obtained by running the model again in the forward mode. The same procedure was iterated for the adaxial and abaxial sides.

PROSPECT computes the total directional–hemispherical reflectance of normal incident light ($\rho_{prospect}$), which includes both the specular and diffuse components. A correction was applied to obtain only the diffuse component (ρ_{diff}) as the specular component was simulated with the Bousquet model (see Eq. (1)):

$$\rho_{diffuse} = \rho_{prospect} - F(\eta_{Pr,\lambda}, 0^\circ) \quad (5)$$

$F(\eta, \theta_i)$ is the Fresnel reflectance of a plate with refraction index η and light incident with an angle θ_i. In this equation, the wavelength-dependant refraction index of the PROSPECT model $\eta_{Pr,\lambda}$ was used. This index is different from the (constant) refraction index of the microfacets model. The refraction index in the PROSPECT model is used to simulate water–cell, water–air and cell–air interfaces in the leaf interior, and is therefore a combination of the refraction indices of cell walls and water, while the microfacets model only concerns the cuticle–air interface, with a relatively constant η [10]. Fig. 3 shows the diffuse reflectance and transmittance spectra for the ten reference trees.

For each individual tree, all leaves were assigned the average leaf spectrum of that tree, assuming that the different spectra of individual leaves in a tree can be substituted by one average spectrum (see Section 2.4.1). A second implicit assumption is that leaves with different spectra are randomly distributed throughout the canopy as the current simulation does not distinguish between sun leaves, shadow leaves and new flush. All leaves are assumed to be sun leaves.

2.2.4.2. Weed leaves. For weed leaves, the same BSDF model was used. All the weeds in the scene are simulated using an average leaf spectrum (Fig. 3). Spectral reflectance and transmittance of healthy grass leaves were obtained from the Leaf Optical Experiment database [34]. Both abaxial and adaxial sides were assumed to be equal and the roughness parameter was set to 0.5.

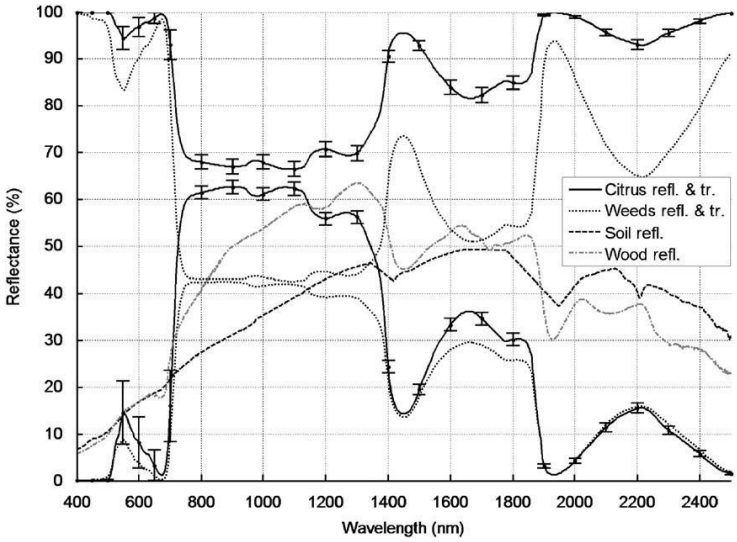

Fig. 3. Reflectance and transmittance spectra of geometric objects. Error bars indicate the ranges of the values for the ten reference leaf spectra.

2.2.4.3. Trunks and branches. For all trees, one measured spectrum (Fig. 3) is used for trunks and branches. For trunks and branches a Lambertian reflectance model was used.

2.2.4.4. Soil. A measured soil spectrum (Fig. 3) of the dominant soil type in the test plot, Albic Luvisol [35], was used. No spatial variability in soil spectra was modeled. Soil reflectance is not Lambertian and many soil types are known to exhibit backscatter. To correctly model this property, the SOILSPECT BRDF model developed by Jacquemoud et al. [25] was implemented. The model accounts for both single and multiple scattering of soil particles, but the single-scattering component is modeled in more detail using a phase function. Two phase functions were used, the first of which models the backscatter peak, while the second phase function is used for forward scattering that is present in wet soils. The BRDF can be represented as

$$f_{\text{soil}} = F(\theta_i, \theta_o, \varphi, \omega_\lambda, h, b, c, b', c') \tag{6}$$

with ω_λ as the single-scattering albedo, h as a roughness parameter and four parameters that determine the width and height of the reflectance peak in the hotspot (b and c) and specular (b' and c') directions. The exact formulas are described in [25]. While the latter five parameters are for the most part wavelength independent and describe the bidirectional properties of the soil, only ω_λ is a wavelength-dependent parameter.

For none of these parameters an exact physical meaning can be given that would allow direct derivation from physical soil properties, but they can be determined using inversion procedures. For all but the single-scattering albedo (ω_λ), values published by Jacquemoud et al. [36] for different general soil types were used. In simulations that focused on individual canopy crowns, default values for a smooth moist sandy soil were used ($h = 0$, $b = -0.03$, $c = 0.31$, $b' = 0.09$, $c' = 0.09$) as the soils below the canopies are irrigated. For simulations at the orchard level, settings for a dry sandy soil were used ($h = 0.18$, $b = 0.17$, $c = 0.06$, $b' = 0.5$ and $c' = -0.06$) as the lanes between the rows were not irrigated but contained the dominant fraction of bare soil at the orchard level. ω_λ was obtained by inverting SOILSPECT using the right sets of bidirectional parameters using soil spectra that were measured with a known illumination angle and a nadir viewing angle. Reference dry soils had an average gravimetric moisture content of 10% and wet soils had a 30% moisture content.

2.2.5. Ray-tracing integrators

For all the scenes, path tracing was used for integrating the surface reflectances. This solution method follows the paths of individual photons through multiple scattering events. Upon each interaction with a surface a new random direction is chosen by sampling the surface BSDF. Although more time consuming than more advanced integrators such as global illumination or photon mapping, this method guarantees unbiased results [21]. For all calculations, at least 655,360 rays were generated to reduce the Monte-Carlo sampling noise.

2.3. Validation of the reference model

Two sets of validations were made. First the RT component of the PBRT model was validated using the RAMI Online Model Checker (ROMC) [37]. This web-based service allows comparing the performance of RT models by intercomparison of simulation outputs for a set of well-described scenarios. The focus in the validation effort was put on heterogeneous and homogeneous scenarios with discrete scatterers. For a comprehensive description of all the simulations and results we refer to [37]. A second validation experiment compared measured and simulated reflectance spectra of individual tree canopies. In the simulations, canopy spectra were generated for the ten reference trees at hourly intervals from 10 to 13 h local time in September, to obtain a dataset with comparable illuminations. Each simulated tree was neighbored with two trees to the north and to the south and five trees in each adjacent row to ensure realistic lateral fluxes comparable to the field data. In addition, a simulation was set up to estimate the uncertainty associated with the Monte-Carlo sampling.

2.4. Testing of assumptions

Assumptions were tested at the tree or orchard level, whichever was more appropriate. For the tree-level simulations between-tree variability was taken into account by averaging the simulation results for the ten reference trees, each of which was assigned a different leaf spectrum and canopy structure (see also the sections describing tree geometry and leaf optical properties).

For the assumptions on leaf BRDF and orchard row orientation, viewing and illumination geometry was found to be critical in describing the assumption errors. In both cases additional simulations were set up to obtain the directional–hemispherical or hemispherical–directional reflectance distribution at the tree or orchard level for individual wavebands.

The general methodology for testing the assumptions was a side-by-side comparison of a 'reference' and one or more 'scenarios'. The reference contained the most detailed model or sub-model while in the scenarios an assumption was introduced (e.g. 'all leaves have a Lambertian reflectance'). Scenario reflectances (ρ_{scenario}) are compared to the reference (ρ_{ref}) and expressed as 'absolute' or relative error in hemispherical–directional reflectance:

$$\text{abs. err} = \rho_{\text{scenario}} - \rho_{\text{ref}} \tag{7}$$

$$\text{rel. err} = \frac{\rho_{\text{scenario}} - \rho_{\text{ref}}}{\rho_{\text{ref}}} \tag{8}$$

For some spectral or structural changes easier to model alternatives are explored by introducing the concept of effective variables. When multiple factors influence the output of a system in a similar way (e.g. leaf angle and gap fraction) and a model of this system is incapable to implement all those factors as variables (e.g. only leaf angle), the 'effective' variables that are being modeled need to be interpreted as a result of all underlying factors and will deviate from the 'true' variables in a systematic way. This technique has been successfully applied in various canopy model inversion processes, e.g. [14,38].

The following paragraphs describe the testing set-up for the different assumptions.

2.4.1. Assumption 1: Optical properties of randomly distributed leaves

The effect of within- and between-canopy differences in leaf spectra was evaluated in two simulations. The first simulation concerned within tree spectral variability. The reference was a single tree of which the leaves have varying optical properties. From the field dataset, a tree was selected of which the leaves covered a broad range in reflectance. A total of 63 measured leaf reflectance spectra were obtained and inverted with the PROSPECT model to estimate transmittance. Other spectral properties (roughness and refraction index) were used from the calibration procedure and were kept constant. The resulting 63 sets of leaf optical properties were randomly assigned to the leaves (10,272 in total) of a representative simulated tree for which the canopy reflectance spectrum was calculated. In the scenario, the average reflectance and transmittance spectrum of the 63 leaves was calculated and assigned to all the leaves of the same tree.

The second simulation evaluated the between-canopy spectral variability. The reference consisted of the default orchard scene, containing random clones of the ten reference trees, each with a different set of leaf optical properties (Fig. 3). The scenario was modeled by assigning the averaged values of these sets of spectra to each tree.

2.4.2. Assumption 2: Leaf adaxial versus abaxial optical properties

The contribution of the abaxial side of leaves to the canopy reflectance was assessed at the tree level. For the ten reference trees, the default sets of optical properties (reflectance, transmittance and roughness) were used with different values for abaxial and adaxial sides. Fig. 8 shows the relative difference between abaxial and adaxial leaf reflectance, which is the largest in the VIS region. The simulated reference canopy spectra were compared for two scenarios:

- In a first scenario both leaf sides were assigned the optical properties of the adaxial side, assuming that a negligible fraction of leaves has its abaxial side on top (i.e. has a leaf angle larger than 90°). Since the optical properties of the scatterers are changed, this scenario is not equivalent to the reference in terms of total energy conservation and overall

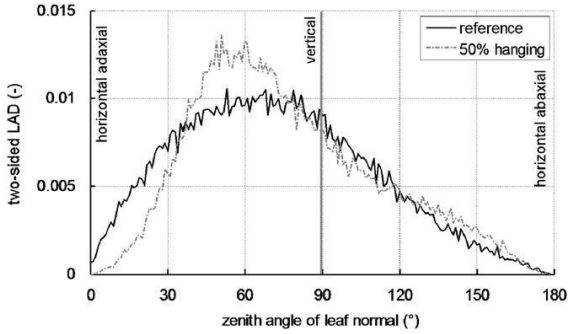

Fig. 4. Extended leaf angle distribution for the averaged for the ten reference trees for default and 50% hanging leaves.

canopy reflectance is not expected to be equal. The importance of this scenario is to assess the magnitude of the errors under realistic conditions.

- Investigation of the leaf angle distribution (Fig. 4) revealed that in the reference trees 26% of the vertically projected leaf area was abaxially oriented (with the bottom side pointing up). Therefore, in a second scenario weighted averages (OP_W) of the adaxial (OP_{AD}) and abaxial (OP_{AB}) optical properties were assigned to both leaf sides. The weighting factor (w) was calculated as the vertical projection (nadir viewing) of the total adaxially oriented leaf surface (leaf zenith angle $\theta < 90^\circ$) divided by the total projection of all leaf surfaces and expresses the relative importance of the adaxial side:

$$OP_w = w\,OP_{AD} + (1 - w)\,OP_{AB} \tag{9}$$

$$w = \int_0^{\pi/2} LAD(\theta)|\cos(\theta)|\,d\theta \Big/ \int_0^{\pi} LAD(\theta)|\cos(\theta)|\,d\theta \tag{10}$$

For a correct interpretation, the definition of 'leaf angle' was extended to take into account the adaxial/abaxial orientation: leaf angle (θ) is redefined as the angle between the vertical upward direction and the normal to the *adaxial* side of the leaf. As such, horizontal leaves with the adaxial side on top have a θ of 0°, vertical leaves have a θ of 90° and horizontal leaves with the abaxial side on top have a θ of 180°.

To assess possible interaction effects with tree structure variability, the experiment was tested on both the reference trees ($w = 0.74$) as for the reference trees with an altered leaf angle distribution (more hanging leaves). As illustrated in Fig. 4, hanging leaves resulted in a smaller fraction ($w = 0.7$) of adaxial sides exposed to a nadir viewing sensor (right half versus left half of the graph).

2.4.3. Assumption 3: Leaf bidirectional scattering distribution function

Three simplified models, one for each scenario, were compared to the reference Bousquet BRDF model. Conceptually, for all calculations the overall leaf reflectance was separated into a diffuse component that is determined by the leaf interior and a specular component caused by the leaf cuticle (Eq. (3)). The diffuse component of the reflectance as well as the (Lambertian) transmittance was identical for all four models.

The first model assumes that the reflectance for the specular component is constant (Lambertian) and equal to the directional–hemispherical reflectance for normal incident light (i.e. leaf reflectance as measured with an integrating sphere and illumination perpendicular to the leaf). This value was obtained from the Bousquet microfacets model, for which the directional–hemispherical reflectance equals 4.6% for the reference leaves with $\sigma = 0.248$ and a normal incident angle. The (implicit) assumptions in this first model are (i) that most leaves in a canopy are oriented perpendicular to the sun and (ii) that viewing geometry can be ignored at the scale of individual leaves.

The second model is based on the hemispherical–hemispherical reflectance or leaf albedo. This assumes that leaves are randomly oriented with respect to the sun's direction. Leaf albedo reflectance was computed by adding the bi-hemispherical integral of the Bousquet BRDF model to the diffuse component of the leaf reflectance:

$$\rho_{spec} = \iint_{\omega_o} \iint_{\omega_i} f_{dd,microfacets}(\omega_i, \omega_o)\,d\omega_i\,d\omega_o \tag{11}$$

$$f_{leaf} = \frac{1}{\pi}(\rho_{spec} + \rho_{diffuse}\,(1 - \rho_{spec})) \tag{12}$$

with ω_i and ω_o the solid incoming and viewing angles. Although this approach requires some pre-computation to obtain a leaf albedo by integration, the input into any RT model or ray tracer is simply a constant reflectance and transmittance spectrum for a Lambertian BRDF. The specular part of the reflectance (ρ_{spec}) in this approximation, for $\eta = 1.5$, ranges from 8.6% ($\sigma = 0.1$) to 5.5% ($\sigma = 0.6$). For a more detailed analysis, see [31].

The third model is hybrid as it considers the incident angle but ignores the reflected angle. The same approach was followed as described in [12], but using a BRDF model that is based on microfacets theory. Although this approach violates the Helmholtz reciprocity principle (i.e. both BRDF reflectance models in this simulation are reciprocal), it may result in an improved accuracy when compared to Lambertian models. This model is expected to be easier to implement in RT models than full BRDF models since only the distribution of incident light angles relative to the leaf orientation needs to be evaluated. The specular component in this version is

$$\rho_{spec}(\omega_i) = \rho_{dh,microfacets}(\omega_i) = \iint_{\omega_o} f_{dd,microfacets}(\omega_i, \omega_o)\, d\omega_o \tag{13}$$

The implementation uses an approximation by multiple regression ($R^2 = 0.999$) to avoid calculating the double integral on each intersection.

In a first experiment, canopy reflectance for the ten reference trees was calculated. As effects of solar position were expected to influence the error, a second more detailed experiment was set up. The bidirectional reflectance of a single tree ($LAI = 7.9$) for all hemispherical viewing angles was simulated at 670 nm (<1% diffuse leaf reflectance) for both the reference BRDF and the normal incidence model. Simulations were made for two illuminations: a realistic solar elevation of 56.4° (March 21, 13 h) and a hypothetical position with only a directional light source in zenith position. By accepting the Helmoltz reciprocity principle at the canopy level, the latter may be interpreted as the bidirectional reflectance of a nadir viewing sensor for all solar angles. See [39] for a detailed analysis on multi-angular remote sensing.

2.4.4. Assumption 4: Representation of leaves as disks

The overall effect of leaf shape and curl was assessed in five sets of simulations. Results were compared to the reference elliptical *Citrus* leaf that has a length–width ratio of 1.7. A slight modification was made to the reference situation to allow a better comparison: all reference leaves were assumed to be flat instead of having a slight curl of 20% as observed during the field campaign. Simulated sets—all having the same LAI—include:

- Disk-shaped (orbicular) leaves with a leaf area equal to the reference leaves. Although orbicular leaves are uncommon in nature, this assumption is often made in RT models [41,7].
- Lanceolate leaves with a length–width ratio of 6.7.
- Reference leaves with a severe curl (60% curl).
- A decreased leaf size (50% leaf area) compensated with an increased leaf density on the branches to maintain the same total leaf area.

An additional simulation with a reduced total leaf area (tree-level $LAI = 75\%$ or reference) with reference leaf size and shape was included to find possible analogies (use of effective parameters) between LAI or leaf size and leaf shape or curl.

2.4.5. Assumption 5: Row-oriented geometry

The effects of row-oriented geometry were evaluated at the orchard level. The default orchard with a tree spacing of 2 m, row spacing of 4.5 m and row azimuth of 7.3° was used as a reference and compared to a scene with a random tree distribution but equal tree density and weed occurrence. Random tree distributions are often assumed in natural forests and multiple-canopy RT models have been adapted for modeling randomly distributed trees [41,42]. The easiest assumption for dealing with row-oriented canopies may thus be to consider them as sparse canopies with random trees. To obtain an equivalent simulation, a random distribution algorithm was designed that avoids placement of trees with trunks at distances smaller than 2 m. This ensures overlaps between canopies to be equal to those in the row geometry. Weeds were randomly distributed over the scene, but not directly under the tree crowns to be consistent with the row-oriented simulation. Total leaf area and leaf size were equal to the row-oriented scene as the same tree density and the same prototype trees were used.

Both scenes were thus designed to be equivalent except for the placement of trees and weed patches. Hence, the reflectance of both scenes for an illumination with a hypothetical zenith light source (and no diffuse light) should almost be identical. The only shading component for such illumination is the vertical crown projections (that are equal in both cases) and there is no mutual crown shading or between-row shading (which is expected to be different). An initial experiment was set up with a 0° zenith light source and no diffuse component to test this presumed equivalence.

Subsequent comparisons were made for six different illumination angles, covering various amounts of between-row and mutual canopy shadings. These simulations were complemented with simulations in a virtual goniometer placed over the forest scene to evaluate the canopy BRDF for wavelengths at 800 nm (infrared plateau) and 670 nm (chlorophyll absorption maximum). The virtual sensor had an FOV of 1° and rotated over the scene at 2000 m distance from the scene center, resulting in a spot size diameter of 34 m for nadir viewing and 102 m for 70° viewing angles. All measurements of

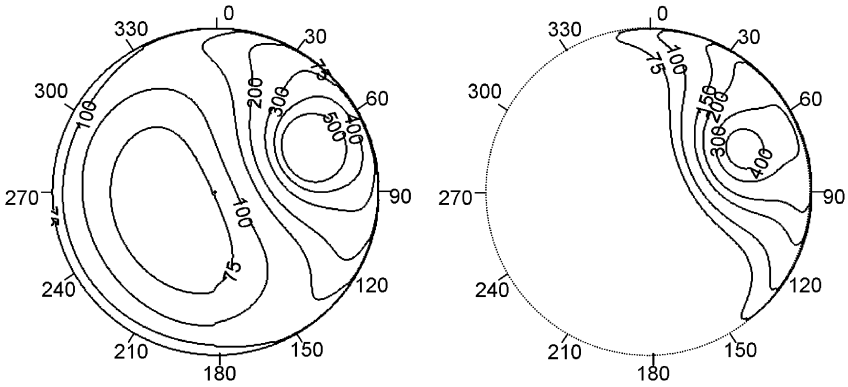

Fig. 5. Angular distribution of diffuse horizontal radiance for a solar elevation of 37.5° and azimuth of 59.4° (March 21, 10 h local time) ($W\,m^{-2}\,sr^{-1}\,mr^{-1}$) for 400 nm (left image) and 670 nm (right image).

viewing angles above 70° were discarded to avoid misinterpretations due to low viewing positions with spot sizes larger than the scene.

2.4.6. Assumption 6: Diffuse sky irradiance at the orchard level

The effect of sky irradiance on the scene illumination was evaluated by testing two assumptions for different combinations of solar position and orchard geometry. Three light distribution models were used of which the first served as a reference, while both others were used in the assumptions:

- A detailed light model with both direct and diffuse light computed with the SBDart RT code was used as reference. The skymaps generated a corona of diffuse light around the solar position, an example of which is illustrated in Fig. 5. The angular distribution of diffuse light decreases with increase in angular distance from the solar position. The amount of scattering at 400 nm is significantly larger at 670 nm.
- A model with only direct light. This tests the assumption that the diffuse component has no significant effect on the canopy reflectance.
- A model with direct light plus isotropic diffuse light. This light model tests the common assumption that diffuse irradiance is approximately evenly distributed over the hemisphere. Simplified skymaps were generated that evenly redistribute the same amount of diffuse irradiance over the hemisphere.

Both assumptions were tested for three different scenarios to analyze the interaction effects caused by illumination, fraction of diffuse irradiance and orchard geometry:

- The reference approximately north–south-oriented orchard with an illumination causing most of the rows to be shaded (elevation 37.5°, azimuth 59.4°; March 21, 10 h).
- The same reference orchard, with maximum solar elevation, causing minimal shading (elevation 79.2°, azimuth 339.6°; December 22, 13 h).
- A random positioning of the same trees, with equal solar position of March 21, 10 h. This scenario tests whether there is an interaction effect between the ratio of diffuse to direct illumination and the positioning of the trees.

The fraction of diffuse clear sky scattering is known to increase with atmospheric turbidity caused by aerosols. To test the effect of this phenomenon on canopy reflectance, each scenario was first calculated with a default aerosol model (horizontal visibility at 550 nm of 30 km) and then repeated for a more turbid atmosphere (horizontal visibility of 15 km), resulting in a higher fraction of diffuse irradiance for all wavelengths.

3. Results and discussion

3.1. Validation of the reference model

The ROMC validation experiment resulted in a close agreement between PBRT and the ROMC reference scenarios. Overall RMSE for a set of four validation scenarios was 0.19% for the principal plane and 0.11% for the orthogonal plane. Overall chi-square statistics (χ^2) were 0.3 for the principal plane and 0.1 for the orthogonal plane. The χ^2 values for all

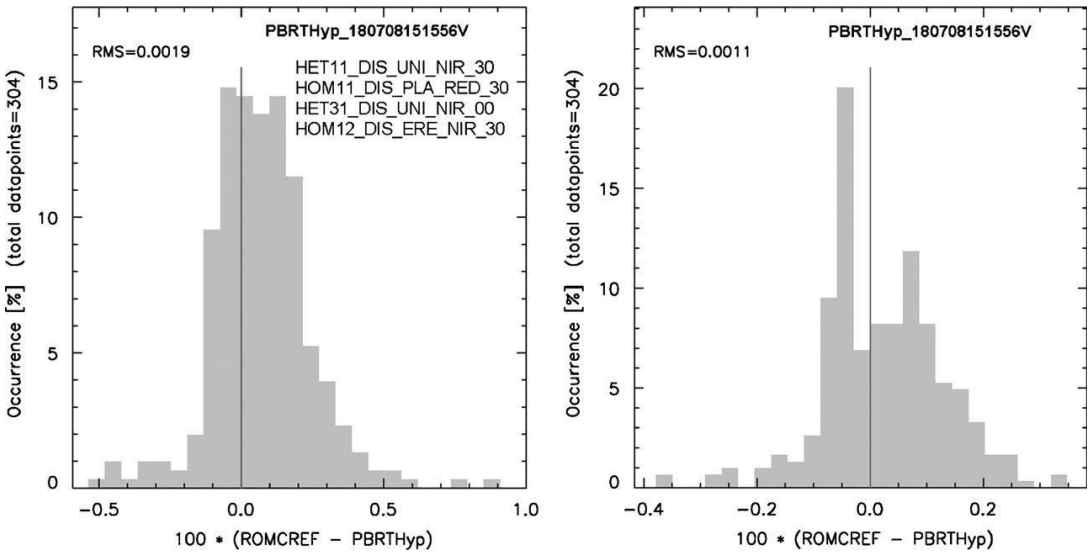

Fig. 6. Histogram of difference in reflectance (%) between PBRT and the ROMC reference for four homogeneous and heterogeneous validation scenarios for the principal plane (left) and the orthogonal plane (right). Results were obtained from the RAMI On-line Model Checker (ROMC) available at http://romc.jrc.ec.europa.eu/.

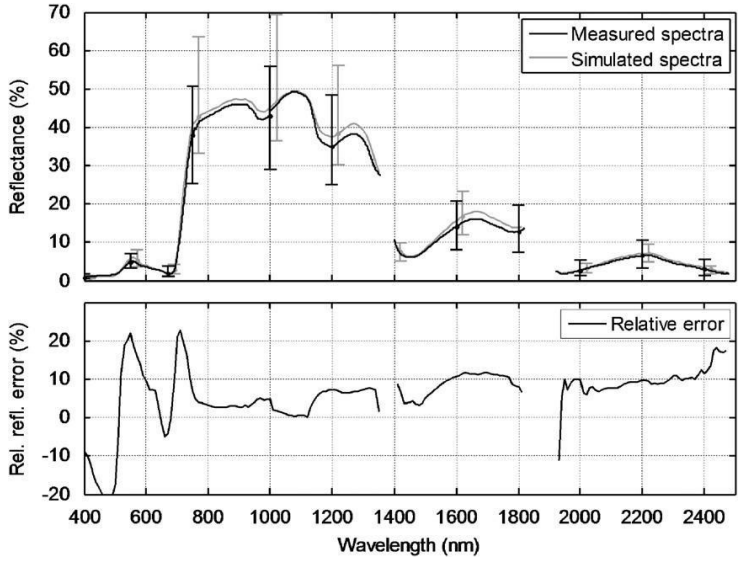

Fig. 7. Measured and simulated canopy spectra expressed as hemispherical–conical reflectance for individual trees (top) and relative error (bottom). The error bars in the top figure show the standard deviation in reflectance for both real and simulated canopies.

individual scenarios were below one and are within the 3% of the ROMC reference. The model skill [37], an integrated value of the agreement of a modeled set of values with a reference set, was 98.2% for the principal plane and 99.7% for the orthogonal plane. Histograms of validation results of four ROMC validation homogeneous and heterogeneous scenarios are presented in Fig. 6a (principal plane) and Fig. 6b (orthogonal plane).

Fig. 7 compares the average hemispherical–conical reflectance for the measured and simulated tree canopy spectra. Error bars indicate the standard deviations in reflectance for both datasets. The bottom figure shows the relative error. Both simulated and calculated datasets contain a high amount of variability, but standard deviations are approximately equal.

The high variability can be explained by differences in leaf spectra, canopy structure and variations in solar illumination (shading) during field work and in the simulations. The standard deviations in both datasets are proportional to the average reflectance values. The (absolute) difference of the average calculated spectrum ranges from −0.4% to +4%, while the RMSE of the averages is 1.3%. The relative difference ranges from −25% (480 nm) to +22% (550 and 710 nm). These values are satisfying since the aim of this research is the use of realistic simulated trees that are representative of trees in commercial orange groves and neither the exact recreation of existing trees nor the inversion of canopy spectra. Considering the comparable ranges of variability of both datasets and the limited deviations of the average spectra, conclusions derived from the simulations are expected to be similar for to real *Citrus* orchards.

In a third experiment, 20 iterations of the same scenario were calculated, each with a different set of random numbers. The standard deviation in reflectance was for all wavelengths below 0.2% in reflectance. Using standard error propagation theory, the uncertainty (standard deviation) due to Monte-Carlo sampling in relative errors (Eq. (8)) was less than 0.5% for all wavelengths.

3.1.1. Assumption 1: Optical properties of randomly distributed leaves

For the first experiment at the tree level, both simulated spectra were almost identical with a maximum absolute error in reflectance of 0.05% at 710 nm and a maximum relative error of 0.9% at 500 nm. Those differences may fall below the numerical accuracy of the ray tracer or may be due to stochastic sampling of a finite number of leaves. This result indicates that the assumption of using averaged optical properties for leaves is valid for at least comparable *Citrus* orchards. The close agreement suggests that generalization to other canopy architectures may even be appropriate, provided (i) that the likelihood of a certain leaf reflectance or transmittance is independent of the position of that leaf within the canopy, and (ii) that leaves with different optical properties have identical angular distributions.

The consequence of condition (i) is that this assumption cannot be used to 'mix' spectra of sun leaves and shadow leaves nor those of mature leaves or new flush (in evergreen canopies), since those leaf types are not randomly distributed over the canopy.

The results of the orchard level experiment resulted in a maximum absolute difference in reflectance of 0.015% at 1220 nm and a maximum relative difference of 0.16% at 590 nm. The previous conclusion may thus be generalized to entire orchard blocks. Note that in this test, spectra were assigned to prototype trees with variable LAI (Table 2). Therefore, the relative contribution to the canopy reflectance of the different leaf spectra was expected to be unequal with leaf spectra of bigger trees having a higher contribution than spectra of smaller trees. The results, however, indicate that for the given conditions (moderate variations in LAI, but approximately equal canopy height and width), a simple averaging is appropriate. Analogous to the previous remark, leaf optical properties should not be averaged over all trees in a plot when trees are not randomly distributed or have distinctly different tree architectures. As such this assumption is expected to fail when mixing, e.g., spectra of under storey leaves with those of upper storey leaves.

3.1.2. Assumption 2: Leaf adaxial versus abaxial optical properties

Fig. 8 shows the results of the experiment by expressing the difference between the reference simulation and the scenario simulations as a relative value (Eq. (7)). For the first scenario (abaxial optical properties are assigned the same value as the adaxial side), the largest error was found in the VIS part of the spectrum: neglecting leaf asymmetry caused a relative decrease in reflectance of approximately 15% at 550 and 670 nm. The shape of the curve is in agreement with the relative difference between the leaf adaxial and abaxial input spectra, but overall differences are smaller, which is due to the larger fraction of adaxial sides exposed to the (nadir) sensor. The relative error increases to more than 25% when leaves hang, which confirms that interaction effects exist between leaf asymmetry and leaf shape and orientation. This may be of high importance in change detection applications, since the results demonstrate that changes in canopy structure may be spectrally equivalent to and confused by changes in leaf albedo (such as chlorosis).

The second 'corrected' scenario that takes into account the properly weighted orientation of the leaf faces produces significantly lower errors, which are less than half the errors of the uncorrected scenario. The remaining error is expected to be due to a correlation between leaf zenith angle and leaf position within the canopy (results not shown): in the constructed trees, leaves in the lower parts of the canopy have higher tendency for abaxial orientation. These results indicate that at least for *Citrus* trees, a correction that attempts to correctly estimate the average single-scattering leaf albedo may provide a more faithful reproduction of canopy reflectance or a better estimation of canopy biophysical parameters in inversion techniques. The error introduced by this assumption in general is expected to depend on the degree of leaf asymmetry and the fractional abaxial leaf area exposed to the sensor. For trees with planophile adaxially oriented leaves such as Hazel (*Corylus avellana* L.) or almost symmetric leaves, the assumption may result in small relative errors.

3.1.3. Assumption 3: Leaf bidirectional scattering distribution function

Fig. 9 shows both the relative (top) and absolute (bottom) errors of the three assumptions when compared to a full BRDF model. All three models result in an overestimation of the canopy reflectance that is the largest in the VIS and SWIR. The approximation of leaf reflectance by directional–hemispherical reflectance at normal incidence (model 1) produces the best results for the given measurement conditions, with relative errors up to 20% in the water absorption bands and absolute errors of up to 0.5% in the NIR and SWIR. The albedo model produces the largest errors, which amount up to 70% in

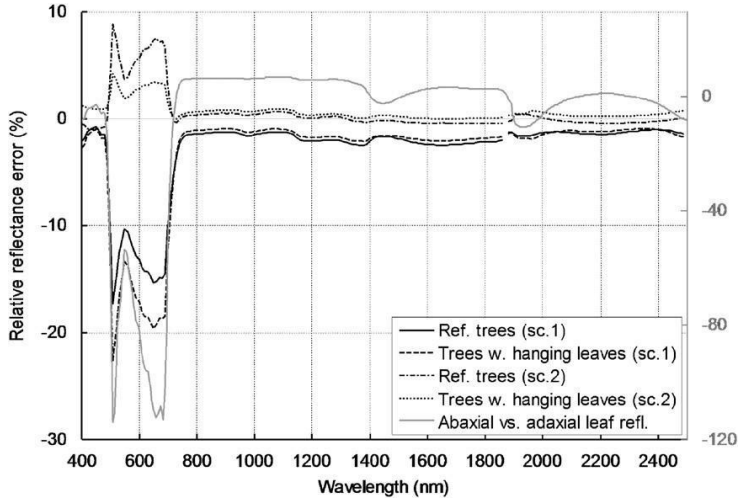

Fig. 8. Relative errors in single tree canopy reflectance for different scenarios when ignoring the adaxial and abaxial reflectance difference. The gray line (right *Y*-axis) shows the relative difference between adaxial and abaxial leaf reflectance. Atmospheric absorption bands (1360–1400 and 1820–1920 nm are masked).

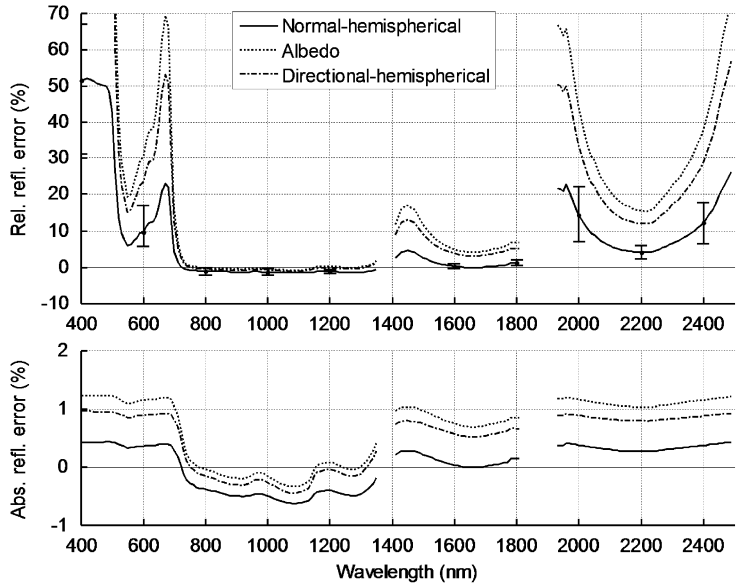

Fig. 9. Relative (top) and absolute (bottom) errors in single tree canopy reflectance for different simplified leaf BRDF models.

relative error and 1.2% in absolute error. The hybrid model, in which the directional effect of incident angles is accounted for, produces slightly smaller errors. The increased complexity of this model is thus not translated in a better accuracy. The error bars show the range of errors for the ten reference trees (only for the first model) and indicate that the relative error is also a function of tree structure and leaf optical properties. The bottom figure shows that overestimations for the three approximations are spectrally constant except for the NIR domain where errors are small ($<0.5\%$ absolute reflectance). Even though the first model results in the smallest errors for the given measurement conditions, the results do not prove that most leaves are indeed oriented with their normals towards the sun as this assumption would result in an equally good performance of the third model which takes into account the exact incident angle.

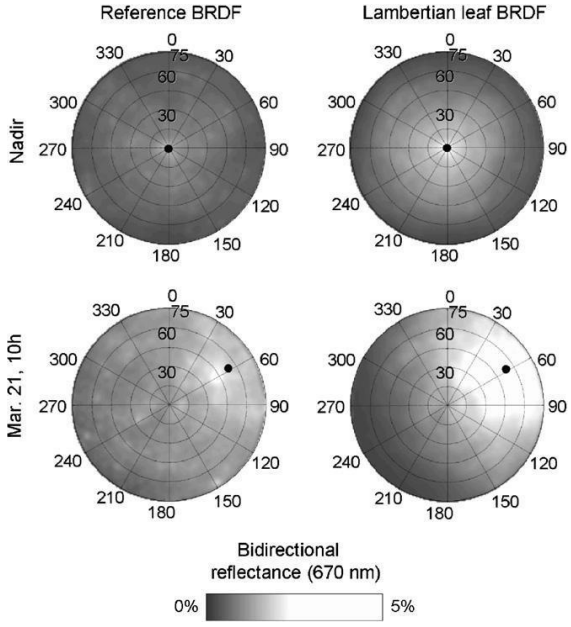

Fig. 10. Bidirectional single tree canopy reflectance at 670 nm for two illuminations for the reference Bousquet BRDF (left) and for the Lambertian BRDF (right). Dots mark the solar position.

Fig. 10 shows the hemispherical bidirectional reflectance distribution at 670 nm obtained from the second experiment. Images are shown for both the reference Bousquet BRDF (left) and the best Lambertian approximation (right). To enhance interpretability, BRDF units are converted to reflectance by multiplying by π. For both illuminations, the Lambertian approximation shows a distinct hotspot (backscatter) around the solar position, while the reference BRDF only has a small hotspot and a more homogeneous canopy reflectance. Analogy can be made with microfacets models that work on a much smaller scale: models such as the Bousquet models assume specular reflectance by the microfacets and result in an almost Lambertian BRDF for very rough surfaces. Microfacets models such as the Oren–Nayar model assume Lambertian microfacets and result in backscatter [21].

The higher reflectance of the Lambertian approximation for identical illumination (bottom images) agrees with the results of the first experiment. When interpreting the top images as hemispherical–directional reflectance, results indicate that for the tree architectures being simulated, nadir reflectance is systematically overestimated with a Lambertian model for all but the lowest solar angles. Although a detailed analysis is beyond the scope of this research, an explanation for this overestimation may be found by considering the leaf angle distributions (Fig. 4 and Table 2) that are slightly erectophile. Leaves with a zenith angle larger than 45° can never scatter direct sunlight into a nadir sensor by specular reflection.

The reported results do not necessarily contradict those reported in [12], which focused on radiation absorption and not canopy reflectance. The more homogeneous distribution of red light within a canopy due to specular reflectance may be important in phytochrome signaling responses [43].

3.1.4. Assumption 4: Representation of leaves as disks

The largest relative effects of leaf shape on canopy reflectance were found in the green and NIR zones as is shown in Fig. 11 (top). Disk-shaped leaves decreased canopy reflectance in the VIS, NIR and SWIR up to 1800 nm, while lanceolate leaves had the opposite effect. The effects were reversed for wavelengths above 2000 nm. The effect may be regarded as a specific case of leaf clumping, used to describe the non-isotropic distribution of scatterers in a medium (e.g. [44]). Elongated leaves result in a more homogeneous distribution of the leaf biomass inside the canopy, while disk-shaped leaves with an equal area are on average closer to the branches, resulting in a higher amount of clumping. Clumping increases the contribution of the soil background by increasing the gap fraction. The same theory can be applied to explain the effects of a decreased leaf size with equal LAI: in this simulation the number of leaves per branch was increased with an equal number of branches, and as a consequence clumping is expected to increase. The relevance for RT models that assume disk-shaped leaves is that deviations in leaf shape (such as lanceolate or elliptic) may be simulated as analogous to changes in leaf size, i.e. by using an 'effective leaf size' which is function of both leaf size and shape. Alternatively, the effects of leaf shape may be modeled using a clumping factor.

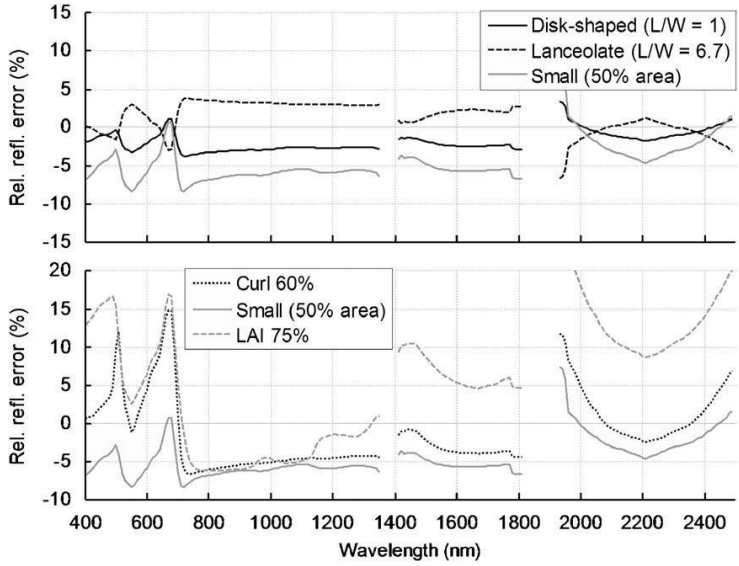

Fig. 11. Relative error in single tree canopy reflectance for different leaf shapes and leaf curl.

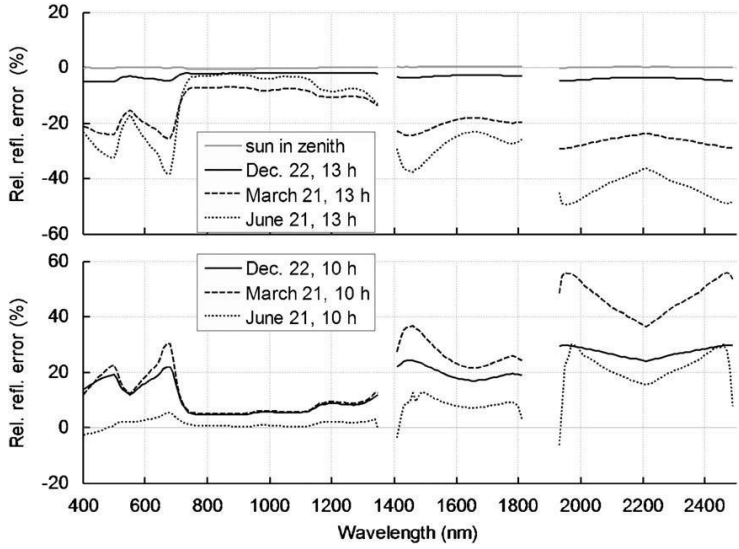

Fig. 12. Relative errors in orchard-level canopy reflectance when ignoring row orientation, for different illumination angles.

Leaf curl (Fig. 11, bottom) causes an increase in the blue and red reflectance, a decrease in the NIR and an increase in the SWIR. The increase in the blue and red can be explained by a higher fraction of abaxial leaf sides being exposed. When ignoring the changes in the VIS region (appropriate for near-symmetrical leaves), spectral changes caused by leaf curl are analogous to the combined effects of an increase in leaf clumping and a decrease in total leaf area. The results suggest that leaf curl may be simulated using effective variables for leaf size, LAI and leaf optical properties.

3.1.5. Assumption 5: Row-oriented geometry

Fig. 12 (top and bottom) shows the relative difference in reflectance at the orchard/stand level for row-positioned trees as compared to randomly positioned trees for seven different illuminations. The results of the validation experiment

(gray lines) confirm that with a zenith light source, both scenes have an almost identical reflectance. The largest simulated difference in reflectance was 0.78% (relative) or 0.45% (absolute), which is small compared to the differences for all other illuminations. This confirms the proposition that differences in reflectance between both scenes are to be interpreted by differences in shading and illumination, including possible non-linear effects.

For all but the highest solar elevation (79.2°, December 21, 13 h), the difference between row-oriented and randomly positioned trees was significant, with relative errors up to 50%. Differences are neither spectrally uniform nor linearly varying with illumination. Most of the variability in spectral regions with low reflectance and transmittance (and a small amount of multiple scattering) may be interpreted as different amounts of shading of tree canopy, soil and weeds. For randomly positioned trees, shading fractions of different orchard components are only a factor of solar zenith, while for row-oriented trees, solar azimuth determines the proportions of shading from canopy to canopy and from canopy to soil/weeds. The low relative differences in the NIR may be a consequence of a high amount of multiple scattering (high reflectance and transmittance) causing small amounts of shading as light can penetrate into the canopy and consequently variations induced by shading are expected to be smaller.

Fig. 13 shows the hemispherical bidirectional reflectance distribution for both row-oriented (top) and randomly distributed (bottom) trees with a zenith illumination and direct light only. Results are simulated for 800 nm (left) and 670 nm (right). The grayscale gradients are scaled between 0% and maximum reflectance. The variations in reflectance in absolute terms are larger at 800 nm, but they are larger in relative terms at 670 nm. For both the row-oriented and random positioned trees, a clear hotspot is visible, which is elliptical for the row-oriented case. The azimuth of the hotspot ellipse major axis is 7.3°, equal to the orchard row azimuth. The row-oriented hemispherical image shows besides a hotspot, a second deviation from the reference (random) image: at low illumination angles perpendicular to the row orientation, the reflectance slightly increases, which is visible on the top left image (800 nm) of Fig. 13 at the left and right edges. This may be attributed to angular variation in canopy gap fraction: direct illumination of the soil caused by sunlight passing above the tops of trees in a row, through the lower and leafless parts of the trees in the adjacent row. This second effect is thus expected to depend on row spacing and on the heights of the upper and lower parts of the canopy.

Abovementioned findings are significant for multi-angular remote sensing. Apart from challenges in BRDF modeling, new opportunities may include innovative algorithms for retrieving row orientation and identification of row plantations. In monitoring applications, where row orientation and planting distances are expected to be known, multi-angular data may help in retrieving canopy architecture parameters and (for orchards) in separating physiological effects from weeds and tree canopies.

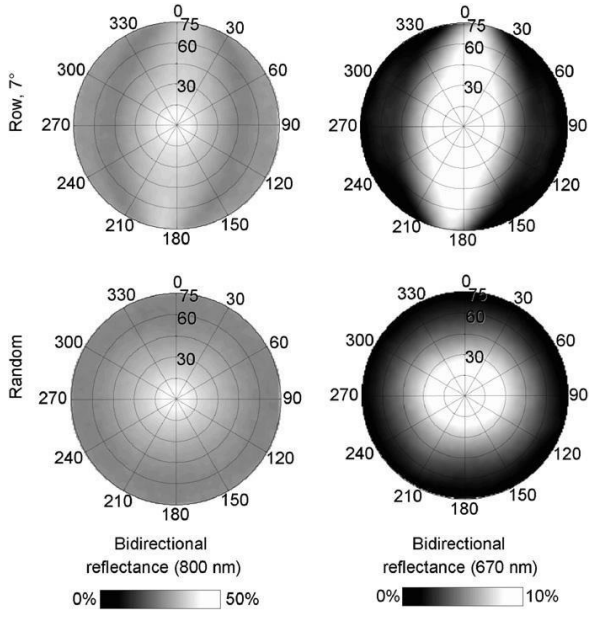

Fig. 13. Hemispherical bidirectional reflectance for row-oriented (top) and randomly positioned (bottom) trees at 800 nm (left) and 670 nm (right). Solar position is in zenith.

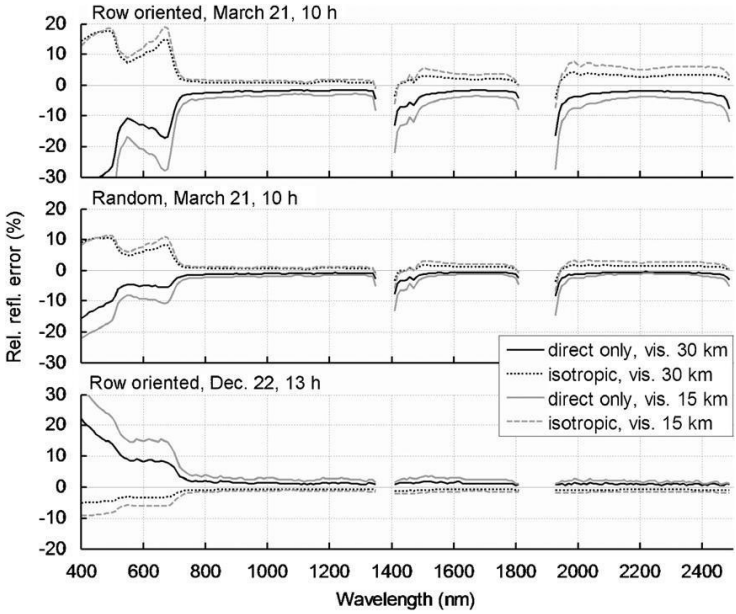

Fig. 14. Relative errors in orchard-level reflectance due to different assumptions of diffuse light distribution for three scenarios and two atmospheric conditions.

3.1.6. Assumption 6: Diffuse sky irradiance at the orchard level

Fig. 14 shows the relative errors induced by both scenarios: only direct light and homogeneously distributed diffuse light. The results for all combinations are grouped per scenario. For each simulation, the effect of ignoring the diffuse component causes the modeled reflectance values to be underestimated for shaded scenes, while for high solar elevations, modeled reflectance is overestimated. The simulated errors are the largest in the visible wavelengths with relative errors of up to 30% in the blue, but are small ($<10\%$) in the NIR and SWIR.

For equal illuminations, the relative errors are significantly larger when applying the assumptions to row-oriented canopies instead of randomly positioned trees. A correct angular distribution of skylight may thus be of higher importance when simulating row-oriented crops or trees.

The assumption of a homogeneous distribution of diffuse light resulted in the opposite effect: reflectance at low and high solar elevations was overestimated and underestimated, respectively. These results can be explained by considering the interaction between illumination and canopy geometries. Diffuse incident light is the main source of illumination for the shaded parts of a scene and will increase reflectance in these zones. At low elevation angles, the shaded fraction of a stand or orchard is high, so the higher the amount of diffuse light, the higher the overall reflectance. The opposite occurs for high solar elevations. The assumption of a homogeneous distribution of diffuse light causes an over-compensation resulting in errors almost as large as those for only direct light. A simple correction to the homogeneous sky model can, however, be considered by introducing an effective value for the fraction of diffuse light, atmospheric turbidity or optical thickness.

These findings are relevant for improving the coupling of canopy RT models and atmospheric correction models. Schemes have already been established in which atmospheric models provide TOC irradiance as well as the wavelength-dependant fraction of diffuse irradiance ([45,46]). Further improvements may include the generation of wavelength-dependant skymaps or, if the canopy model assumes isotropic diffuse illumination, a correction to the fraction of diffuse irradiance to account for its angular variation.

4. Conclusions

In this case study six different assumptions commonly made in vegetation RT modeling were evaluated using a calibrated and validated model of a *Citrus* orchard within a ray-tracing system. A first set of three assumptions focused on leaf optical properties and evaluated the effects of the spectral mixing of randomly distributed leaves, leaf asymmetry and leaf bidirectional reflectance. The fourth assumption investigated the structure effects of variations in leaf shape and leaf curl. The last two assumptions were tested at the orchard level and dealt with the row orientation of trees and the angular

distribution of diffuse irradiance. Pairwise comparisons were made between the reference and multiple scenarios in which assumptions were made. Only the first assumption concerning the optical properties mixing of randomly positioned leaves was not invalidated. All other assumptions resulted in non-negligible and wavelength-dependant relative errors.

The largest effects in relative and absolute terms were found when ignoring the row orientation of trees (assumption no. 5). Therefore, the use of RT models capable of handling row orientation may prove to be a requisite for remote sensing in horticulture.

For the assumptions on leaf asymmetry (no. 2) and leaf shape (no. 4), results suggest that the use of 'effective variables' may at least partially compensate the errors, although further research is required to establish correction methods and evaluate their robustness. The assumptions on leaf BSDF (no. 3) and diffuse illumination (no. 6) indicate that some simple corrections—such as using a leaf albedo instead of directional–hemispherical reflectance or assuming an isotropic distribution of skylight—do not necessarily lead to better representation of the ground truth and may even decrease model fidelity.

Assumption nos. 1–4 can affect all spatial scales of remote sensing, while the last two assumptions are specific for medium- and low-resolution remote sensing, where individual pixels are larger than the crown size. This may provide perspectives for the use of high-resolution remote sensing (such as Quickbird) in situations such as horticulture where assumption nos. 5 and 6 may lead to significant errors.

Assumption errors, expressed in relative terms, were not found to be spectrally uniform (flat line) and often the largest relative errors appeared in the VIS region. A consequence is that values of almost all existing simple ratio and standardized difference vegetation indices will be significantly influenced by factors such as leaf asymmetry, leaf shape, row orientation and atmospheric turbidity in addition to e.g. solar zenith and leaf angle distribution.

A major implication for the use of uncorrected canopy models and vegetation indices in monitoring applications is that the errors (with a possible exception for assumption no. 3) are not temporally constant since they depend on canopy architecture (nos. 2 and 4), solar position (no. 5) and atmospheric conditions (no. 6).

Although testing on different production systems with different canopy architectures and optical properties is required, many conclusions derived here for *Citrus* are expected to be useful to similar crops in horticulture and beyond. Although this research sheds some light on the order of magnitude of errors caused by different assumptions, it has also been demonstrated that the real size of assumption-related errors depends on multiple factors such as illumination and viewing conditions, canopy structure and field or forest lay-out. Whether or not the magnitude of these errors warrants the use of more complicated models will be determined by the field of application and the knowledge of the system being modeled.

Acknowledgements

Funding support for this project has been provided by K.U. Leuven. The authors would like to thank Dr. Graham Barry from Citrus Research International (Stellenbosch) and the Faculty of Agriculture at the University of Stellenbosch, South Africa, for logistic support. We are grateful to Prof. L.G. Albrigo (University of Florida) for his valuable comments and to the European Commission for their support for the ROMC.

References

[1] Goel N. Models of vegetation canopy reflectance and their use in estimation of biophysical parameters from reflectance data. Remote Sensing Rev 1988;4:1–212.
[2] Liang S. Quantitative remote sensing of land surfaces. New York: Wiley; 2004.
[3] Widlowski JL, et al. The third RAdiation transfer Model Intercomparison (RAMI) exercise: documenting progress in canopy reflectance modeling. J Geophys Res 2007;112.
[4] Disney MI, et al. Monte Carlo raytracing in optical canopy reflectance modeling. Remote Sensing Rev 2000;18:163–96.
[5] Gastellu-Etchegorry JP, et al. An interpolation procedure for generalizing a look-up table inversion method. Remote Sensing Environ 2003;87:55–71.
[6] Ross J, Marshak A. The influence of leaf orientation and the specular component of leaf reflectance on the canopy bidirectional reflectance. Remote Sensing Environ 1989;27:251–60.
[7] Kuusk A. A two-layer canopy reflectance model. JQSRT 2001;71:1–9.
[8] Verhoef W, Bach H. Simulation of hyperspectral and directional radiance images using coupled biophysical and atmospheric radiative transfer models. Remote Sensing Environ 2003;87:23–41.
[9] Malenovský Z, et al. Influence of woody elements of a Norway spruce canopy on nadir reflectance simulated by the DART model at very high spatial resolution. Remote Sensing Environ 2008;112:1–18.
[10] Bousquet L, et al. Leaf BRDF measurements and model for specular and diffuse components differentiation. Remote Sensing Environ 2005;98:201–11.
[11] Govaerts Y, Verstraete MM. Raytran: a Monte Carlo ray-tracing model to compute light scattering in three-dimensional heterogeneous media. IEEE Geosci Remote Sensing 1998;36:493–505.
[12] Chelle M. Could plant leaves be treated as Lambertian surfaces in dense crop canopies to estimate light absorption? Ecol Mod 2006;198:219–28.
[13] Disney MI, et al. 3D modelling of forest canopy structure for remote sensing simulations in the optical and microwave domains. Remote Sensing Environ 2006;100:114–32.
[14] Smolander S, Stenberg P. Simple parameterizations of the radiation budget of uniform broadleaved and coniferous canopies. Remote Sensing Environ 2005;94:355–63.
[15] Drouet J-L, Kiniry JR. Does spatial arrangement of 3D plants affect light transmission and extinction coefficient within maize crops? Field Crops Res 2008;107:62–9.
[16] Wu M, et al. The BRDF model and analysis of hotspot effect of row crops. IGARSS 2002;6:3302–4.
[17] Widlowski JL, et al. Horizontal radiation transport in 3-D forest canopies at multiple spatial resolutions: simulated impact on canopy absorption. Remote Sensing Environ 2006;103:379–97.

[18] CIE-Commission Internationale de l'Éclairage. Spatial distribution of daylight-CIE Standard General Sky. CIE Standard S 011/E:2003. Vienna: CIE Central Bureau; 2003.
[19] Ricchazzi P, et al. SBDART: a research and teaching software tool for plane–parallel radiative transfer in the Earth's atmosphere. Bull Am Meteorol Soc 1998;79:2101–14.
[20] Govaerts Y. A model of light scattering in three-dimensional plant canopies: a Monte Carlo ray tracing approach. Belgique: Departement de Physique, Univ Catholique de Louvain-la-Neuve; 1995.
[21] Pharr M, Humphreys G. Physically based rendering. From theory to implementation. San Fransisco: Morgan Kaufmann; 2004.
[22] Zarco-Tejada PJ, et al. FluorMODgui V3.0: a graphic user interface for the spectral simulation of leaf and canopy chlorophyll fluorescence. Comput Geosci 2006;32:577–91.
[23] Atrashevskii YI, et al. The reflection and scattering of light by a plant leaf. J Appl Spectrosc 1999;66:105.
[24] Cohen S, Fuchs M. The distribution of leaf area, radiation, photosynthesis and transpiration in a Shamouti orange hedgerow orchard. Part I. Leaf area and radiation. AFM 1987;40:123–44.
[25] Jacquemoud S, Baret E, Hanocq JFJ. Modeling spectral and bidirectional soil reflectance. Remote Sensing Environ 1992;41:123–32.
[26] Somers B, et al. A conceptual framework for the simultaneous extraction of sub-pixel spatial extent and spectral characteristics of crops. Photogramm Eng Remote Sensing, 2008, forthcoming.
[27] Weber J, Penn J. Creation and rendering of realistic trees. In: Proceedings of the Siggraph, 1995.
[28] Diesel W. Abraro project, 2007: 〈http://arbaro.sourceforge.net〉.
[29] Jonckheere I, et al. A fractal dimension-based modelling approach for studying the effect of leaf distribution on LAI retrieval in forest canopies. Ecol Mod 2006;197:179–95.
[30] Ashikhmin M, Premoze S, Shirley P. A microfacet-based BRDF Generator, 2000. In: Proceedings of the Siggraph, 2000.
[31] Bousquet L. Mesure et modélisation des propriétés optiques spectrales et directionnelles des feuilles. Paris: Ecole Doctorale des Sciences de l'Environnement d'Ile de France; 2007.
[32] Jacquemoud S, et al. Estimating leaf biochemistry using the PROSPECT Leaf Optical Properties Model. Remote Sensing Environ 1996;56:194–202.
[33] Biliouris D, et al. A compact laboratory spectro-goniometer (CLabSpeG) to assess the BRDF of materials. Presentation, calibration and implementation on *Fagus sylvatica* L. leaves. Sensors 2007;7:1846–70.
[34] Hosgood B, et al. Leaf Optical Properties EXperiment 93 (LOPEX93); EUR 16095 EN. Ispra: European Commission—Joint Research Centre; 1994.
[35] FAO. Soils map of the world: revised legend. Rome: Food and Agriculture Organization of the United Nations; 1988.
[36] Jacquemoud S, Baret F, Hanocq JF. Modélisation de la réflectance spectrale et directionnelle des sols. Application au concept de droite des sols. Cah Orstom, sér Pédol, vol. XXVIII 1993;1:31–43.
[37] Widlowski J-L, et al. The RAMI on-line model checker (ROMC): a web-based benchmarking facility for canopy reflectance models. Remote Sensing Environ 2008;112. 1144:1150.
[38] Pinty B, et al. Synergy between 1-D and 3-D radiation transfer models to retrieve vegetation canopy properties from remote sensing data. J Geophys Res 2004;109.
[39] Capderou M. Confirmation of Helmholtz reciprocity using scarab satellite data—an earth observing system experiment. Remote Sensing Environ 1998;64:266–85.
[41] North P. Three-dimensional forest light interaction model using a Monte-Carlo method. IEEE Trans Geosci Remote Sensing 1996;34:946–56.
[42] Kuusk A, et al. Validation of the forest radiative transfer model FRT. Remote Sensing Environ 2008;112:51–8.
[43] Taiz L, Zeiger E. Plant physiology. Fourth ed. Sunderland: Sinauer Associates; 2006.
[44] Rosema A, et al. A new forest light interaction model in support of forest monitoring. Remote Sensing Environ 1992;42:23–41.
[45] Houborg R, Boegh E. Mapping leaf chlorophyll and leaf area index using inverse and forward canopy reflectance modeling and SPOT reflectance data. Remote Sensing Environ 2008;112:186–202.
[46] Verhoef W, Bach H. Coupled soil–leaf-canopy and atmosphere radiative transfer modeling to simulate hyperspectral multi-angular surface reflectance and TOA radiance data. Remote Sensing Environ 2007;109:166–82.

Chapter 5

Physiology of a hyperspectral time series in a citrus orchard

In review: Stuckens, J., Dzikiti, S., Verreynne, S., Verstraeten, W.W., Swennen, R., Coppin, P., Physiological interpretation of a hyperspectral time series in a citrus orchard. Agricultural and Forest Meteorology.

Physiology of a hyperspectral time series in a citrus orchard

Jan Stuckens[a], Sebinasi Dzikiti[b], Stephan Verreynne[b,c], Willem W. Verstraeten[a], Rony Swennen[d,e], and Pol Coppin[a]

[a] K.U.Leuven, Department of Biosystems, M3-BIORES, W. de Croylaan 34, BE-3001 Leuven, Belgium
[b] Stellenbosch University , Department of Horticultural Science, Private Bag X1, Matieland, 7602, South Africa
[c] Citrus Research International, Department of Horticultural Science, Private Bag X1, Matieland, 7602, South Africa
[d] K.U.Leuven, Department of Biosystems, Division of Crop Biotechnics, Kasteelpark Arenberg 13, box 2455, BE-3001 Leuven, Belgium
[e] Bioversity International, Honorary Research Fellow, Kasteelpark Arenberg 13, box 2455, BE-3001 Leuven, Belgium

Abstract

Hyperspectral remote sensing for the monitoring of horticultural production systems demands a good understanding how canopy reflectance is affected by physiology, canopy structure, management and solar elevation during different stages of the phenological cycle. This research describes the construction and interpretation of a hyperspectral time series for a mature and healthy citrus orchard in the Western Cape province of South Africa. Biophysical parameters at the canopy level were derived and related to known observed physiological and phenological changes at the leaf level and to orchard management.

Mature fruit, flowers (at anthesis), and sunburnt leaves had small cover fractions (2.1%, 3.1% and 7% respectively), but the high spectral contrast between flowers and leaves allowed a successful classification of flowering intensity into three broad classes. Canopy level time series of vegetation indices were sensitive to changes in solar elevation and soil reflectance. An empirical soil line correction reduced this influence for the most affected indices. Leaf reflectance measurements were inverted into a time series of biophysical parameters, including a separation of new vegetative flushes and sunburnt leaves. Most trends in vegetation indices at the canopy level could be explained by a combination of these changes at the leaf level, changes in canopy structure (leaf area index and leaf angle distribution) and changes in cover fractions of vegetative flushes, flowers and sunburnt leaves. The index MCARI/OSAVI was best related to leaf level trends in chlorophyll content, with a noticeable influence of sunburn and vegetative flush. Seasonal changes in the photochemical reflectance index (PRI) were linked to inverse changes in carotenoid-to-chlorophyll ratio. Canopy structure indices (MTVI2 and sLAIDI) were sensitive to changes in LAI, average leaf angle as well to management interactions (pruning and harvest). Monitoring of canopy water status was highly impacted during the spring flush by the presence of expanding leaves that concealed trends in the underlying mature leaves.

Seasonal trends in soil and weeds reflectance, important for the up-scaling of reflectance factors from the canopy to the field level, were related to seasonal changes in volumetric soil water content and to the earlier and reduced growth period of non-irrigated weeds.

Keywords: hyperspectral, time series, evergreen, canopy, citrus

1. Introduction

Remote sensing has an important potential to optimize the performance of agricultural production systems. In horticulture, for example, optimal performance of orchards is manifested by warning systems that observe shortcomings in growth at an early stage, enabling the grower to adapt the field management immediately, resulting in no or very limited reduction of yield. This leads to an increased economic output, reduced environmental impact e.g. by improved nutrient and water usage and better logistics planning based on phenological predictions. Current orchard monitoring methods are primarily based on field surveys, climatology recording and soil or leaf nutrient sampling (Hrubovcak, 1999). Most field surveys depend on human interpretation which may cause subjective differences

between assessors as well as over time. Climatology monitoring often obtained through local weather stations, needs interpretation or modelling, as it measures the plant system input and not its state (health) or output (yield). Finally, nutrient analysis, while being an objective and direct assessment, is generally restricted to a limited number of samples due to the elevated costs involved. Major benefits of remote sensing data as a complementary tool, are its fast and objective, quantitative nature and the spatial and temporal resolution provided by present day sensors and platforms. Disadvantages are indirect parameter estimates that require processing and may include bias.

Both active sensors (e.g. microwave) and passive sensors, measuring reflectance or thermal emission, have been used to monitor agricultural systems (Dorigo et al., 2007), either on satellite or airborne platforms. Technological advances and demands for higher spectral resolutions from vegetation sciences and mineralogy exploration have lead to the development of hyperspectral sensors that combine high spectral resolution in the 400-2500 nm domain with a high spatial resolution (Goetz, 2009). Important efforts have been made in porting well-established relationships predicting leaf level biochemistry from spectroscopic measurements to their hyperspectral equivalents at canopy and field levels (Goetz, 2009). Three major applications of hyper- and multispectral data in horticulture and, by extension in crop production in general, include the prediction of chlorophyll content and related stresses (e.g. Haboudane et al., 2002; Zarco-Tejada et al., 2004; Wu et al., 2008), the estimation of leaf area index (LAI) (e.g. Baret & Guyot, 1991; Haboudane et al., 2004) and the detection of water status (e.g. Cheng et al., 2006; Colombo et al., 2008; Clevers et al., 2010; Suarez et al., 2010). Less common examples are monitoring rice phenology (Sakamoto et al., 2005), the prediction of sugar cane harvest date (El Hajj et al., 2009) and the direct estimation of citrus yield (Somers et al., 2010). Accurate retrieval of most biophysical parameters at the canopy level is often hampered by the large number of structure and biochemical parameters affecting the reflectance (Stuckens et al., 2009b), often in overlapping spectral regions, a problem referred to as the ill-posed inverse problem. Therefore, prior information is generally required to obtain reliable parameter estimates. An important category of such prior information consists of a typical time dependent distribution (or baseline) of biophysical variables (Combal et al., 2002), which substantially narrows the valid range for unknown variables in inversion schemes.

The use of time series has been well developed for applications based on sensors with low spatial resolution. For platforms as the Advanced Very High Resolution Radiometer (AVHRR), Moderate Resolution Imaging Spectroradiometer (MODIS) and Spot Vegetation (VGT), multi-day composites of common vegetation indices such as the Normalized Difference Vegetation Index or NDVI (Rouse et al., 1973) and the Enhanced Vegetation Index (EVI) are part of standard processing chains (e.g. USGS, 2010). While important for larger scale applications such as regional yield predictions (Dorigo et al., 2007) or fire risk monitoring, their lower spatial resolution currently limits uses at field scale. Current research on multi- or hypertemporal time series for individual fields or even tree crowns is therefore limited. Examples in horticulture are the monitoring of mite damage in peach orchards using field measurements of crowns and leaves (Luedeling et al., 2009), the monitoring of vegetation water content in crops and woodlands with Landsat Thematic Mapper 5 time series (Yilmaz et al., 2008) and the detection of water stress in orchards with airborne multispectral data (Suarez et al., 2010).

In this research a hyperspectral time series is established by the year-round monitoring of citrus physiology and phenology. Such time series can either serve as a baseline in remote sensing data assimilation or can be used to further our understanding of the interactions between physiology/phenology and canopy reflectance. The use of ground-based top-of-canopy measurements allows a characterization of seasonal trends unhampered by inaccuracies linked to the pre-processing of remotely sensed images, such as registration and atmospheric correction errors.

Timelines of many remotely sensed parameters in citrus, being an evergreen crop, can be significantly different from those in annual crops, that are characterized by rapid increases in both vegetative cover and chlorophyll at the start of the growing season and senescence and leaf drop towards the fall (White et al., 1997; Kodani et al., 2002). The continual presence of leaves in evergreens conversely poses specific challenges. Examples are (i) the presence of mature leaves during a vegetative flush potentially hampering the detection of chlorotic stresses and (ii) smaller seasonal dynamics in LAI combined with a high year-round leaf density that may lead to saturation effects in which canopy reflectance becomes insensitive to limited changes in LAI (Delalieux et al., 2008). Finally, although year-round monitoring enables longer seasonal time series, the larger range in solar elevation angles will cause more pronounced bidirectional reflectance effects that need to be accounted for (Hilker et al., 2008).

The objectives of this research are to establish a hyperspectral time series for a mature and healthy citrus orchard, to derive structural and biophysical parameters at the canopy level and to relate those to known physiological and phenological changes and management actions. Research questions are: (i) Which components are important in the determination of the overall canopy and orchard level reflectance? (ii) How do structural and biochemical variables and solar illumination interact to determine canopy reflectance? (iii) How does the evergreen nature of citrus, including the presence of leaves of different age classes, influence year-round monitoring?

2. Materials and methods

2.1. Site description

All measurements were made in a 12 year old Midknight Valencia orange orchard [*Citrus sinensis* (L.) Osbeck] grafted on Carrizo citrange rootstock [*Citrus sinensis x Poncirus trifoliata*]. The orchard is situated at Sand Rivier Estate near the town of Wellington, Western Cape province, South Africa (33° 35’ 28” S, 18° 55’ 45” E) at 115 m above sea level. This region has a Mediterranean climate with cool, wet winters and warm, dry summers. Within a representative orchard block, 30 healthy trees in two adjacent rows were selected for the collection of a time series of the spectral and non-spectral data. Selected trees were not shaded by adjacent windbreaks during year-round spectral reflectance measurements. The soil type was a shallow Albic luvisol (Somers et al., 2009b). Trees were planted on ridges of 0.5 - 0.6 m height with a between row spacing of 4.5 m, a within row tree spacing of 2 m and a row azimuth of 7.3° (Stuckens et al., 2009b). The average tree height was 3.3 m with elliptic crowns having a major axis perpendicular to the row of 2.7 m and a minor axis of approximately 2 m with limited intertwining of adjacent crowns.

Each year all trees are pruned manually between September and November (Figure 1) by cutting back branches in the top part of the canopy to improve light penetration. Trees are irrigated with micro-sprinklers situated near the base of the trunks delivering 6 litres of water per hour. Fertilizer applications comprised a main urea application in August (200 kg/ha) for flowering and smaller applications in December (35 kg/ha) and April (75 kg/ha). Potassium nitrate was applied in December and January to enhance fruit growth. Corrective foliar applications of urea, potassium nitrate, mono ammonium phosphate and micronutrients (e.g. zinc, copper, manganese and boron) were applied at different stages in the growing season based on leaf nutrient analyses.

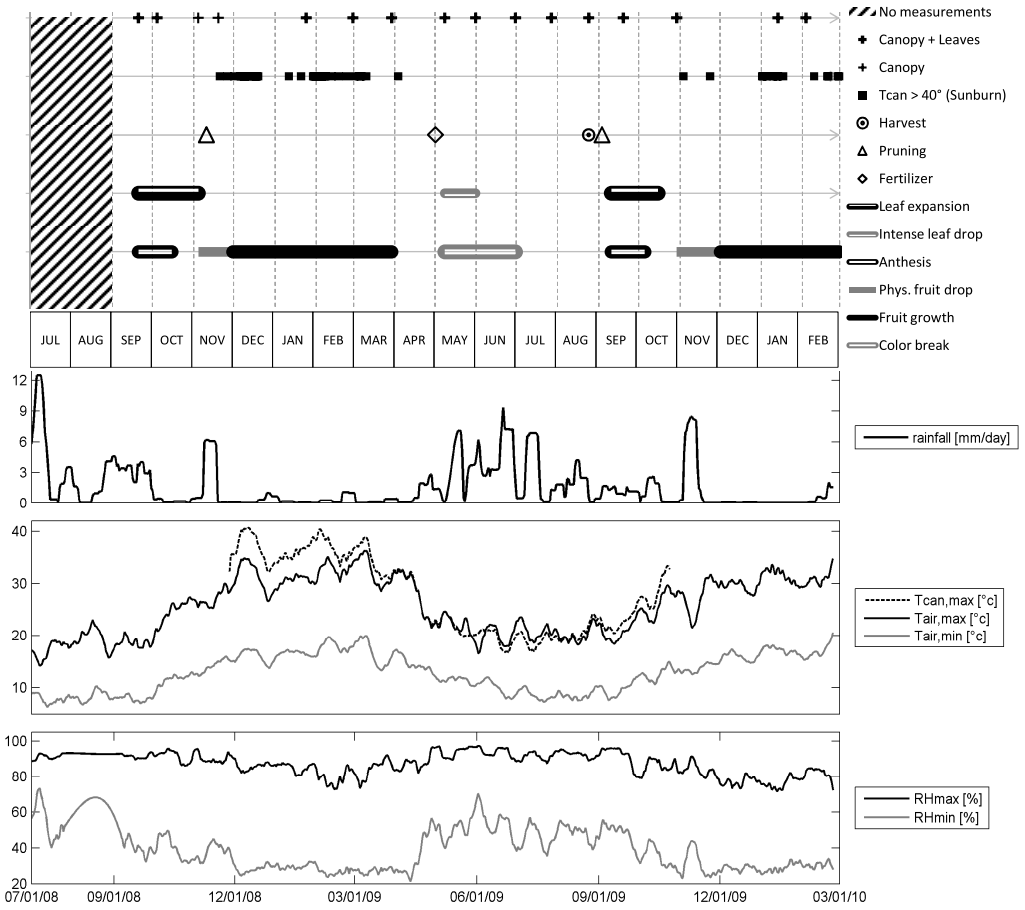

Figure 1. Measurement dates, phenological calendar, management actions and climatogram with rainfall, temperature and humidity at the test site from 07/01/2008 until 03/01/2010.

2.2. Climatology

Air temperature, relative humidity, rainfall and wind speed were continuously recorded at 5 min. intervals by an on-site automatic weather station. Missing data e.g. due to power cuts or sensor malfunctioning was filled in with data from nearby weather stations at Landau Estate (4.3 km distance) and Diemerskraal Estate (3.9 km distance). Periods of overlapping data were used to construct linear regression functions to account for small systematic between-site differences. Canopy temperature was measured with two precision infrared radiometers (Campbell Scientific, Logan Utah, USA) mounted over a single tree from October 2008 until October 2009.

2.3. Canopy structure

Leaf area index (LAI) measurements were taken on five dates between November 2008 and February 2010. LAI was measured with an AccuPAR LP-80 ceptometer (Decagon devices, Inc., Pullman, Washington state, USA) by measuring below-canopy and above-canopy PAR. On each tree, a minimum of five below-canopy and two above-canopy readings were made. All measurements were made on uniformly overcast days, without direct beam radiation. LAI was calculated according to the method described in Norman & Campbell (1989):

$$LAI = \tau / 0.283 + 0.785a - 0.159a^2 \quad (1)$$

with τ the ratio of below-to-above canopy downward radiation and a the leaf absorptivity, which was fixed at 0.9 (Decagon, 2007). This method is an indirect estimation method and thus the retrieved values may be biased and should only be used for comparison of trends at the same location.

Leaf angle distribution (LAD) was measured on three dates: twice in August 2009, directly before and after harvest to assess the impact of fruit weight on leaf angle and orientation and in March 2010 to assess the impact of high temperatures and high irradiance, including photodamage. Discrimination was made between upward (positive angle) and downward (negative angle) facing leaves as well as between adaxially (top side facing up) and abaxially (bottom side facing up) oriented leaves.

2.5. Spectral measurements

The spectral time series started in September 2008 and data reported in this manuscript ends in February 2010, comprising 18 months with 16 measurement sets (Figure 1) at approximately monthly intervals. Canopy, soil and weed reflectance spectra were collected on cloud-free days around solar noon, using a full-range ASD spectroradiometer (350 - 2500 nm) with a 25° field-of-view (FOV) bare fiber optic (Analytic Spectral Devices, Boulder, CO). The spectral resolution (full width half maximum) was 3 nm between 350 and 1050 nm and 20 nm between 1050 and 2500 nm (ASD, 1999). Contact spectra of fruit, leaves and flowers were taken by the same instrument with a contact probe and light source attached. Contact measurements were made in the field or immediately after the field visit with intermediate storage in sealed plastic bags.

Canopy spectra were taken from a scaffold positioned between the rows at an average height of one metre above the top of canopy, from positions were the operator and instrument did not cast shadows onto the trees. Per tree, two to five canopy spectra were collected and white reference spectra were taken after every six trees to account for any changes in the ambient radiation. Top-of-canopy pictures were taken with a 7 megapixel Sony DSC-P200 digital still camera for each tree on every measurement day for a visual assessment and quantitative analysis of canopy structure.

Leaf reflectance spectra were measured with a contact probe immediately after picking on a minimum of 50 randomly picked leaves from the top part of the canopy, using a spectralon whitepanel (Labsphere inc., North Sutton, New Hampshire, USA) as a background to normalize for multiple scattering effects (Stuckens et al., 2009a). New flush leaves and mature leaves were separated until three months after bud break. In 2010, sunburn affected leaves, showing typical photodamage induced chlorosis and necrosis spots, were separated from healthy leaves. Flower and fruit spectra were taken whenever flowers or sufficiently large fruit were present. Soil and weed spectra were collected from June 2009 onwards on six tagged positions randomly situated in the row middles, with five spectra per position.

2.6. Leaf biochemistry from model inversion

Leaf biochemistry was obtained from the leaf reflectance spectra by inverting a Dorsiventral Leaf Model (DLM) as described in Stuckens et al. (2009a), using a Spectralon whitepanel background and by excluding the near-infrared wavelengths (900-1300 nm) from the inversion. Retrieved elements are the contents of total chlorophyll, total carotenoids, water and dry matter. Derived parameters are the carotenoid-to-chlorophyll ratio (car/chl) and the water concentration (fraction of fresh mass). DLM inversion validated on multi-species datasets including citrus using destructive measurement produced root mean squared errors (RMSE) of 4.1 $\mu g/cm^2$ for chlorophyll, 2.5 $\mu g/cm^2$ for carotenoids, 1.6 mg/cm^2 for water, 0.4 mg/cm^2 for dry matter and 2.4% for water concentration. An additional validation dataset obtained in a water stress experiment on *Miho Wase* Satsuma mandarin [*Citrus unshiu* Marcovitch] (Dzikiti et al., 2010) resulted in higher errors for water and dry matter contents (RMSE of 1.9 mg/cm^2 and 1.1 mg/cm^2 respectively) but a better estimate for water concentration (RMSE of 1.8%).

2.7. Soil line correction

An empirical soil line correction was applied to reduce the combined impact of changes in soil reflectance and changes in the fraction of sunlit soil in measured spectra. This correction is based on the soil line principle (Chi, 2003;

Pinty et al., 2009) assuming a linear correlation between the contribution of the soil in a mixed canopy spectrum for any pair of wavelengths and for a fixed soil type. A measured spectrum $\rho_{meas,i,\lambda}$ of a canopy j is approximated as a linear mixture of a fraction f_{soil} of sunlit soil with reflectance $\rho_{soil,\lambda}$ and a fraction f_{can} of pure crown signals ($\rho_{crown,j,\lambda}$):

$$\rho_{meas\ j,\lambda} = f_{soil}\rho_{soil,\lambda} + f_{can}\rho_{can\ j,\lambda} \quad (2)$$

A critical part in applying a correction is the existence of a stable region in the pure canopy reflectance where the total variance in the measured spectrum is explained by changes in the soil fraction. Such a spectral region exists in the water absorption band between 1960 and 1980 nm (Buitenveld et al., 1994). This region is precisely outside of the major water vapour absorption band while liquid water absorption is sufficiently high to ensure almost complete absorption of all intercepted radiation by non-sparse healthy canopies. In this correction, we consider as 'canopy' all fractions except the sunlit soil fraction ($f_{can} = 1 - f_{soil}$). A small base canopy reflectance of 1% caused by the glossy leaf cuticles is assumed, as is derived from measured and simulated spectra, so that:

$$\rho_{meas,j,1970} \approx f_{soil}\rho_{soil,1970} + (1 - f_{soil})\,0.01 \quad (3)$$

from which f_{soil} can be retrieved and any measured canopy signal can be converted to pure canopy reflectance. Since the light interaction between crowns and soil, particularly in the near infrared wavelengths, is non-linear (Somers et al., 2009a), this correction procedure can only provide adequate corrections when the total contribution of soil reflectance to the measured signal is small. Both corrected and uncorrected time series will be described.

2.8. Simulation of bidirectional effects

To estimate the possible impact of changing solar elevations on the measured time series (Hilker et al., 2008), canopy reflectance factors were simulated for seven individual tree crowns placed in a virtual orchard with identical tree spacings as in the Sandrivier study site. Full details of the orchard construction and geometry can be found in Stuckens et al. (2009b). Tree structures for all prototype trees were recalibrated to better match the selected trees using measured values for LAI and LAD. Hyperspectral reflectances, from 350 to 2500 nm at 10 nm intervals, were simulated in a physically based ray tracing environment (pbrt) for seasonally varying illumination conditions at the same time of day (solar elevation and azimuth) as the actual measurements. For each solar position, the angular distributions of diffuse light (skymaps) were simulated using the SBDart atmospheric radiative transfer model (Ricchiazzi et al., 1998). Virtual cameras were placed above the tree crowns at nadir viewing positions with a FOV similar to that of the spectroradiometer (25°). Since the virtual tree structures and soil reflectances were unaltered between different simulations, the constructed time series only contains changes induced by changing solar position and is therefore used to estimate the magnitude of the resulting bidirectional effects. These simulations were subsequently used to construct a time series of hyperspectral canopy indices (see section 2.9) similar to the field measurements, but without seasonal trends in physiology or phenology.

Simulations are set up to closely approximate field measurement conditions with spectroradiometers and therefore focus on individual tree crowns, without major influences of the surrounding soil and weeds. Bidirectional effects at the entire field level such as detected by airborne or spaceborne sensors will include mixtures of soils, weeds and shadow casting by tree crowns and produce substantially different BRDF effects (Stuckens et al., 2009b; Stuckens et al., 2010).

2.9. Hyperspectral indices

To monitor tree physiology and phenology at the crown level, multiple vegetation indices were calculated. According to the parameter they predict, these indices are divided into the following four groups: leaf area index, chlorophyll, carotenoid/xanthophyll pigments and water status. The list of indices evaluated, equations, references and main uses of these indices are listed in Table 1. Different indices for the same parameter were selected to assess the impact of differences in equation structure (e.g. TCARI/OSAVI versus MCARI/OSAVI) or constituent wavelengths (e.g.

sLAIDI versus MTVI2). For each measurement date, all vegetation indices were computed on the averaged canopy reflectance for all trees. For the detection of flowering intensity, no published indices were found and a new index was developed and tested (see subsection 3.3.3).

Table 1. Overview of selected canopy level vegetation indices.

Index	Full name	Equation	Reference	Variable	Comments
MTVI2	Modified Triangular Vegetation Index	$\frac{1.5[2.5(\rho_{800}-\rho_{670})-1.3(\rho_{800}-\rho_{550})]}{\sqrt{(2\rho_{800}+1)^2-(6\rho_{800}-5\sqrt{\rho_{670}})-0.5}}$	Haboudane et al., 2004	green LAI	Modified version of the original Triangular Vegetation index with low sensitivity to changes in soil reflectance and chlorophyll
sLAIDI	standardized Leaf Area Index Determining Index	$\frac{5(\rho_{1050}-\rho_{1250})}{\rho_{1050}+\rho_{1250}}\rho_{1550}$	Delalieux et al., 2008	LAI	Developed and tested on citrus trees
TCARI/OSAVI [705,750]	Transformed Chlorophyll Absorption Ratio Index; Optimised Soil Adjusted Vegetation Index	$\frac{3\left[(\rho_{750}-\rho_{705})-0.2(\rho_{750}-\rho_{550})\frac{\rho_{750}}{\rho_{705}}\right]}{(1+0.16)(\rho_{750}-\rho_{705})/(\rho_{750}+\rho_{705}+0.16)}$	Wu et al., 2008	chlorophyll	Revised version of original index of [Daughtry2000] for better linearity and lower sensitivity to LAI, shadow and soil reflectance.
MCARI/OSAVI [705,750]	Modified Chlorophyll Absorption Ratio Index	$\frac{[(\rho_{750}-\rho_{705})-0.2(\rho_{750}-\rho_{550})](\rho_{750}-\rho_{705})}{(1+0.16)(\rho_{750}-\rho_{705})/(\rho_{750}+\rho_{705}+0.16)}$	Wu et al., 2008	chlorophyll	Revised version of original index of [Daughtry2000] for better linearity and lower sensitivity to LAI, shadow and soil reflectance.
ANMB [650,725]	Area under curve Normalised to Maximal Band depth	$\frac{0.5\sum_{j=1}^{n-1}(\lambda_{j+1}-\lambda_j)(\rho_{j+1}+\rho_j)}{MDB_{650-725}}$ With $MDB_{650-725}$ the maximum band depth of the continuum removed reflectance curve at 677 nm	Malenovský et al., 2006	chlorophyll	Area under curve Normalised to Maximal Band depth
PRI	Photochemical Reflectance Index	$\frac{\rho_{531}-\rho_{570}}{\rho_{531}+\rho_{570}}$	Gamon et al., 1992	xanthophyll ; carotenoid to chlorophyll ratios	Originally developed for xanthophyll pigments, but later [Sims2002] found to be better related to carotenoid-to-chlorophyll ratios
MSI/SR	Moisture Stress Index / Simple Ratio	$\frac{\rho_{1553}/\rho_{816}}{\rho_{816}/\rho_{680}}$	Colombo et al., 2008	leaf EWT	Double ratio index to normalize water content for changes in LAI, i.e. to convert canopy EWT into leaf EWT
SIWSI	Shortwave Infrared Water Stress Index	$\frac{\rho_{860}-\rho_{1640}}{\rho_{860}+\rho_{1640}}$	Fensholt et al., 2003	leaf EWT	Originally developed for MODIS bands 6 and 2, using band centres
FII	Flowering Intensity Index	$\frac{\rho_{470-480}-\rho_{360-370}}{\rho_{470-480}+\rho_{360-370}}$	Section 3.3.3	flowering intensity	Only to be used during spring flowering season, developed for citrus

2.10. Canopy component fraction estimates from digital photos

To assess the relative importance of different canopy components (leaf types, flowers, fruit), top of canopy pictures were classified. Three binary classifiers were constructed to discriminate (i) flowers, (ii) fruit after colour break and (iii) sunburnt leaves from other canopy components, mainly leaves and soil background caused by gaps. Prior to classification, canopy boundaries were manually delineated on the pictures and used as a mask. The original three channels (red, green and blue) for each picture and for each classifier were transformed - by ratioing and differencing - into two dimensions by making transformations that maximized class separability. Due to the high contrast present in most pictures (shaded and sunlit parts), preference was given to decision boundary classifiers in which the decision line was manually fitted in a two-dimensional feature space. Per classifier, multiple pictures were randomly selected for validation on which the components (e.g. flowers vs. other canopy elements) were manually digitized, enabling an accuracy assessment and correction of over- or underclassification. Corrected fractions for flowers, fruit and for each component (f_c) were obtained from original classified fractions (f_0) as:

$$f_c = f_0\, UA / PA \tag{4}$$

with *UA* the user's accuracy (1-commission error) and *PA* the producer's accuracy (1-omission error). The commission error for a specific component (e.g. flower) is defined as the fraction of the total area classified as that component that belongs to the 'other components' class. The omission error is the fraction of the total area that belongs to a specific component but is classified as 'other components'.

3. Results and discussion

3.1. Seasonal climatology and phenology

Figure 1 presents an overview at the same time scale (July 2008 until end of February 2010) of the local climatology, measurement days, phenology and management. As expected for Mediterranean conditions, precipitation is concentrated during the winter season. Total annual rainfall was 632 mm in 2008 and 583 mm in 2009 which is below the yearly average of 674 mm (Wellington weather station, approximately 5 km from the test site; FAO, 2005). Daily maximum air temperatures can exceed 40 °C on clear summer days while no freezes occurred with an absolute minimum of 2.5 °C. The temperature graph shows canopy temperature exceeding air temperature when air temperatures exceed 20 °C. The occurrence of sunburn (photo-oxidative stress) caused by excess heat and radiation is a widespread phenomenon in the Western Cape province in South Africa (Huysamer, 1997). Although different tissues have varying sensitivities, sunburn in apple fruit was found to occur when the tissue temperature exceeds 45 °C (Schrader et al., 2003). As leaf and fruit surface temperature can exceed canopy temperature by 2 to 6 °C (Jifon & Syvertsen, 2003), days with an elevated risk for sunburn are selected as those where the daily maximum canopy temperature exceeds 40 °C. They are indicated on the second line of the top scheme of Figure 1. Most occurred in 2008 and 2009 from November until March, with a high concentration in January and February. The bottom graph shows the maximum and minimum relative humidity. This corresponds well with rainfall events and air temperature, with high relative humidities in periods of abundant rainfall and lower temperatures. Daily minimum relative humidity drops below 30% on hot clear summer days around and after solar noon.

Yearly pruning was executed in November 2008 and immediately after harvest in September 2009. For 2008, canopy spectra immediately after and before pruning were collected. Seasonal phenology in 2008 started with bud break around mid September. Spring flush, anthesis and petal drop/fruit set lasted until the end of October, followed by physiological fruit drop (November) and fruit growth (December - March). Color break was completed in May 2009. In 2009, bud break, anthesis, fruit set and leaf expansion were advanced by one to two weeks, in early September. This caused by the relatively early warming up of the late winter weather or by the higher average winter temperatures in 2009 (Figure 1) that can advance flowering (Albrigo, 2004). For both years, inductive requirements for citrus flowering (18-15°C/13-8°C; day/night; Moss, 1969) are fulfilled. Leaf drop in 2009 occurred during the April - June period, but was mostly concentrated in April. Observations indicate that the 2010 leaf drop started in late February, possibly due to drought stress starting in January.

3.2. Seasonal and diurnal BRDF effect simulations

To limit the impact of solar elevation on the measured canopy reflectance factors, all measurements were concentrated in a 2-3 hour time window around solar noon. Seasonal effects on the other hand are inevitable. To enable a physiological interpretation of the hyperspectral time series and the derived indices, a simulation experiment was set up to allow us to assess the impact of solar zenith angle (SZA) on the reported hyperspectral indices. For seven virtual reference citrus trees (see section 2.7), nadir viewing canopy spectra were simulated at monthly intervals and results were averaged over all trees. As this experiment focuses on the effect of solar elevation, canopy structure, reflectance and transmittance of canopy components and soil were kept constant, at average values. For each month, eight vegetation indices (Table 1) were calculated. The soil line correction procedure described in section 2.7 was also applied to the simulated spectra.

Both corrected and uncorrected simulated timelines are plotted in Figure 2. The magnitude of the seasonal variation of the simulated data (only changing solar position), compared to the magnitude of the variation of the index derived from real trees, is a measure of the sensitivity of each index to SZA. Optimally, simulated indices are constant

in time. Most indices however clearly exhibit an influence of SZA, with a maximum or minimum in June (winter solstice) depending on the nature of the index. The indices for LAI (MTVI2 and sLAIDI) show a limited sensitivity, with simulated effects mostly opposite to measured effects. This indicates that measured trends in LAI are most likely caused by true changes in physiology or phenology and may be even more pronounced than what is actually illustrated. Soil line correction slightly decreases the flatness of the curve.

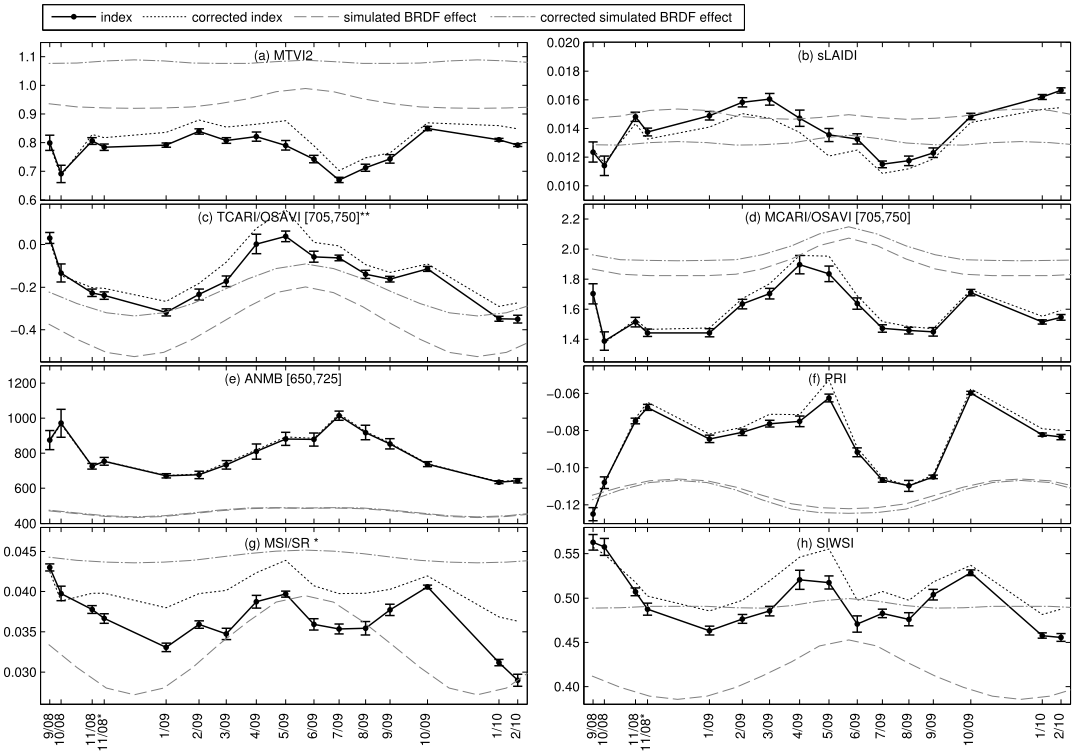

Figure 2. Time series of canopy level vegetation indices: MTVI2, (b) sLAIDI, (c) TCARI/OSAVI[705,750], (d) MCARI/OSAVI[705,750], (e) ANMB[650,725], (f) PRI, (g) MSI/SR and (h) SIWSI. (*) after pruning, (**) original index has been transformed to obtain a positive relationship with the predicted variable.

The chlorophyll indices TCARI/OSAVI and MCARI/OSAVI are sensitive to SZA, with simulated trends of the same magnitude as measured trends. TCARI/OSAVI has similar trends for simulated and measured indices. Consequently, seasonal trends are harder to relate to physiology as they may partly be caused by changes in SZA. The ANMB index on the other hand shows a very low sensitivity to SZA. Soil line correction can reduce this BRDF effect only for TCARI/OSAVI.

The PRI shows a moderate to low sensitivity to SZA with simulated trends different from measured trends and almost no influence from the soil line correction. This trend is remarkably opposite to simulations by Barton & North (2001) who found PRI to increase with increasing SZA. This may indicate that the impact of BRDF on PRI depends on canopy structure and/or soil reflectance.

Both water indices (MSI/SR and SIWSI) exhibit a large influence of BRDF, that is almost completely removed by applying the soil line correction. This can be explained by the high difference in reflectance between canopy and sandy soils in the shortwave infrared (SWIR) as compared to visible (VIS) and near infrared (NIR) wavelengths. This effect is emphasized in row-oriented vegetations, where for summer measurements (high solar elevations) the soil below and surrounding the canopies is sunlit, while during the winter, most of the soil is shaded by adjacent rows

(Stuckens et al., 2010). As a result, spectra collected under summer conditions can contain a higher contribution of the soil background.

In interpreting these results, it is important to consider that the impact of BRDF is only one aspect of the overall performance of an index. Other factors include the sensitivity of each index to the variable it's assumed to measure, the impact of background reflectance, LAI and leaf orientation (Haboudane et al., 2002).

3.3. Discriminating between canopy components

3.3.1. Estimation of component cover fractions

Figure 3 shows a feature space representation for the classification of mature fruit versus other canopy elements (mainly leaves and soil background) for a subset of points from a validation image using the methodology as described in section 2.10. The decision boundary shows a clear separation between both groups, except for the highest values with a maximum digital number (DN) of 255, that are saturated. Saturation in the green channel is caused by glossy reflectance of leaves and fruit. For saturated pixels, no reliable classification could be made and in a conservative approach they were assigned to the 'other canopy elements' class. Similar feature space separations were obtained for both other binary classifiers. Table 2 summarizes the results, presenting the image acquisition date, the construction of the transformed feature space, user's and producer's accuracy, uncorrected and corrected fraction estimates and standard deviation of estimates for all images.

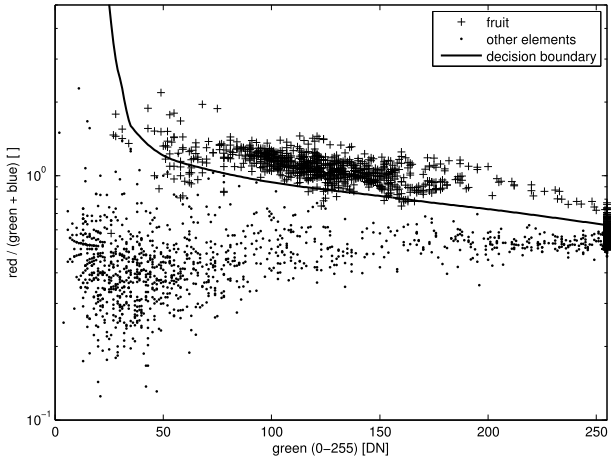

Figure 3. Feature space representation of the validation data for the binary classification of fruit on digital photographs with band combinations on the Y axis and digital numbers (DN) on the X-axis.

For all classifiers, user's accuracy was between 75% and 90%. The lower producer's accuracies were caused by the conservative approach favouring omission errors to commission errors. Mean corrected fractions for fruit (2.1%) and flowers (3.1%) are lower than those for sunburnt leaves (7.1%). Considering these small cover fractions, it is clear that large spectral differences between flowers or fruit and leaves are required to enable quantitative assessments.

Since each image represents a single canopy, the standard deviation of fractions over all images can be used as a rough estimate of between-tree variability. Fruit show the lowest standard deviation (relative to the mean), with a higher value for flowers. This indicates that early between-tree differences in flowering intensity are levelled off towards fruit maturation. The large standard deviation for sunburnt leaves can be a result of relatively large differences in tree susceptibility to photodamage, although they are all genetically identical.

Table 2: Overview of input data, feature space composition and classification results for binary classifiers for flowers, fruit and sunburnt leaves. R = red, G = green, B = blue, std.dev. = standard deviation.

Classifier	Fruit after colour break	Flowers	Sunburnt leaves
Date of images	Jun. 30, 2009	Oct. 5-16, 2008	Feb. 3, 2010
Number of images	26	14	29
Feature space (2 dimensions)	R/(G+B), G	B, G+R	R+G, G+B
User's accuracy (%)	90	75	87
Producer's accuracy (%)	63	67	91
Mean classified fraction (%)	1.5	2.8	7.4
Mean corrected fraction (%)	2.1	3.1	7.1
Std. dev. fraction (%)	0.6	1.4	4.6

3.3.2. Spectral differences

Figure 4 presents average reflectance spectra of canopy components: mature leaves, sunburnt leaves, young leaves during spring flush, abaxial (bottom) sides of mature leaves, mature fruit after colour break and flower petals. Due to the high density of leaves in all trees being monitored, cover fractions of stems and twigs were found to be lower than 1%. These components were not further considered, although their presence may still impact the overall canopy reflectance.

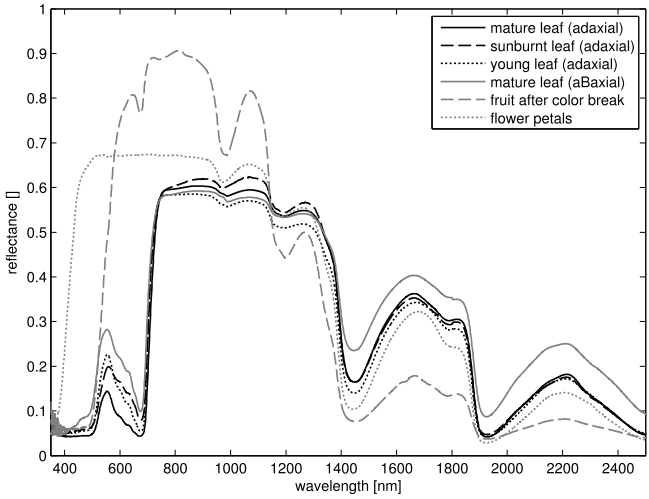

Figure 4. Average measured reflectance of canopy elements: mature leaves (adaxial), sunburnt leaves (adaxial), young spring flush leaves (adaxial), mature leaves (abaxial), fruit after full color break and flower petals.

Among the different leaf types, the most notable differences exist in the VIS, with higher overall reflectance of young spring flush leaves (September - October) and sunburnt leaves (January - March). Both sunburnt and spring flush leaves show an increased reflectance around 550 nm (green), which may lead to errors for vegetation health indices based on these wavelengths. Sunburn in addition results in a higher increase in reflectance between 600 and 700 nm, which can reflect different pigment ratios. Other discriminating features are the deeper water absorption curves for spring flush leaves (e.g. around 1450 nm) and the slope of spectra around 800 nm, which is horizontal for healthy leaves and sloping up for sunburnt leaves. The latter indicates the presence of oxidated or polymerized phenolics (brown pigments; Macheix et al., 1990; Peñuelas & Filella, 1998). See also Felicetti & Schrader (2009b) who found a decrease in idaein phenolics in the sunburnt areas of apple fruit.

Abaxial reflectance of leaves is higher than adaxial reflectance over almost the entire spectrum, except the infrared region, which is typical for most dorsiventral leaves with well-developed palisade and mesophyll layers (Stuckens et al., 2009a). Based on these observations, hyperspectral indices may fail to accurately discriminate higher fractions of dorsiventrally oriented leaves from leaf chlorosis (green and NIR wavelengths) or water stress (SWIR wavelengths).

Mature fruit have an increased reflectance in the VIS for wavelengths beyond 600 nm. The high fruit NIR reflectance can be caused by multiple scattering in the thick peel flavedo and albedo. Markedly lower reflectances in the water absorption bands around 960 nm, 1200 nm and 1450 nm are explained by the high water contents of the fruit. These results indicate that a high spectral contrast between healthy leaves and flowers or mature fruit may still be sufficient to spectrally detect changes in component fractions, notwithstanding their small cover fractions.

Flower petals can be well discriminated from other components in the VIS wavelengths with a high almost uniform reflectance between 65 and 70%, but an equally low UV-B reflectance (around 350-370 nm), indicating the presence of UV absorbing pigments. The most contrasting spectral region is between 470 and 480 nm, where the flowers have a reflectance of approximately 67% while other components' reflectances are below 8%. For wavelengths between 500 nm and 600 nm the contrast is still high, but variability between other components is higher (mature, young, sunburnt leaves and their abaxial sides). For higher wavelengths, the spectral contrast between flowers and fruit is lower. Simultaneous presence of flowers and fruit is uncommon in South Africa, but does occur in other regions, such as Florida where off-season flowering is more common and where mature fruits are left on trees for extended periods to spread harvest time (Valiente & Albrigo, 2004).

3.3.3. Flowering intensity index

The high between-tree variability in flowering intensity (Table 2) necessitates the creation of a flowering intensity index. The critical step in the construction of such an index is contrasting flowers with other canopy elements. As shown in section 3.3.2, the most contrasting region is 470-480 nm. In addition to these differences in diffuse reflectance, specular reflectances are present in both pictures and spectra. These are caused by the refraction of light by the cuticles of glossy leaves and fruit and can cause offsets in reflectance for the entire spectrum (Bousquet et al., 2005). Therefore, to normalize for the specular component, an additional wavelength band is required where all components have an equal and low reflectance, which is found around 350-370 nm. As the signal-to-noise ratio of spectroradiometers decreases in the lowest wavelengths (ASD, 1999), the 350-360 nm range is excluded. The resulting flowering intensity index (FII) is constructed as a normalized difference index:

$$FII = \frac{\rho_{470-480} - \rho_{360-370}}{\rho_{470-480} + \rho_{360-370}} \quad (5)$$

Its performance is compared by visual assessment of flowering intensity during peak anthesis in October 2008. The flowering intensity was evaluated by determining the mean number of flower buds per unit length of the spring shoot in a one square meter quadrant of the canopy on ten trees. The intensity was then broadly categorised into "low" (<0.20 buds/cm), "medium", (0.20 - 0.30) and "high" (>30). Simultaneously, 24 canopy spectra were taken and after applying the soil line correction (section 2.7) the FII was derived. Results for each category are plotted in boxplots on Figure 5, showing a good separation of the three categories. Although this experiment is not a full validation, it proves that spectral detection of flowering intensity at the level of tree crowns is possible during anthesis, even though the average cover fraction of flowers in a canopy at anthesis is low (3.1%). The feasibility of this index in airborne or satellite remote sensing will depend on additional factors such as the sensor's spectral sensitivity, the amount of atmospheric scattering in the UV-B and the amount of spectral mixtures.

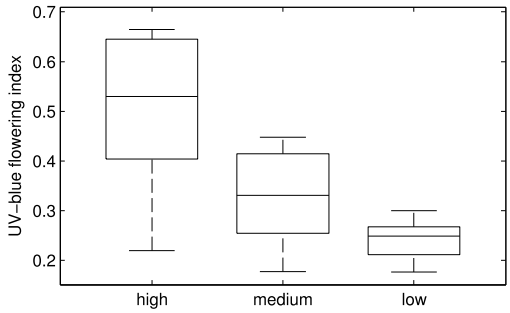

Figure 5. Boxplots of Flowering Intensity Index for trees with high, medium and low flowering intensity. Canopy spectra were made on 10/4/2008.

No specific indices for fruit and sunburn of leaves have been developed here. For detection of crop load, it is important to consider that the presence of fruit produces additional effects that may be spectrally detected, such as alteration of the tree structure (twig bending) due to the weight and blocking of multiple scattering in the infrared spectral region by fruit deeper inside the canopy (Somers et al., 2010). The effects of leaf sunburn are described in the following sections by a combination of chlorophyll breakdown and changes in pigment ratios that are picked up by existing hyperspectral indices.

3.4. Monitoring of leaf biochemistry

Figure 6 shows the results of the DLM model inversion in time lines of contents of total chlorophylls (a + b), total carotenoids, water and dry matter as well as two derived parameters: fraction of water (of the total leaf mass) and the car/chl ratio. Due to the lower relative accuracy of the carotenoid inversion results (section 2.6), only well pronounced trends in carotenoid contents will be interpreted as real physiological changes. Each value includes two error bars: the grey bars show +/- 1 standard deviation (SD) for individual leaves and represent between-leaf variability. The black error bars show the group standard deviation (+/- 1 SD) for each sample and are error bounds for the plotted mean values.

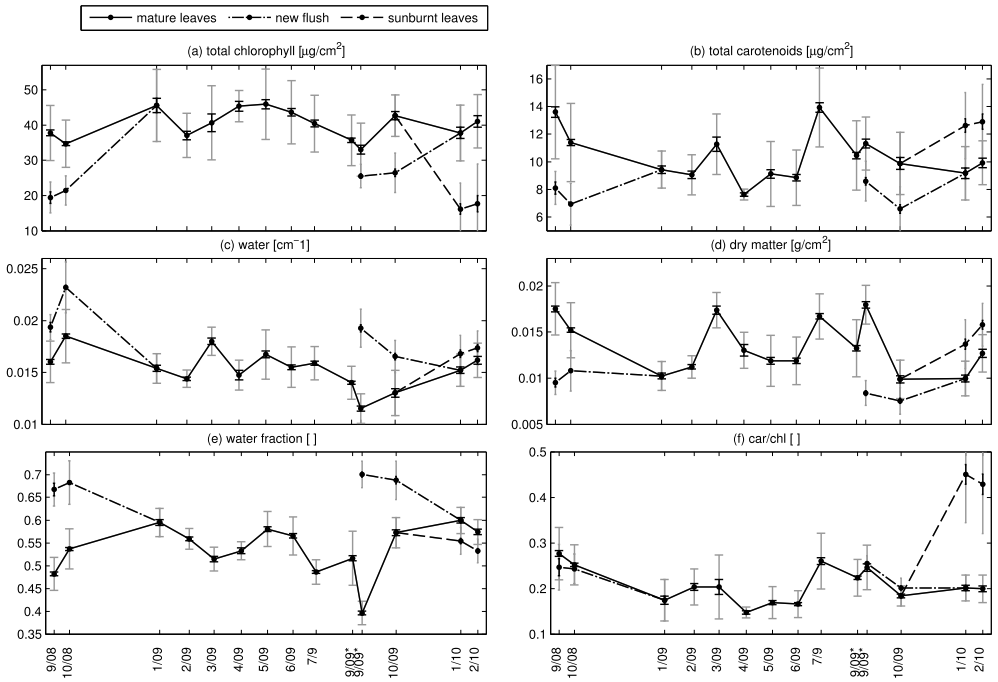

Figure 6. Time series of leaf biochemistry for (a) chlorophyll content, (b) carotenoid-to-chlorophyll ratio, (c) water content, (d) dry matter content, (e) water fraction and (f) carotenoid-to-chlorophyll ratio. (*) measurements before and after vegetative bud break.

Starting at the 2008 spring flush, new leaves clearly have lower chlorophyll, carotenoid and dry matter contents. The water contents are higher than in mature leaves. There is only a small difference in car/chl ratio which indicates that the photosystems gradually develop towards maturity. From January onwards, no discrimination is made between new and old growth. After an initial decrease in chlorophyll content (with constant carotenoid contents) from January to February, the trend is reversed and trees reach their maximum chlorophyll contents around May after which contents start to decline until September. These observations confirm results obtained by Sari et al. (2005) who found maximum chlorophyll contents on navel orange trees [*Citrus sinensis* (L), Osbeck] during the fruit maturity and harvest period, followed by a decline in the dormancy period caused by senescence. Carotenoid contents show rather unstable behaviour with a peak value in July. Water content and water fraction are relatively stable until mid September 2009 where a noticeable drop concurs with the onset of a new vegetative flush. As the climatographs of Figure 1 show no drought during this month, this observation can indicate that the water consumption by the newly expanded leaves and opened flowers temporarily exceeds the root water uptake. This confirms to findings by Syvertsen et al. (1981) who noticed a high water consumption by new flush leaves and opened flowers since the stomatal regulation of water loss in the young shoot leaves is not well developed (Spiegel-Roy & Goldschmidt, 1996). Maintaining turgor pressure in all leaves may be at the expense of water content in mature leaves.

The 2009 spring season shows a similar pattern for spring flush leaves as the previous year, but trends in mature leaves show a decrease rather than increase in water content. From January 2010 on, sunburnt and healthy leaves are treated separately. Sunburn clearly induces a steep drop in chlorophyll contents. The increase in carotenoid contents is explained by an initial photoprotective reaction of the leaves to increased irradiance, i.e. production of carotenes and xanthophylls (Felicetti & Schrader, 2009a). This is most pronounced by the sharp rise in the car/chl ratio. Water contents are only slightly affected, while sunburnt leaves show a small increase in dry matter contents.

3.5. Monitoring of pigments at canopy level

The indices TCARI/OSAVI, MCARI/OSAVI and ANMB (see Table 1) are developed to monitor chlorophyll at the canopy level. The first two are based on the same discrete wavelengths (550, 705 and 750 nm), but use a different equation. ANMB (Figure 2 e) is a continuum removal index normalized for differences in LAI. The timelines of the three indices are clearly different, although some similarities exist. Both TCARI/OSAVI and MCARI/OSAVI show a general decrease from September until January for both years (Figure 2 c, d). For MCARI/OSAVI, this trend is less apparent. The main explanatory factor is the spring flush, in which two opposite trends occur: maturation increases the chlorophyll content of new leaves, while leaf expansion increases the fraction of new shoots in the canopy, thereby reducing observed canopy chlorophyll content. Citrus growth is sympodial, where most shoots emerge from axiliary buds near the tips of the old shoots (Spiegel-Roy & Goldschmidt, 1996) and will therefore often cover the existing mature leaves, increasing their proportional cover for top-of-canopy measurements. As the leaf expansion phase in citrus takes from 4 to 6 weeks (Davies & Albrigo, 1994), most leaves are fully expanded by November. The further drop in canopy chlorophyll content from November until January is thus unlikely to be caused by leaf expansion. Therefore, MCARI/OSAVI, where an initial decrease in chlorophyll content is reversed after October 2008 presents a more realistic timeline. The earlier 2009 spring flush may cause the drop in chlorophylls from August to September, followed by an increase. Alternatively, excessive heat from the end of November (Figure 1) may have caused early sunburn related chlorosis, although this is less likely considering the small fraction of sunburn affected leaves (7.1 %; Table 2). According to TCARI/OSAVI and MCARI/OSAVI, chlorophyll contents peak in April-May 2009, which corresponds to the increase in leaf chlorophyll contents. From July until the new flush in September, chlorophyll contents in mature leaves decrease. The peak in value of ANMB in July does not correspond to leaf level values. For the entire time series, most but not all trends at leaf level were expressed in canopy level indices, with MCARI/OSAVI exhibiting the best correspondence.

Seasonal and diurnal trends in PRI (Figure 2 f) were found to be positively correlated with canopy net CO_2 uptake and with photosystem II efficiency and negatively correlated with carotenoid to chlorophyll ratios (Sims & Gamon, 2002; Stylinski et al., 2002). The timeline of PRI is thus best compared to the car/chl ratio. The trend is described by a sharp rise in September to reach maximum values around October-November, a relatively stable period during the summer season with a temporary and smaller decline, until PRI levels drop again in May. The main trend corresponds well to PRI time series on Pine forests as reported by Weng et al. (2006), with an obvious six months shift (northern versus southern hemisphere). The drop in PRI from July to September indeed agrees with elevated car/chl in the same period which confirms this relationship and may indicate a decrease in photosynthetic efficiency during the winter months. This is confirmed by Ribeiro et al. (2009) who related the lower photosynthetic performance during the winter months to lower temperatures impairing stomatal and stem hydraulic conductances, while photoinhibition by high summer irradiances did not appear to have a significant negative impact on photosynthesis. The smaller decrease around January may be caused by adaptation to high irradiance levels (production of xanthophyll or other carotenoid pigments).

3.6. Monitoring of tree structure

Averages and standard deviations of measured relative tree level LAI are summarized in Table 3. The first two measurements, directly before and after pruning show a decrease in relative LAI of 0.9 or 19%. The third measurement, approximately 10 months later and before the new spring flush, shows almost the same value, even though it includes the leaf drop period from April to June 2009. During this period, no (minor) summer flush was observed. The fourth measurement in November, shows the combined impact of spring flush and pruning resulting in an increase by 0.7 or 18%. The overall increase in leaf area by new leaves is thus approximately twice as large as the removal of leaves by pruning. The subsequent drop in LAI towards February does not correspond to expected seasonal phenology. Field visits in February 2010 however confirmed moderate levels of leaf shedding. Related experiments at the same site reveal a substantial drop in soil water content between December 2009 and February 2010 to below 15%, while the field capacity for this soil type (Albic luvisol) equals 20%. The decrease in LAI can therefore be

explained by water stress induced leaf abscission (Ben-Yehoshua & Aloni, 1974) that may be caused by irrigation malfunctioning during the 2009-2010 summer drought period.

Table 3: Measured averages, standard deviations and change relative to the previous measurement of relative tree level LAI in different phenological stages.

Date	Phenology/management	Average LAI	St.dev. LAI	% change in LAI
2008-11	before pruning, after flush	4.8	0.4	
2008-11	after pruning, after flush	3.9	0.4	-19%
2009-09	before pruning, before flush	3.8	0.5	-3%
2009-11	after pruning, after flush	4.5	0.6	18%
2010-02	fruit growth	3.6	0.4	-20%

Table 4 shows the average values of leaf angle and orientation at three different dates. Leaf angles were recorded relative to the horizontal plane with positive angles for upwards pointing leaves and negative angles for downwards pointing leaves. This discrimination is important in interpreting physiology, e.g. downwards pointing leaves are under water stress while spring flush leaves can be pointing upwards. In canopy radiative transfer, rather the absolute leaf angle determines the patterns of light scattering. The last column shows the abaxial leaf orientation (f_b). It is calculated as the fraction of the total projected leaf area that is abaxially oriented:

$$f_b = \sum_{i \in b} \cos \alpha_i \Big/ \sum_{i \in b+a} \cos \alpha_i \qquad (6)$$

where α is the leaf angle, b stands for abaxial (downward facing) and d for adaxial (upward facing). The increase in average leaf angle after harvest by 7.6° shows the impact of fruit weight on the bending of twigs and branches, pulling down the attached leaves. The absolute leaf angle on the other hand decreases towards a more planophile distribution. After harvest, fewer leaves are abaxially oriented. The third measurement in early March 2010 was taken after a drought period with high air temperatures (exceeding 35 °C) and low relative humidity (25%) (Figure 1). It shows only small changes in leaf angle and absolute leaf angle: the impact of high irradiance and drought on leaf angles seems to be limited, even with leaf shedding occurring from February onwards. The fraction of abaxial orientations however has increased. Considering the higher albedo of the abaxial side (Figure 4), this may be part of a photoprotective mechanism.

Table 4: Sample sizes, measured leaf angle, absolute leaf angle and leaf orientation at three different dates.

Date	Phenology/management	Sample size	Average leaf angle [°]	Average absolute angle [°]	Abaxial orientation
2009-08	before 2009 harvest	137	19.2	38.9	0.29
2009-08	after 2009 harvest	121	26.8	33.7	0.10
2010-03	fruit growth	63	26.3	35.7	0.20

Most of the trends in LAI and LAD can be observed in MTVI2 and sLAIDI (Figure 2 a, b), both of which are positively correlated with LAI. Spring flushes in October-November 2008 and September-October 2009 induce an increase in the index values. Pruning events in November 2008 and early September 2009 have a clear impact on sLAIDI but only result in a minor effect on MTVI2. From November until January (2008 and 2009), sLAIDI shows a further increase although leaf expansion ends in November. From February onwards both indices show a gradual but consistent decrease until minima are reached in July. One cause is the gradual shedding of senescent leaves of the

2007 spring flush, that were approximately 17 months old in February. Erickson & Brannaman (1960) found that leaf drop in Citrus occurs in two stages: a first short but intensive drop of young and mature leaves during the spring flush and a second prolonged drop during the fall. The latter can explain the observed gradual decline.

The clear subsequent increase in both indices in August reveals the likely impact of the presence of fruit. Changes in leaf angle and leaf area can cause very similar effects on nadir viewing canopy reflectance (Asner, 1998). Gradual twig and branch bending by growing fruit (Table 4) and the resulting changes in average leaf angle can therefore explain part of the large decrease in both indices from February until July. sLAIDI and MTVI2 also show an apparent decrease from January to February 2010 that was not present in the previous year and is attributed to accelerated leaf drop by drought stress (Table 3).

3.7. Monitoring of canopy water status

Both water indices MSI/SR and SIWSI (Figure 2 g, h) require careful interpretation due to their high sensitivity to seasonal variation, although the soil line correction procedure severely reduced the dynamic ranges for both indices (section 2.7). In the uncorrected version, the trend starts with a decrease from September 2008 until January 2009, followed by an increase until May and a small drop in June. In 2009 there is an opposite trend with increasing values from August until October and a clear drop until February. For the corrected indices, the trend for SIWSI remains, but the January 2009 drop in MSI/SR has almost disappeared. The limited range of both corrected indices coincides with a limited range in leaf water content, with the exception of a larger dynamic during the vegetative flushes (section 2.6). The combined presence of mature and new leaves may explain why trends at the canopy level only partly correspond to water status at leaf level (Figure 6 c and e). High values in September-October can be related to new expanding leaves with a high water content. These do not reflect the water status of the mature leaves that indicate a temporary water stress. Monitoring of water status at the canopy level during spring leaf growth may thus result in biased estimates. The summer minimum in leaf water content is in February 2009 while at the canopy level it occurs earlier, in January. The steep drop in canopy water indices in the first months of 2010 corresponds well with observed water stress in the orchard (leaf drop, low soil moisture content, see section 3.6) but is not detected at the leaf level. The major impact of the new vegetative flushes, not only on water status indices, but also on chlorophyll and car/chl indices that are mainly used to monitor vegetation health leads to the suggestion to consider the new flush as the start of a new growing season rather than as the continuation of a trend.

Note that although mature fruit represent a large volume of water, fruit harvest between the July and August measurements has no real impact on either index. This could be because of cultural practices in citrus orchards in the Western Cape wherein sunburnt and split fruit (normally at the top of the canopy) is removed early in the growing season since such fruit has no market value and poses competition on the marketable fruit. As a consequence, the influence of the fruit on the top of canopy spectral measurements is negligible at harvest since most harvestable fruit is concealed inside and on the peripherals of the canopy.

3.8. Seasonal evolution of soil and weeds reflectance

Spaceborne remote sensing in orchards, except at very high resolutions (0.5 m and smaller) will inevitably result in mixed signals, containing not only fractions of canopy components but also soil and weeds. Therefore this concluding analysis describes the evolution of soil and weeds reflectance. Figure 7 shows average spectra taken at fixed spots during six consecutive measurement days. The trend in soil reflectance shows an increase from June/July until a maximum in January followed by a decrease in February. Changes can be explained by a combination of three factors: (i) higher volumetric water contents causing an overall darkening due to the lower contrast in the refractive index between water (n=1.33) and soil (n=1.5) as compared to air (n=1) and soil. This decreases the amount of multiple scattering and therefore the probability of absorption (Twomey et al., 1986); (ii) water absorption bands centred at 1430, 1915 and 2500 nm (Buitenveld et al., 1994) will further decrease the reflectance and (iii) differences in illumination direction will induce BRDF effects in soils (Hapke, 1981) with an increased nadir reflectance at high solar elevations (summer) due to the hotspot effect. The clear monotonic trend in soil reflectance, specifically in the water absorption bands, suggests a gradual evolution with higher soil moisture contents in the winter season and dry soils during summer. Such a trend can be expected under the Mediterranean climate of the test site.

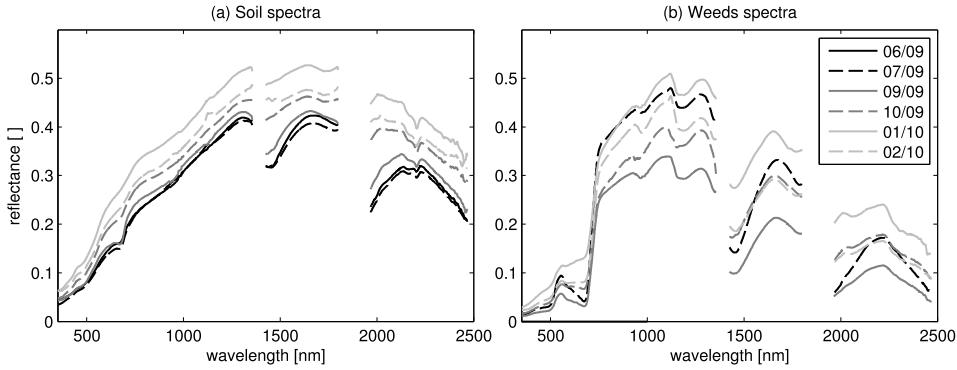

Figure 7. Time series of (a) soil reflectance and (b) weeds reflectance from 06/2009 until 02/2010.

The trends for weeds - mainly grasses not irrigated by the sprinklers - are more complex as they combine spectral changes due to growth, senescence and management (mowing) with changes in the underlying soil background. The high NIR reflectance in July, combined with a green (550 nm) peak reveals sprouting of new grasses after sufficient winter precipitation. The decreased overall reflectance in September 2009 can be a combined effect of maturation (550 nm, increase in chlorophyll content) and structural changes that also decrease the NIR reflectance. From October onwards, weeds spectra show an increased mixture of soil which indicates decreased vegetation cover and senescence. This is confirmed by visual observations and photographs. The phenological calendars of weeds and citrus are thus not simultaneous, with weeds preceding citrus by approximately two months and exhibiting a greater physiological amplitude in a shorter time scale.

Optical remote sensing applications in citrus and other orchards will need to take into account seasonal changes in soil reflectance e.g. by modelling the soil spectral reflectance (Somers, 2009). Knowledge of weeds physiology becomes important in interpreting spectral changes at orchard level, specifically in irrigated orchards with abundant weed cover, and asynchronous physiology of weeds and trees.

4. Conclusions

In this research, an overview is presented of the monitoring of physiology and phenology in a commercial citrus orchard and the impact of each phenological stage on the reflectance of the entire canopy and its components (leaves, fruit, flowers). Classification of individual canopy components allowed an assessment of their potential impact on the canopy spectral reflectance. An experimental Flowering Intensity Index was constructed with which three classes of flowering intensity could successfully be discriminated. Leaf reflectance measurements were inverted into time series of biophysical parameters using a validated Dorsiventral Leaf Model. Separation of new vegetative flushes and sunburnt leaves in these time series provided insights that were key in interpreting canopy level spectral changes.

Prior to interpretation of canopy level spectral time series, an analysis and simulation experiment was set up to quantify the impact of solar elevation on canopy level spectral indices, revealing the sensitivity of mainly chlorophyll (TCARI/OSAVI and MCARI/OSAVI) and water content predicting indices (MSI/SR and SIWSI). Applying a soil line correction to remove the influence of the underlying soil greatly reduced the influence of solar elevation on the water content indices.

Most trends in vegetation indices at the canopy level could be explained by a combination of changes at the leaf level, changes in leaf area index and leaf angle distribution and changes in relative cover fractions of different components (new vegetative flushes, flowers and sunburnt leaves). Different indices predicting the same variable (chlorophyll, water content or LAI) revealed similar trends, but noticeable differences were found in which some trends could be better related to known structural or spectral changes in the canopies. The MCARI/OSAVI index was best related to leaf level trends in chlorophyll content. Seasonal changes in PRI could be linked to inverse changes in

carotenoid-to-chlorophyll ratio. Both canopy structure indices (MTVI2 and sLAIDI) were found to be sensitive to changes in LAI as well as average leaf angle. The major management interactions, pruning and harvest, lead to noticeable changes in these vegetation indices. Monitoring of canopy water status was highly impacted by the presence of new, expanding leaves between September and November that hampered a physiological interpretation of trends in the mostly underlying mature leaves.

Seasonal trends in soil and weed reflectance, that are important when upscaling reflectance factors from the canopy to the field level (spectral mixtures), could be explained in terms of predictable seasonal changes in volumetric soil water content and the earlier and reduced growth period of weeds.

5. Acknowledgements

Funding support for this project was provided by the K.U. Leuven (OT-04047) and the IS-HS (In-Situ, HyperSpectral) project funded by the Flemish government. The authors are grateful to the Stellenbosch University , Department of Viticulture and Oenology, South Africa and in particular to Mr Albert Strever for the use of their spectroradiometer and to Citrus Research International for logistic support. We also gratefully acknowledge the Claude Leon Foundation for the postdoctoral funding for the second author, the Agricultural Research Council of South Africa for providing the weather data and Mr Stephan Strauss of Sandrivier Estates for providing the trial site.

References

ASD, 1999. Technical Guide 3rd Ed. Analytical Spectral Devices, 3rd edition.

Albrigo, G. & Saúco, G., 2004. Flower bud induction, flowering and fruit-set of some tropical and subtropical fruit tree crops with special reference to citrus. Acta Horticulturae, 632, 81-90.

Asner, G., 1998. Biophysical and biochemical sources of variability in canopy reflectance. Remote Sens. Environ., 64(3), 234–253.

Baret, F. & Guyot, G., 1991. Potentials and limits of vegetation indices for LAI and APAR assessment. Remote Sens. Environ., 35(2-3), 161–173.

Barton, C. & North, P., 2001. Remote sensing of canopy light use efficiency using the photochemical reflectance index. Model and sensitivity analysis. Remote Sens. Environ., 78(3), 264–273.

Ben-Yehoshua, S. & Aloni, B., 1974. Effect of water stress on ethylene production by detached leaves of Valencia orange (Citrus sinensis L. Osbeck). Plant Physiology, 53, 863–865.

Bousquet, L., Lachérade, S., Jacquemoud, S., & Moya, I., 2005. Leaf BRDF measurements and model for specular and diffuse components differentiation. Remote Sens. Environ., 98(2-3), 201–211.

Buitenveld, H., Hakvoort, J.M.H., & Donze, M., 1994. The optical properties of pure water, in Ocean Optics XII. In J.S. Jaffe, editor, Proc. SPIE, 2258, 174–183.

Cheng, Y.B., Zarco-Tejada, P., Riaño, D., Rueda, C., & Ustin, S., 2006. Estimating vegetation water content with hyperspectral data for different canopy scenarios: Relationships between AVIRIS and MODIS indexes. Remote Sens. Environ., 105(4), 354–366.

Chi, H., 2003. Practical atmospheric correction of NOAA-AVHRR data using the bare-sand soil line method. International Journal of Remote Sensing, 24(17), 3369–3379.

Clevers, J., Kooistra, L., & Schaepman, M., 2010. Estimating canopy water content using hyperspectral remote sensing data. International Journal of Applied Earth Observation and Geoinformation, 12(2), 119–125.

Colombo, R., Meroni, M., Marchesi, A., Besetto, L., Rossini, M., Giardino, C., & Panigada, C., 2008. Estimation of leaf and canopy water content in poplar plantations by means of hyperspectral indices and inverse modeling. Remote Sens. Environ., 112(4), 1820–834.

Combal, B., Baret, F., Weiss, M., Trubuil, A., Macé, D., Pragnère, A., Myneni, R., Knyazikhin, Y., & Wang, L., 2002. Retrieval of canopy biophysical variables from bidirectional reflectance using prior information to solve the ill-posed inverse problem. Remote Sens. Environ., 84(1), 1–15.

Davies, F. & Albrigo, L., 1994. Citrus. CABI Publishing, Wallingford, UK.

Decagon, 2007. PAR/LAI ceptometer model LP-80. Operator's manual version 5. Decagon devices, Inc.

Delalieux, S., Somers, B., Hereijgers, S., Verstraeten, W.W., Keulemans, W., & Coppin, P., 2008. A near-infrared narrow-waveband ratio to determine Leaf Area Index in orchards. Remote Sens. Environ., 112(10), 3762–3772.

Dorigo, W., Zurita-Milla, R., de Wit, A., Brazile, J., Singh, R., & Schaepman, M., 2007. A review on reflective remote sensing and data assimilation techniques for enhanced agroecosystem modeling. International Journal of Applied Earth Observation and Geoinformation, 9(2), 165–193.

Dzikiti, S., Verreynne, J., Stuckens, J., Strever, A., Verstraeten, W., Swennen, R., & Coppin, P., 2010. Determining the water status of Satsuma mandarin trees [Citrus Unshiu Marcovitch] using spectral indices and by combining hyperspectral and physiological data. Agricultural and Forest Meteorology, 150(3), 369–379.

El Hajj, M., Bégué, A., Guillaume, S., & Martiné, J.F., 2009. Integrating SPOT-5 time series, crop growth modeling and expert knowledge for monitoring agricultural practices - The case of sugarcane harvest on Reunion Island. Remote Sens. Environ., 113(10), 2052–2061.

Erickson, L. & Brannaman, B., 1960. Abscission of reproductive structures and leaves of orange trees. Proc. Am. Soc. Hort. Sci., 75, 222–229.

FAO, 2005. New LocClim 1.06. Technical Report Working paper No. 20, Environment and Natural Resources Service (SDRN).

Felicetti, D. & Schrader, L., 2009a. Changes in pigment concentrations associated with sunburn browning of five apple cultivars. I. Chlorophylls and carotenoids. Plant Science, 176(1), 78–83.

Felicetti, D. & Schrader, L., 2009b. Changes in pigment concentrations associated with sunburn browning of five apple cultivars. II. Phenolics. Plant Science, 176(1), 84-89.

Goetz, A., 2009. Three decades of hyperspectral remote sensing of the Earth: A personal view. Remote Sens. Environ., 113(1), S5–S16.

Haboudane, D., Miller, J., Pattey, E., Zarco-Tejada, P., & Strachan, I., 2004. Hyperspectral vegetation indices and novel algorithms for predicting green LAI of crop canopies: Modeling and validation in the context of precision agriculture. Remote Sens. Environ., 90(3), 337–352.

Haboudane, D., Miller, J., Tremblay, N., Zarco-Tejada, P., & Dextraze, L., 2002. Integrated narrow-band vegetation indices for prediction of crop chlorophyll content for application to precision agriculture. Remote Sens. Environ., 81(2-3), 416–426.

Hapke, B., 1981. Bidirectional reflectance spectroscopy 1. Theory. Journal of Geophysical Research, 86(B4), 3039–3054.

Hilker, T., Coops, N., Hall, F., Black, T., Wulder, M., Nesic, Z., & Krishnin, P., 2008. Separating physiologically and directionally induced changes in PRI using BRDF models. Remote Sens. Environ., 112(6), 2777–2788.

Hrubovcak, J., Vasavada, U., & Aldy, J.E., 1999. Green technologies for a more sustainable agriculture. Agriculture information bulletin, no. 752, Economic Research Service, US Department of Agriculture, Washington, DC.

Huysamer, M., 1997. Integrating cultivar, rootstock and environment in the export-driven South African deciduous fruit industry. Acta Horticulturae, 451, 755–760.

Jifon, J. & Syvertsen, J., 2003. Moderate shade can increase net gas exchange and reduce photoinhibition in citrus leaves. Tree Physiology, 23, 119–127.

Kodani, E., Awaya, Y., Tanaka, K., & Matsumura, N., 2002. Seasonal patterns of canopy structure, biochemistry and spectral reflectance in a broad-leaved deciduous Fagus crenata canopy. Forest Ecology and Management, 167(1-3), 233–249.

Luedeling, E., Hale, A., Zhang, M., Bentley, W., & Dharmasri, L., 2009. Remote sensing of spider mite damage in California peach orchards. International Journal of Applied Earth Observation and Geoinformation, 11(4), 244–255.

Macheix, J.-J., Fleuriet, A, & Billot, J., 1990. Fruit phenolics. CRC Press, Boca Raton, Florida, USA.

Moss, G., 1969. Influence of temperature and photoperiod on flower induction and inflorescence development in sweet orange (Citrus sinensis L. Osbeck). Journal of Horticultural Science, 44, 311–320.

Norman, J. & Campbell, G., 1989. Canopy structure. Plant physiological ecology: Field methods and instrumentation. Chapman and Hall, London.

Peñuelas, J. & Filella, I., 1998. Visible and near-infrared reflectance techniques for diagnosing plant physiological status. Trends in Plant Science, 3(4), 151–156.

Pinty, B., Levergne, T., Widlowski, J.L., Gobron, N., & Verstraete, M., 2009. On the need to observe vegetation canopies in the near-infrared to estimate visible light absorption. Remote Sens. Environ., 113(1), 10–23.

Ribeiro, R.V., Machado, E.C., Santos, M.G., and Oliveira, R.F., 2009. Photosynthesis and water relations of well-watered orange plants as affected by winter and summer conditions. Photosynthetica, 47(2), 215-222.

Ricchiazzi, P., Yang, S., Gautier, C., & Sowle, D., 1998. SBDART: A Research and Teaching Software Tool for Plane-Parallel Radiative Transfer in the Earth's Atmosphere. Bulletin of the American Meteorological Society, 2101–2114.

Rouse, J., Haas, R., Schell, J., Deering, D., & Harian, J., 1973. Monitoring vegetation systems in the great plains with ERTS. In Third ERTS Symposium, SP-351, pages 309–317. NASA.

Sakamoto, T., Yokozawa, M., Toritani, H., Shibayama, M., Ishitsuka, N., & Ohno, H., 2005. A crop phenology detection method using time-series MODIS data. Remote Sens. Environ., 96(3-4), 366–374.

Sari, M., Sonmez, N., & Kurklu, A., 2005. Determination of seasonal variations in solar energy utilization by the leaves of Washington navel orange trees (Citrus sinensis L, Osbeck). International Journal of Remote Sensing, 26(15), 3295–3307.

Schrader, L., Zhang, J., & Sun, J., 2003. Environmental stresses that cause sunburn of apple. Acta Horticulturae, 618, 397–405.
Sims, D.A. & Gamon, J.A., 2002. Relationships between leaf pigment content and spectral reflectance across a wide range of species, leaf structures and developmental stages. Remote Sens. Environ., 81(2-3), 337–354.
Somers, B., 2009. Hyperspectral unmixing for plant production system monitoring. Ph.D. thesis, K.U.Leuven.
Somers, B., Cools, K., Delalieux, S., Stuckens, J., Van der Zande, D., Verstraeten, W.W., & Coppin, P., 2009a. Nonlinear hyperspectral mixture analysis for tree cover estimates in orchards. Remote Sens. Environ., 113(6), 1183–1193.
Somers, B., Delalieux, S., Verstraeten, W.W., & Coppin, P., 2009b. A conceptual framework for the simultaneous extraction of sub-pixel spatial extent and spectral characteristics of crops. Photogrammetric Engineering and Remote Sensing, 75(1), 57–68.
Somers, B., Delalieux, S., Verstraeten, W., Vanden Eynde, A., Barry, G., & Coppin, P., 2010. The contribution of the fruit component to the hyperspectral citrus canopy signal. Photogrammetric Engineering and Remote Sensing, 76(1), 37–47.
Spiegel-Roy, P. & Goldschmidt, E., 1996. Biology of citrus. 229. Cambridge University Press.
Stuckens, J., Verstraeten, W.W., Delalieux, S., Swennen, R., & Coppin, P., 2009a. A dorsiventral leaf radiative transfer model: Development, validation and improved model inversion techniques. Remote Sens. Environ., 113(12), 2560–2573.
Stuckens, J., Somers, B., Delalieux, S., Verstraeten, W.W., & Coppin, P., 2009b. The impact of common assumptions on canopy radiative transfer simulations: A case study in Citrus orchards. Journal of Quantitative Spectroscopy and Radiative Transfer, 110(1-2), 1–21.
Stuckens, J., Somers, B., Albrigo, G.L., Dzikiti, S., Verstraeten, W.W., Swennen, R., Verreyne, S., & Coppin, P., 2010. Off-nadir viewing for reducing spectral mixture issues in citrus orchards. Photogrammetric Engineering and Remote Sensing, in press.
Stylinski, C., Gamon, J., & Oechel, W., 2002. Seasonal patterns of reflectance indices, carotenoid pigments and photosynthesis of evergreen chaparral species. Oecologia, 131(3), 366–374.
Suarez, L., Zarco-Tejada, P., González, V., Berni, J., Sagardoy, R., Morales, F., & Fereres, E., 2010. Detecting water stress effects on fruit quality in orchards with time-series PRI airborne imagery. Remote Sens. Environ., 114(2), 286–298.
Syvertsen, J., Smith, M., & Allen, J., 1981. Growth rate and water relations of citrus leaf flushes. Annals of Botany, 47, 97–105.
Twomey, S., Bohren, C., & Mergenthaler, J., 1986. Reflectances and albedo differences between wet and dry surfaces. Applied Optics, 25, 431–437.
USGS, 2010. Land processes distributed active archive center. MODIS products table. Available from: https://lpdaac.usgs.gov/lpdaac/products/modis_products_table [Accessed 14 May 2010].
Valiente, J. & Albrigo, L., 2004. Flower bud induction of sweet orange trees [Citrus sinensis (L.) Osbeck]: effect of low temperatures, crop load, and bud age. Journal of the American Society for Horticultural Science, 129, 158–164.
Weng, J.H., Liao, T.S., Hwang, M.Y., Chung, C.C., Lin, C.P., & Chu, C.H., 2006. Seasonal variation in photosystem II efficiency and photochemical reflectance index of evergreen trees and perennial grasses growing at low and high elevations in subtropical Taiwan. Tree Physiology, 26(8), 1097–1104.
White, M., Thornton, P., & Running, S., 1997. A continental phenology model for monitoring vegetation responses to interannual climatic variability. Global Biogeochemical Cycles, 11(2), 217–234.
Wu, C., Niu, Z., Tang, Q., & Huang, W., 2008. Estimating chlorophyll content from hyperspectral vegetation indices: Modeling and validation. Agricultural and Forest Meteorology, 148(8-9), 1230–1241.
Yilmaz, M., Hunt Jr., E., & Jackson, T., 2008. Remote sensing of vegetation water content from equivalent water thickness using satellite imagery. Remote Sens. Environ., 112(5), 2514–2522.
Zarco-Tejada, P., Miller, R., Morales, A., Berjón, A., & Agüera, J., 2004. Hyperspectral indices and model simulation for chlorophyll estimation in open-canopy tree crops. Remote Sens. Environ., 90(4), 463–476.

Chapter 6

Evaluation and normalization of cloud obscuration related BRDF effects in field spectroscopy

Published as: Stuckens, J., Somers, B., Verstraeten, W.W., Swennen, R., Coppin, P., 2009. Evaluation and normalization of cloud obscuration related BRDF effects in field spectroscopy. Remote Sensing 1, 496-518.

OPEN ACCESS

Remote Sensing

ISSN 2072-4292

www.mdpi.com/journal/remotesensing

Article

Evaluation and Normalization of Cloud Obscuration Related BRDF Effects in Field Spectroscopy

Jan Stuckens [1,*], Ben Somers [1], Willem W. Verstraeten [1], Rony Swennen [2] and Pol Coppin [1]

[1] M3 BIORES, K.U. Leuven, de Croylaan 34, 3001 Leuven, Belgium;
E-Mails: Ben.Somers@biw.kuleuven.be (B.S.); Willem.Verstraeten@biw.kuleuven.be (W.W.V.);
Pol.Coppin@biw.kuleuven.be (P.C.)

[2] Division of Crop Biotechnics, K.U. Leuven, Kasteelpark Arenberg 13, 3001 Leuven, Belgium;
E-Mail: Rony.Swennen@biw.kuleuven.be (R.S.)

[*] Author to whom correspondence should be addressed; E-Mail: Jan.Stuckens@biw.kuleuven.be;
Tel.: +32 16 32 97 49.

Received: 1 July 2009; in revised form: 7 August 2009 / Accepted: 11 August 2009 /
Published: 25 August 2009

Abstract: The impact of target bidirectional reflectance in dual field of view spectroscopy was described and quantified using field measurements and ray-tracing simulations. A data-driven normalization method was developed to convert reflectance factors under cloud obscured conditions into clear sky reflectance by decomposing the target bidirectional reflectance into an isotropic target-specific component and a group-specific bidirectional component. An evaluation on tree, grass and gravel targets suggests a reduction in relative reflectance error obtained by normalization from 15% to less than 5% between 400 and 1800 nm. At higher wavelengths a decreased signal-to-noise ratio increases the errors.

Keywords: dual field-of-view; spectroradiometer; hyperspectral; BRDF; clouds; obscuration

1. Introduction

During the last decades, field spectroscopy has become an established technique for characterizing reflectance of surfaces in situ, for supporting calibration of airborne and satellite sensors (vicarious calibration) and for providing a means of up-scaling data from small surfaces such as leaves, branches and

stones to composite scenes such as canopies and ultimately to pixels [1]. The comparably small footprint of spectroradiometers combined with their high spectral resolution enables a precise characterization of an object's reflectance, without signal deterioration due to atmospheric interactions of the reflected radiance. This higher detail comes at the expense of significantly larger efforts required to establish field datasets. Since single field of view reflectance spectroscopy is based on taking the ratio of sequentially measured target radiance to whitepanel radiance, stable illumination conditions are imperative, which can only be guaranteed under cloudless conditions [2, 3]. Unfortunately, occurrence of such necessary conditions for many regions in the world is subject to seasonality and the dominant sky type may include various amounts of cloud cover (the fraction of the sky hemisphere covered by clouds) and cloud obscuration (the optical depth of the cloud layer obscuring the solar disk and the surrounding corona). Even at visually optimal conditions, measurements can still be deteriorated due to optically thin cirrus clouds passing before the sun disk [4]. While single date dataset collections may permit waiting for optimal conditions, the establishment of time series does not offer such flexibility. In single field of view spectroscopy, often (linear) interpolations are made of the target radiance before and after a set of target scans to account for smoothly varying irradiance such as that due to varying solar zenith angle at clear sky conditions [5]. This interpolation technique, however, can hardly be applied to account for the typically rapid, unpredictable and nonlinear changes in irradiance caused by cloud obscuration. To alleviate these restrictions, dual field of view (DFOV) methods have been designed that rely on the simultaneous measurement of reference and target providing more precise field spectra than results collected using a single-beam mode [3]. Different DFOV implementations have been developed, either by implementing into a single instrument an oscillating shutter or mirror to interleave signals from target and reference or by simultaneously triggering scans of two individual instruments [6]. In both designs, the reference measurement may be either the radiance of a reference panel (*bi-conical*) or the irradiance obtained by a cosine receptor (*cos-conical*). For dual instrument designs, intercalibration functions (ICF) are implemented to account for differences in spectral response of both sensors. Research by [6] demonstrated that ICFs depend on the irradiance spectrum and are therefore best established under field conditions approximating those of the target measurements. The significant additional expense of a second spectroradiometer for DFOV measurements has lead to the development of techniques for estimating the irradiance spectrum by only sampling a limited number of fixed wavelength bands using a much simpler filter-based radiometer [5, 7].

Although DFOV techniques can successfully overcome errors caused by varying irradiance, cloud obscuration also causes an increase in incident light scattering. As a consequence, the diffuse to direct ratio of incident light as well as the angular distribution of diffuse light will be altered. The impact of this phenomenon may be limited for light and invisible cirrus clouds under which circumstances DFOV spectroscopy is commonly applied. For obscurations by optically thicker cloud types such as cumulus and stratus clouds, the irradiance distribution will be significantly altered, causing a different sampling of the target's bidirectional reflectance distribution function (BRDF) and consequently different values of measured reflectance (hereafter named reflectance factor) for most surfaces [8, 9]. Most structured earth surfaces are known to exhibit different amounts of backscatter (soil, vegetation) and/or forward scattering (water bodies). Moreover, also the non-Lambertian behavior of commonly used reference panels such as Spectralon material (Labsphere Inc.) has been well investigated [10, 11, 12]. When taking the ra-

tio of target radiance to reference radiance to obtain re?ectance factors, target and reference panel BRDF effects may either compensate or reinforce each other. A cos-conical configuration can suffer from analogous issues as many commercially available cosine diffusers are based on spectroradiometer fore-optics exhibiting a sub-optimal cosine response [13]. An additional restriction in DFOV under severely obscured conditions is the reduced irradiance resulting in a reduced signal-to-noise ratio (SNR) of the measurements.

The objectives of this research are:

- to gain better insights in the mechanisms in which different levels of cloud obscuration affect DFOV spectroscopy. More specifically, the focus will be put on the effects of decreased irradiance (noise level) and target/whitepanel BRDF.
- to evaluate whether, for measurement series over similar targets, the target BRDF can be decomposed into an isotropic target-specific component and a group-specific bidirectional component.
- to use this decomposition for developing a data-driven normalization procedure for converting, by means of an initial dataset obtained from a representative target, measured reflectance factors into reproducible reflectance measures, independent of cloud obscuration.

The theoretical background section presents the processing of DFOV measurements and the calculation of SNR using error propagation theory. Expressions for quantifying BRDF effects are derived and a normalization procedure is developed. Evaluation of BRDF effects and the normalization procedure relies on both reference data obtained over Citrus canopy, grass sod and gravel targets with DFOV spectroscopy and on hyperspectral ray-tracing data.

2. Theoretical Background

In the first section, the use of instrument intercalibration is discussed. Subsequently, three major effects of cloud obscuration on incident light are considered: (i) the decrease in the total amount of transmitted irradiance due to scattering and absorption by cloud particles, (ii) an increase in the fraction of diffuse light due to a higher amount of scattering and (iii) a different angular distribution of the diffuse light. Finally, a normalization procedure for the second and third effect is developed.

2.1. Overview of Radiometric Units

Table 1 lists a description of the radiometric symbols and units used in this work. For a complete description, we refer to standard works in remote sensing such as [14].

Table 1. List of radiometric symbols and units.

Symbol	Name	Units
L	radiance	$W\,m^{-2}sr^{-1}$
$L(\lambda)$	spectral radiance	$W\,m^{-2}sr^{-1}nm^{-1}$
E	irradiance	$W\,m^{-2}$
$E(\lambda)$	spectral irradiance	$W\,m^{-2}nm^{-1}$
f	BRDF or bidirectional reflectance	sr^{-1}
ρ	reflectance factor	-
γ	fraction of direct irradiance	-

2.2. Processing of Dual Field of View Measurements

In DFOV spectroscopy, measurements are made with two identical instruments, one measuring the radiance of a reference whitepanel (L_{ref}) which is used as a surrogate for total incident irradiance [15], and the other measuring the target's radiance (L_{tar}). The resulting absolute reflectance factor (ρ_{tar}) after correcting for the reference panel reflectance (ρ_{ref}) is:

$$\rho_{tar}(\lambda) = \frac{L_{tar}(\lambda)}{L_{ref}(\lambda)}\,\rho_{ref}(\lambda) \tag{1}$$

in which λ represents the wavelength (nm). Generally, both instruments are not completely identical and measure slight differences in radiance due to small errors in calibration or small waveband shifts. Without correction, the resulting spectra can exhibit significant noise levels and therefore intercalibration functions are often applied [6, 16]. Instrument intercalibration is obtained by measuring the radiance with both instruments of a constant intercalibration surface (L^{ic}) illuminated with a stable light source. The reflectance factor is then multiplied with an wavelength specific intercalibration term, $IC(\lambda)$, that equals the ratio of both instruments measured radiances. Although in this form, the intercalibration appears as a constant spectrum, its value depends on the shape of the irradiance spectrum [6]. Intercalibration functions are thus best established under illumination conditions approximating those under which the field measurements are collected. To reduce notational complexity, intercalibration is omitted in subsequent formulations, although it is consistently applied when processing real measurements.

2.3. Impact of Cloud Obscuration on Signal Noise

Spectroradiometers exhibit different sensitivities along the wavelength spectrum they are designed to measure. Measurement noise is commonly expressed as noise equivalent radiance (NER) and is measured as the standard deviation in radiance of a sufficiently large number of 1 s scans over a target illuminated with a perfectly stable light source [2]. For a given measured radiance of a target L_{tar}, the signal to noise ratio (SNR) in radiance units can be expressed as:

$$SNR(\lambda)_{tar,rad} = \frac{L_{tar}(\lambda)}{NER(\lambda)\,\sqrt{T}} \tag{2}$$

with T being the scan time in seconds, expressing a decrease in noise level according to the square root law (of sample size). Since the property of interest is target reflectance, the SNR of the reflectance factor can be expressed using the standard error rule of a ratio:

$$SNR(\lambda)_{refl} = \frac{1}{\sqrt{\frac{1}{SNR(\lambda)^2_{tar,rad}} + \frac{1}{SNR(\lambda)^2_{WP,rad}}}} \tag{3}$$

with $SNR_{WP,rad}$ as the signal-to-noise ratio of the whitepanel measured with the same illumination. Equation 3 can be used to estimate SNR of an intended measurement series if approximations of the irradiance spectrum and target reflectance are available.

2.4. BRDF Effects Caused by Illumination Conditions

This section discusses the impact of cloud cover on the fraction of diffuse irradiance and the angular distribution of diffuse light. Differences in cloud cover during a measurement series will cause a different sampling of the target's BRDF and result in different measured reflectance values. In addition, the non-Lambertian BRDF of whitepanels should be taken into account [16]. Both statements can be explained by expressing target and reference surface radiance as functions of the direct and diffuse irradiance components. For isotropic surfaces, where the BRDF only depends on the relative difference between viewing (φ_v) and illumination azimuths (φ_i), the radiance of a target can be expressed as:

$$L_{tar} \;=\; E_{dir}\, f_{tar}\,(\theta_i, \theta_v, \varphi_i - \varphi_v) + \int_0^{2\pi}\int_0^{\pi/2} f_{tar}\,(\theta, \theta_v, \varphi - \varphi_v)\;\; L_{dif}(\theta, \varphi \mid i)\;\cos\theta\;\sin\theta\,\mathrm{d}\theta\,\mathrm{d}\varphi \tag{4}$$

with θ_i and θ_v the illumination and viewing zenith angles, f_{tar} the BRDF of the target surface, E_{dir} the direct (projected) irradiance and L_{dif} the angular distribution of the diffuse irradiance (skylight) under specific illumination conditions (i). Note that BRDF (f) and reflectance factor (ρ) are related by a constant, i.e., $\rho = \pi\, f_{tar}$. Equation 4 can also be used to obtain the reference panel radiance (L_{ref}) when replacing f_{tar} by f_{ref}, the reference panel BRDF. For nadir viewing angles, Equation 1 can be converted using basic mathematical operations into (see appendix section):

$$\rho^{nadir}_{tar} = \frac{\gamma_{dir}\, f_{tar}\,(\theta_i, 0) + (1-\gamma_{dir})\;\int_0^{\pi/2} f_{tar}\,(\theta, 0)\;\; w\,(\theta \mid i)\;\mathrm{d}\theta}{\gamma_{dir}\, f_{ref}\,(\theta_i, 0) + (1-\gamma_{dir})\;\int_0^{\pi/2} f_{ref}\,(\theta, 0)\;\; w\,(\theta \mid i)\;\mathrm{d}\theta}\rho^{nadir}_{ref} \tag{5}$$

in which γ_{dir} is the fraction of direct irradiance on a horizontal surface and $w\,(\theta\,|i)$ expresses the distribution of diffuse irradiance under specific illumination conditions (i) as a weighting function. This expression no longer depends on absolute (radiometric) measures of light flux. Different (polynomial) expressions exist to describe the BRDF of Spectralon material [10, 17, 18] that is commonly used as the reference surface, so we assume f_{ref} to be known. Its impact on reflectance factors measured under obscured conditions is discussed in Section 4.3. The other parameters are harder to determine since they depend on the BRDF shape of the (unknown) target and on the specific illumination conditions at the time of measurement.

All variables also depend on wavelength. For f_{tar} and f_{ref} this is inherent to the BRDF itself. γ_{dir} depends on the amount of scattering by air and cloud particles and therefore increases with increasing wavelength (Rayleigh scattering) while water absorption regions also impact its magnitude [19]. Wavelength dependencies of γ_{dir} and the weight function (w) are discussed in Section 4.2.

2.5. Normalization Factor for Dual-Beam BRDF Effects

In this section a normalization strategy is developed to convert the measurements from a dataset with different levels of cloud obscuration to quasi clear sky reflectance. The normalization is data-driven without the requirement of additional data on atmospheric conditions or reference or target BRDF shape and relies on the similarity in BRDF shape of similarly structured targets. The term "quasi clear sky" (QCS) will be used for prevailing partly cloudy conditions with no clouds obscuring the solar disk or the surrounding corona, i.e., the CIE white-blue sky with distinct solar corona (type V.4) [20]. "Clear sky" (CS) then refers to a cloudless sky as defined in the CIE Standard Clear Sky (type IV.4). The similarity between both sky types, with respect to the normalization procedure, is discussed in Section 4.2.

The function f_{tar} in Equations 4 and 5 describes the target bidirectional reflectance under different illumination conditions and is the key factor in obtaining QCS reflectance factors. When no multi-angular observations are available, f_{tar} cannot be derived from field spectroscopy data. Prior knowledge or assumptions are thus required. This is achieved by decomposing f_{tar} for an arbitrary viewing and illumination geometry into the product of (i) a target specific reflectance factor, $\bar{\rho}_{tar}(\lambda)$ independent of viewing and illumination geometry and (ii) a bidirectional component, $\kappa_{tar}(\lambda, \theta_i, \theta_v, \varphi_i - \varphi_v)$ determined by the general structure of the target type and describing the relative shape of the BRDF. The shape of κ_{tar} as a function of viewing and illumination angles should thus be approximately equal for different targets of the same type. The decomposition described here is thus based on the same principle as the kernel-driven MODIS Albedo product for sparse angular sampling [21]. For nadir viewing, it allows the retrieval of $\bar{\rho}_{tar}(\lambda)$ from Equation 5 if κ_{tar}, κ_{ref},γ_{dir}, w and f_{ref} are known.

During a short measurement series with constant solar elevation under partly cloudy conditions over a constant target, variations in cloud obscuration (COD) are considered to be the dominant atmospheric parameter influencing the angular distribution of incident light (w) and the fraction of direct incident light (γ_{dir}). Short-term (hourly) variations in other atmospheric parameters such as atmospheric haze (expressed as atmosphere optical depth or AOD) are not considered here. Research by [22] indicates that although diurnal fluctuations in AOD can be considerable, hourly fluctuations are smooth (as opposed to sudden changes in COD) and limited in magnitude. From Equation 5 can now be derived that the ratio of two reflectances obtained form the same target, one measured with a certain level of cloud obscuration (COD = x) and the other with a (quasi) clear sky (QCS or COD = 0), is no longer a function (g) of the target specific reflectance factor $\bar{\rho}_{tar}$. This ratio only depends on the bidirectional shape parameters (κ_{ref} and κ_{tar}) and illumination conditions (θ_i,γ_{dir} and w):

$$\frac{\rho^{x}_{tar}(\lambda)}{\rho^{QCS}_{tar}(\lambda)} = g\left(\gamma^{QCS}_{dir},\, w^{QCS},\, \gamma^{x}_{dir},\, w^{x} \mid \theta_i,\, \kappa_{tar},\, \kappa_{ref},\, \lambda\right) \tag{6}$$

The function g, for specified values of θ_i, κ_{tar} and κ_{ref}, can be experimentally determined (e.g., using quadratic regression) for each wavelength (λ) using only reflectance factors obtained over a constant

target for a range of COD values (see Figure 5 for examples).

For practical DFOV applications however, it is preferred to reformulate g as a function of incident radiance (L) or irradiance (E) quantities that, unlike γ_{dir} or w, are automatically measured by the spectroradiometer making the reference measurements. Simulations with atmospheric radiative transfer models (see also Section 4.2) demonstrate that, with increasing levels (x) of COD, the total irradiance (E^x_{tot}) monotonically decreases while γ^x_{dir} also monotonically decreases and w^x evolves towards a fixed distribution. Under such conditions a unique relationship exists between E^x_{tot} on one hand and γ^x_{dir} and w^x on the other hand. Consequently Equation 6 can be reformulated as:

$$\frac{\rho^x_{tar}(\lambda)}{\rho^{QCS}_{tar}(\lambda)} = g\left(\frac{E^x_{tot}}{E^{QCS}_{tot}} \mid \theta_i,\ \kappa_{tar},\ \kappa_{ref},\ \lambda\right) \tag{7}$$

The technique described here is analogous to empirical relationships established to derive atmospheric properties such as turbidity and clear sky index from relative total irradiance [23]. As an easier alternative, measurements may be discretized into a "quasi clear sky set" containing scans with no obscuration and an "obscured sky set" containing scans with full obscuration (high values of COD), turning g into a constant spectrum. Once determined for a single target, g can be applied as a normalization factor (nf) to convert reflectance factors of other targets with a similar structure (e.g., trees of the same species, stand and age class) measured under cloud obscuration (but equal solar elevation angle) into QCS reflectance (ρ^{QCS}_{tar}). As a consequence, the proposed normalization procedure does not require a full characterization of the target BRDF nor a full description of κ_{tar}, but rather of a group of targets by a nf derived under equal illumination conditions. This nf may be obtained at the start of a field dataset collection by fixing the target spectroradiometer over a representative target such as a tree crown or a part of a grass sod, and simultaneously measuring reflectance factors and spectral irradiance under varying levels of clouds for approximately 15 to 30 minutes. Porting an established nf to different measurement days is possible as long as illumination conditions, such as cloud type and solar elevation, are almost equal.

3. Materials and Methods

3.1. Field Measurements

Five hyperspectral field datasets were collected in Leuven, Belgium (50°52'N, 4°42'E) over three different targets: a grass sod (*Lolium perenne* L.) on a loamy soil, potted Citrus trees placed on a loamy soil and gravel. Solar zenith angles (SZA) during measurement time range between 36° and 63°. Yearly minimal and maximal SZA at solar noon at the measurement site are 27° and 74°. All datasets were collected under a partly cloudy sky (CIE types IV.2, IV.3 and IV.4) with different levels of cumulus clouds as such that each set contains several clouds obscuring the solar disk. The length of each series was restricted to approximately 40 minutes to minimize effects in impact of changing solar elevation. Table 2 summarizes the measurement conditions, including the approximate range of total irradiance. Total irradiance was estimated by converting the measured whitepanel radiance into irradiance. Two independent dataset (different trees of equal cultivar, age and phenology) were obtained for Citrus under comparable illumination conditions. The first is intended for derivation of the normalization factor (nf) while the second set is intended to test the normalization procedure.

Table 2. Overview of measurement conditions and targets for field measurements.

target	day, time	solar zenith (°)	min. irradiance ($W\ m^{-2}$)	max. irradiance ($W\ m^{-2}$)
Citrus tree canopies (set 1)	8-24-2008, 13h10	41°	158	886
Citrus tree canopies (set 2)	30-4-2009, 13h00	36°	190	859
grass sod (0.05 m height)	9-10-2008, 14h00	46°	160	752
grass sod (0.05 m height)	9-10-2008, 17h00	63°	136	385
gravel	9-11-2008, 14h00	46°	203	785

Field measurements were made with two Spectra-Vista HR-1024 spectroradiometers with spectral resolutions of 3.5 nm between 350 and 1,000 nm, 8.5 nm between 1,000 and 1,850 nm and 6.5 nm between 1,850 and 2,500 nm. A reference instrument with a 4° FOV fore-optic was mounted on a tripod over a Spectralon whitepanel placed 0.5 m below the sensor lens. The second target instrument with a 25° FOV fore-optic was mounted on a second tripod at 1.7 m height for measurements of the grass sod and gravel surfaces. For the tree canopies, the instrument was attached with a fixture onto a scaffold at 3.5 m height. The larger spot size of the 25° FOV fore-optic, approximately 0.08 m² at 1.5 m distance [24], assures a more representative sampling of ground targets while the 4° FOV fore-optic assures a correct focusing on the center of the whitepanel. Per series between 30 and 50 scans were made, each of 10 s length with varying levels of obscuration and overall sky cloud cover. Both instruments were manually triggered to start measuring at exactly the same time (less than 0.1 s time difference). During a measurement series, the sensor gain of each instrument was automatically determined at the start of each individual scan. This assured optimal signal-to-noise ratios at the light intensity level of each individual scan. Measurements where light intensity substantially increased during the scan time resulted in saturation effects in the detectors and those saturated spectra were filtered during data preprocessing. All spectra were collected in radiance mode ($W\ m^{-2}\ sr^{-1}\ nm$). For each measurement set, intermediate intercalibration scans were made with both instruments measuring a level Spectralon whitepanel to obtain an ICF under field conditions as suggested by [6].

3.2. Ray Tracing Simulations

Three different virtual targets were constructed: gravel surface, grass sods and *Citrus sinensis* L. (Osbeck) trees. For each target, measurements were simulated in a ray tracing environment for different solar elevations and atmospheric conditions. The ray tracer, PBRT, is a physically based ray tracer [25] adapted for hyperspectral radiative transfer simulations and validated with the RAMI Online Model Checker [26]. Measurements were simulated from 400 nm to 2,500 nm in 10 nm increments. Per simulation, 250,000 random rays were cast, which guarantees a relative error in reflectance below 0.4% for all wavelengths [27]. Simulations were set up to approximate (but not to equal) field conditions with similar targets, atmospheric conditions and sensors. Since the aim of the simulations was a theoretical analysis of BRDF effects with DFOV sensors for various conditions and targets, no attempt was made to obtain an exact calibration for the specific measurement settings.

A virtual 25° field of view camera was positioned at 5 m height for the tree simulations (3 m above the top-of-canopy) and at 3 m height for the sod and gravel targets. The gravel surface was simulated as a simple flat surface using the Hapke-Jacquemoud soil BRDF model [28] and bidirectional coefficients for pebble surfaces ($h = 0.09$, $b_0 = 1.11$, $c_0 = 0.53$, $b_1 = 0.33$, $c_1 = -0.11$). The single scattering albedo was obtained by inversion of reflectance spectra collected with a Spectra-Vista HR-1024 spectroradiometer.

The grass sod was simulated as randomly placed disks with a 0.01 m radius, an elevation between 0 and 0.1 m and an erectophile leaf angle distribution as defined in [29]. Grass leaf reflectance and transmittance were simulated as Lambertian surfaces with spectra (*Phleum sp.*) obtained from the LOPEX dataset [30].

The Citrus tree structures were calibrated on ten Citrus trees in a commercial orchard in Wellington, South-Africa [31]. The calibration procedure is described in [27]. Citrus stem reflectance was Lambertian and leaf reflectance and transmittance were calibrated on measured spectra with the Bousquet microfacets model [32]. The ten calibrated trees used in the simulations comprise a set with large variations in both tree canopy structure (e.g., LAI at tree level ranges from 3.2 to 11) and leaf reflectance (e.g., average leaf chlorophyll content per tree from 47 to 89 $\mu g\, cm^{-2}$). The underlying soil, identical for each tree, was simulated as a moist loamy soil (coefficients $h = 0.09$, $b_0 = 1.11$, $c_0 = 0.64$, $b_1 = 0.18$, $c_1 = -0.05$) using the Hapke-Jacquemoud BRDF model. An identical inversion procedure on measured spectra was used to obtain the single scattering albedo of a loamy soil (Alfisol). Total direct and diffuse irradiance as well as the angular distribution of diffuse irradiance were simulated with the SBDart atmospheric model [33] for wavelengths from 400 to 2,500 nm (per 10 nm) at an angular resolution of 2° and subsequently implemented as direct and hemispherical (diffuse) light sources in pbrt. Simulations were made for solar zenith angles of 20, 30, 40, 50 and 60° and for ten levels of cloud optical depth (COD) between 0 and 100 at logarithmic increments. Cloud height (4,000 m), cloud thickness (400 m), aerosol optical depth (0.3) and atmospheric water vapor ($2.5\ g\, cm^{-2}$) and ozone ($0.3\ g\, cm^{-2}$) concentrations were fixed at typical values for mid-latitude atmospheric conditions. Cloud cover was simulated as a uniformly overcast sky. In all simulations, the effect of the reference panel BRDF was included using a fourth order polynomial approximation of the panel BRDF as established by [18].

4. Results and Discussion

In the first set of simulations, the impact of the reduced irradiance (signal strength) due to cloud obscuration on the measured SNR is discussed. Subsequently, ray-tracing simulations combined with atmospheric radiative transfer models are used to reproduce BRDF effects of different targets for varying illumination conditions. Results are compared to field collected datasets and recommendations are formulated for optimal measurement conditions. In the last step, the normalization procedure is evaluated on synthetic and real measurements.

4.1. Impact of Cloud Cover on the Signal-to-Noise Ratio

To assess the impact of cloud cover on signal quality, the NER of both spectroradiometers was determined using 20 consecutive 1 s scans. SNR in spectral radiance units ($W\, m^{-2}\, sr^{-1}\, nm$) was obtained

from Equation 2 using measured radiance of a grass sod target for a 10 s scan time (T). Obtained results agree with manufacturer provided instrument specifications. SNRs were calculated for four different illumination conditions consisting of combinations of low (36°) and high (63°) solar zeniths with obscured and non-obscured conditions. Analogously, SNR for the instrument measuring the reference panel were obtained for the same measurement conditions. Both values were combined into the SNR of reflectance (Equation 3) as illustrated in Figure 1, from 350 to 2,500 nm. Although these results are specific for the combination of instrument type, target and illumination conditions being used, it allows to make some general inferences. Due to a low instrument NER in combination with high spectral irradiance, the SNR in the 450–900 nm region is at least one order of magnitude larger than in the higher wavelengths, even for the vegetative target that has a low reflectance in the visible part of the spectrum (VIS, 400–700 nm). For the unfavorable combination of a low zenith angle and obscured illumination, the SNR in this region still exceeds 100. The usability of the 1,000–1,800 nm region is heavily impacted by both solar elevation and cloud thickness. The SNR drops below 10 above 2,000 nm in the case of cloud obscuration. DFOV spectroscopy applied under cloud obscured conditions will thus require longer measurement times or a larger number of scans from the same target to achieve equal SNR levels as compared to clear sky conditions. Alternatively broader spectral regions around the atmospheric water absorption regions or even the entire 1,800–2,500 nm region may need to be excluded from analysis. This analysis indicates that DFOV time series can be established even with low illumination conditions for the monitoring of chlorosis-related stresses such as nitrogen deficiencies that show up in the VIS spectrum [34] and canopy structure changes that are most pronounced in the near-infrared (NIR) [35]. Monitoring of changes that appear in the short-wave infrared (SWIR) may on the other hand be restricted. Further reductions in noise levels under prevailing atmospheric conditions can be obtained by applying advanced noise filtering techniques [36].

Figure 1. Signal-to-noise ratios for dual FOV measurements using Spectra-Vista HR-1024 instruments and 10 s integration times. Measurements at Leuven, Belgium, 10/9/2008, 14h00 local time (SZA = 36°) and 17h00 local time (SZA = 63°).

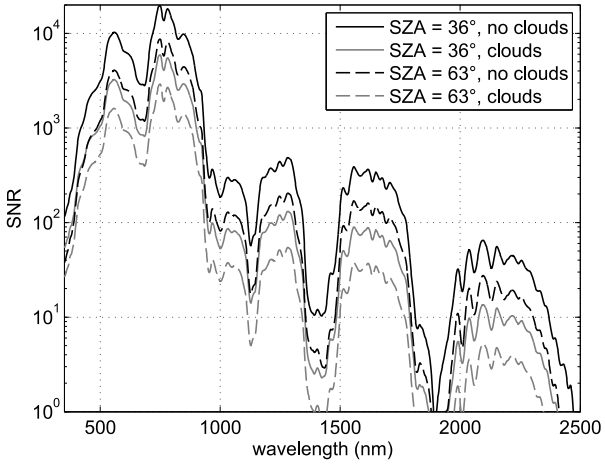

4.2. *Wavelength Dependency of Fraction of Diffuse Radiance and Weight Function*

Figure 2 shows fractions of direct irradiance (γ_{dir}) simulated with the atmospheric radiative transfer model SBDart for some typical mid-latitude illumination conditions and different levels of cloud optical depth (COD). For overcast skies (COD $\geq$ 5, black dotted line at the bottom) almost all the light is diffuse so that γ_{dir} is equal or close to zero for all wavelengths.

Figure 2. Fraction of direct irradiance for different values of solar zenith angle (SZA) and cloud optical depth (COD) simulated with SBDart. Simulations used fixed values for atmosphere optical depth (0.3), cloud altitude (4,000–4,400 m), water vapor content ($2.5\ g\ cm^{-2}$) and ozone content ($0.3\ atm\ cm^{-1}$).

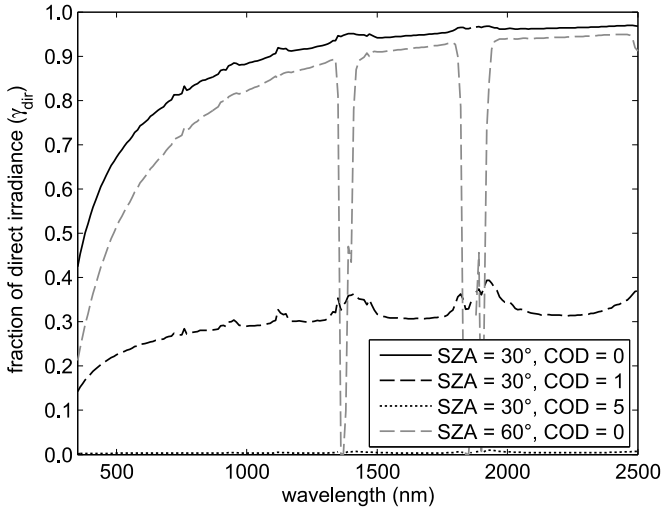

Figure 3 shows the angular distributions of diffuse light projected onto a horizontal plane, simulated with SBDart and normalized as a weight function as described in Section 2.4. Curves are plotted for a solar zenith angle of 60°, aerosol optical depth of 0.3 and different cloud optical depths (left figure) and wavelengths (right figure). As a reference on the left figure, the weight function is plotted of a hypothetical isotropic distribution that takes the shape of a half sine curve (grey dotted line). Large differences exist between the different weight functions, demonstrating the importance of accounting for angular distributions of diffuse light to obtain good quality normalizations of BRDF effects in DFOV spectroscopy. To increase optical depths, the weight function first concentrates around the solar disk (COD = 0.5) and for higher values (COD > 5) it converges into a fixed distribution, with a maximum weight around the 40° sky zenith angle (grey dashed line). Different simulations confirm that for COD = 100, the weight function becomes largely independent of wavelength with the exception of the higher SWIR wavelengths (R^2 between weight functions at different wavelength > 0.99 from 350 to 1,340 nm and from 1,520 to 1,790 nm), solar zenith angle (R^2 between 10° and 80° > 0.99) and aerosol optical depth. The CS weight functions (right figure) have more articulated maxima for increasing wavelengths due to more atmospheric Rayleigh scattering in addition to the Mie scattering by clouds. The right figure

in addition shows the weight functions derived for the CIE white blue sky and clear sky types as defined in [20] at a 60° SZA. The coefficient of determination between both functions ranges from 0.99 for a 10° SZA to 0.97 for a 80° SZA. These observations indicate that at least for the visible wavelengths (CIE is defined as luminance) the difference between CS and QCS reflectance factors as defined in section 2.5 will be limited.

Figure 3. Angular distribution of diffuse incident light expressed as a weight function, for different values of cloud optical depth (left figure) and wavelengths (right figure) simulated with SBDart or derived from the CIE formulations [20] for a 60° solar zenith angle.

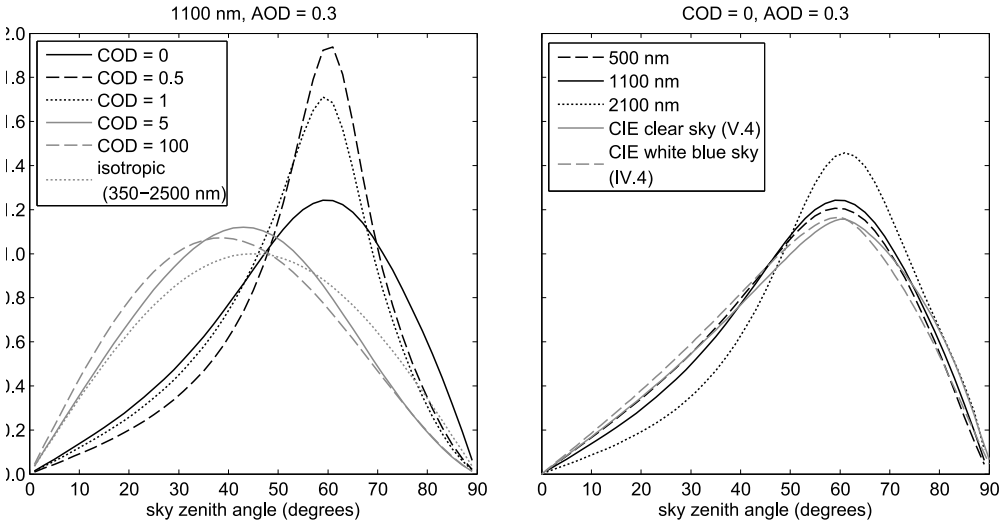

4.3. Impact of Reference Panel BRDF

Figure 4 shows the reflectance factor of a Spectralon whitepanel for different illumination conditions, calculated using Equation 5 with wavelength dependent skylight distributions (weighting factors) and fractions of direct irradiance simulated with SBDart. The target BRDF is derived from the correction factor for the non-Lambertian behavior of Spectralon material as established by [18]. The BRDF effects caused by a small cloud optical depth (COD = 1) compared to a clear sky (COD = 0), with a SZA fixed at either 30° (dashed and solid black lines) or 60° (dashed and solid grey lines) are below 1%. For high cloud thickness (COD = 100, equal for all SZAs), deviations from CS reflectance range from approximately 1% to more than 3%. For low solar azimuths (SZA = 30°), obscuration causes an underestimation of the panel CS reflectance factor, while for high solar azimuths, this effect reverses. It is thus expected that the use of a reference panel in DFOV spectroscopy will substantially contribute to BRDF effects if not corrected for. In the establishment of a time series over a span of several months, single FOV spectroscopy will also likely require corrections for reference panel BRDF unless a field protocol is adopted to measure under constant solar elevation. Whether the non-Lambertian nature of the reference panel will intensify or (partly) compensate BRDF effects of different targets will depend

on the specific BRDF shape of those targets and more specifically on the dominant optical scattering process (geometric-optical or volume scattering) that determines this shape [21].

Figure 4. Reflectance factor of Spectralon whitepanel for different cloud optical depths and solar zenith angles calculated with polynomial approximations of [18].

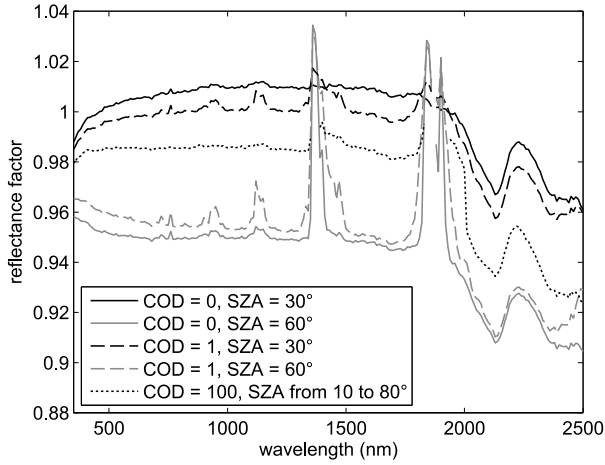

4.4. Effect of Fluctuations in COD and Irradiance During Scan Time

The normalization procedure developed in Section 2.5 relies on the measurement of total irradiance. When measuring under partly cloudy conditions, however, the optical depth of clouds obscuring the solar disk and corona and therefore also total irradiance can exhibit large fluctuations during a measurement scan. Measured total irradiance can be the result of either an almost constant illumination under intermediate cloud thickness or a mixture of high irradiance with unobscured and low irradiance with obscured conditions caused by a thick cloud layer. To assess the impact of varying illumination during a scan, effects were simulated of clouds moving before the solar disk during a short (10 s) time interval. For a 10 s scan, reflectances were calculated ranging from a clear sky (CS, COD = 0) to fully obscured sky (OS, COD = 100) for different mixture levels (α) ranging from 0% obscuration (of the scan time) to 100% obscuration. Since spectroradiometers collect radiance rather than reflectance, the result is a linear mixture of reflected radiances (L), but is non-linear with respect to reflectance factors (ρ):

$$\rho^{\alpha}_{meas}(\lambda) = \frac{\alpha\, L^{CS}_{tar}(\lambda) + (1-\alpha)\; L^{OS}_{tar}(\lambda)}{\alpha\, L^{CS}_{ref}(\lambda) + (1-\alpha)\; L^{OS}_{ref}(\lambda)} = \frac{\alpha\, E^{CS}(\lambda)\, \rho^{CS}_{tar}(\lambda) + (1-\alpha)\; E^{OS}(\lambda)\, \rho^{CS}_{tar}(\lambda)}{\alpha\, E^{CS}(\lambda)\, \rho^{CS}_{ref}(\lambda) + (1-\alpha)\; E^{OS}(\lambda)\, \rho^{CS}_{ref}(\lambda)}$$

with L^{CS}_{tar}, L^{OS}_{tar}, L^{CS}_{ref} and L^{OS}_{ref} the target and reference reflected spectral radiances and E^{CS} and E^{OS} the total spectral irradiances for both clear and obscured conditions.

Figure 5 shows the results of simulations for different combinations of wavelengths, solar elevations and targets. The X-axis shows the relative total irradiance, scaled to the maximum value (CS conditions). The Y-axis shows the reflectance relative to CS conditions and thus equals the inverse of the

normalization factor (nf) to convert to CS conditions. Each simulation is shown as two curves forming a loop of which the thick line contains (from left to right) decreasing levels of COD and the thin line contains (from left to right) increasing fractions (α) of CS illumination. The difference between both lines is apparent for most simulations and presents a dilemma for applying a normalization based on total irradiance: if no instantaneous irradiance measurements but only the average irradiance is collected during a scan, it is not possible to discriminate scans with stable and intermediate levels of COD (between 1 and 10) from scans with strong fluctuations in COD. As a consequence the normalization factor can take any value between the upper and lower curve of a loop. A solution is restricting measurements to scans with assured stable illumination conditions (i.e., the outer edges where both curves converge) with either high (>10) or low (<1) values of COD, possibly in combination with a reduction of the scan time. The COD threshold values may change depending on target type and maximum BRDF-induced bias and values used here ascertain relative deviations on Citrus tree canopies to be below 5% (see Figure 5A). This allows field measurement scans to be subdivided into "quasi clear sky scans" and "obscured sky scans", with a normalization applied only to the latter group. The relative flatness of the upper curves for CODs between 20 and 100 indicates an approximately constant normalization factor once cloud thickness (COD) reaches a certain level. Conversely, the steep slope of the curve for low COD values indicates that even thin (cirrus) clouds may trigger a substantial BRDF effect. The shape of the lower curves of the loops stresses the importance of stability of the illumination conditions during the scan time, as even a small mixture fraction of direct sunlight greatly impacts the relative reflectance.

Figure 5. Relative reflectance compared to clear sky reflectance simulated with pbrt and SBDart for gradually increasing cloud optical depth (thick curves) and different mixtures between clear and obscured conditions (thin curves). Simulations for (a) three different wavelengths, (b) five solar zenith angles and (c) three surface types.

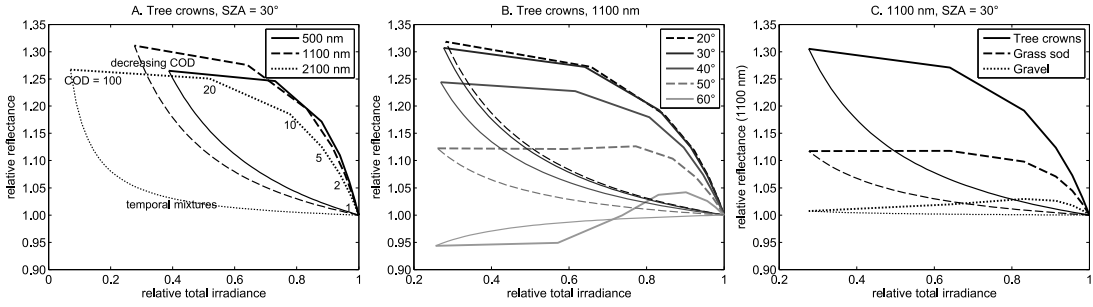

For most simulations, reflectance under obscured conditions is higher than under CS conditions (relative reflectance > 1). Only for tree canopies simulated with low solar elevation angles (middle figure, SZA = 60°) an inversion occurs. The BRDF shape of vegetation targets and, to a lesser extent, of rough soil surfaces (gravel) thus seems opposite to the BRDF effects of the whitepanel (Figure 4). Hence the ratio of both radiances (Equation 5) will reinforce rather than compensate the overall BRDF effect.

The differences between the loops on the three figures show that each combination of target type and solar zenith angle requires a different wavelength-dependent normalization factor. For DFOV time series

this implicates that for the same type of target, throughout a measurement season different normalization factors may need to be established.

4.5. Evaluating the Decomposition of the Target BRDF

The normalization strategy developed in Section 2.5 relies on the assumption that the BRDF of a target can be split into a target specific component independent of viewing and illumination geometry and a bidirectional component that describes the behavior of a group of targets, i.e., $f_{tar} \approx \rho_{tar}^{dh} \kappa_{tar}$. A simulation was set up to evaluate the impact of this assumption on the performance of the normalization procedure. The evaluation was made for the Citrus tree canopy targets that showed the largest BRDF effects (Figure 5c). Ten iterations were set up for solar zenith angles of 30° and 60° in which subsequently each of the ten calibrated Citrus trees was used as a reference to construct a normalization factor (nf) as the ratio of reflectance with obscured sky (COD = 100) and clear sky (COD = 0). In each iteration the nf was used to normalize the obscured sky reflectances of the nine remaining trees to clear sky conditions. The performance of the procedure was expressed as the relative root mean square error (RRMSE) between true and normalized clear sky reflectance (Figure 6). The results show that not correcting reflectance for BRDF effects results in substantial errors between 20% and 40% for solar elevations of 30°. At an elevation of 60° the uncorrected relative errors fall below 10%. Both results corresponds to Figure 5b. Applying the nf results in an improvement for the 30° SZA simulation and a smaller improvement (except between 1400 and 2000 nm) for the 60° SZA simulation. Normalized spectra consistently have an average RRMSE below 5%. This is comparatively low considering the large variations in canopy structure and leaf reflectance present in the Citrus tree dataset (see Section 3.2 and [27]). Whether or not errors of this magnitude are acceptable will be application-dependent.

Figure 6. Relative error in reflectance of the simulated Citrus trees under cloudy conditions (COD = 100) using a clear sky reflectance (COD = 0) as a reference, simulated with pbrt and SBDart. Averages for 10 Citrus tree canopy targets and two solar zenith angles. Black curves: uncorrected reflectance, grey curves: corrected reflectance.

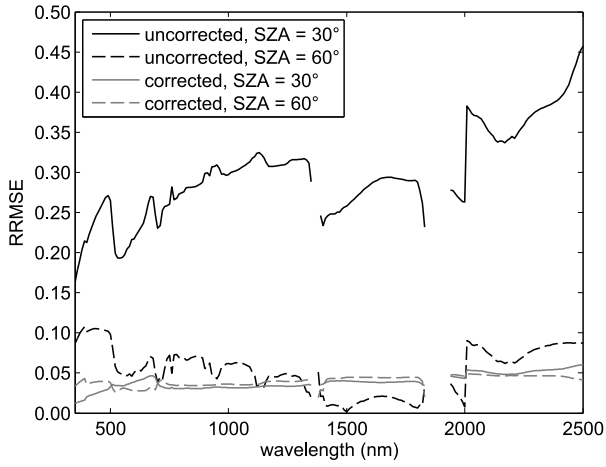

4.6. Interpretation of Measured BRDF Effects

Figure 7 shows, for four different measurement sets, the relative reflectance factor between 1,050 and 1,150 nm (around the peak NIR reflectance of vegetations) as a function of total irradiance. Reflectance factors for each figure were normalized to average reflectance under unobscured conditions. Irradiance values were normalized to the maximum total irradiance per measurement sets. Most of the points on the scatter-plots are grouped into two clusters (black dots): one for high irradiance (unobscured) and one for low irradiance (obscured). The limited number of intermediate points (grey dots) show large fluctuations. This agrees with the simulations in Section 4.4 (Figure 5) where intermediate measurements could take any position between the upper and lower curve of a loop. Most intermediate points have relative reflectances closer to 1 indicating that most of them are caused by irradiance fluctuations during the scan time.

Figure 7. Measured relative reflectance factor between 1,050 and 1,150 nm, normalized to reflectance at quasi clear sky conditions (10 percentile highest values). The X-axis shows the relative total irradiance, scaled to the highest measured value.

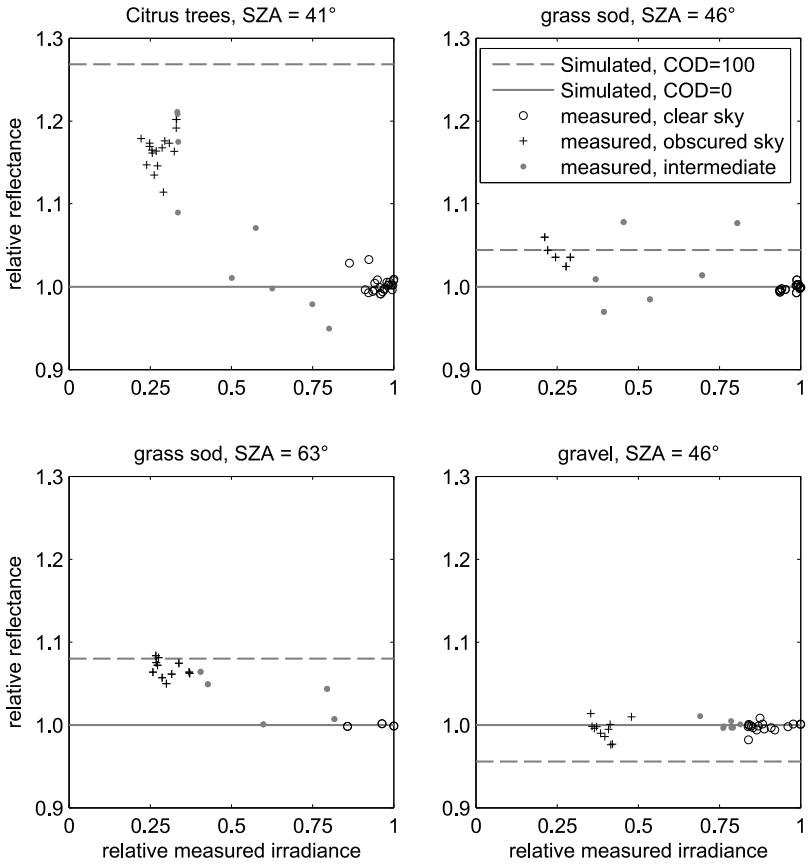

For each measurement set a virtual model was constructed with a comparable canopy or soil structure and reflectance and simulated with PBRT (see Section 3.2) under an approximately equal illumination (solar elevation), for both clear and obscured conditions. For each simulation, a wavelength-dependent nf was derived using the procedure of Section 2.5. The nfs calculated for the same wavelength interval are drawn as horizontal dashed lines on Figure 7. For an ideal agreement between simulated and measured datasets, these line should thus pass through the centers of the point clusters for obscured conditions. The simulated nf for tree canopies is overestimated, the nfs for the grass sods under high and low solar elevations show good agreement with the measurements and the nf for the gravel surface is underestimated. Similar results were obtained for other wavelengths (results not shown here). In general both simulated and measured datasets show a similar behavior of relative reflectance as a function of relative irradiance, although the magnitude of the effects are not always equal. It can be concluded that relative differences in reflectance factor related to differences in illumination are well explained and described by the theory presented in Sections 2.4 and 2.5. The use of synthetic nfs to correct DFOV measurements can however be questioned.

4.7. Data-Driven Normalization

The alternative to synthetic nfs is a data-driven approach in which an nf is obtained from a reference target with equal solar elevation and varying grades of cloud cover. Figure 8 shows spectral nfs obtained for the four different field-collected datasets. The nfs for each dataset were obtained as the ratios of average QCS to average OS reflectance factors, while intermediate values (>150% of lowest total irradiance and <80% of highest total irradiance) were removed to minimize irradiance fluctuations during scan time (see Sections 4.4 and 4.6). Removed spectra accounted for less than 20% of the measurements in each dataset. As predicted from the simulation data, the values of the nfs are spectrally variant, depend on the solar elevation angle and show large differences between target types (grass sod, tree canopy, gravel). Both negative and positive values occur.

Figure 8. Normalization factors derived for four field measurements sets.

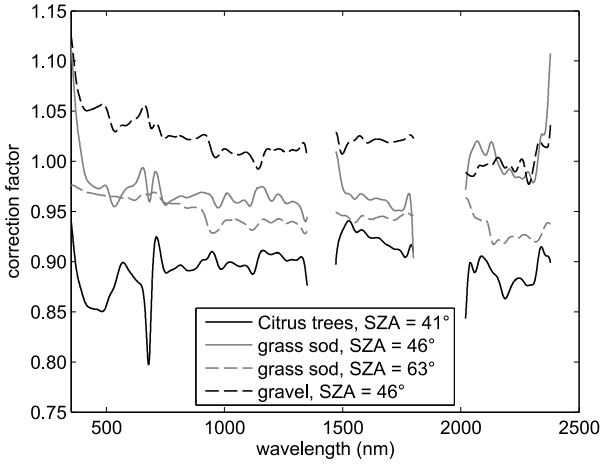

A nf derived from a DFOV dataset of measured Citrus tree canopy reflectance (black solid line) was subsequently applied to normalize a second DFOV dataset of different Citrus trees (same variety and phenology) with comparable structure, measured under similar illumination conditions (difference in average SZA below 4°). Figure 9 compares measured reflectance under obscured conditions (grey lines) to the average unobscured reflectance factor (black line) for both original uncorrected and normalized data. The normalized results show a better fit over the entire spectrum although the normalized reflectance still shows a small overestimation in the NIR.

Figure 9. Reflectance factor of Citrus trees measured under obscured conditions (grey lines, individual scans) with a reference (black line, average value) measured under unobscured conditions. Top figure: uncorrected spectra. Bottom figure: after multiplication with a normalization factor.

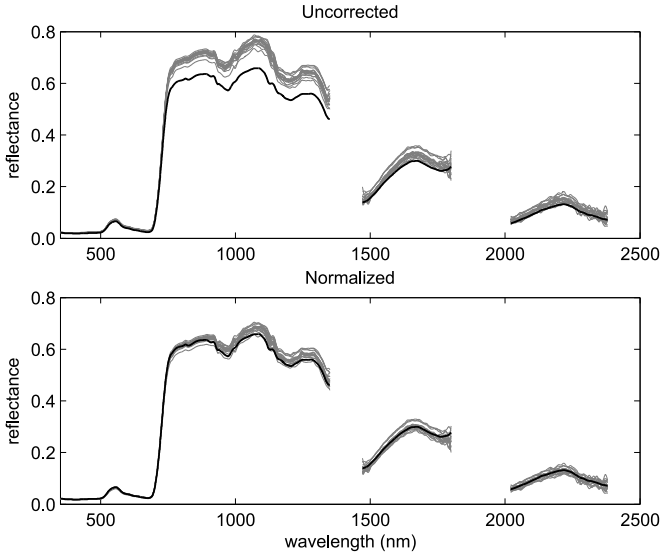

Figure 10 shows the RRMSE of the cloud obscured data compared to the unobscured data. Without normalization, relative errors range between 10% and 20%. After normalization, relative errors fall below 6% up to 1,800 nm, but reach values up to 10% for higher wavelengths. As compared to the simulations of Figure 6, the magnitude of the errors is comparable up to 1,800 nm. To separate BRDF-related bias from noise (which is not present in the simulations), the RRMSE of the average of the normalized measurements is also plotted. In this average spectrum the noise term is reduced by a factor of 4.1 (17 scans) so that it represents an upper bound to BRDF-related bias. The low values between 1,500 and 2,500 nm indicate that for the individual normalized scans (solid black line), the increased RRMSE beyond 1800 nm is no bias, but caused by a low SNR (see Figure 1) related to severely reduced irradiance. As a second reference the relative standard deviation of the unobscured (reference) measurements is plotted on Figure 10, which is consistently below 4%. It reflects the error term under quasi clear sky conditions and is attributed to electronic sensor noise, small target changes (wind) or BRDF effects due to small changes in illumination (AOD) or solar elevation during a measurement set [4].

Figure 10. Relative error in reflectance (RRMSE) of measurements under obscured conditions using unobscured measurements as a reference.

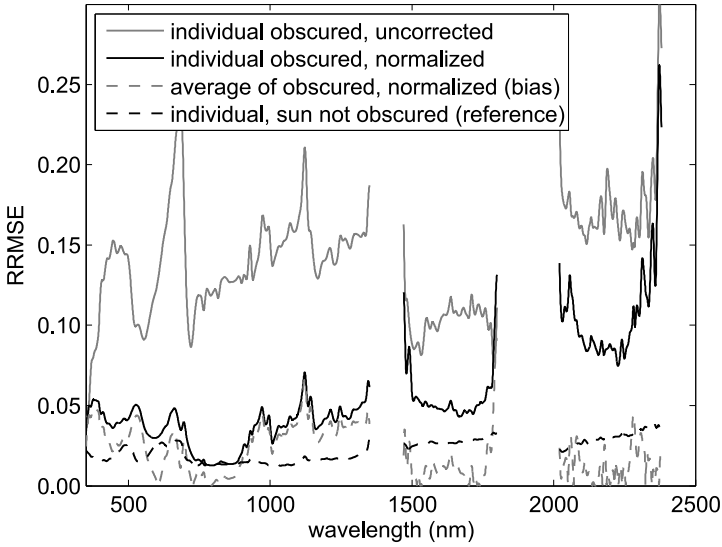

For vicarious calibration, normalization to (quasi) clear sky conditions as presented here is still required. The construction of time series in field spectroscopy on the other hand can benefit from a normalization to standardized illumination conditions to separate BRDF effects due to illumination conditions (solar elevation) from changes in target reflectance, e.g., due to vegetation physiology. The same approach can therefore inverted to normalize to reflectance with a homogeneous cloud obscured sky. When the COD is sufficiently high (>5), for all wavelengths in the 400–2,500 nm region, almost all the incident light is diffuse ($\gamma_{dir} \approx 0$) and the weight function is almost constant (see Section 4.2) and approximately isotropic [20, 37]. The reflectance factor measured under overcast conditions will therefore offer an approximation of hemispherical-directional reflectance (ρ^{hd}) with nadir viewing angle or directional-hemispherical reflectance (ρ^{hd}, or black-sky albedo) with zenith illumination according to the Helmholtz reciprocity principle.

5. Conclusions

The impact of reduced irradiance caused by cloud cover on the SNR of the measured reflectance factor was quantified. Results suggest that data quality standards (minimal SNR) can be converted into instrument and wavelength specific lower bounds for illumination conditions (spectral irradiance) under which DFOV spectroscopy can be deployed.

BRDF effects in DFOV measurements could be modeled and described using synthetic data in a ray tracing environment. Solar elevation, wavelength and target type (structural composition) were found to be the determinant factors affecting differences between reflectance factors under obscured and unobscured conditions, while the reference panel BRDF will often reinforce this effect.

A data-driven normalization procedure and its underlying assumption (decomposition of the BRDF into a target specific isotropic and a group specific bidirectional component) were evaluated on both synthetic and real datasets. Results indicate that most of the bias in cloud obscured measurements can be removed by applying a normalization factor obtained by from a representative target under equal illumination conditions, without the need to obtain an exact description of the bidirectional component of the target BRDF (κ_{tar}). Field protocols should avoid or remove measurements that include large irradiance fluctuations during scan time as well as measurements made with intermediate COD values corresponding to intermediate irradiance levels. Threshold values depend on the acceptable bias. Normalized spectra show low relative errors up to 1,800 nm, but at higher wavelengths, an increase in relative error was attributed to a reduced SNR. For DFOV applications requiring the full 350–2,500 nm spectrum, a larger number of scans per individual target may be required to lower the noise level. The inclusion of a BRDF normalization, in addition to an intercalibration factor shows good promise to deploy DFOV spectroscopy for physiological monitoring applications in mid-latitude climate regions where a dominance of partly cloudy and overcast skies can prevent establishment of clear sky time series. The low relative errors obtained by this combined normalization (on average 5% below 1,800 nm) may meet the requirements of physiological investigations that require the detection of trends in specific zones of the spectrum.

Prior to implementation, more testing is required under a broader range of illumination conditions with different cloud types and different targets. In addition, this method can be tested in inverse mode to normalize reflectance under standardized overcast illumination conditions that are largely independent of solar elevation. This would be advantageous for the separation of physiological changes from BRDF effects in seasonal time series of vegetated targets.

6. Acknowledgments

This research was funded by the Katholieke Universiteit Leuven, Biosystems Department as part of the Special Research Fund program OT04047.

Appendix

This section describes the conversion of Equation 1 into Equation 5. For nadir (n) viewing directions ($\theta_v = 0$) the relative azimuth between viewing and illumination ($\varphi_i - \varphi_v$) can take arbitrary values with no influence on an object's reflected radiance. The target reflected radiance from Equation 4 can therefore be simplified into:

$$\begin{aligned} L^n_{tar} &= L^n_{dir} + L^n_{dif} \\ L^n_{dir} &= E_{tot}\,\gamma_{dir}\,f_{tar}\,(\theta_i, 0) \\ L^n_{dif} &= \int_0^{2\pi}\int_0^{\pi/2} f_{tar}\,(\theta, 0)\;L_{dif}(\theta, \varphi \mid i)\;\cos\theta\;\sin\theta\,\mathrm{d}\theta\,\mathrm{d}\varphi \end{aligned}$$

The integral part of the last equation can be simplified by defining $\overline{L_{dif}}\,(\theta) = \int_0^{2\pi} L_{dif}\,(\theta,\varphi)\,\mathrm{d}\varphi$, multiplying by $\frac{E_{dif}}{E_{dif}} = \frac{(1-\gamma_{dir})E_{tot}}{E_{dif}}$ and expanding the denominator as a radiometric integral so that:

$$L_{dif}^{n} = (1 - \gamma_{dir}) \frac{\int_0^{\pi/2} f_{tar}\,(\theta, 0)\ \overline{L_{dif}}\,(\theta)\ \cos\theta\ \sin\theta\,\mathrm{d}\theta}{\int_0^{\pi/2} \overline{L_{dif}}\,(\theta)\ \cos\theta\ \sin\theta\,\mathrm{d}\theta}$$

This equation takes the shape of a weighted average with a weight function w defined as $w(\theta \mid i) = \overline{L_{dif}}\,(\theta)\ \cos\theta\ \sin\theta$. The same conversion can be applied to the reference radiance so that the measured reflectance can be written as Equation 5.

References

1. Milton, E.; Schaepman, M.; Anderson, K.; Kneubühler, M.; Fox, N. Progress in field spectroscopy. *IEEE International Conference on Geoscience and Remote Sensing Symposium, IGARSS 2006*, Denver, CO, USA, July 31–August 4, 2006; pp. 1966–1968.
2. *ASD Technical Guide*, 3rd ed.; Analytical Spectral Devices: Boulder, CO, USA, 1999.
3. Milton, E.; Rollin, E.; Emery, D. *Advances in Environmental Remote Sensing*; Wiley: Chichester, UK, 1995; pp. 9–32.
4. Sandmeier, S.R. Acquisition of bidirectional reflectance factor data with field goniometers. *Remote Sens. Environ.* **2000**, *73*, 257–269.
5. Milton, E.; Rollin, E. Estimating the irradiance spectrum from measurements in a limited number of spectral bands. *Remote Sens. Environ.* **2006**, *100*, 348–355.
6. Anderson, K.; Milton, E.; Rollin, E. Calibration of dual-beam spectroradiometric data. *Int. J. Remote S.* **2006**, *27*, 975–986.
7. Milton, E.; Goetz, A. Atmospheric influences on field spectrometry: observed relationships between spectral irradiance and the variance in spectral reflectance. In *Seventh International Symposium on Physical Measurements and Signatures in Remote Sensing*, Courchevel, France, April 7-11, 1997; *Vol. 1*, pp. 109–114.
8. Gilabert, M.-A.; Meliá, J. Solar angle and sky light effects on ground reflectance measurements in a citrus canopy. *Remote Sens. Environ.* **1993**, *45*, 281–293.
9. Abdou, W.A.; Helmlinger, M.C.; Conel, J.E.; Bruegge, C.J.; Pilorz, S.H.; Martonchik, J.V. Ground measurements of surface BRF and HDRF using PARABOLA III. *J. Geophys. Res.* **2000**, *106*, 967–976.
10. Sandmeier, S.; Müller, C.; Hosgood, B.; Andreoli, G. Sensitivity analysis and quality assessment of laboratory BRDF data. *Remote Sens. Environ.* **1998**, *64*, 176–191.
11. Rollin, E.; Milton, E.; Emery, D. Reference panel anisotropy and diffuse radiation - some implications for field spectroscopy. *Int. J. Remote Sens.* **2000**, *21*, 2799–2810.
12. Bruegge, C.; Chrien, N.; Haner, D. A spectralon BRF data base for MISR calibration applications. *Remote Sens. Environ.* **2001**, *76*, 354–366.
13. Michalsky, J.; Harrison, L.; Berkheiser, W. Cosine response characteristics of some radiometric and photometric sensors. *Sol. Energy* **1995**, *54*, 397–402.
14. Schott, J. *Remote Sensing: The Image Chain Approach*, 2th Ed.; Oxford Press: New York, NY, USA, 2007.

15. Kimes, D.; Kirchner, J. Irradiance measurement errors due to the assumption of a Lambertian reference panel. *Remote Sens. Environ.* **1982**, *12*, 141–149.
16. Gu, X.; Guyot, G. Effects of diffuse irradiance on the reflectance factor of reference panels under field conditions. *Remote Sens. Environ.* **1993**, *45*, 249–260.
17. Flasse, S.; Verstraete, M.; Pinty, B.; Bruegge, C. Modeling Spectralon's bidirectional reflectance for in-flight calibration of Earth-orbiting sensors. In *Proc. SPIE, 1993*, Orlando, FL, USA, April 16, 1993.
18. Schopfer, J. *Spectrodirectional ground-based remote sensing using dual-view goniometry: field BRF retrieval and assessment of the diffuse irradiance distribution in spectrodirectional field measurements*. PhD thesis, University of Zurich, Zurich, Switzerland, 2008.
19. Platt, U.; Pfeilsticker, K.; Vollmer, M. *Springer Handbook of Lasers and Optics*; Springer: New York, NY, USA, 2007; pp. 1165–1203.
20. CIE, Spatial distribution of daylight-CIE Standard General Sky. Technical Report CIE Standard S 011/E:2003, CIE Central Bureau, Vienna, Austria, 2003.
21. Lucht, W.; Schaaf, C.; Strahler, A. An algorithm for the retrieval of albedo from space using semiempirical BRDF models. *IEEE T. Geosci. Remote Sens.* **2000**, *38*, 977–998.
22. Giavis, G.; Kambezidis, H.; Sifakis, N.; Toth, Z.; Adamopoulos, A.; Zevgolis, D. Diurnal variation of the aerosol optical depth for two distinct cases in the Athens area, Greece. *Atmosph. Res.* **2005**, *78*, 79–92.
23. Igawa, N.; Koga, Y.; Matsuzawa, T.; Nakamura, H. Models of sky radiance distribution and sky luminance distribution. *Sol. Energy* **2004**, *77*, 137–157.
24. *HR-1024 User Manual*, rev. 1.3 ed.; Spectra Vista Corporation: New York, NY, USA, 2008.
25. Pharr, M.; Humphreys, G. *Physically Based Rendering: From Theory to Implementation*; Morgan Kaufmann: San Francisco, CA, USA, 2004.
26. Widlowski, J.-L.; Robustelli, M.; Disney, M.; Gastellu-Etchegorry, J.-P.; Levergne, T.; Lewis, P.; North, P.; Pinty, B.; Thompson, R.; Verstraete, M. The RAMI On-line Model Checker (ROMC): A web-based benchmarking facility for canopy reflectance models. *Remote Sens. Environ.* **2008**, *112*, 1144–1150.
27. Stuckens, J.; Somers, B.; Delalieux, S.; Verstraeten, W.; Coppin, P. The impact of common assumptions on canopy radiative transfer simulations: A case study in Citrus orchards. *J. Quant. Spectrosc. Ra.* **2009**, *110*, 1–21.
28. Jacquemoud, S.; Baret, E.; Hanocq, J. Modeling spectral and bidirectional soil reflectance. *Remote Sens. Environ.* **1992**, *41*, 123–132.
29. Bunnik, N.J.J. The Multispectral Reflectance of Shortwave Radiation of Agricultural Crops in Relation with Their Morphological and Optical Properties. PhD Thesis, Mededelingen Landbouwhogeschool Wageningen, Wageningen, The Netherlands, 1975.
30. Hosgood, B.; Jacquemoud, S.; Andreoli, G.; Verdebout, J.; Pedrini, A.G.S. Leaf Optical Properties EXperiment 93 (LOPEX93). Technical report, Joint Research Centre, Institute for Remote Sensing Applications, Unit for Advanced Techniques, TP 272, Ispra (VA), Italy, 1994.

31. Somers, B.; Delalieux, S.; Verstraeten, W.; Coppin, P. A conceptual framework for the simultaneous extraction of sub-pixel spatial extent and spectral characteristics of crops. *Photogramm. Eng. Remote Sens.* **2009**, *1*, 57–68.
32. Bousquet, L.; Lachérade, S.; Jacquemoud, S.; Moya, I. Leaf BRDF measurements and model for specular and diffuse components differentiation. *Remote Sens. Environ.* **2005**, *98*, 201–211.
33. Ricchiazzi, P.; Yang, S.; Gautier, C.; Sowle, D. SBDART: A research and teaching software tool for plane-parallel radiative transfer in the Earth's atmosphere. *Bull. Am. Meteorol. Soc.* **1998**, *79*, 2101–2114.
34. Carrer, G. Ratios of leaf reflectances in narrow wavebands as indicators of plant stress. *Int. J. Remote Sens.* **1994**, *15*, 697–704.
35. Haboudane, D.; Miller, J.; Pattey, E.; Zacro-Tejada, P.; Strachan, I. Hyperspectral vegetation indices and novel algorithms for predicting green LAI of crop canopies: Modeling and validation in the context of precision agriculture. *Remote Sens. Environ.* **2004**, *90*, 337–352.
36. Roberts, M. *Signals and Systems: Analysis of Signals Through Linear Systems*; McGraw-Hill Higher Education: Whitby, Ontario, L1N 9B6, Canada, 2003.
37. Schaepman-Strub, G.; Schaepman, M.; Painter, T.; Dangel, S.; Martonchik, J. Reflectance quantities in optical remote sensing - definitions and case studies. *Remote Sens. Environ.* **2006**, *103*, 27–42.

Chapter 7

Off-nadir viewing for reducing spectral mixture issues in citrus orchards

Published as: Stuckens, J., Somers, B., Albrigo, G.L., Dzikiti, S., Verstraeten, W.W., Swennen, R., Verreynne, S., Coppin, P., 2010. Off-nadir viewing for reducing spectral mixture issues in orchards. Photogrammetric Engineering and Remote Sensing 76, 1261-1274.

Off-nadir Viewing for Reducing Spectral Mixture Issues in Citrus Orchards

Jan Stuckens, Ben Somers, Gene L. Albrigo, Sebinasi Dzikiti, Willem W. Verstraeten, Rony Swennen, Stephan Verreyne and Pol Coppin

Abstract

A modeling approach to determine optimal viewing angles that reduce the impact of signal mixtures in orchards was evaluated on citrus. Orchards statistics from high-resolution images in Florida and Western Cape province (South Africa) citrus producing areas show that pixel unmixing between adjacent fields can be avoided for pixel sizes below 10 to 15 m, while within fields mixing (canopy, soil, and weeds) is inevitable with multi- and hyperspectral sensors. A virtual 3D environment was constructed in which off-nadir pointing simulations were made for different field orientations. Spectral similarity based contribution indices were derived to find overflight times and viewing angles that reduce the impact of seasonality, soil and weeds. Although no single optimal view direction was found for all scenarios, optimal results in mature orchards were consistently obtained by early acquisitions and low oblique viewing perpendicular to or at a 45° angle with the row orientation, opposite to the solar azimuth.

Introduction

The development of remote sensing applications for early stress detection, yield prediction, and phenology monitoring in horticulture has a large potential but still faces many challenges. A critical factor is a thorough understanding of the structural, biophysical, and optical factors contributing to the measured signals. Generally, remotely sensed reflectance data of vegetation is a mixture of different contributions of reflectance of soil, stems, fruits, weeds, and litter in addition to the leaf reflectance and transmittance (Roberts *et al.*, 1993). In agriculture or horticulture, one is generally interested in changes in the spectral crop response while other factors such as soil, branches, weeds, and litter are sources of undesired variability that need to be accounted for. In addition, differences in solar zenith and azimuth position cause different fractions of the soil and vegetation to be shaded, which adds to the variability (Ranson *et al.*, 1985; Gilabert and Meliá, 1993).

For passive sensors in the optical, near, and short wave infrared wavelengths (400 to 2,500 nm), the main focus in this paper, this spectral mixture question is tightly coupled to the scale level of observation, i.e., the pixel size of the imagery. Considering field sizes in horticulture of up to multiple hectares (ha), high-resolution (HR, between 4 and 30 m pixel size) and very high-resolution (VHR, pixel size <4 m) sensors are of utmost importance. Moderate resolution sensors such as MODIS are more suitable for significantly larger field or stand sizes, commonly encountered in large scale forestry or agriculture (Fritz *et al.*, 2007). For observations in orchards (e.g., viticulture, citriculture, pomology), HR sensors compared to VHR sensors have the benefit of a higher spectral resolution and/or a larger image footprint. VHR sensors on the other hand, may be capable of observing individual tree crowns, minimizing the signal variability due to changes in soil reflectance, shading, or occurrence of weeds in the middle of the orchard rows. This comes at the cost of a severely reduced spectral resolution, often limited to a single panchromatic band at the highest resolution supplemented with multiple bands at a lower spatial resolution. Intensive research has focused on "normalizing" HR data and remove or compensate the influence of soil, weeds, and shadow. Vegetation indices, such as the normalized difference vegetation index or NDVI (Tucker, 1979) have been modified to reduce the influence of soils. The basic assumption of these soil-adjusted vegetation indices is that soils are characterized by a unique linear relationship between the Near InfraRed (NIR) and visible (VIS) reflectance, i.e., the soil line (Richardson and Wiegand, 1977) or the coefficients of the soil line (e.g., Baret and Guyot, 1991; Qi *et al.*, 1994; Rondeaux *et al.*, 1996) are used to normalize vegetation indices for soil background effects. In a separate approach, Pinty and Verstraete (1992) designed the Global Environment Monitoring Index (GEMI) to reduce both the soil and the atmospheric effects on satellite data. Despite these efforts, the success of the soil-adjusted indices is limited because the soil line is not as generic as assumed and the technique is mainly restricted to corrections in the

Jan Stuckens, Ben Somers, Willem W. Verstraeten, and Pol Coppin are with K.U.Leuven, Department of Biosystems, M3-BIORES, W. De Croylaan 34, BE-3001 Leuven Belgium, (Jan.Stuckens@biw.kuleuven.be).

Gene L. Albrigo is with the University of Florida, Citrus Research and Education Center, Lake Alfred, FL 33850.

Sebinasi Dzikiti is with Stellenbosch University, Department of Horticultural Science, Private Bag X1, Matieland 7602, Stellenbosch, South Africa.

Rony Swennen is with K.U.Leuven, Department of Biosystems, Division of Crop Biotechnics, Kasteelpark Arenberg 13, bus 2455, BE-3001 Leuven, Belgium, and Bioversity International, BE-3001 Leuven, Belgium.

Stephan Verreyne is with Stellenbosch University and with Citrus Research International, Department of Horticultural Science, Private Bag X1, Matieland 7602, Stellenbosch, South Africa.

Photogrammetric Engineering & Remote Sensing
Vol. 76, No. 11, November 2010, pp. 1261–1274.

0099-1112/10/7611–1261/$3.00/0

VIS-NIR spectral domain (Rondeaux *et al.*, 1996; Gilabert *et al.*, 2002). Other subpixel cover maps generated from HR imagery use spectral unmixing techniques (Asner and Heidebrecht, 2002; Van der Meer and De Jong, 2000). The spatial extent of soil background and shadows can as such be quantified as well as the spatial variability in crop structure parameters such as canopy cover and width, above ground biomass, and Leaf Area Index (Peddle and Smith, 2005). Recently, Somers *et al.* (2009c) presented a conceptual approach assimilating a radiative transfer model for soil surfaces (Lobell and Asner, 2002) and spectral unmixing. These authors thus extract the pure information on the vegetation spectrum from each pixel, discarding effects from soil background and shadows. Despite the fact that preliminary results were promising, the technique is still in development.

This study aims at developing and evaluating the potential of an alternative sensing strategy to minimize the impact of mixing fractions for monitoring plant growth and development in horticulture. Many recently launched HR satellite platforms such as Proba-1, Earth Observer 1, and even older platforms such as SPOT5 have off-nadir (oblique) pointing capabilities to decrease the revisit time and/or to produce stereo pairs. Imagery from different viewing angles has been combined to derive forest structure information (Widlowski *et al.*, 2004) or bidirectional reflectance distribution functions (Strahler *et al.*, 1999). Off-nadir observations in row oriented crops, which are common in horticultural trees, may have the additional potential to severely reduce the impact of soil, weeds and different fractions of shading. This can be illustrated by considering a North-South oriented orchard. When observed from a westward direction (perpendicular to the row orientation), a large fraction of the soil and weeds is occluded from view by the canopies. Shadows cast by tree crowns onto the orchard floor will further reduce the contribution of soils and weeds in the overall signal. Similar properties have been described by *Pinter et al.* (2003) for thermal remote sensing in agriculture, while Bausch and Diker (2001) concluded that 15° off-nadir viewing decreased the influence of soil on vegetation indices in corn fields.

Optimal combinations of viewing angles and solar positions may generally be defined as those in which the largest fractions of the soil and weeds components are either invisible or shaded, therefore minimizing their contribution to the total signal. From a remote sensing point of view, the analysis of this problem can be considered as an optimization question for an anisotropic bidirectional reflectance distribution function (BRDF). While reflectance in most commonly used BRDF models only depends on the view and illumination zeniths and the difference in azimuth between view and illumination directions (three geometric parameters), for row plantations this is increased with a fourth parameter, the row azimuth, that introduces an azimuthal anisotropy. Platform specifications such as overflight time and maximum tilt angles will restrict the degrees of freedom. Furthermore, the pros of off-nadir sensing need to be weighed against the cons, such as geometric distortions in pixel shape (Jensen, 2004) and larger atmospheric path lengths (Campbell, 2002).

In this study, we will focus on deriving optimal sensor and platform specifications in order to reduce the spectral mixture problem. For our study, we use *Citrus sinensis* (L.) *Osbeck* as a prototype since its evergreen nature allows year-round remote sensing of foliage, combined with a high economical importance worldwide cultivation (FAO, 2006).

An important part of this research is determining optimal viewing angles in combination with different platform overflight times. It is therefore crucial (a) to separate changes caused by viewing or illumination geometry from changes in crop physiology and cover, soil moisture, or weeds physiology and cover, (b) to exactly quantify those changes, and (c) to evaluate a considerable number of viewing/illumination combinations at exactly the same time for different areas. Therefore, a calibrated virtual 3D environment was used in which different orchard fields were simulated with explicit geometric descriptions up to the individual leaf level (Stuckens *et al.*, 2009a). As such, exact reference data (e.g., leaf area index or canopy cover) could easily be obtained and altered in scenario simulations. For the sake of representative and realistic results, a statistical GIS analysis is made for two citrus growing areas.

The next section presents an overview of the aerial and satellite images used along with regional orchard statistics, the field data collection and the models and model inputs used for the simulations. Next, pixel sizes are discussed for the monitoring of orchard physiology at two scale levels, and subsequently off-nadir pointing capabilities, revisit time, and acquisition time of satellite platforms are discussed. Simulations are evaluated using multiple criteria to derive optimal viewing angles for different scenarios. Considerations are made on the extrapolation to different orchard systems and on the combination of off-nadir viewing and image processing techniques such as spectral unmixing.

Materials and Methods

Basic Geometric Statistics of Orchards

Orchard geometry statistics were obtained from very high-resolution orthorectified images of Lake Alfred (Polk County, Florida, 28°06' N, 81°42' W) and Citrusdal (Olifants Rivier basin, Western Cape Province, South Africa, 32°36' S, 19°0' E). Both are regions with high concentrations of citrus groves. The latitude of both regions lies within the world citrus belt, that ranges from 40° North to 40° South, with the majority of commercial citrus grown between 20° and 40° latitude (Spiegel-Roy and Goldschmidt, 1996). Image data of Lake Alfred was acquired by US Geological Survey (USGS) in December 2007, around solar noon, with a 0.26 m pixel size. Image data of Citrusdal was acquired with QuickBird-2 on 25 November 2005 with a 0.6 m pixel resolution. Digital elevation data was acquired from the Shuttle Radar Topography Mission (SRTM) at 1 arc-second (30 m) resolution for Lake Alfred and 3 arc-second (90 m) resolution for Citrusdal.

From each site, 80 randomly selected orchard field perimeters were digitized. Per field, three tree crown centers were digitized using visual inspection: a first reference tree, a second tree separated by 19 trees within the same row, and a third tree separated by nine rows from the first tree, along a line perpendicular to the row orientation. From these three points, row orientation and tree spacing were derived using simple geometric operators. Average slope and slope aspect were derived from the same fields. Average tree height could be estimated from tree shadow casts of the Lake Alfred imagery. Since the image resolution over Citrusdal was insufficient for tree height estimation, tree size statistics were collected during field visits on fully grown trees in a commercial farm in Citrusdal, from July to September 2009.

Average field size is 3.6 ha in Citrusdal and 5.7 ha in Florida. Both areas can be considered as relatively flat, with an average slope of 1.9° for the Florida fields and 2.3° for the Citrusdal fields. Slope and aspect will therefore only have a minor impact in remotely sensed observations of

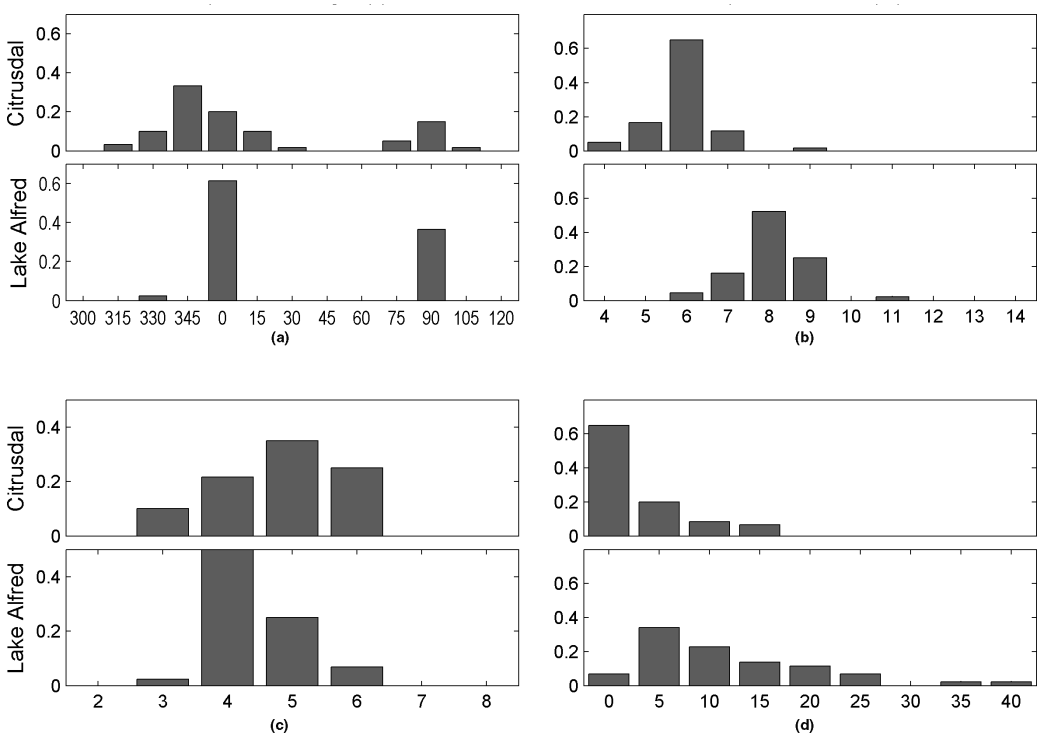

Figure 1. Orchard statistics: Histograms of (a) orchard orientation azimuth angle (°), (b) row distance (m), (c) tree spacing (m), and (d) missing fraction percentages of missing trees or replants in Citrusdal and Lake Alfred.

these citrus orchards. Figure 1 shows four histograms for basic orchard parameters, derived from Citrusdal and Lake Alfred, each with the Y-axis scaled to the fractional occurrence of each class. For both regions, orchards are dominantly North-South oriented, with also an important fraction of East-West oriented fields. There is a larger variation in orientations in Citrusdal, whereas Lake Alfred fields are almost perfectly aligned at either 0° (North-South) or 90° (East-West). The dominant orientation in Citrusdal is slightly tending towards the West, which may be explained by the 345° orientation of the Olifantsrivier valley in which the orchards are situated. Remote sensing applications involving citrus groves in either region will need to take into account both dominant row orientations, while intermediate orientations may have some influence in Citrusdal, but are hardly of any importance in Lake Alfred.

Most fields have a between row spacing of approximately 6 m in Citrusdal and 8 m in Lake Alfred (Figure 1b). This can be related to the generally larger and wider canopies in the Florida production system as compared to South Africa. Rather than absolute measures, the importance for remote sensing applications is mainly determined by the ratios of tree height and width to between row spacing, which impacts the shading of soil and trees. Within row spacing (Figure 1c), conversely, is larger in Citrusdal (mode value of 5 m) than in Lake Alfred (mode value of 4 m). Many Citrusdal fields are planted in a relatively square grid (rectangularity or the ratio of within row spacing to between row spacing equal to one), while hedging is slightly more common in Lake Alfred. Off-nadir observations in fields of low rectangularity (e.g., 1:2 or 1:3) can be expected to have more shading of the soil by the canopies and therefore provide lower fractions of sunlit soil and a higher contribution of the canopy in the mixed signal. Both regions also differ in the fraction of missing trees or replants (Figure 1d). These are identified as gaps within rows (missing trees) or trees with an estimated canopy diameter smaller than 50 percent of the average diameter (replants). The number of missing trees or replants is higher in Lake Alfred. A plausible explanation is the combined impact of diseases (blight, canker, Phytophtora) and severe hurricanes in 2004 and 2005 that affected a large fraction of Florida citrus orchards (Albrigo *et al.*, 2005; Rogers *et al.*, 2009). High fractions of missing and replanted trees are expected to increase the contribution of sunlit soil in the mixed signal.

Statistics however, are not to be extrapolated to all other citrus producing regions: VHR aerial imagery from the Valencia region (Spain; 39°26" 38.31" N, 0°26'51.27" W) reveal a less strict North-South / East-West dominance with smaller field sizes around 1 ha, while VHR imagery near

Bebedouro (Brazil, 21°01'25.31" S, 48°28'13.72" W) reveal a dominance of large fields with row orientations following contour cropping.

Field Data Collection

Field data were collected in commercial orchards near Wellington (Western Cape province, South Africa, 33°35'58.51" S, 18°55'32.44" E) and in Citrusdal. All canopy, soil and weed spectra were collected using an ASD FR spectroradiometer (Analytical Spectral Devices, Boulder, Colorado) ranging from 350 to 2,500 nm with a spectral resolution of 3 nm in the VIS and NIR and 10 nm in the SWIR. A 25° field of view (FOV) bare fiber optic was used. Top of canopy measurements were made on a 4 m mobile scaffolding platform with the sensor at approximately 1.5 m above the canopy. Off-nadir spectra were collected on a ladder from the sunlit side of the canopy at an approximate angle of 45° zenith. At least five spectra were collected for 16 trees at each sensor position on typically cloudless days in September 2009. Target radiance spectra were normalized against a 0.3 m Spectralon (Labsphere Inc., North Sutton, New Hampshire) reference plate to obtain reflectance factors and converted to absolute reflectance using a calibrated reflectance spectrum of the panel.

Ray Tracing Simulations in Virtual Orchards

The virtual orchards used in this study are based on a commercial citrus field of Midknight Valencia oranges near Wellington (Stuckens *et al.*, 2009a). Each consists of an explicit 3D geometric description of the orchard, from leaf level to field level. Key geometric parameters at the tree level include leaf geometry, angular distribution, branching patterns, stem size, tree height, and pruning dimensions. A total of ten representative trees were calibrated to represent actual trees. Random replicas of these trees were placed in an orchard pattern. Weeds were simulated as pseudo-random patches in the row-middles. Citrus leaf, stem, fruit, weed leaf, and soil optical properties were collected and used to calibrate bidirectional scattering distribution functions (BSDF). Illumination was simulated for different solar positions with both direct and diffuse solar radiation components derived from the SBDart (Ricchiazzi *et al.*, 1998) atmospheric radiative transfer model. Simulations are made using a modified version of a physically based ray-tracer *(pbrt,* Pharr and Humphreys, 2004), adapted for spectral rendering from 350 to 2,500 nm in 10 nm increments. A detailed description including calibration and validation procedures for both the geometric orchard description and the ray tracing environment (including the RAMI Online Model Checker, Widlowski *et al.*, 2008) can be found in Stuckens *et al.* (2009a). Orchard dimensions and orientations in the Wellington orchard deviate from the average orchard parameters in the two study areas, Citrusdal and Lake Alfred. Therefore the original tree spacing, tree dimensions, and weed occurrence were adjusted to obtain orchard fields representative for both areas, while maintaining the same leaf sizes, optical properties, angular distributions, and branching patterns. Valencia oranges are the second most planted in the Western Cape Province, after Navel oranges (C.G.A, 2008) and the dominant citrus variety in Polk County (Bronson *et al.*, 2009). Basic field level parameters of the original Wellington orchard and from the derived Citrusdal and Lake Alfred orchards are summarized in Table 1. Figure 2 shows side-by-side a 30 × 30 m section of the reference orchard in Lake Alfred and of its simulated counterpart for similar illumination conditions. All subsequent simulations used a view window of 70 × 70 m in Citrusdal and 100 × 100 m in Lake Alfred positioned at the center of the fields to avoid boundary effects.

TABLE 1. GEOMETRIC AND GEOGRAPHIC PROPERTIES OF SELECTED ORCHARD FIELDS

Property \ Location	Wellington	Citrusdal	Lake Alfred
Row orientation (°)	7.0	351.0	359.6
Between row spacing (m)	4.5	5.5	7.7
Within row spacing (m)	2.0	4.0	4.6
Average tree height (m)	3.0	3.3	5.0
Average canopy width (m)	2.5	3.7	4.9
Fraction of missing trees (%)	11	3	6
Weed cover (%)	22	18	8
Field dimensions (m)	125 × 125	170 × 170	200 × 200

By using an explicit 3D model, many assumptions from analytical radiative transfer models no longer restrict the accuracy of the simulations (Stuckens *et al.*, 2009a). Specifically for the purposes of this research, this includes that (a) contributions of shaded zones to the total signal can be accounted for, i.e., due to diffuse light and canopy transmission, shades are not perfectly "black" (Roberts *et al.*, 1993), (b) the impact of missing trees or replants in a row plantation can be realistically modeled, (c) the influence of weed occurrence can be accounted for, and (d) non-linearities in the spectral mixing between soil and canopy and within canopies can be accurately simulated.

Pixel Size and Signal Mixtures

For passive remote sensing in the optical domain, different sensor specifications may be considered, which vary in pixel size, footprint (image area), spectral resolution, and signal quality (signal-to-noise ratio, bit depth). In this analysis, we will focus on the pixel size, given its impact on the spectral mixture problem. Two scale levels are evaluated: field scale and tree scale.

Signal Mixtures between Adjacent Fields

For physiology monitoring at a field scale, a determining factor is the fraction of pixels that are spatially constrained within individual fields. When a large fraction of an orchard field is covered by pixels overlapping with adjacent land-cover classes or fields, difficulties arise in separating the fraction of the signal coming from the observed field. Since many fields are rectangular and have different orientations and sometimes irregular shapes, an analysis cannot be restricted to simply comparing pixel size to average or minimum field size. A total of 530 field perimeters in Citrusdal and 81 in Lake Alfred were digitized using high-resolution aerial or satellite images as a reference. Both areas were overlayed by grids of different sizes, ranging from 4 m to 100 m. For each individual field and for all overlapping grid cells, the fraction of overlap was calculated from which on a per field basis the fraction of "pure" pixels was derived. When adhering to a strict definition, a pure pixel lies 100 percent within the field perimeter. In a more pragmatic definition, a pixel is pure when a large fraction of it (90 percent) lies within the field. Figure 3 shows the average values for both the Citrusdal and Lake Alfred fields, using a strict (100 percent) and a 90 percent threshold. The larger and more regular fields in Lake Alfred result in a higher fraction of pure pixels for all pixel sizes. For pixels sizes up to 10 m, more than 85 percent of the total orchard area is covered by pure pixels. For 20 m pixels, this drops below 60 percent for Citrusdal and 80 percent for Lake Alfred. For pixel sizes above 30 m this fraction drops below 80 percent for both regions, even using the 90 percent threshold. According to this analysis, it can be suggested that pixel

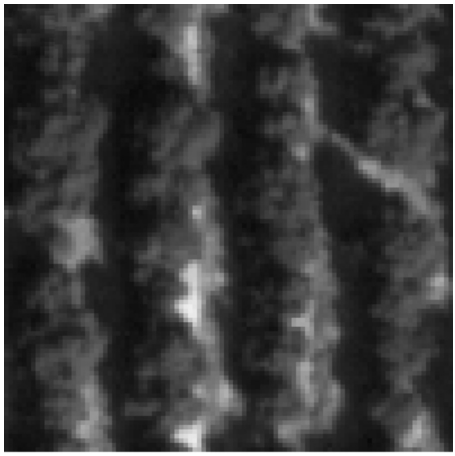

(a)

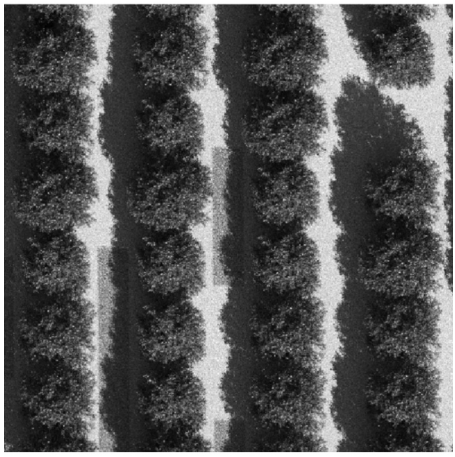

(b)

Figure 2. (a) A 30 m × 30 m aerial image of a segment from the reference orchard in Lake Alfred at 0.3 m pixel resolution with original RGB colors converted to greyscale ©U.S. Geological Survey and Photo Science, Inc., December 2007, and (b) Greyscale simulation of an equally sized segment of the virtual orchard with comparable illumination conditions (22 December, 10:30 LST).

sizes up to 30 m are adequate for Lake Alfred region, while in Citrusdal, smaller pixels are recommended.

Signal Mixtures within a Field

Beyond the field scale, we now explore the pixel size threshold from which most individual pixels fall entirely within the tree crown perimeter so that unmixing may be greatly simplified or even become redundant. An experiment was set up using the modeled fields in Citrusdal and Lake Alfred. More details on field properties are provided in Table 1. Analogous to the previous experiment, each field was intersected with grids of increasing pixel size and per grid cell, the fractions of tree crown + stems and soil + weeds were calculated. This was technically achieved with the *pbrt* ray-tracer by assigning a single waveband to each of these cover types and restricting calculations to single scattering with hypothetical nadir viewing and zenith illumination (hotspot without shading). Figure 4 shows for both regions the average fractions of pure pixels (i.e., belonging by more than 90 percent to one of the two cover types) as a function of pixel size. Even at very small pixel sizes of 0.1 m, approximately

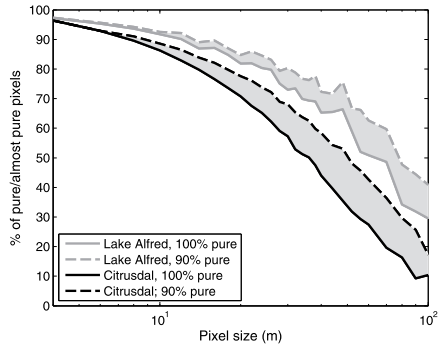

Figure 3. Impact of pixel size on mixing at tree level: fraction of almost pure tree pixels as a function of pixel size for a representative orchard field in Citrusdal and Lake Alfred.

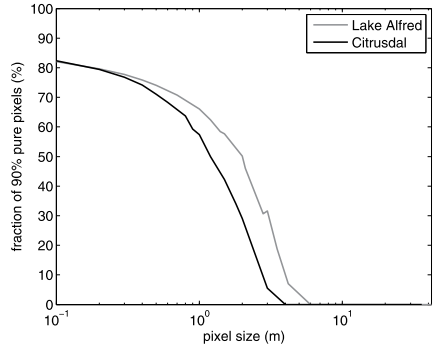

Figure 4. Impact of pixel size on mixing at tree level: fraction of almost pure tree pixels as a function of pixel size for a representative orchard field in Citrusdal and Lake Alfred.

18 percent of the pixels is still mixed. These pixels are mostly situated in the boundary region between crown and soil. For pixel sizes larger than 4 m in Citrusdal and 6 m in Lake Alfred, no more pure pixels can be found. To obtain a minimum of 50 percent pure pixels, pixel sizes should be no larger than 1 m for Citrusdal and no larger than 2 m for Lake Alfred.

Analysis of Off-nadir Viewing Capabilities

Platform and Sensor Limitations

This section discusses the impact of orbit, platform and sensor characteristics of earth observing satellites on the monitoring of horticulture and specifically citriculture. Two dominant orbits designs for earth-observing satellites exist, geostationary and sun-synchronous (Campbell, 2002), of which the latter are designed to reduce variations in illumination caused by differences in time-of-day, while enabling a full world coverage within a limited time frame (e.g., 16 days for Landsat and MODIS-nadir, *circa* 1.5 days for MODIS off-nadir). Most sun-synchronous orbits are designed to acquire imagery between 09:30 and 10:30 local solar time (LST). This is considered as a trade-off between ideal illumination and time of minimum cloud cover in tropical regions (Campbell, 2002) while also avoiding specular reflections of flat surfaces (Capderou, 2005). Notwithstanding their almost fixed LST of observation, seasonal variations in solar zenith and azimuth are still considerable for sun-synchronous orbits. Figure 5 plots for both regions the seasonal variations in solar position for 09:30 and 10:30 LST overpass orbits. Summer observations (June in Lake Alfred, December in Citrusdal) at 09:30 LST occur with a solar azimuth of approximately 90° (East), which shifts to approximately 30° (Citrusdal) and 150° (Lake Alfred) for winter observations. Corresponding solar zenith angles increase from 34° to 67° and 34° to 63°, respectively. Yearly oscillations in solar positions will therefore cause differences in shading during observation time: e.g., for a North-South oriented field, summer observations cast shadows perpendicular to the row orientation while winter observations cause more crown-on-crown shading. For the 10:30 LST observations, the ranges are similar with higher zenith angles and azimuths shifted towards the North (Citrusdal) or South (Lake Alfred).

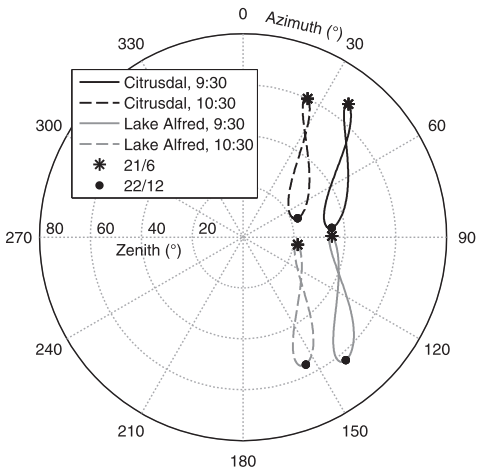

Figure 5. Polar plot of seasonal variations in solar zenith and azimuth angles for 09:30 and 10:30 local solar time (LST) orbits in Citrusdal and Lake Alfred.

Satellite platforms can be equipped with along-track and across-track pointing capabilities for off-nadir observations. This increases the platform's versatility by allowing a higher revisit frequency or observations from multiple viewing angles that can be used in estimating target BRDF parameters (e.g., Schaaf *et al.*, 2002) or vegetation structure parameters (e.g., Goel *et al.*, 1997; Widlowski *et al.*, 2004). Current examples of off-nadir viewing platforms are Terra and Aqua (8.55° for SWIR and 24° for VIS/NIR cross-track pointing), Worldview-1 (40°), SPOT4 (27°). Instruments such as the Multi-angle Imaging SpectroRadiometer are even specifically designed for multi-angular observations (up to 70.5°).

Optimal Sensing Geometry

Results from the previous section indicate that while mixtures of different land cover types (orchard / non-orchard) can be largely avoided for pixel sizes no larger than 10 to 15 m, within orchard mixtures between tree, soil, and weeds are almost inevitable with current sensor technology. Therefore seasonal changes in soil/weeds shading at acquisition time as well as spectral changes of the soil (e.g., due to soil moisture or organic matter accumulation) or weeds (e.g., tillage, spraying or drought stress) will be reflected in the mixed signal and need to be minimized to retrieve the spectral changes in crown canopies with good accuracy. To improve the insight in the feasibility of off-nadir sensing combined with variations in acquisition time, the North-South oriented field in Citrusdal is treated as an example. Figure 6 shows the simulated reflectance factors of a 30 m × 30 m subset of this field for a panchromatic band (450 to 900 nm), simulated on 21 March 10:30 LST with the sun in 39° zenith and 37° azimuth, 60 km horizontal visibility. The four images represent different viewing angles. In the nadir image some shadows are cast onto the orchard floor, but the largest fraction of both soil and weeds is sunlit. Within the rows, crown closure is not perfect and gaps exist. The north viewing image shows an even lower fraction of shadows, but the apparent crown closure is higher. The soil is slightly brighter since the viewing direction is closer to the hotspot (direction where viewing and illumination directions are equal). In the eastward viewing image, almost all shadows have disappeared. On the other hand, the apparent between row spacing is reduced due to the viewing direction that is almost perpendicular to the row orientation. A large fraction of the weed patches is hidden behind the crowns. This increases the canopy fraction and decreases the soil and weeds fractions in the image. Finally, in the westward viewing image, almost the entire fraction of visible soil is shaded with the sunlit fractions hidden from sight behind the tree crowns. Identical to the previous image, the apparent between row spacing is reduced. Due to the relatively large tree spacing and the solar azimuth direction, sunlit soil is visible between trees. For each of these viewing directions, differences in solar illumination will alter the amounts of shading of soil and canopy.

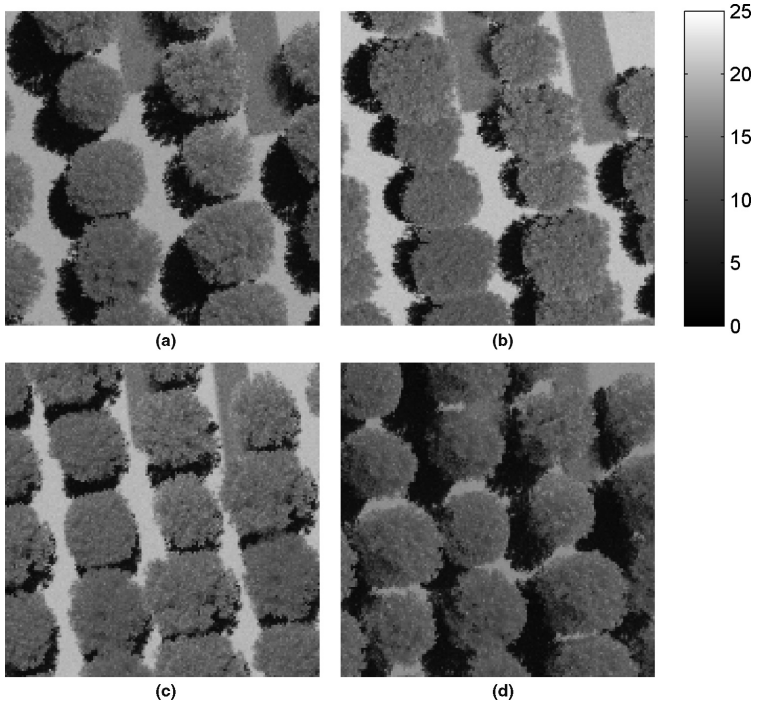

Figure 6. Simulated panchromatic reflectance (450 to 900 nm) of a segment of an approximately North-South (351° azimuth) oriented field in Citrusdal observed from different nadir and off-nadir viewing directions: (a) Nadir (30 m × 30 m), (b) North (VZA = 40°, VAA = 0°, 30 m × 39 m), (c) East (VZA = 40°, VAA = 90°, 39 m × 30 m), and (d) West (VZA = 40°, VAA = 270°, 39 m × 30 m) Image titles contain view zenith angle (VZA), view azimuth angle (VAA), and image dimensions (width × height).

Scenario Evaluation Criteria

For the given illumination conditions and orchard layout properties, an optimal viewing direction can be defined as one that maximizes the sensitivity to the tree physiology while minimizing the sensitivity to weed physiology or soil spectral changes (e.g., caused by changes in soil moisture). Based on the example presented in the *Optimal Sensing Geometry Subsection*, one may thus attempt to achieve this by minimizing the fraction of visible soil and weeds in general and specifically the sunlit fraction of soil and weeds. To compare and evaluate these different viewing angles, it is necessary to construct a quantitative statistic. We will focus on four criteria:

Changes in Trees

Different viewing angles may have a different efficiency at capturing changes in tree biochemistry (e.g., chlorosis), phenology (e.g., fruiting) or structure (e.g., leaf loss).

Seasonal Changes in Illumination

Similar to agriculture in general, in horticulture, seasonal changes in physiology and phenology as well as in solar position will induce changes in the measured reflectance factors (Stuckens *et al.*, 2009a). Failing to separate both factors may lead to erroneous conclusions. An optimal viewing angle will minimize the impact of illumination.

Impact of Soil

Considering the relatively low canopy cover fraction in orchards, soil reflectance has a major impact on the retrieved signal (Somers *et al.*, 2009a). Changes in soil reflectance may be caused by variations in soil moisture (rainfall, irrigation systems) or organic matter (decomposition, litter) (Müller and Décamps, 2001) and need to be separated from changes in the tree canopy.

Impact of Weeds

Although the total weed cover fraction is often limited, weeds can undergo large variations in cover fraction due to their rapid growth and orchard management practices such as mowing and spraying. In addition, weed physiology can undergo large fluctuations, e.g., caused by drought stress, since the middle lanes in orchards are typically not irrigated by sprinklers or microjets. Changes in weed occurrence and physiology may be hard to separate from similar changes in trees, e.g., by unmixing algorithms due to

spectral similarities since both are vegetation types (Somers *et al.*, 2009b and 2009d).

Similarity and Contribution Indices for Scenarios

To derive the optimal viewing angles, sensitivity to changes in trees need to be compared to the sensitivity to illumination conditions and to soil and weeds spectral changes. To express the similarity between two spectra, the Spectral Information Divergence (SID) measure will be used (Du *et al.*, 2004). SID is an entropy-based statistic expressing the discrepancy of probabilistic behaviors between two spectra. Its performance surpassed that of traditionally used measures such as Spectral Angle Mapper (SAM) (Du *et al.*, 2004). Given spectra x and y, SID is defined as:

$$SID(x,y) = \sum_{i=1}^{N} p_i \log(p_i/q_i) + \sum_{i=1}^{N} q_i \log(p_i/q_i) \quad (1)$$

where

$$p_i = x_i \Big/ \sum_{i=1}^{N} x_i;\ q_i = y_i \Big/ \sum_{i=1}^{N} y_i \quad (2)$$

with p_i and q_i the normalized values of x_i and y_i, respectively, restricted to the range 0 to 1. The higher the similarity between both spectra, the smaller SID. The normalizations in p_i and q_i make SID insensitive to a linear scaling of spectra so that it only measures changes in spectral shape. As a consequence it can be used as a generic performance indicator for simple ratio and normalized difference vegetation indices that are also insensitive to scaling.

For each orchard five different scenarios were set up:

1. Scenario I, containing the calibrated orchard (*ref*).
2. Scenario II, varying the tree structure and physiology ($\delta tree$). To provide a realistic simulation, a general decline in tree health was simulated with a 25 percent loss in leaf area index (LAI) and a 25 percent loss of chlorophyll content. Leaf loss was simulated by decreasing the number of leaves for each tree. The loss in chlorophyll content is simulated by replacing the reference leaf reflectance and transmittance spectra by spectra simulated for leaves with 25 percent less chlorophyll content. All reference and scenario spectra are calculated using a Dorsiventral Leaf Model (DLM; Stuckens *et al.*, 2009b) and calibrated with measured citrus leaf spectra by model inversion (Stuckens *et al.*, 2009a).
3. Scenario III, assessing seasonal changes in solar illumination ($\delta season$). Three different dates were considered: 22 December (northern winter or southern summer solstice), 21 March (equinox), and 21 June (northern summer or southern winter solstice).
4. Scenario IV, in which the soil spectrum is changed ($\delta soil$). While the reference spectrum is a slightly moist course sandy soil with 4 to 5 percent gravimetric moisture content, in this scenario drying of the soil was simulated as by using a soil spectrum from a sample with 0 to 0.5 percent gravimetric moisture content. Soil spectra were collected in a field experiment in Citrusdal with coupled moisture content measurements as described in Somers *et al.* (2009c).
5. Scenario V that varies the weeds cover and its physiology ($\delta weeds$). A severe drought stress with senescence was simulated with a 50 percent loss in water content, a 50 percent loss in chlorophyll content and a 50 percent reduction in weeds LAI.

For each viewing angle, we can define three contribution indices (CI): a Temporal Contribution Index (TCI) expressing seasonal changes, a Soil Contribution Index (SCI), and a Weed Contribution Index (WCI). Each expresses the sensitivity to unwanted changes in the spectrum as compared to changes that are to be detected, using the following equation:

$$CI = SID(ref, \delta scen)/SID(ref, \delta tree) \quad (3)$$

in which $\delta scen$ is replaced by $\delta season$, $\delta soil$ and $\delta weeds$ for TCI, SCI, and WCI, respectively. A contribution index equal to 1 indicates that the spectral change of an undesired effect (e.g., soil influence) is as large as the spectral change in the tree canopies. To evaluate the possible differences in optima between two different regions, all simulations were run for orchards in Citrusdal and Lake Alfred. Simulations were set up for representative fields in the two dominant azimuths for each region (351° and 90° for Citrusdal and 0° and 90° for Lake Alfred). For each of these four fields, the above described scenarios were simulated. To compare the impact of satellite overflight time, all simulations were made for 09:30 and for 10:30 LST solar positions in three seasons: 22 December, 21 March, and 21 June. Note that the solar position on 21 September is very close to that on 21 March (see Figure 5). To express the overall year-round impact, values of WCI and SCI were averaged over the three dates. The TCI is derived from the previous scenarios: the 21 March simulation was taken as the reference (*ref*), while $\delta season$ consisted of the December and June simulations. In each simulation, 17 different viewing angles were tested: nadir (0° view zenith angle or VZA), 20° VZA combined with 0°, 45°, 90°, 135°, 180, 225°, 270°, and 315° view azimuth angle (VAA) and the same eight directions for a 40° VZA.

Scenario Results

Considering the large number of scenarios and hence results, detailed results for each viewing direction will be presented for one field (i.e., 351° azimuth in Citrusdal). Results for the other fields are discussed and Figures summarized. Finally, for all combinations of field type, season and overflight time, the contribution indices (TCI, SCI, and WCI) of the optimal viewing direction will be compared to contribution indices from the nadir viewing.

To illustrate similarity between different reflectance spectra, Figure 7 shows example simulated spectra for the 351° azimuth field in Citrusdal, 21 March, 09:30 LST. Atmospheric

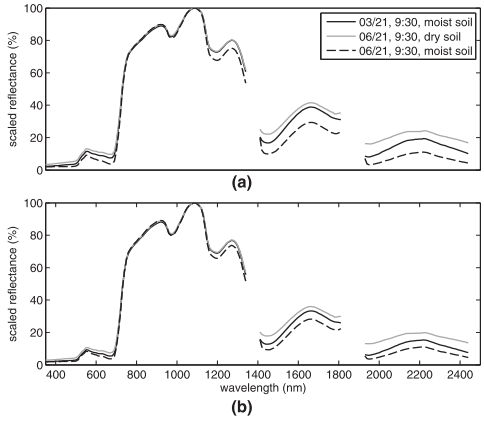

Figure 7. Simulated scaled reflectance spectra of a 351° azimuth orchard field in Citrusdal for (a) nadir observations and (b) a viewing direction of 40° zenith and 270° azimuth.

water absorption zones (1,360 to 1,400 nm, 1,820 to 1,940 nm and 2,450 to 2,500 nm) have been removed. To better assess the changes in spectral shape, all spectra were linearly scaled to their maximum value around 1080 nm. The solid and black dotted lines in the top of Figure 7 illustrate the impact of solar illumination. In this simulation, it is of the same order of magnitude as changes in the soil spectrum (from moist to dry, grey line). The bottom of Figure 7 illustrates that for well-chosen viewing angles (in this case 270° VAA, 40° VZA, approximately perpendicular to the row orientation), the impact of soil spectral changes and illumination direction is clearly reduced.

Figure 8 shows three polar plots of the contribution indices. The angular axis shows the eight azimuthal directions and the radial axis holds the contribution index. The values for the nadir direction are plotted as circles (dotted lines) for better comparison. For seasonal variation (Figure 8a), a 09:30 LST acquisition has a lower TCI than a 10:30 LST acquisition, which is attributed to the lower solar elevation at 09:30 LST that is almost perpendicular to the row orientation (see inset image). This causes more shading of the soil. The 20° VZA simulations (dashed lines) show moderate differences when compared to the nadir simulations with TCI for VAA in the quadrant between 225 and 315° azimuth. For VAAs in the 45° to 135° quadrant off-nadir viewing increases the TCI. Similar to nadir viewing, earlier acquisitions substantially reduce the TCI. The lowest VZA of 40° provides the best opportunities to reduce the TCI, certainly when combined with early acquisitions (black solid line). The 225° and 315° VAAs provide slightly better results than the 270° VAA.

Results for the SCI (Figure 8b) are in the same order of magnitude, but the conclusions are somewhat different. The 09:30 LST simulations are still outperforming the 10:30 LST simulations, with even larger differences. The additional benefit of off-nadir viewing is smaller, but is still substantial for 225° and 315° VAAs. The 270° VAA no longer provides an improvement on nadir viewing.

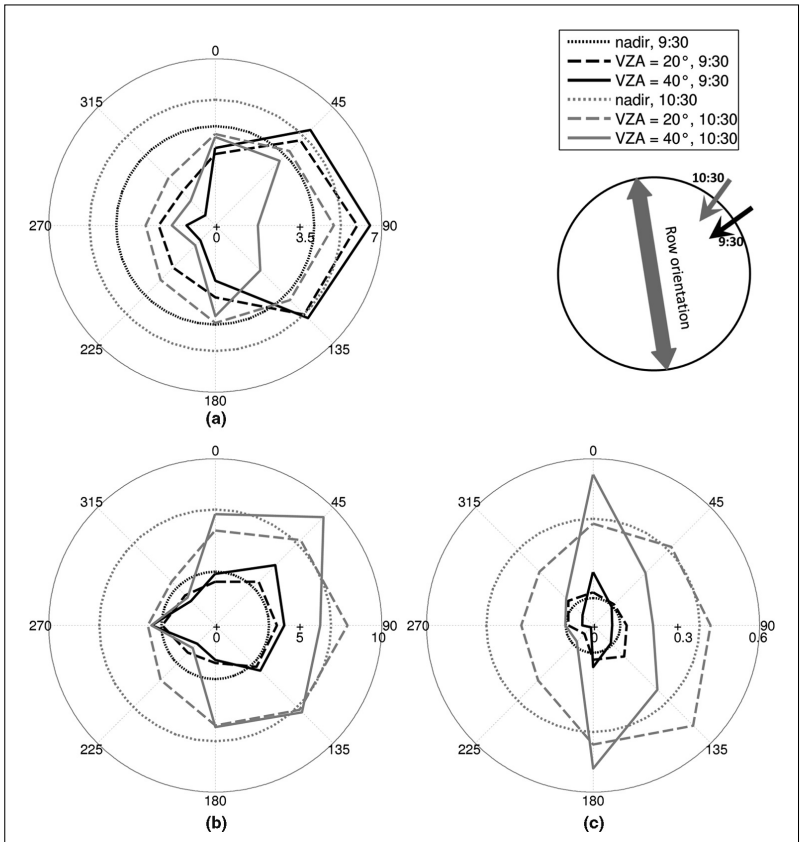

Figure 8. (a) Temporal Contribution Index (TCI), (b) Soil Contribution Index (SCI), and (c) Weeds Contribution Index (WCI) for a North-South (351° azimuth) oriented field in Citrusdal on 21 March at 09:30 (black lines) and 10:30 LST (grey lines) for different viewing angles. The inset image shows the row orientation and the solar azimuth angles.

The results for weeds (Figure 8b) lead to similar conclusions: 09:30 LST, when combined with the optimal VAAs, is consistently better than 10:30 LST, and higher oblique viewing (40° VZA) can provide the lowest (but also the highest) WCI values. The WCI values are approximately ten times smaller than the TCI and SCI values. These lower values can be explained by the lower weed cover fraction (16.5 percent weeds versus 39.6 percent for pure soils and 44.1 percent for tree canopy) and by the position of the weeds. In both scenarios and similar to many commercial fields, a strip of soil next to the trees is permanently cleared of weeds (see Figures 2 and 6) so that for low solar elevations, all weed patches can be shaded before the entire row is shaded. The same deduction can be made for low viewing angles perpendicular to the rows.

The simulations results for the three other fields are comparable but with different optimal azimuth angles. The Citrusdal East-West oriented field (no Figure) has the lowest TCI and WCI for a 40° VZA / 180° VAA pair, while the lowest SCI is approximately equal between 135° and 225° VAA and 40° VZA. In this case, looking perpendicular to the row orientation thus provides the lowest contribution indices. For the Florida fields, the North-South oriented field has optimal viewing conditions for a 40° VZA / 315° VAA viewing direction for both TCI and SCI, while the WCI becomes very small (<0.1) for all azimuths with a 40° VZA. Since solar azimuths on Northern and Southern hemispheres are mirrored around the East-West (270° to 90° azimuth) axis, the 315° VAA for Lake Alfred is consistent with the 225° VAA for Citrusdal. The optimal viewing direction for the Florida East-West oriented field is at 40° VZA / 0° VAA for the TCI, SCI, and WCI. This is also a mirror of the optimal VAA for Citrusdal.

For these four fields, the best viewing angles to reduce the combined effects of seasonality (TCI), soil (SCI), and weeds (WCI) are thus somewhat variable, but are mostly obtained by combining early acquisitions (09:30 LST) with highly oblique viewing (40° VZA). The optimal azimuth angle for North-South fields is not perpendicular to the rows but at a slant angle (45°) while for East-West fields it is perpendicular to the rows. In each of the four cases, the best viewing direction is the one most opposite to the solar zenith.

Figure 9 provides an alternative and comprehensive view of these results to better assess the potential improvements of off-nadir viewing. For each field the optimal viewing angles (40° VZA combined with 225°, 180°, 315°, and 0° VAA for Citrusdal N-S, Citrusdal W-E, Lake Alfred N-S and Lake Alfred W-E), respectively, are compared with nadir viewing as a reference. For each of the four fields, the summer simulation (December for Citrusdal, June for Lake Alfred) which consistently produces the highest contribution

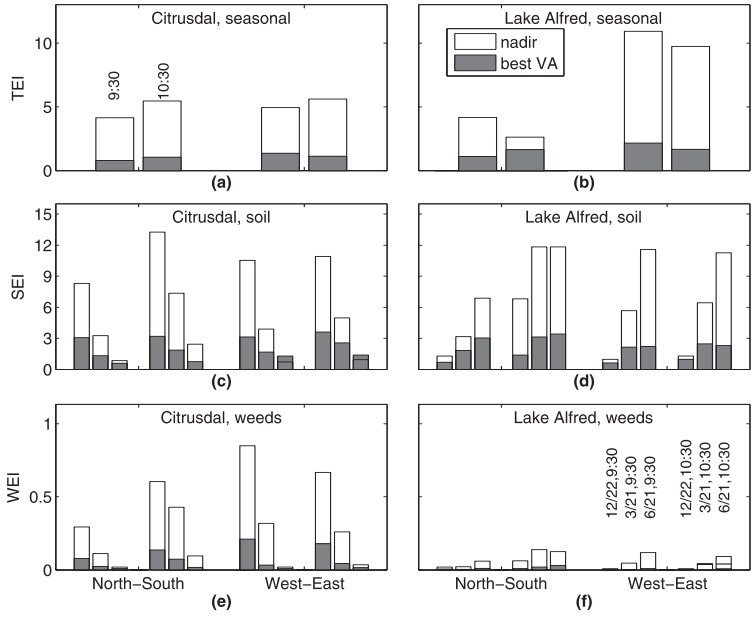

Figure 9. Temporal Contribution Index (TCI), Soil Contribution Index (SCI) and Weeds Contribution Index (WCI) for Citrusdal and Lake Alfred, for the two dominant row orientations (North-South and East-West), two overflight times (09:30 and 10:30 LST) at three dates (22 December, 21 March, and 21 June). White bars are for a nadir viewing angle and grey bars are for the best off-nadir viewing angle (VA): (a) Citrusdal seasonal, (b) Lake Alfred seasonal, (c) Citrusdal soil, (d) Lake Alfred soil, (e) Citrusdal weeds, and (f) Lake Alfred weeds.

indices also shows the largest improvements for off-nadir viewing (difference between white and grey bars). Provided the right viewing angle is selected, similar improvements can be obtained for North-South and East-West oriented fields for both regions, although seasonal variability is still higher in the East-West oriented fields. For the four fields, differences between 09:30 and 10:30 LST solar positions are generally small, although North-South oriented fields are best observed earlier (09:30 LST), while for East-West oriented fields results are mixed: 10:30 LST is better for TCI and WCI, but 09:30 LST is better for SCI.

Discussion

The analysis of signal mixtures between fields suggests pixel sizes of 30 m and smaller for remote sensing in Citrus orchards. These values must be treated as absolute upper bounds, since (a) the spatial response of a sensor is often substantially larger than the boundaries of a square pixel that represents it (Huang *et al.*, 2002), and (b) the adjacency effect, caused by atmospheric scattering (path radiance) induces additional degradation (Richter *et al.*, 2006). The analysis of signal mixtures within a field determined threshold resolutions for pure canopy spectra in orchards between 1 m (Citrusdal) and 2 m (Lake Alfred). Such resolutions can be matched by the panchromatic band of very high-resolution satellites such as Ikonos (0.82 m nadir viewing), QuickBird (0.61 m), and GeoEye-1 (0.41 m). The multispectral bands however have a lower spatial resolution (e.g., 1.65 m for GeoEye-1) while these sensors provide no full spectral information. Thus, the combination of high spatial and spectral resolution can, hitherto, only be provided by aerial remote sensing. On the other hand, the 1 to 4 m scale level has potential in unmixing applications, since a fair number of mostly pure pixels allows the extraction of image based endmembers (Bateson *et al.*, 2000; Plaza *et al.*, 2004).

The results reported in the *Optimal Sensing Geometry* Subsection lead to the presumption that off-nadir viewing provides important improvements in the monitoring of citrus physiology and orchard physiology in general as well as for other row-oriented crops (e.g., maize). Before extrapolating these results to other geographic regions and other crops, it is important to better understand the major limitations (1 to 4) and assumptions (5 and 6) of off-nadir viewing:

1. Due to the fixed nature of satellite orbits, VAA and VZA can not be exactly chosen, but only approximated. For platforms with smaller revisit times, the spacing between tracks increases. For across-track pointing, the LST of observations is not exactly equal to the LST of nadir viewing angles, but differences are limited (e.g., +/− 17 minutes for the Terra orbit).
2. Off-nadir viewing results in geometric distortions in pixel shape (Jensen, 2004) and the spectral signal is more affected by atmospheric interactions due to the larger atmospheric path lengths (Campbell, 2002).
3. As described in the *Optical Sensing Geometry Subsection*, optimal viewing angles for one row orientation (North-South) often result in no improvement or even an increase in the contribution indices for other orientations. For full coverage of an area, the number of image acquisitions has to equal the number of dominant orientations (two in the cases treated here). For flat areas in the subtropics, a dominance of North-South orientations may be expected since this provides optimal light interception (Aubert and Vullin, 1998). Additional complications can arise for orchards planted on hill-slopes, which is a common practice in Brazil and in Asian countries such as India, China, and Japan (Ladaniya, 2007). Hill-slope orientation often determines the orchard orientation (along or across the hill), and steep hills can cause differences in shadow casting.
4. Large tree spacings as well as a large fraction of replants or missing trees will prevent full shading of the orchard floor.
5. When considering viewing/illumination geometry, optimal performance was found for directions where direct sunlight is blocked by the tree crowns (shading of soil and weeds) and/or where the view of soil and weeds is blocked by these crowns. This assumes a low transmissivity of the tree canopy, ideally resulting in a perfectly "black" shade or no visibility of "hidden" soil and weeds. Figure 10 shows the measured and simulated radiance of shaded spots of soil and weeds in a Wellington (South Africa) orchard, divided by the radiance of the same spots when they receive direct sunlight. The graphs therefore show relative reflectance of shaded soil and weeds. Both measurements and simulations for weed patches and bare soil provide similar results. The high values of up to 15 percent in the blue and green wavelengths (350 to 550 nm) are caused by diffuse incident light (Rayleigh scattering). The relative impact in these wavelengths will depend on the atmospheric aerosol concentrations (optical depth). The high values of up to 20 percent in the near infrared (800 to 1,300 nm) are caused by transmittance of light through the canopy. Aerosol concentrations are highly variable in time and space. Canopy transmittance will depend on crop type and management and is determined by vegetation structure parameters such as leaf area index, leaf angle distribution, clumping factor and leaf optical properties. As a consequence, the relative shading of rows may be lower for crops with optically "thinner" canopies such as grapes and apples.
6. Finally, an implicit assumption in off-nadir viewing certainly at low angles, is that the signal obtained from the side-view of the canopy equals the top-of-canopy (nadir) signal or at least provides similar information. Figure 11 shows average top-of-canopy reflectance measured in the Wellington orchard on 12 trees (five spectra per tree) as well as the average measured reflectance of the same trees taken at an approximate angle of 45° perpendicular to the row and pointing towards the sunlit side to avoid self-shading. Differences are small between 350 and 1,100 nm. For higher wavelengths, limited but clear differences appear that can be caused by canopy BRDF effects and/or by variable influence of the soil component in these signals. It is therefore recommendable not to mix canopy spectral endmembers obtained from different viewing angles and to obtain

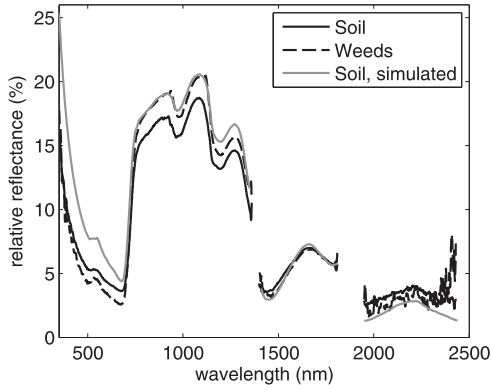

Figure 10. Relative reflectance of shaded soil and shaded weeds in an orchard field in Wellington: measured and simulated values. Spectra were collected on 29 October 2009 at 12:00 LST (sunlit) and 14:50 LST (shaded)

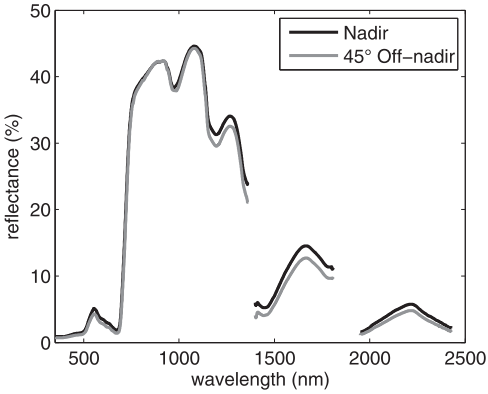

Figure 11. Average measured reflectance in the Wellington orchard (5 spectra per tree, 12 trees) taken from nadir direction (black line) and at an approximate angle of 45° (grey line). Spectra were collected on 19 September 2009 between 11:40 and 13:00 LST.

different image acquisitions in a time series all from the same viewing angle. For VAA opposite to the SAA, as suggested here, the observed side of the canopy will often be shaded, resulting in an alteration (decrease) of the magnitude, but not necessarily the shape, of the spectrum.

Although off nadir viewing could substantially reduce the impact of seasonality, soil, and weeds, the remaining influence of soil and seasonality is too large to be neglected. Therefore, the benefit of off-nadir viewing should always be combined with either unmixing algorithms, canopy radiative transfer models or robust soil-adjusted indices to normalize for any changes in soil spectral reflectance. In contrast to soil and seasonality, the impact of weeds using nadir and off-nadir viewing was found to be much smaller. This leads to the question whether changes in weeds physiology still need to be taken into account. Some considerations need to be made. Weed occurrence for both situations was moderate (Citrusdal) to low (Lake Alfred), which is a consequence of local management practices and should not be extrapolated to, e.g., orchards with continuous grass sods. The high spectral similarity between two types of vegetation, trees and grasses, may also be more difficult to deal with in spectral indices or unmixing algorithms than the vegetation versus soil case. Finally, simulated changes in weeds and tree physiology and soil water content, though within realistic bounds, are still arbitrary choices (e.g., weeds may also be almost entirely removed by spraying and moving) that are valid for comparing different combinations of viewing and solar positions. They are not intended to compare the general impact of weeds versus soil versus seasonality.

Further improvements may be achieved by including soil reflectance models to simulate spectral variability caused by soil moisture (Bach and Mauser, 1994) or by merging hyperspectral data with VHR data from which crown canopy, weeds and soil cover fractions may be estimated (Ye *et al.*, 2007). Future evaluations are planned as a side-by-side year-round comparison of nadir and off-nadir imagery acquired by the Sumbandila-sat multispectral sensor (Mostert *et al.*, 2008) using Citrusdal as a test area.

Conclusions

A radiative transfer model for virtual citrus orchards was constructed and used to search for optimal viewing angles for different dominant row orientations. An initial GIS analysis provided statistics on the Citrusdal and Lake Alfred citrus production areas. Results show that, while tree spacings are highly variable, two dominant row orientations exist in these regions. An analysis was made on the impact of pixel size on signal mixture at two scale levels: current sensors with moderate to high spectral resolution and pixel sizes no larger than 10 to 15 m can avoid the unmixing problem between adjacent fields or fields, but not within the fields at the tree/soil/weeds level. The off-nadir pointing capabilities of recent platforms can provide additional degrees of freedom to reduce the impact of mixtures of weeds and soil. Simulations in a virtual 3D environment were used to determine optimal off-nadir viewing directions for North-South and East-West oriented fields in both areas for earlier (09:30 LST) and later (10:30 LST) image acquisition times. Objective comparisons between different viewing and illumination geometries were made using spectral similarity based contribution indices. Three criteria were used to find optimal values: (a) reducing the impact of seasonality (illumination angle), (b) of soil spectral changes (mainly due to moisture conditions), and (c) of weeds spectral changes (weed physiology, weed cover). For North-South oriented fields, 315° (Citrusdal, southern hemisphere) or 225° (Lake Alfred, northern hemisphere) azimuth angles provided the best performance for the three criteria. This is at a 45° angle with the row orientation. For the East-West oriented fields, the best azimuths for Citrusdal and Lake Alfred are 180° and 0°, respectively, which is perpendicular to the row orientation. The optimal view azimuth is consistently in the direction opposite to the solar azimuth. High oblique zenith angles (40°) performed better or equal to near-nadir angles (20°). Early overflights 09:30 LST) resulted in better performance than later (10:30 LST) overflights, which is attributed to more shadowing of soil and weeds. Optimal viewing azimuths for one row orientation were often sub-optimal for the other perpendicular row orientation. Considering the dominance of North-South and East-West orientations in both areas, monitoring applications will require at least two image acquisitions in each critical stage of the production process.

Acknowledgments

Funding support for this project was provided by the K.U. Leuven (OT-04047) and the IS-HS (In-Situ, HyperSpectral) project funded by the Flemish government. The authors are grateful to the University of Stellenbosch, Department of Viticulture and Oenology and in particular to Mr Albert Strever for the use of their spectroradiometer and to Citrus Research International for logistic support.

References

Albrigo, L., R. Buker, J. Burns, W. Castle, S. Futch, C. McCoy, R. Muraro, M. Rogers, J. Syvertsen, and L. Timmer, 2005. The impact of four hurricanes in 2004 on the Florida citrus industry: Experiences and lessons learned, *Proceedings of Florida State Horticultural Society*, 118:66-74.

Asner, G., and K. Heidebrecht, 2002. Spectral unmixing of vegetation, soil and dry carbon cover in arid regions: Comparing multispectral and hyperspectral observations, *International Journal of Remote Sensing*, 23(19):3939-3958.

Aubert, B., and G. Vullin, 1998. *Citrus Nurseries and Planting Techniques*, CIRAD, Montpellier, France, 183 p.

Bach, H., and W. Mauser, 1994. Modelling and model verification of the spectral reflectance of soils under varying moisture conditions, *Proceedings of IGARSS '94*, Volume 4, pp. 2354-2356.

Baret, F., and G. Guyot, 1991. Potentials and limits of vegetation indices for LAI and APAR assessment, *Remote Sensing of Environment*, 35(2-3):161-173.

Bateson, C., G. Asner, and C. Wessman, 2000. Endmember bundles: A new approach to incorporating endmember variability into spectral mixture analysis, *IEEE Transactions on Geoscience and Remote Sensing*, 38(2):1083-1094.

Bausch, W., and K. Diker, 2001. Innovative remote sensing techniques to increase nitrogen use efficiency of corn, *Communications in Soil Science and Plant Analysis*, 32:1371-1390.

Bronson, C., J. Geuder, N. Mongiovi, and R. Gaskalla, 2009. *Florida Agricultural Statistics, Commercial Citrus Inventory 2008, Technical Report*, USDA, NASS, Florida Field Office.

Campbell, J., 2002. *Introduction to Remote Sensing*, Third edition, Taylor & Francis, London, UK, 621 p.

Capderou, M., 2005. *Satellites, Orbits and Missions*, Springer-Verlag, France, 544 p.

C.G.A, 2008. *Key Industry Statistics 2008*, Citrus Growers Association of Southern Africa, 47 p.

Du, Y., C. Chang, H. Ren, C. Chang, J. Jensen, and F. D'Amico, 2004. New hyperspectral discrimination measure for spectral characterization, *Optical Engineering*, 43(8):1777-1784.

FAO, 2006. *Fresh and Processed Citrus Fruit Annual Statistics, Technical report*, Commodities and Trade Division Food and Agriculture Organization of the United Nations, Rome, Italy.

Fritz, S., M. Massart, I. Savin, J. Gallego, and F. Rembold, 2007. The use of MODIS data to derive acreage estimations for larger fields: A case study in the south-western Rostov region of Russia, *International Journal of Applied Earth Observation and Geoinformation*, 10(4):453-466.

Gilabert, M., J. Gonzalez-Piqueras, F. Garcia-Haro, and J. Melia, 2002. A generalized soil-adjusted vegetation index, *Remote Sensing of Environment*, 82(2-3):303-310.

Gilabert, M.A., and J. Meliá, 1993. Solar angle and sky light effects on ground reflectance measurements in a citrus canopy, *Remote Sensing of Environment*, 45(3):281-293.

Goel, N., W. Qin, and B. Wang, 1997. On the estimation of leaf size and crown geometry for tree canopies from hotspot observations, *Journal of Geophysical Research, BOREAS Special Issue*, 102(D24):29543-29554.

Huang, C., J. Townshend, S. Liang, S. Kalluri, and R. DeFries, 2002. Impact of sensor's point spread function on land cover characterization: Assessment and deconvolution, *Remote Sensing of Environment*, 80(2):203-212.

Jensen, J.R., 2004. Introductory Digital Image Processing: A Remote Sensing Perspective, Third edition, Prentice Hall, Upper Saddle River, New Jersey, 526 p.

Ladaniya, M.S., 2007. *Citrus Fruit: Biology, Technology and Evaluation*, Academic Press (Elsevier), San Diego, California, 576 p.

Lobell, D., and G. Asner, 2002. Moisture effects on soil reflectance, *Soil Science Society of America Journal*, 66:722-727.

Müller, E., and H. Décamps, 2001. Modeling soil moisture-reflectance, *Remote Sensing of Environment*, 76(2):173-180.

Mostert, S., H. Steyn, H. Burger, and H. Bosman, 2008. Sumbandilasat, An operational technology demonstrator, *Acta astronautica*, 63(11-12):1273-1282.

Peddle, D., and M. Smith, 2005. Spectral mixture analysis of agricultural crops: Endmember validation and biophysical estimation in potato plots, *International Journal of Remote Sensing*, 26(3):4959-4979.

Pharr, M., and G. Humphreys, 2004. *Physically Based Rendering, From Theory to Implementation*, Morgan Kaufmann, San Fransisco, California, 1019 p.

Pinter, P., J. Hatfield, Jr, J. Schepers, E. Barnes, M. Moran, C.S.T. Daughtry, and D. Upchurch, 2003. Remote sensing for crop management, *Photogrammetric Engineering & Remote Sensing*, 69(6):647-664.

Pinty, B., and M. Verstraete, 1992. GEMI: A non-linear index to monitor global vegetation from satellites, *Vegetation*, 101(1):15-20.

Plaza, A., P. Martinez, R. Perez, and J. Plaza, 2004. A quantitative and comparative analysis of endmember extraction algorithms from hyperspectral data, *IEEE Transactions on Geoscience and Reomote Sensing*, 42(3):650-663.

Qi, J., A. Chehbouni, A. Huete, Y. Kerr, and S. Sorooshian, 1994. A modified soil adjusted vegetation index, *Remote Sensing of Environment*, 48(2):119-126.

Ranson, K.J., C.S.T. Daughtry, L.L. Biehl, and M.E. Bauer, 1985. Sun-view angle effects on reflectance factors of corn canopies, *Remote Sensing of Environment*, 18(2):147-161.

Ricchiazzi, P., S. Yang, C. Gautier, and D. Sowle, 1998. SBDART: A research and teaching software tool for plane-parallel radiative transfer in the earth's atmosphere, *Bulletin of the American Meteorological Society*, 79(10):2101-2114.

Richardson, A., and C. Wiegand, 1977. Distinguishing vegetation from soil background information., *Photogrammetric Engineering & Remote Sensing*, 43(2):1541-1552.

Richter, R., M. Bachmann, W. Dorige, and A. Muller, 2006. Influence of the adjacency effect on reflectance measurements, *Transactions on Geoscience and Remote Sensing Letters*, 3(4):565-569.

Roberts, D., M. Smith, and J. Adams, 1993. Green vegetation, nonphotosynthetic vegetation, and soils in AVIRIS data, *Remote Sensing of Environment*, 44(2-3):255-269.

Rogers, M., L. Timmer, and T. Spann (editors), 2009. *Florida Citrus Pest Management Guide, SP 043*, University of Florida, IFAS, Lake Alfred, Florida, 170 p.

Rondeaux, G., M. Steven, and F. Baret, 1996. Optimization of soil-adjusted vegetation indices, *Remote Sensing of Environment*, 55(13):95-107.

Schaaf, C., Gao, F., Strahler, A., Lucht, W., Li, X., Trsang, T., Strugnell, N., Zhang, X., Jin, Y., Muller, J.P., P. Lewis, M. Barnsley, P. Hobson, M. Disney, G. Roberts, M. Dunderdale, C. Doll, R. d'Entremont, B. Hu, S. Liang, J. Privette, and D. Roy, 2002. First operational BRDF, Albedo nadir reflectance products from MODIS, *Remote Sensing of Environment*, 83(1-2):135-148.

Somers, B., K. Cools, S. Delalieux, J. Stuckens, D. Van der Zande, W.W. Verstraeten, and P. Coppin, 2009a. Nonlinear hyperspectral mixture analysis for tree cover estimates in orchards, *Remote Sensing of Environment*, 113(6):1183-1193.

Somers, B., S. Delalieux, J. Stuckens, W.W. Verstraeten, and P. Coppin, 2009b. A weighted linear spectral mixture analysis approach to address endmember variability in agricutrural production systems, *International Journal of Remote Sensing*, 30(9):139-147.

Somers, B., S. Delalieux, W.W. Verstraeten, and P. Coppin, 2009c. A conceptual framework for the simultaneous extraction of sub-pixel spatial extent and spectral characteristics of crops, *Photogrammetric Engineering & Remote Sensing*, 75(1):57-68.

Somers, B., S. Delalieux, W.W. Verstraeten, J. Verbesselt, S. Lhermitte, and P. Coppin, 2009d. Magnitude and shape related feature integration in hyperspectral mixture analysis to monitor weeds in citrus orchards, *IEEE Transactions on Geoscience and Remote Sensing*, 47(11):3630-3642.

Spiegel-Roy, P., and E. Goldschmidt, 1996. *Biology of Citrus, 229*, Cambridge University Press.

Strahler, A., W. Lucht, C. Schaaf, T. Trang, F. Gao, X. Li, J.P. Muller, P. Lewis, and M. Barnsley, 1999. *MODIS BRDF/Albedo Product: Algorithm Theoretical Basis Document Version 5.0. Technical Report*, NASA - MODIS Science Team.

Stuckens, J., B. Somers, S. Delalieux, W.W. Verstraeten, and P. Coppin, 2009a. The impact of common assumptions on canopy radiative transfer simulations: A case study in citrus orchards, *Journal of Quantitative Spectroscopy and Radiative Transfer*, 110(1-2):1-21.

Stuckens, J., W.W. Verstraeten, S. Delalieux, R. Swennen, and P. Coppin, 2009b. A dorsiventral leaf radiative transfer model: Development, validation and improved model inversion

techniques, *Remote Sensing of Environment*, 113(12):2560-2573.

Tucker, C., 1979. Red and photographic infrared linear combination for monitoring vegetation, *Remote Sensing of Environment*, 8(2):127-150.

Van der Meer, F., and S. De Jong, S., 2000. Improving the results of spectral unmixing of Landsat Thematic Mapper imagery by enhancing the orthogonality of end-members, *International Journal of Remote Sensing*, 21(15):2781-2797.

Widlowski, J.L., B. Pinty, N. Gobron, M. Verstraete, D. Diner, and A. Davis, 2004. Canopy structure parameters derived from multi-angular remote sensing data for terrestrial carbon studies, *Climatic Change*, 67(2):403-415.

Widlowski, J.L., M. Robustelli, M. Disney, J.P. Gastellu-Etchegorry, T. Levergne, P. Lewis, P. North, B. Pinty, R. Thompson, and M. Verstraete, 2008. The RAMI On-line Model Checker (ROMC): A web-based benchmarking facility for canopy reflectance models, *Remote Sensing of Environment*, 112(3):1144-1150.

Ye, X., K. Sakai, S.I. Asada, and A. Sasao, 2007. Use of airborne multispectral imagery to discriminate and map weed infestations in a citrus orchard, *Weed Biology and Management*, 7(1):23-30.

(Received 08 January 2010; accepted 06 April 2010; final version 17 April 2010)

Errata

Section 2.1, par.1, line 7:

"...with a 0.6 m pixel resolution" should be "...with a 0.6 m pixel size".

Section 2.1, par. 3, line 8:

"The dominant orientation in Citrusdal is slightly tending towards the West, which may be explained by the 345° orientation of the Olifantsrivier valley in which the orchards are situated."

should be

"The dominant orientation in Citrusdal (351°) is slightly tending towards the West. Most of these orchards have their row orientations approximately aligned with the axis of the Olifantsrivier valley (345°) in which they are situated. This may explained by practical (access to orchards) or historical reasons (land ownedship)."

Section 2.1, figure 1B and 1C:

"row distance" should be "between row spacing"

"tree distance" should be "within row spacing"

Section 2.3, par. 1, line 4:

"A total of 10 representative trees were calibrated to represent actual trees."

should be

"A total of 10 virtual trees were generated to represent actual field trees. The virtual tree structure parameters were iteratively calibrated using allometric measures and gap fraction analysis."

Section 4.3, list item 2

"*Seasonal changes in illumination.* Similar to agriculture in general, in horticulture, seasonal changes in physiology and phenology as well as in solar position will induce

changes in the measured reflectance factors (Stuckens et al., 2009a). Failing to separate both factors may lead to erroneous conclusions. An optimal viewing angle will minimize the impact of illumination."

should be

"*Seasonal changes in illumination.* For a fixed observation time (LST), seasonal changes in solar position will induce changes in the measured reflectance factors even when tree structure or biochemistry would not be altered (Stuckens et al., 2009a). Failing to separate these from physiological changes that are to be detected will lead to erroneous conclusions. An optimal viewing angle will minimize the impact of illumination."

Chapter 8

Conclusions and future perspectives

8.1 Conclusions

8.1.1 Overview

The two objectives of this manuscript, as formulated in chapter 1, were (i) improving the understanding of the processes that translate biophysical changes into changes detectable by optical remote sensing technology using a bottom-up approach, and (ii) improving the sensitivity and robustness of data extraction methods to detect subtle changes in the plant state. The first research objective is addressed in chapters 2 (biophysical processes), 3.1 (leaf RT model development), 4, 5 (up-scaling from leaf to canopy level to field level) and 7.1 (up-scaling to satellite level) from the smallest scale level (plant processes) to the satellite level. The second objective is addressed in chapters 3.2 (inversion strategies), 6 (time series for field reference spectra) and 7.2 (optimal viewing angles). Relationships and chapter numbers are indicated in figure 8.1 that is repeated here from the first chapter for the reader's convenience.

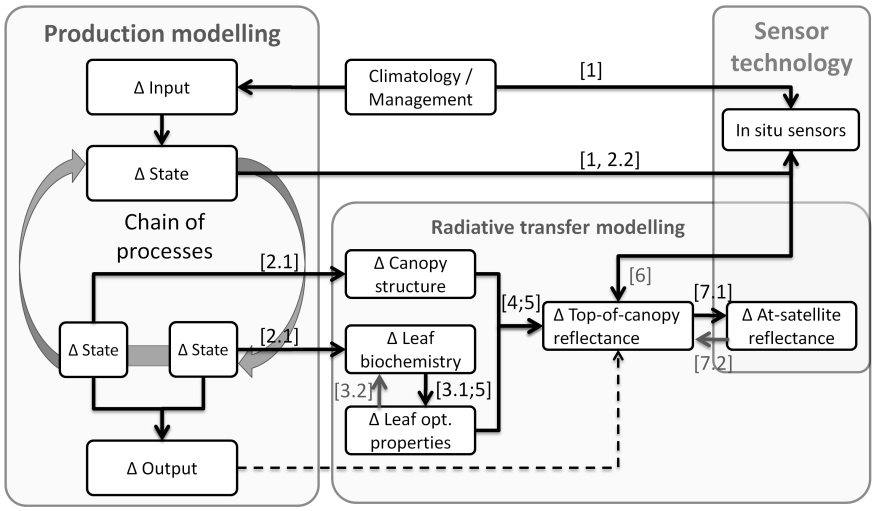

Figure 8.1: *A bottom-up modeling approach that integrates plant production modeling and radiative transfer modeling. Chapter numbers are between square brackets. Black numbers: objective one;* gray *numbers: objective two.*

Table 8.1 presents for each chapter an overview of the collected data, the constructed models and the field and model experiments that were conducted.

Table 8.1: *Overview of the collected data, models and field and simulation experiments for each chapter. Original chapter titles are abbreviated.*

Chapter, Part	Data	Experiments and models
2. Carbohydrate flows in citrus	- Literature review - Leaf spectra - Chemical analysis (starch, sugar)	- Statistical model fitting
3. Dorsiventral Leaf Model	- Leaf spectra - Chemical analysis (chlorophyll, carotenoids) - Leaf water and dry matter contents	- Model construction: Dorsiventral Leaf Model - Model sensitivity analysis - Model inversion
4. Assumptions in canopy RT	- Canopy spectra - Hemispherical photography - Allometry	- Model construction: ray-tracing model - Model simulations: impact of model simplifications on bias
5. Physiology of a hyperspectral time series	- Contact spectra (leaves, fruit) - Canopy spectra - Soil and weeds spectra - Meteorology	- Observations of phenology (18 months at monthly intervals) - Model simulations: impact of solar zenith angle
6. BRDF normalization in field spectroscopy	- Canopy and soil spectra - Solar irradiance	- Observations under different illuminations (from overcast to clear sky) - Model simulations: different illuminations
7. Off-nadir viewing	- High resolution satellite and aerial images + digitized field geometry	- GIS analysis - Model simulations: different viewing angles

8.1.2 Evaluation of hypothesis

Both objectives are used to evaluate the hypothesis that (i) hyperspectral reflectance of perennial fruit tree canopies holds information on the plant's internal state, that this information is expressed (ii) in the dynamics of leaf biochemistry and (iii) in mixtures and structural organizations of canopy components (leaves, fruit, flowers,...) and (iv) that this information can be accurately extracted for integration in biophysical models.

For the ***first part*** of this hypothesis (***information content***), an overview is presented of the variables that can be retrieved by hyperspectral remote sensing (chapter 1). The importance of variables such as chlorophyll and water contents has already been well explored for a number of production systems with relevance for citrus. For other variables with known absorption features, and specifically for (leaf level) soluble sugars and starch, a lack of knowledge was detected on their retrieval using hyperspectral remote sensing. On the other hand, a considerable amount of research exists, supporting evidence about their importance for the citrus production process. Therefore, existing physiological knowledge was summarized in a dynamic and deterministic/empirical conceptual model (chapter 2.1), focused on the carbohydrate flows in citrus. Seasonal

dynamics in soluble sugar and starch contents at the leaf level clearly reflect phenology, although differences between climatological regions exist. In many production systems, a large increase in starch contents precedes the vegetative flush, after which the levels drop during flowering, fruit set and fruit expansion. The potential relevance of both parameters for different stages in the production process is high, provided that their dynamics can be understood and that the internal and external processes that affect their values can be separated. Monitoring of leaf carbohydrate contents has potential to infer information about (i) yield losses due to physiological fruit drop, (ii) about the inclination of trees towards alternate bearing, (iii) about temperature conditioning or cold hardiness in cooler climates, and (iv) to scout for possible infections that block phloem transport, such as HLB.

The ***second part*** of the hypothesis focused on the ***expression*** of this information ***in leaf biochemistry*** through changes in the optical properties of leaves and in the ***structural organization of canopy elements***.

At the *leaf level*, the molecular absorption of *total chlorophyll, total carotenoids, water and total dry matter* has been well described and a fundamental approach was preferred by the development of a static mechanistic Dorsiventral Leaf radiative transfer Model (DLM, chapter 3.1). DLM considers the asymmetric distribution of pigments, water and dry matter in dorsiventral leaves. By running the model in forward mode, optical properties of both faces of a wide variety of leaves, including citrus, can be accurately simulated with good precision. This facilitates improvements in canopy radiative transfer modeling (the next step in bottom-up modeling), since dorsiventral properties of leaves can have a significant impact on canopy reflectance.

To gain a better understanding on the role of *canopy structure* in orchards, a static mechanistic hyperspectral ray-tracing model was developed in which realistic simulations of radiative transfer (including canopy reflectance) can be generated in virtual 3D environments (chapter 4). The model was calibrated and successfully validated in a virtual citrus orchard, realistically modeled based on an existing commercial orchard. Subsequent simulation experiments were set up to evaluate six assumptions commonly made in less complicated analytical radiative transfer models. The first three assumptions focused on leaf optical properties. They tested (i) whether a random mixture of leaves with different optical properties can be substituted by one leaf type with average optical properties, (ii) the impact of leaf asymmetry and (iii) leaf bidirectional reflectance (glossy cuticular reflections). Assumption (iv) compared variations in leaf shape and curl to the common representation of flat, disk-shaped leaves. The last two assumptions tested are (v) the impact of row orientation on canopy reflectance as compared to a random distributions of the same trees, and (vi) the impact of the diffuse component of sunlight on canopy reflectance under clear-sky conditions. The first assumption (optical properties mixtures) was not invalidated, but all other assumptions caused substantial errors. The largest effects in relative and absolute terms were found by ignoring the row orientation of trees, (assumption (v)). Models capable of dealing with row orientations seem to be a requisite for using remote sensing technology in horticulture. Deviations in leaf asymmetry (ii) and shape (iv) may be partly compensated using 'effective model variables'. The assumptions on leaf bidirectional reflectance (iii) and

diffuse illumination (vi) indicate that such simple corrections often applied to account for model generalizations do guarantee a better model fidelity. All errors, expressed in relative terms, were wavelength-dependent, so that many vegetation indices derived from model outputs are affected by model assumptions. Since reported errors depend on canopy architecture, solar position and atmospheric conditions, they are not temporally invariant and will affect vegetation monitoring applications. Many conclusions derived for citrus are expected to be valid for similar crops in horticulture and beyond.

The information obtained through both models and simulations was *validated* and placed in a *dynamic* context using a hyperspectral *time series of field data* in a commercial citrus orchard (chapter5). The impact of each phenological stage on the reflectance of the entire canopy and its components could be described. Leaf reflectance measurements were inverted into time series of biophysical parameters using the DLM (see chapter 3.1). The contribution of the individual canopy components (flowers, fresh, old and sun-burnt leaves) to the overall canopy spectral reflectance could be assessed by classification of digital camera images. An experimental Flowering Intensity Index allowed to discriminate three classes of flowering intensity. The separation of new vegetative flushes and sun-burnt leaves from healthy mature leaves provided insights in interpreting canopy level spectral changes. A simulation experiment was set up to quantify the impact of solar elevation on canopy level spectral indices, revealing the sensitivity of indices for chlorophyll and water content. This effect could be mitigated by applying a correction that removes the impact of the underlying soil. Most other trends in vegetation indices at the canopy level could be explained by a combination of changes in leaf biochemistry, leaf area index, leaf angle distribution and cover fractions of the components: old leaves, new flushes, flowers and sun-burnt leaves. Different vegetation indices predicting the same variable (chlorophyll content, water content or LAI) revealed similar trends, but some indices were better related to known structural or spectral changes in the canopies. The MCARI/OSAVI index was best related to leaf level trends in chlorophyll content. Seasonal changes in PRI could be linked to inverse changes in carotenoid-to-chlorophyll ratio. Canopy structure indices (MTVI2 and sLAIDI) were related to changes in LAI as well as to changes in leaf angle. Management (pruning and harvest) leads to noticeable changes in vegetation indices. Monitoring of canopy water status was highly impacted by the presence of new expanding spring leaves between and hampered a physiological interpretation of trends in the underlying mature leaves. Seasonal trends in soil and weed reflectance, important for the up-scaling of reflectance to the field level (spectral mixtures), was explained by seasonal changes in volumetric soil water content and by the weeds phenology.

The ***last part*** of the hypothesis was the ***existence of accurate data extraction methods***. Therefore different methods and strategies were developed to improve existing extraction methods at three scale levels: the leaf level for contact measurements, the canopy level for field measurements and finally the satellite level:

- At the *leaf level*, different strategies were developed to optimize the inversion of DLM (chapter 3.2) , i.e. to retrieval biophysical parameters from measured leaf reflectance spectra. Results of an initial sensitivity analysis followed by validation on two independent datasets (LeuvenV and LOPEX) revealed that inversion can

be improved using two techniques. The first is to exclude the 720-1350 nm region of the spectrum, which is the most sensitive to unknown variations in the leaf's internal structure and to variability in the dry matter specific absorption spectrum. The second is to measure reflectance on a 100% reflecting background. This knowledge was applied in different inversion schemes to retrieve pigments, water and dry matter contents. The best performing inversion schemes for both datasets show a good prediction accuracy for total chlorophylls, water and total dry matter (R^2 resp. 0.95, 0.94 and 0.97) and a moderate accuracy for carotenoids (R^2 of 0.58). Further development of DLM is required for the simulation of additional molecular groups that were not yet included. Soluble sugars and starch could however be reliably predicted from contact sensing measurements using statistical model fitting (chapter 2.2). Prediction accuracy depends on the type of measurement (e.g. type of background, fresh or dry leaf), on the applied statistical methods and the preprocessing procedures of the measured spectra. Good accuracies (R^2 of 0.91) were obtained for starch, while lower values for sugars (R^2 of 0.70) are attributed to the smaller range of sugar concentrations in the reference dataset.

- At the *canopy level*, the collection of ground-based canopy and soil hyperspectral measurements is often constrained by mixed meteorological conditions. While traditional dual field-of-view (DFOV) spectroscopy can overcome some of these restrictions (variations in total irradiance), it can not yet compensate for changes in angular light distribution (e.g. different proportions of diffuse and direct light). Therefore research was set up to better describe the effects of varying amounts of cloud cover (chapter 6). In a first simulation experiment, the impact of reduced irradiance caused by cloud cover on the signal-to-noise ratio (SNR) of measured canopy and soil reflectance factors was quantified. Results suggest that instrument specific lower bounds for illumination conditions (irradiance) can be defined above which DFOV spectroscopy can be successfully deployed. BRDF effects in DFOV measurements were modeled and described using synthetic data in a ray tracing environment (pbrt). Solar elevation, wavelength and target structure were the determinant factors affecting differences between target reflectance under obscured and unobscured conditions, while the anisotropy (BRDF) of the reference panel often reinforces this effect. A data-driven normalization procedure was developed by decompositing of the BRDF into an isotropic component specific for each individual target and a bidirectional component specific for a group of similar targets. The procedure was evaluated on synthetic and on real datasets. Results indicate that most of the bias in cloud obscured measurements can be removed by applying a normalization factor obtained from a representative target under equal illumination conditions. Field protocols should avoid or remove measurements that include large irradiance fluctuations during scan time as well as measurements made under intermediate cloud cover. Normalized spectra show low relative errors up to 1800 nm (on average 5%). At higher wavelengths, the errors increase due to a reduced signal-to-noise ratio. The inclusion of a BRDF normalization, in addition to existing intercalibration factors shows good promise to deploy DFOV spectroscopy for physiological monitoring applications. This can be important in mid-latitude climates where the dominance of partly cloudy and overcast skies

prevents the establishment of clear sky time series.

- At the *satellite level*, pixels from orchards (and other row structured plantations) contain the spectral signature of the tree crowns, but also variable mixtures of weeds and soil. To obtain a better insight in the composition and variability of these mixtures, the radiative transfer model for citrus orchards (see chapter 4) was adapted (chapter 7). A GIS analysis provided statistics on orchard geometry from two test areas: Citrusdal (South Africa) and Lake Alfred (Florida). Supplemented with simulations in virtual orchards constructed for both regions, information on the composition of pixel mixtures was obtained. Results indicate that moderate and high resolution satellite sensors (pixel sizes from 0.5 up to 15 m) can avoid the mixture problem between adjacent fields, but not the within-field mixtures between trees, soil and weeds. The effective estimation of these fractions and reverting the mixed spectrum to a pure canopy spectrum is the scope of (spectral) unmixing research and was not researched in this dissertation. Alternatively and in addition to the algorithmic solutions of unmixing, the *off-nadir pointing* capabilities of recent platforms provide additional opportunities to reduce the impact of mixtures of weeds and soil. A second set of simulations was used to determine optimal off-nadir viewing directions for North-South and East-West oriented fields in both areas for different acquisition times. Comparisons between different viewing and illumination geometries were made using spectral similarity based indices. Three evaluation criteria were used: (i) the impact of seasonality caused by illumination angle, (ii) the impact of soil spectral changes caused by varying soil moisture contents and (iii) the impact of spectral changes in weeds (weed physiology and ground cover). For North-South oriented fields, azimuth angles of 315° (southern hemisphere) and 225° (northern hemisphere) provided the best performance for the three criteria. For the East-West oriented fields, the best azimuths for the northern and southern hemisphere are 180° and 0° respectively, which is perpendicular to the row orientation. The optimal view azimuth is thus consistently in the direction opposite to the solar azimuth. High oblique zenith angles (40°) performed better or equal to near-nadir angles (20°). Early overflights (9:30 LST) resulted in better performance than later overflights (10:30 LST). This is attributed to increased shadowing of soil and weeds. Optimal viewing azimuths for one row orientation were often sub-optimal for the other perpendicular row orientation. Considering the dominance of both North-South and East-West orientations in many commercial citrus production regions, monitoring applications may require image acquisitions from two different azimuth angles in each critical stage of the production process.

8.1.3 Relevance for scientific research and for the citrus industry

The main contributions of this dissertation to the progress in ***science*** are better insights obtained in radiative transfer of leaves and canopies, the construction of tools to further investigate this radiative transfer on any crop type and the development of improved data capturing and extraction methods.

The main insight in radiative transfer is that - as stated in the hypothesis - the canopy reflectance can be considered as an integration of the contributions of the different

components (mainly leaves, but with contributions of twigs, fruit and flowers and the soil background) and the leaf biochemistry expressed in these components. The development of phenological stages and stresses can be explained by variations component's fractions, in their spatial organization and in detectable biochemical changes. Many aspects of canopy structure influence the overall reflectance, including the shape and cuticular structure of leaves, the difference between their adaxial and abaxial optical properties and the distribution of incident light. Accurate modeling of canopy reflectance requires to take these aspects into account.

Two modeling tools have been developed: DLM at the leaf level and a hyperspectral version of pbrt at the canopy level. Both models are not crop specific and can easily be ported to other production systems to retrieve leaf biochemistry and to provide accurate simulations of canopy reflectance.

Two of the improved data capturing and extraction methods include the improved model inversion scheme for DLM and the dual field-of-view method for the collection of time series under variable meteorological conditions. They can be readily applied on other research in the domain of hyperspectral remote sensing of vegetation. The third method, the use of off-nadir observations in row oriented crops has important potential, but is currently based on simulations and requires validation using satellite data series.

The main relevance of this research for the ***citrus industry*** must be situated in a longer time frame, as it further supports the construction of the anticipated integration of *in situ* and hyperspectral data to monitor, model and steer agricultural production systems.

The good results obtained in predicting leaf biochemistry from spectral contact measurements (chapters 2.2 and 3.2) indicate that these techniques may not only be a step in a scientific modeling framework. They can also be adapted for operational use for *in situ* instruments. This can be of importance for the citrus industry and other horticultural industries as it can provide a fast and low cost method to detect water stress (water content), biomass accumulation (dry matter content), chlorosis (chlorophyll), different stresses (chlorophyll to carotenoid ratio) and information about the carbohydrate flows (alternate bearing, diseases). The technological challenge in developing low-cost field-portable instruments to detect these variables involves substituting full spectral measurements by a limited number of wavebands measured by bandpass filter sets. Currently, this technology has only been commercialized for chlorophyll meters and fluorimeters.

8.2 Future perspectives

The biophysical modeling of horticultural crops is a research topic in its own right, that has only briefly been touched in chapters 1 and 2, but recommendations can be made for integration of submodels, model parametrization and data assimilation and choice of model crop. The radiative transfer modeling tools developed in this research can be further refined and additional steps are required to achieve an integrated model that simulates all optical interactions from leaf biochemistry to the sensor level. In

addition, the virtualization offered by ray-tracing models offers important potential for the modeling of photosynthesis. The data capture and inversion techniques introduced to improve the robustness of data retrieval can be further optimized and require further validation.

8.2.1 Biophysical modeling

Integration and parametrization of sub-models

Important biophysical relations specific for fruit tree crops are being incorporated into existing biophysical models such as CropSyst (Stöckle et al., 2003). This includes light interception by row crops, cold accumulation to simulate bud induction and thermal time accumulation for fruit ripening and cold hardiness. These models can be further developed by including additional interrelationships between compartments or by including existing sub-models. Sub-models can be species-specific such as the Decision Information Systems for Citrus (DISC; Albrigo et al., 2002) for flowering or the fruit growth model CITROS (Bustan et al., 1999) for grapefruit or more generic such as the fruit growth model of Henton et al. (1999).

Alternatively, strategies for a correct and site/cultivar-specific parametrization of the different crop coefficients requires more attention: CropSyst (version 4.13; 2010) defines 67 crop-specific parameters for a single fruit cultivar. Other variables and parameters such as meteorology, management and site description (soil type and fertility, terrain) are easier to define objectively.

Data assimilation and fusion with other technologies

In contrast to the large number of biochemical molecules involved in a plant's physiology, only a limited number have known absorption features in the 350-2500 nm wavelength range and can be detected by optical sensors. This includes chlorophyll a and b, carotenoids, anthocyanins, brown pigments (oxidized polyphenols), soluble sugars, starch, proteins, (hemi-)cellulose, lignin and water (see section 1.4). Only for a small number of these, chlorophyll, water and possibly carotenoid-to-chlorophyll ratio, can be retrieved with reasonable or good accuracy using existing multi- or hyperspectral remote sensing technology and algorithms. Others such as total dry matter, soluble sugars and starch can be determined at the leaf level. While these variables are related to different biophysical processes, knowledge is lacking to describe their expected or optimal values for different crops and cultivars during each phenological stage. In contrast, such knowledge bases exist for mineral nutrients in soil and leaf tissue and are being used to calculate fertilizer requirements. A successful introduction of remote sensing technology in horticulture (and by extension in agriculture) depends on the accurate retrieval of a set of biophysical parameters, but also on the knowledge of their expected dynamics during the production cycle and on a diagnostic interpretation of anomalous values.

As outlined in the introduction of this manuscript (section 1.4), thermal remote sensing and active and passive radar can provide valuable additional information that is hard to obtain using only passive optical remote sensing. The most important parameters are

related to the plant-soil water relations, namely the latent heat of (evapo)transpiration and soil moisture. Fusion of both technologies may further knowledge on modeling and monitoring of complex production systems.

Choice of model crop

Research in this dissertation used citrus as a model crop. Transferring this knowledge to different horticultural crops may benefit from knowledge gathered on citrus, but different crop-specific adaptations will be required. This not only considers the biophysical modeling itself, but also the up-scaling from leaf to canopy levels. Two examples are given:

- Banana (*Musa spp.*) plantations generally form a closed vegetation cover. This is expected to minimize the contribution of soils and weeds so that spectral unmixing may be facilitated or even redundant. On the other hand, phenological stages of individual plants in plantations are not synchronized, but their stochastic behavior can be modeled (Dens et al., 2008).
- Modern high density pear (*Pyrus communis*) training and pruning systems often create thin hedgerows (Mitcham & Elkins, 2007). These can have a proportionally small cover fraction as compared to citrus (approximately 40-60%; chapter 7) and thus a smaller contribution of the trees to the mixed spectrum. In addition, pear orchard floors are often maintained as continuous sods. Spectral mixtures of two vegetation signals (tree and grass) were found to be harder to separate than mixtures of only tree canopy and soil (Somers et al., 2010a). Remote sensing in such orchards may require oblique viewing as described in chapter 7 to reduce the spectral contribution of the sods.

8.2.2 Improvements on radiative transfer models

From leaf biochemistry to leaf optical properties

The current version of the DLM is restricted to four biochemical parameters: total chlorophyll, total carotenoids, water and total dry matter. The good prediction accuracy for dry matter indicates that it may be possible to quantify the contents of some of the dry mass constituents (e.g. cellulose, lignin, protein, sugar and starch). This is underpinned by recent research in which concentrations of soluble sugars and starch could be accurately determined in fresh and dry citrus leaves using statistical methods (Devarrewaere, 2010, see also chapter 2). Including these components in the DLM would only require the measurement of their in-vivo specific molecular absorption spectra.

From leaf to canopy

The up-scaling of radiative transfer from the leaf to the canopy level can be accomplished by either *analytical models* using stochastic parameters that describe averages and distributions for an entire forest, orchard or field or by a *rendering algorithm* (such as ray-tracing) that requires an explicit 3D modeling of all canopy elements (leaves, stems,

fruit). The computational speed of analytical models makes them suitable candidates for fast model inversion on remotely sensed datasets, but their large number of assumptions can lead to substantial deviations, as demonstrated in chapter 4. The largest deviation, caused by ignoring the row structure of orchards, requires dedicated radiative transfer models for row crops, such as the recent work by Zhao et al. (2010). The impact of other assumptions may be mitigated by using effective parameters, i.e. values deviating from true parameter values but producing a more correct simulated canopy reflectance. This raises the question of how such effective parameters can be derived from the true parameters (e.g. LAI) measured in the field. An alternative approach may focus on substantially improving the computational speed of rendering algorithms. One of many possibilities is to apply the technique of decomposition of the radiation field (Liang, 2004) on ray-tracing models and to explicitly model the zero- and first scattering orders, but to approximate higher scattering orders with stochastic algorithms.

Another field of research involves understanding the combined effect that many stresses and phenological events exert on both canopy structure and leaf biochemistry. Recent research on citrus indicates that water stress may initially impact canopy structure by alteration of leaf angles and leaf curl (Dzikiti 2010, unpublished data), while spectrally detectable water loss only occurs under more severe and persisting stress (Dzikiti et al., 2010). Additional research required for the detection of water stress is the spectral separation of wetting and drying of the soil background from changes in canopy water content.

From at-sensor radiance to sensor retrieved signals

While many radiometers are capable of producing relatively noiseless spectra in the visible and near-infrared wavelengths (350-1400 nm), the lower power of sunlight at higher wavelengths decreases the signal-to-noise ratio in the short-wave infrared (1400-2500 nm). This leads to substantial amounts of noise (ASD, 1999) hampering data extraction methods that require narrow wavebands or spectral derivatives. Other causes that can result in errors in radiometric measurements[1] include stray light (Zong et al., 2007), incorrect dark current subtraction and wavelength shifts (ASD, 1999). Most of these errors can be simulated by error models for well-characterized instruments. This can provide the last step in the up-scaling process to increase the realism of simulations and provide the necessary means to test the robustness of data extraction algorithms for specific sensors.

Modeling of light interception at the leaf level

Exact knowledge of canopy structure, as provided by 3D virtual environments (chapter 4) can also be used to simulate light interception at the level of individual leaves rather than to aggregate it at the canopy level. Such an approach has already been applied in forestry environments (Van der Zande et al., 2010) to provide detailed input for the modeling of photosynthesis or transpiration (Van der Zande et al., 2009). It may be

[1] In this discussion we exclude geometric distortions, although these can also be modeled if necessary parameters such as lens distortions, spatial point spread and uncertainties of satellite tilt and pitch are known.

adapted for orchards to evaluate the efficiency of different layouts, row orientations and pruning systems.

8.2.3 Robust data retrieval

Focus on model inversion strategies

The different model inversion schemes that were compared in chapter 3 reveal that the commonly used unweighted least squares approach often produces sub-optimal results. Alternative cost functions in optimization techniques have been reviewed by Baret & Buis (2008). On a canopy scale, inversions are often ill-posed and may require ancillary data or prior information to achieve accurate results (Baret & Buis, 2008).

Better normalization for dual field-of-view measurements

The normalization technique for ground based spectroradiometric measurements introduced in chapter 6 converts measurements under overcast conditions to clear sky conditions with a minimal bias. This is the correct procedure for vicarious calibration, but the resulting time series are still affected by BRDF effects caused by seasonal changes in solar position. An alternative approach is to modify this procedure and normalize all measurements to illumination under standard overcast conditions as these are almost insensitive to solar elevation.

Off-nadir viewing

The conclusions of chapter 7 are based on extensive and realistic simulations, but still require validation by field data. A validation experiment requires at least a one-year multi- or hyperspectral time series collected by a high resolution satellite sensor with off-nadir viewing capabilities (e.g. CHRIS-Proba or Sumbandilasat) coupled with ground spectroradiometer measurements for reference data.

8.3 References

(1999). ASD Technical guide 3rd Ed. Analytical Spectral Devices, 3rd edition.

Albrigo, L.G., Valiente, J.I., & Beck, H.W. (2002). Flowering expert system development for a phenology based citrus decision support system. *Acta horticulturae*, 584, 247–254.

Baret, F. & Buis, S. (2008). Advances in land remote sensing: system, modelling, inversion and application, chapter Estimating canopy characteristics from remote sensing observations: review of methods and associated problems, pages 173–202. Springer Science+Business Media B. V.

Bustan, A., Goldschmidt, E.E., & Emer, Y. (1999). Progress in the development of 'CITROS' - a dynamic model of citrus productivity. *Acta Horticulturae*, 499, 69–80.

Dens, K.R., Swennen, R.L., Romero, R.A., & Turner, D.W. (2008). Simulation of banana plant growth (Musa spp. AAA, Cavendish subgroup) based on temperature and ontogeny. *Acta Horticulturae*, 803, 181–186.

Devarrewaere, W. (2010). The use of hyperspectral remote sensing for the detection of carbohydrates in citrus foliage. Master's thesis, K. U. Leuven, Faculty of Bioscience Engineering.

Dzikiti, S., Verreynne, J.S., Stuckens, J., Strever, A., Verstraeten, W.W., Swennen, R., & Coppin, P. (2010). Determining the water status of Satsuma mandarin trees [Citrus Unshiu Marcovitch] using spectral indices and by combining hyperspectral and physiological data. *Agricultural and Forest Meteorology*, 150, 369–379.

Henton, S.M., Piller, G.J., & Gandar, P.W. (1999). A fruit growth model dempendent on both carbon supply and inherent fruit characteristics. *Annals of Botany*, 83, 509–514.

Liang, S. (2004). Quantitative remote sensing of land surfaces. John Wiley & Sons.

Mitcham, E.J. & Elkins, R.B., editors (2007). Pear. Production and handling manual. University of California, Agriculture and Natural Resources.

Somers, B., Delalieux, S., Verstraeten, W.W., van Aardt, J.A.N., Albrigo, G., & Coppin, P. (2010a). An automated waveband selection technique for optimized hyperspectral mixture analysis. *International Journal of Remote Sensing*, in press.

Stöckle, C.O., Donatelli, M., & Nelson, R. (2003). CropSyst, a cropping systems simulation model. *European Journal of Agronomy*, 18, 289–307.

Van der Zande, D., Mereu, S., Nadezhda, N., Cermak, J., Muys, B., Coppin, P., & Manes, F. (2009). 3D upscaling of transpiration from leaf to tree using ground-based LiDAR: Application on a Mediterranean Holm oak (Quercusilex L.) tree. *Agricultural and Forest Meteorology*, 149, 1573–1583.

Van der Zande, D., Stuckens, J., Verstraeten, W.W., Muys, B., & Coppin, P. (2010). Assessment of light environment variability in broadleaved forest canopies using terrestrial laser scanning. *Remote Sensing*, 2, 1564–1574.

Zhao, F., Gu, X., Verhoef, W., Wang, Q., Yu, T., Liu, Q., Huang, H., Qin, W., Chen, L., & Zhao, H. (2010). A spectral directional reflectance model of row crops. *Remote Sensing of Environment*, 114, 265–285.

Zong, Y., Brown, S.W., Meister, G., Barnes, R., & Lykke, K.R. (2007). Characterization and correction of stray light in optical instruments. In Proceedings of the SPIE Conference. Florence, Italy.

Chapter 9

Curriculum vitae

Articles in internationally reviewed journals

- **Stuckens, J.**, Somers, B., Albrigo, G.L., Dzikiti, S., Verstraeten, W.W., Swennen, R., Verreynne, S., Coppin, P., 2010. Off-nadir viewing for reducing spectral mixture issues in orchards. Photogrammetric Engineering and Remote Sensing 76, 1261-1274.
- Van der Zande, D., **Stuckens, J.**, Verstraeten, W.W., Muys, B., Coppin, P. Assessment of light dynamics in broadleaved forest canopies using terrestrial laser scanning. Remote Sensing 2, 1564-1574.
- Verstraeten, W.W., Vermeulen, B., **Stuckens, J.**, Lhermitte, S., Van der Zande, D., Van Ranst, M., Coppin, P., 2010. Webcams for bird detection and monitoring: a demonstration study. Sensors 10, 3480-3503.
- Dzikiti, S., Verreynne, S.J., **Stuckens, J.**, Strever, A., Verstraeten, W.W., Swennen, R., Coppin, P., 2010. Determining the water status of Satsuma mandarin trees [Citrus Unshiu Marcovitch] using spectral indices and by combining hyperspectral and physiological data. Agricultural and Forest Meteorology 150, 369-379.
- **Stuckens, J.**, Somers, B., Verstraeten, W.W., Swennen, R., Coppin, P., 2009. Evaluation and normalization of cloud obscuration related BRDF effects in field spectroscopy. Remote Sensing 1, 496-518.
- Somers, B., Cools, K., Delalieux, S., **Stuckens, J.**, Van Der Zande, D., Verstraeten, W.W., Coppin, P., 2009. Nonlinear Hyperspectral Mixture Analysis for tree cover estimates in orchards. Remote Sensing of Environment 113, 1183-1193.
- **Stuckens, J.**, Somers, B., Delalieux, S., Verstraeten, W.W., Coppin, P., 2009. The impact of common assumptions on canopy radiative transfer simulations: A case study in Citrus orchards. Journal of quantitative spectroscopy & radiative transfer 110, 1-21.
- Somers, B., Delalieux, S., **Stuckens, J.**, Verstraeten, W.W., Coppin, P., 2009. A weighted linear spectral mixture analysis approach to address endmember variability in agricultural production systems. International journal of remote sensing 30, 139-147.
- Biliouris, D., Van Der Zande, D., Verstraeten, W.W., **Stuckens, J.**, Muys, B., Dutré, P., Coppin, P., 2009. RPV model parameters based on hyperspectral bidirectional reflectance measurements of Fagus sylvatica L. leaves. Remote Sensing 1, 92-106.
- **Stuckens, J.**, Verstraeten, W.W., Delalieux, S., Swennen, R., Coppin, P., 2009. A dorsiventral leaf radiative transfer model: development, validation and improved model inversion techniques. Remote Sensing of Environment 113, 2560-2573.
- Van Der Zande, D., Jonckheere, I., **Stuckens, J.**, Verstraeten, W.W., Coppin, P., 2008. Sampling design of ground-based lidar measurements of forest canopy structure and its effect on shadowing. Canadian journal of remote sensing 34, 526-538.

- **Stuckens, J.**, Coppin, P., Bauer, M., 2000. Integrating contextual information with per-pixel classification for improved land cover classification. Remote sensing of environment 71, 282-296.

Articles in review

- **Stuckens, J.**, Dzikiti, S., Verreynne, S., Verstraeten, W.W., Swennen, R., Coppin, P. Physiological interpretation of a hyperspectral time series in a citrus orchard. Agricultural and Forest Meteorology.
- Biliouris, D., Van der Zande, D., Verstraeten, W.W., **Stuckens, J.**, Muys, B., Dutré, P., Coppin, P. The importance of leaf BRDF in forest canopy bidirectional reflectance. A case study using simulated canopy architecture and PBRT ray tracing. International Journal of Remote Sensing.

Papers at international conferences and symposia, published in full in proceedings

- Dzikiti, S., Verreynne, S.J., **Stuckens, J.**, Strever, A., Verstraeten, W.W., Swennen, R., Coppin, P., 2010. Integrating hyperspectral and physiological data to determine water status of Satsuma mandarin trees. Proceedings of the Combined Crops, Soils, Horticulture & Weeds Congress 2010.
- Dzikiti, A., Verreynne, S.J., Strever, A., **Stuckens, J.**, Verstraeten, W.W., Swennen, R., Coppin, P., 2009. Detecting citrus tree water status by integrating hyperspectral remote sensing with physiological approaches in a water-flow storage model. IGARSS2009.
- Van Der Zande, D., **Stuckens, J.**, Verstraeten, W.W., Muys, B., Coppin, P., 2009. Monitoring within-season dynamics in the light environment of a broadleaved forest stand using ground-based LIDAR datasets. MULTITEMP2009 94-100.
- **Stuckens, J.**, Somers, B., Verstraeten, W.W., Coppin, P., 2009. Normalization of illumination conditions for ground-based hyperspectral measurements using dual filed-of-view spectroradiometers and BRDF corrections. IGARSS2009.
- Somers, B., **Stuckens, J.**, Tits, L., Verstraeten, W.W., Coppin, P., 2009. A solution for the mixture problem in agricultural remote sensing. IGARSS2009.
- **Stuckens, J.**, Somers, B., Verstraeten, W.W., Coppin, P., 2009. Modeling of Physiology Related Changes in a Virtual Citrus Orchard as Detected by Remote Sensing Platforms. Acta Horticulturae; Proc. IS on Appl. of Precision Agric. for Fruits and Vegetables 824, 37-48.
- Van Der Zande, D., Jonckheere, I., **Stuckens, J.**, Verstraeten, W.W., Coppin, P., 2008. Impact of the sampling design on the quality of ground-based LiDAR datasets. SilviLaser 2008 305-315.

Meeting abstracts, presented at international conferences and symposia, published or not published in proceedings or journals

- **Stuckens, J.**, Dzikiti, S., Verstraeten, W.W., Verreynne, J.S., Swennen, R., Coppin, P., 2010. Impact of physiology, structure and BRDF in hyperspectral time series of a Citrus orchard. Geophysical Research Abstracts 12.
- Somers, B., Tits, L., **Stuckens, J.**, Verstraeten, W.W., Coppin, P., 2009. Hyperspectral signal unmixing: a next step towards site-specific crop production monitoring. Remote Sensing Applications in Environmental Science.
- **Stuckens, J.**, Verstraeten, W.W., Delalieux, S., Coppin, P., 2009. Development, validation and inversion of a dorsiventral leaf radiative transfer model. Geophysical Research Abstracts 11.
- Van Der Zande, D., Dieussaert, K., **Stuckens, J.**, Verstraeten, W.W., Coppin, P., 2009. Light environment modeling in Populus plantations using voxel-based light interception. Geophysical Research Abstracts 11.
- Somers, B., Cools, K., Delalieux, S., **Stuckens, J.**, Van Der Zande, D., Verstraeten, W.W., Coppin, P., 2009. Estimation of tree cover in orchards using a novel nonlinear hyperspectral mixture analysis technique. Geophysical Research Abstracts 11.
- **Stuckens, J.**, Somers, B., Verstraeten, W.W., Coppin, P., 2008. Simulation of physiology induced hyperspectral changes in a virtual citrus orchard as detected by medium and high resolution remote sensing platforms. Geophysical Research Abstracts 10.

Other journal publications

- Dzikiti, S., Verreynne, J., **Stuckens, J.**, Somers, B., Verstraeten, W.W., Swennen, R., Coppin, P. 2010. Hypersprectral remote sensing: prospects and challenges for monitoring fruit production. SA Fruit Journal, April/May, 55-58.

Arenberg Doctoral School of Science, Engineering & Technology
Faculty of Bioscience Engineering
Department of Biosystems
Research group Measure, Model & Manage Bioresponses
Address Willem de Croylaan 34, B-3001 Leuven, Belgium

KATHOLIEKE UNIVERSITEIT LEUVEN

ASSOCIATIE K.U.LEUVEN